Anzon Australia
LIMITED

BASKER-5
WELL COMPLETION REPORT
VOLUME 2
INTERPRETIVE DATA

September 2007

VIC/L26
OFFSHORE GIPPSLAND BASIN
VICTORIA

A. Cernovskis, K. Grieves, P. Hunt, B. Messent, S.Y. Wong and H. Zammitt

Document Control Number: 34262-DR-01-0033

Anzon Australia LIMITED

TABLE OF CONTENTS

1. WELL DATA RECORD 3

2. INTRODUCTION 4

3. SUMMARY OF WELL RESULTS 8

4. GEOLOGICAL DISCUSSION 12

5. GEOPHYSICAL DISCUSSION 18

6. OPEN-HOLE WIRELINE LOG ANALYSIS 23

7. MDT PRESSURE INTERPRETATION, FLUID CONTACTS AND SAMPLING 38

8. SAMPLE ANALYSES USING QEMSCAN 40

(i) Appendix 1 - X-Ray Diffraction Traces
(ii) Appendix 2 – QEMSCAN Reports
(iii) Appendix 3 - Photomicrographs

LIST OF FIGURES

Figure 2.1 Basker-5 Location Map 4
Figure 2.2 Basker-5 Location Map (Detail) 4
Figure 2.3 Basker Field Well Spider 5
Figure 2.4 Plan View of the Basker-5 Well Path 6
Figure 2.5 Vertical Cross Section along the Basker-5 Well Path 7
Figure 3.1 Basker-5 Flow Rates During the Well Cleanup 9
Figure 3.2 Basker-5 Pressure and Temperatures during the Cleanup Phase 10
Figure 4.1 Basker-5 Chronostratigraphy 12
Figure 4.2 Basker Palaeo-transport directions for Basker-2, -3, -4 and -5 14
Figure 4.3 Example from Basker-5 showing results of QEMSCAN 16
Figure 5.1 Composite Structure Map, Top of Basker Field Zone 2 Reservoir and Top of Manta Field Zone 7 Reservoir (Contour Interval 20m) 18
Figure 5.2 Seismic Line through the Basker and Manta Fields, Showing the Reservoir Intervals 19
Figure 5.3 Bathymetry Map (Contour Interval 10m), Showing Location of the Basker Field 20
Figure 5.4 Structure Map, Top of Basker Zone 0 Reservoir (Contour Interval 10m) 21
Figure 5.5 Structure Map, Top of Basker Zone 1.2 Reservoir (Contour Interval 10m) 21
Figure 5.6 Structure Map, Top of Basker Zone 2 Reservoir (Contour Interval 10m) 22
Figure 6.1 Basker-5 Hydrocarbon Type, example of methodology 26
Figure 6.2 Basker-5 NGT Composite Plot 27
Figure 6.3 Basker-5 Core-Log Comparison 28
Figure 6.4 Basker-5 PHIT-RT crossplot water sand interval 3000-3083mMD 29
Figure 6.5 Basker-5 PHIT-RT crossplot Hydrocarbon Interval 3204-3230mMD 30
Figure 6.6 Basker-5 Core Porosity-Permeability Crossplot 31
Figure 7.1 Basker-5 MDT Pressure vs Depth Plot 38

LIST OF TABLES

Table 3.1 Perforation intervals 9
Table 3.2 Basker-5 Predicted Versus Actual Formation Tops 11
Table 4.1 Sequence Boundaries in Hydrocarbon Section 13
Table 6.1 Open Hole Wireline Log Analysis General Data 24
Table 6.2 Basker-5 Reservoir Summation 32
Table 6.3 MSCT TEST Schedule (Part 1) 33
Table 6.4 Analysis Parameters (Zones of Interest) 35
Table 6.5 Schlumberger PEX Log Suite-1 Run1 Main Pass 36
Table 7.1 Basker-5 Approximate Fluid Contacts 39

LIST OF ENCLOSURES

Enclosure 1 Basker Field Correlation
Enclosure 2 Basker-5 Composite Well Log
Enclosure 3 Arbitrary Seismic Line along the Basker-5 Well Path
Enclosure 4 Basker-5 Petrophysical Evaluation Log (Complex Lithology Model)

1. WELL DATA RECORD

Well Name	BASKER-5
Designation	Development
Permit Name	VIC/L26 Production Licence
Title Holders	Anzon Australia Limited (Anzon) 50% and Beach Petroleum Limited (Beach) 50%
Operator (per P(SL)A Well Operations Regulations)	Anzon Australia Limited
Surface Location (GDA94, GRS80, MGA, UTM Zone 55)	Latitude 38º 17' 59.33"S Longitude 148º 42' 23.80"E 649229.0mE 5759541.6mN
Bottom Hole Location	Latitude 38º 18' 22.88"S Longitude 148º 43' 01.33"E 650127.195mE 5758798.562mN
Project Manager	Upstream Petroleum Pty Ltd
Start of Basker-5 Operations	08:00 hrs 25 February, 2006
Spud Time/Date	09:30 hrs 26 February, 2006
TD date	16:30 hrs 27 March, 2006
End Batch Drilling/Start Batch Completion Phase	03:00 hrs 26 May, 2006
Final Rig Release from Basker-5 Batch Completions Operations	22:00 hrs 29 June, 2006
Total Time Rig on Contract	36.71 days
Water Depth	155.5m (LAT)
Rotary Table – Sea Level	21.5m
Difference MSL to LAT	0.866m
Drilling Contractor / Rig Name / Type	Diamond Offshore General Company / Ocean Patriot / Semi-submersible
Well Status	Suspended for production with sub-sea completion
Total Depth (Drillers)	3640mMDRT (3383.7mTVDRT)
Maximum Deviation	33.18° @ 2816.36m MDRT / 2632.09m TVDRT
Bottom Hole Location offset	743.0m South and 898.2m East, on an Azimuth of 129.6° from surface location

2. INTRODUCTION

The Basker-5 development well (Figures 2.1 and 2.2) was planned for oil and gas production and for possible use as a gas injection well. It was drilled as a deviated well with the "Ocean Patriot" semi-submersible drilling rig and was part of the 2006 Basker-Manta Project Full Field Development (FFD) drilling campaign. It was spudded in 155.5m of water on 26th February 2006, with a wellhead adjacent to the Basker Field sub-sea production manifold and reached a TD south east of the production manifold near the crest of the Basker Field on 27th March 2006 (Figure 2.3).

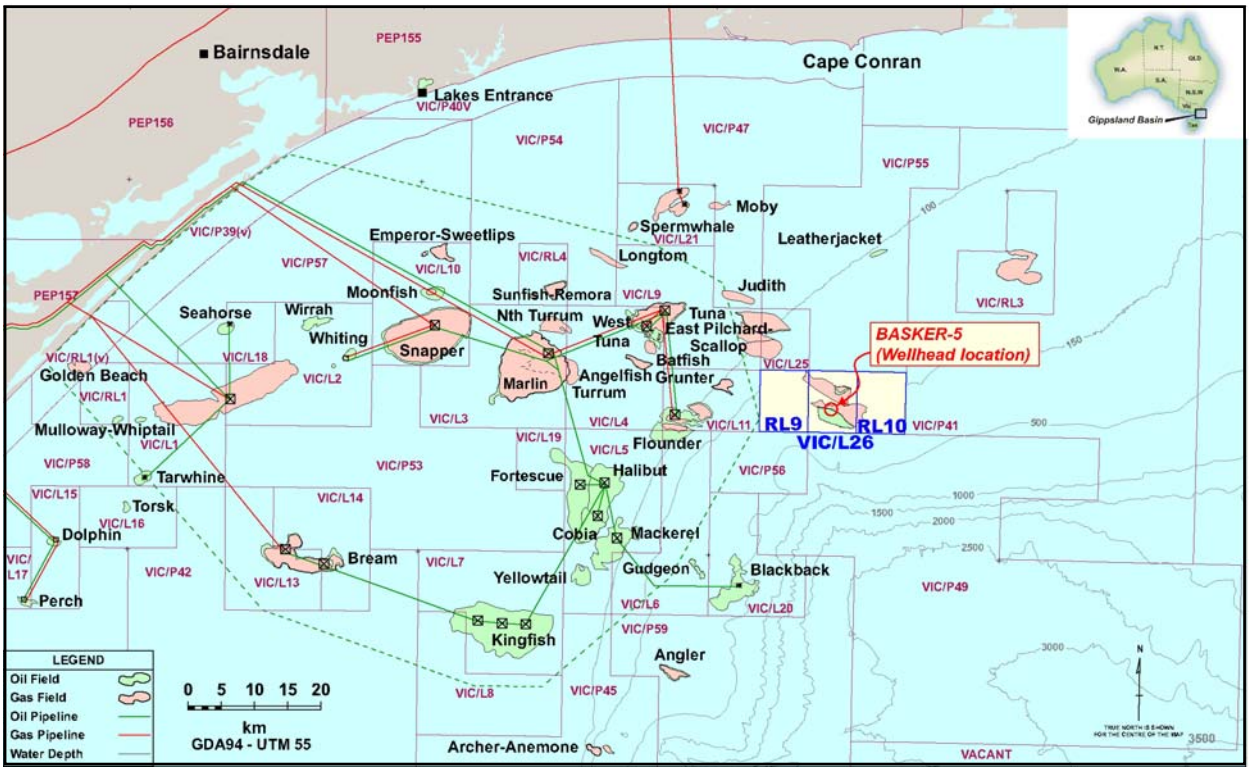

Figure 2.1 Basker-5 Location Map

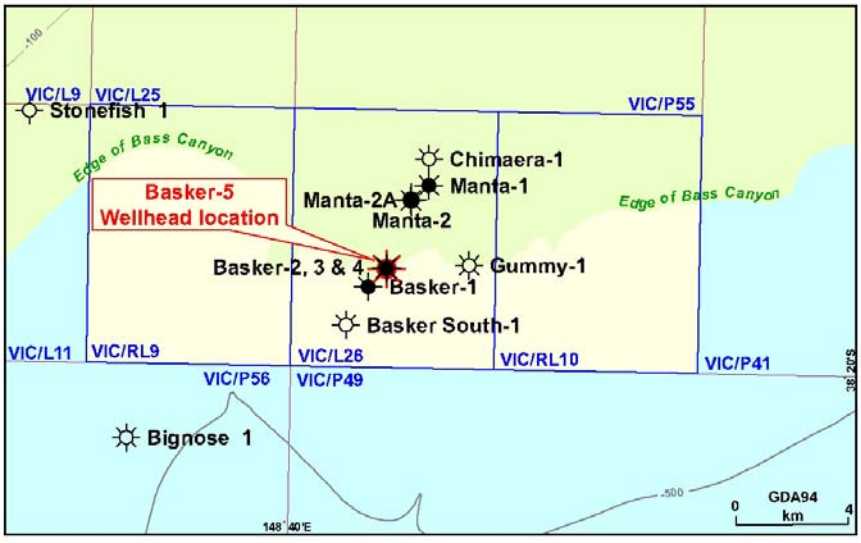

Figure 2.2 Basker-5 Location Map (Detail)

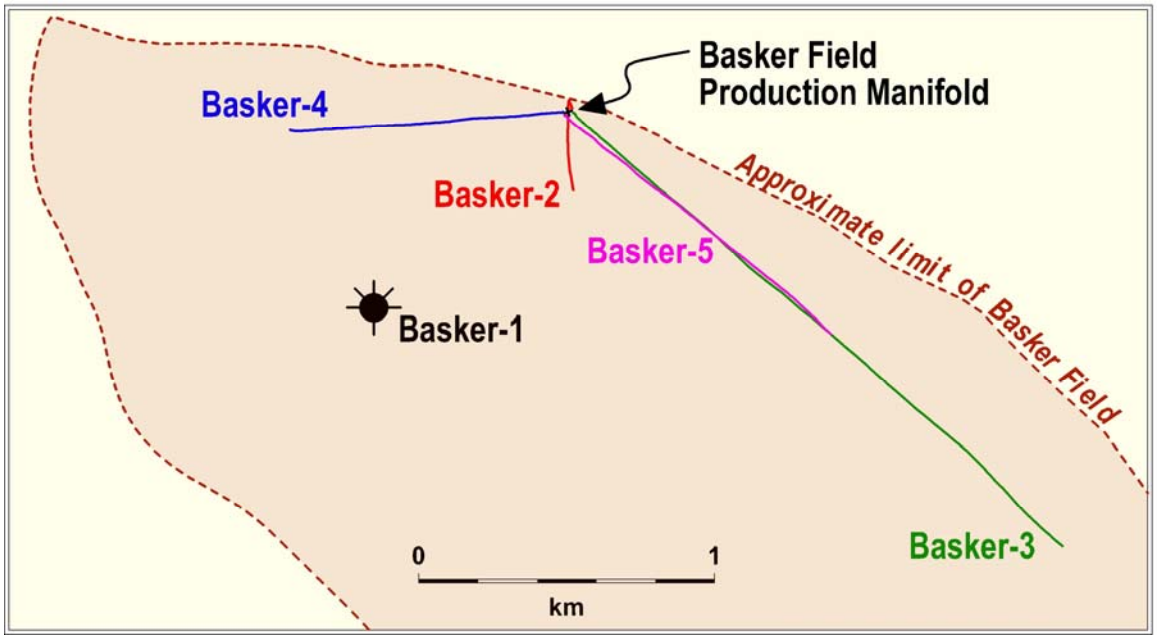

Figure 2.3 Basker Field Well Spider

The FFD well operations utilised "batch drilling and completion" wherever possible. Batch drilling and batch completion provided significant cost reductions and gains in operating efficiency. Rig time consumed in changing hole size was minimized by drilling all of the 36", 17½" and 12¼" holes in a continuous operation. Similarly, the completion phase of well operations was batched by running the completions back-to-back. The rig movement required to move the Ocean Patriot between wellheads (to facilitate batch drilling) was accomplished by adjustment of the rig's anchor chains.

Basker-5 was the second of the four FFD wells to be spudded (following Manta-2A and preceding Basker-4 and Basker-3). It was the second well to reach total depth and the second last well to be completed. The Ocean Patriot was released from the Basker-5 batch completion operations on 29th June 2006.

The primary objective of the well was to maximise future production from the oil and gas reservoirs discovered by Basker-1 and Basker-2, by intersecting them near the structural crest of the field. The well was also intended as a possible gas injection well, following evaluation of all four of the Basker development wells, to determine which was the most suitable for injection. The target for Basker-5 (at the top of the Zone 2 reservoir) was selected to conform with the 200 acre drainage circles allowed for each of the Basker FFD wells (so as to optimize development well spacing) and required drilling as a "build and hold" directional well (Figure 2.5). The TD is offset 1172.0m from the wellhead, on a bearing of 129.6° (Figure 2.4).

Basker-5 was suspended awaiting hook-up to the Basker field production manifold and the "Crystal Ocean" FPSO (floating production, storage and offtake vessel).

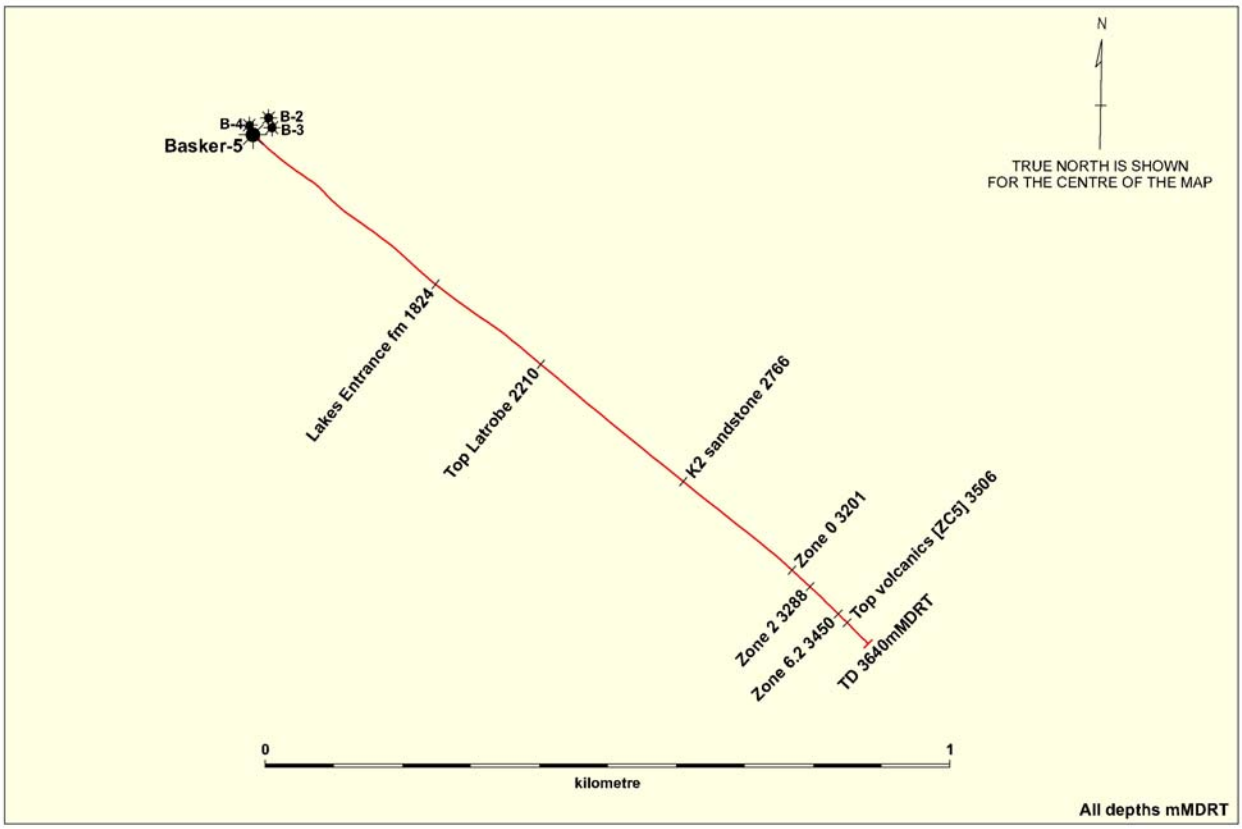

Figure 2.4 Plan View of the Basker-5 Well Path

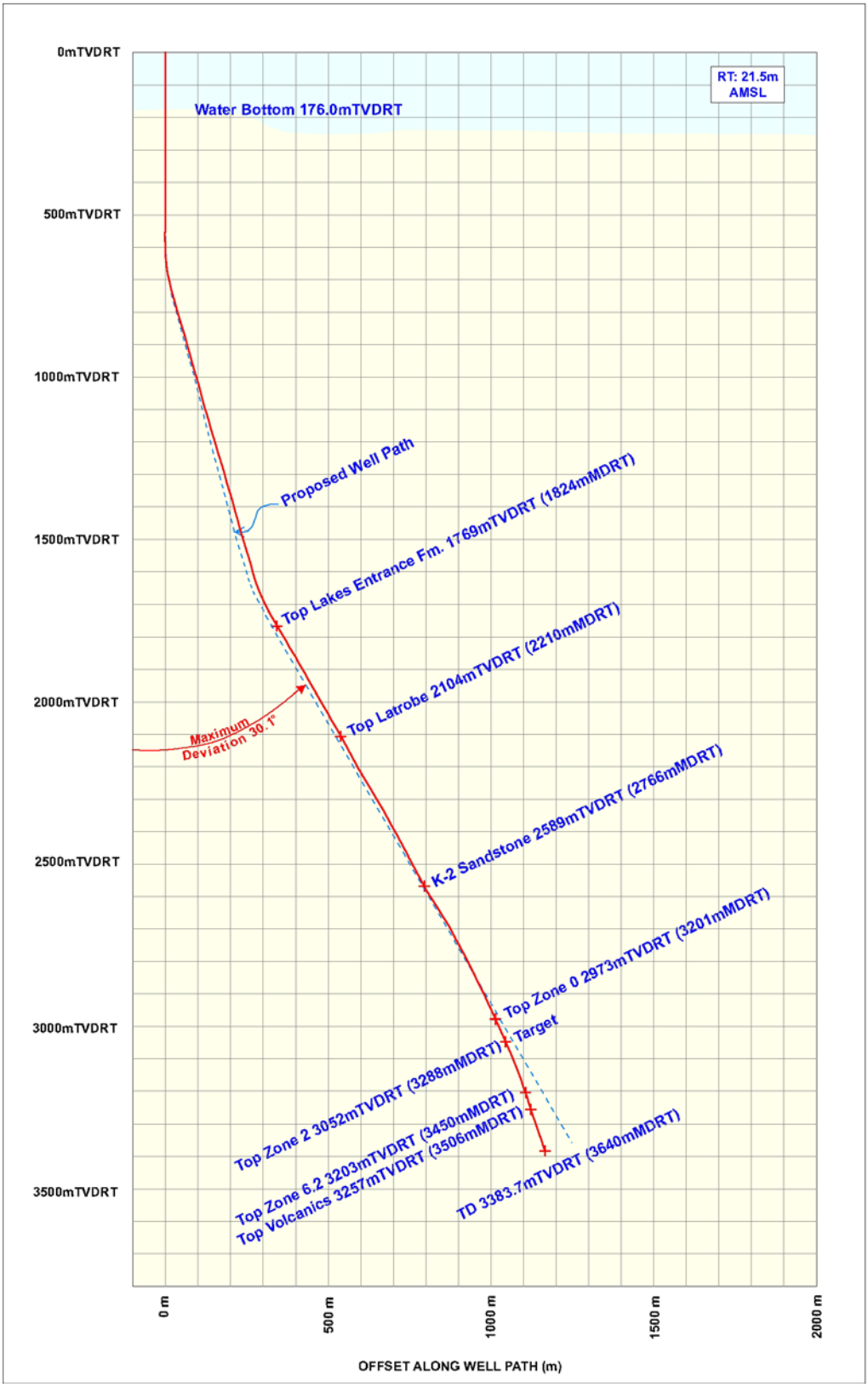

Figure 2.5 Vertical Cross Section along the Basker-5 Well Path

3. SUMMARY OF WELL RESULTS

The oil and gas reservoirs encountered in Basker-5 are similar to those encountered in the other Basker wells but there are a number of key differences (Enclosure 1):

1) Two new hydrocarbon zones containing both gas and oil were encountered in Basker-5. These intervals are grouped as Zone -1.

2) The Zone 0 reservoir is present in Basker-5, is oil-bearing and is in pressure communication with the other wells (as indicated by pressure depletion); the sand quality is good.

3) Zone 1.1 is water bearing.

4) The Zone 1.2 reservoir contains gas and is in pressure communication with the other wells.

5) Zone 2 contains 2 gas bearing sands: the upper is not in pressure communication with Basker 2, indicated by a lack of draw-down; the lower sand is interpreted to be in communication with nearby wells.

6) Zone 3 contains no reservoirs.

7) Zone 4 contains a number of oil and gas sands with separate fluid contacts identified in 4.3, 4.4 and 4.6 units.

8) No significant hydrocarbons are interpreted to be present in Zone 5.

9) A gas reservoir was intersected in Zone 6.1.2 which has the same GWC at 3185mTVDSS as seen in Basker-3.

10) Two gas reservoirs were intersected in Zone 6.2; pressure data is indicative of communication with nearby wells.

11) Zone 7.5 contains two thin gas reservoirs that are not in communication with nearby wells.

The interpreted total net oil pay was 24.2m and the total net gas pay 26.6m. Further details of the hydrocarbon intersections are provided in Section 6 and further details of the reservoir pressure interpretation in Section 7.

Basker-5 was perforated in the three Zones 0, 4.1, 4.3, 4.4, 4.5 and 7 as shown in the following table.

Table 3.1 Perforation intervals

Reservoir Zone	Perforation Interval (mMDRT)	Perforation Interval (mTVDSS)	Total (mMDRT)
Zone 0 (Oil)	3205.0 to 3208.0	-2955.5 to -2958.5	3.0
Zone 0 (Oil)	3211.0 to 3219.0	-2960.5 to -2968.5	8.0
Zone 4 (Oil)	3335.0 to 3338.0	-3074.5 to -3077.5	3.0
Zone 4 (Oil)	3352.0 to 3354.5	-3090.5 to -3093.0	2.5
Zone 4 (Oil)	3372.0 to 3374.5	-3108.5 to -3111.0	2.5
Zone 4 (Oil)	3378.0 to 3380.5	-3114.5 to -3117.0	2.5
Zone 7 (Oil)	3489.5 to 3493.5	-3219.5 to -3223.5	4.0
Zone 7 (Oil)	3497.0 to 3499.0	-3226.5 to -3228.0	2.0
		Total	27.5

The Performance of Basker-5 during the well cleanup operations is shown in the following figures. Please note that the declining oil rate during the first five hours of the cleanup was unreliable. The correct oil rate was restored after the Edge-X computer was back on line from about 13:50 hours.

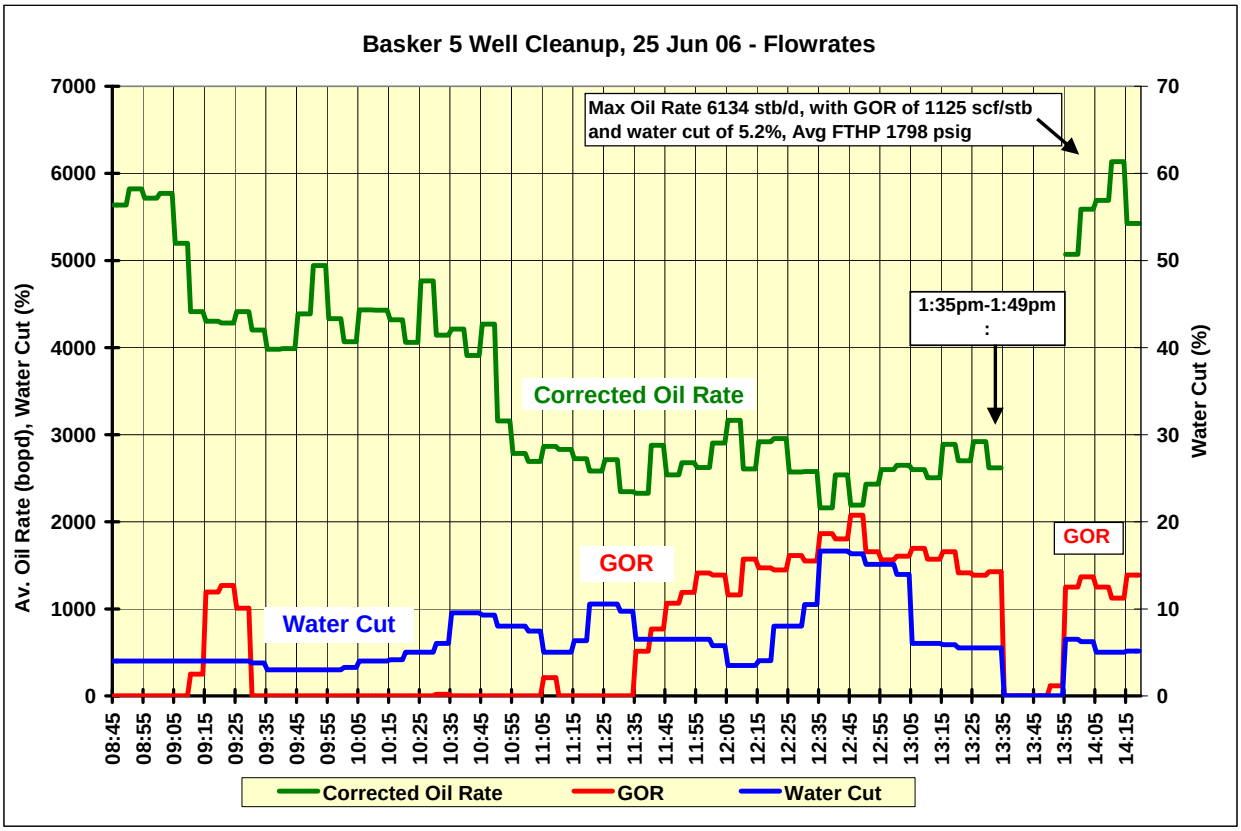

Figure 3.1 Basker-5 Flow Rates During the Well Cleanup

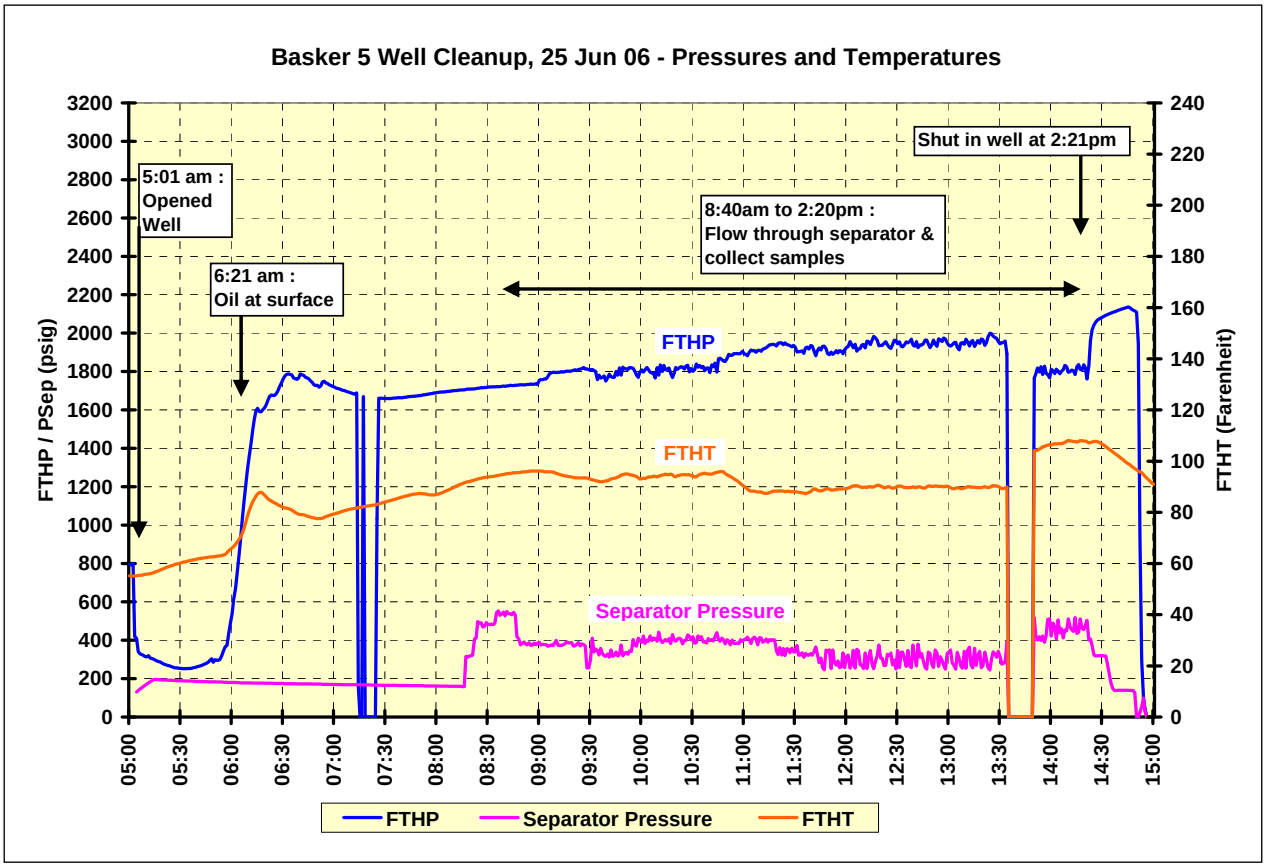

Figure 3.2 Basker-5 Pressure and Temperatures during the Cleanup Phase

The predicted and actual formation tops penetrated in Basker-5 are summarised in Table 3.3. There was a degree of uncertainty with depth prediction in Basker-5 because of difficulties with both depth conversion (further discussed in Section 5) and reservoir correlation (further discussed in Sections 4 and 6).

The reservoir top picks shown in Table 3.3 are at the top of the uppermost hydrocarbon-bearing sand or at the equivalent stratigraphic level, if no reservoir quality sand is present. Depths were predicted for eight of the twelve reservoirs intersected by Basker-5.

Basker-5 has shown that the eastern part of the Basker Field is shallower than was expected. All of the main reservoirs were high to prediction. This indicates that the south eastern extent of the field is potentially larger than as mapped pre-drill.

Table 3.2 Basker-5 Predicted Versus Actual Formation Tops

Formation:	Predicted Depth (mMDRT)	Predicted Depth (mTVDSS)	Actual Depth (mMDRT)	Actual Depth (mTVDSS)	Difference (mTVDSS)
Sea Floor	177.0	-155.5	176.0	-155.5	0m high
Top Lakes Entrance Formation	1884.3	-1779.0	1823.5	-1747.4	23.0m low
Top Latrobe Group	2238.8	-2086.0	2210.2	-2082.0	4.0m high
Top Zone 0 Reservoir Equivalent	3267.8	-2973.0	3201.4	-2952.0	21.0m high
Top Zone 1.2 Reservoir	3347.8	-3042.0	3271.8	-3016.0	26.0m high
Top Zone 2 Reservoir	3357.1	-3050.0	3287.7	-3030.6	19.4m high
Top Zone 4 Reservoir	3413.8	-3099.0	3319.6	-3060.0	39.0m high
Top Zone 5 Reservoir Equivalent	3491.5	-3166.0	3417.0	-3151.0	15.0m high
Top Zone 6.2 Reservoir Equiv.	3535.5	-3204.0	3449.5	-3181.8	22.2m high
Top Zone 7 Reservoir or Equiv.	3573.8	-3237.0	3488.1	-3218.4	18.6m high
Top of Volcanics Unit 1	3584.2	-3246.0	3506.4	-3235.6	10.4m high
Top Zone 8 Reservoir Equivalent	3617.8	-3275.0	NI		NI
TD	3689.6	-3337.0	3640.0	3362.2	25.2m high

NI: not intersected

4. GEOLOGICAL DISCUSSION

The well drilled a section of Recent to Campanian age sediments. A generalised chronostratigraphic summary is presented in Figure 4.1. The hydrocarbon reservoir section is Lower F. longus to T. lillei in age. TD of the well was 50mMD into the volcanic section. The ages are based on the correlation and the palynology carried out in Basker-1 and Manta-1.

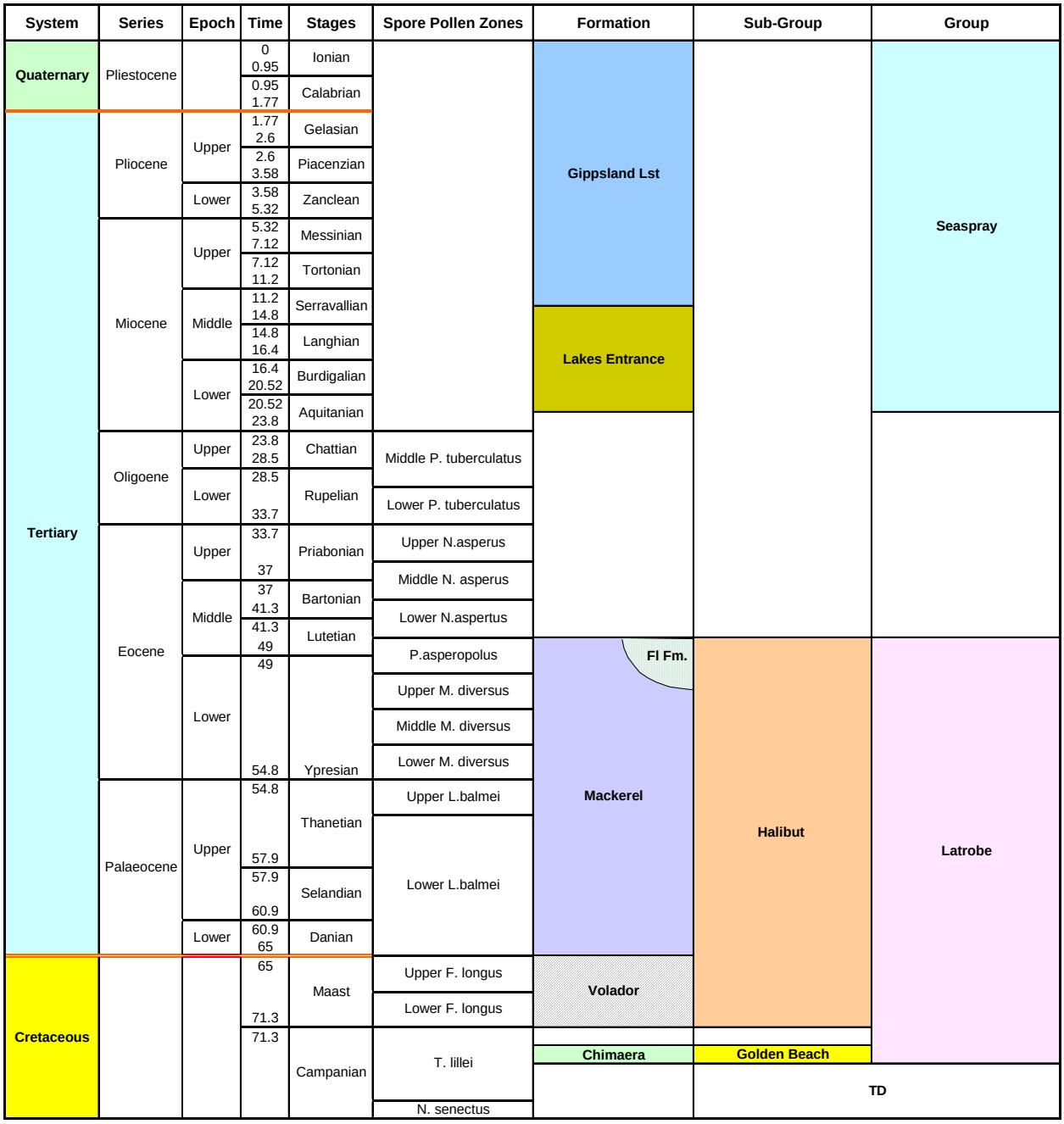

Figure 4.1 Basker-5 Chronostratigraphy

A summary of the palaeogeography for the Latrobe section can be found in Bernecker and Partridge (2005) and other papers.

The hydrocarbon reservoir section is located between the Ma2 Marker 3069.4mMDRT (-2832.6mTVDSS) and top Volcanics 3506.4mMDRT (-3235.6mTVDSS). Deposition occurred in a coastal plain environment consisting of interbedded sandstones, siltstones, claystones and coals.

The reservoir section is comprised of two sequences:

1) Sequence 1 is T. lillei in age. The base is not interpreted in the well. The system tracts present are late HST (Highstand System Tract) and LST (Lowstand System Tract).

2) Sequence 2 is lower F. longus in age, a complete section is present.

The major sequence boundaries in Basker-5 are shown in Table 4.1

Table 4.1 Sequence Boundaries in Hydrocarbon Section

Sequence	mMD	mTVDSS
Sequence 3 Base	3094.5	-2855.1
Sequence 2 Base	3412.0	-3146.4
Sequence 1 Base	Not penetrated	

The distribution of sandstone reservoirs is influenced by their position in the sequence. Using the model of Bohacs and Suter (1997), sandstone bodies of late HST/ early LST are amalgamated, and have more sheet-like characteristics. In Basker this equates to Zones 0 - 2. Channel bodies in the other system tracts have a more meandering characteristic.

For the reservoir section the palaeo-transport directions for the different wells are summarised in Figure 4.2, over page.

Basker-5 Hydrocarbon zones and the major stratigraphic boundaries are identified in the Composite Well Log. (Enclosure 2)

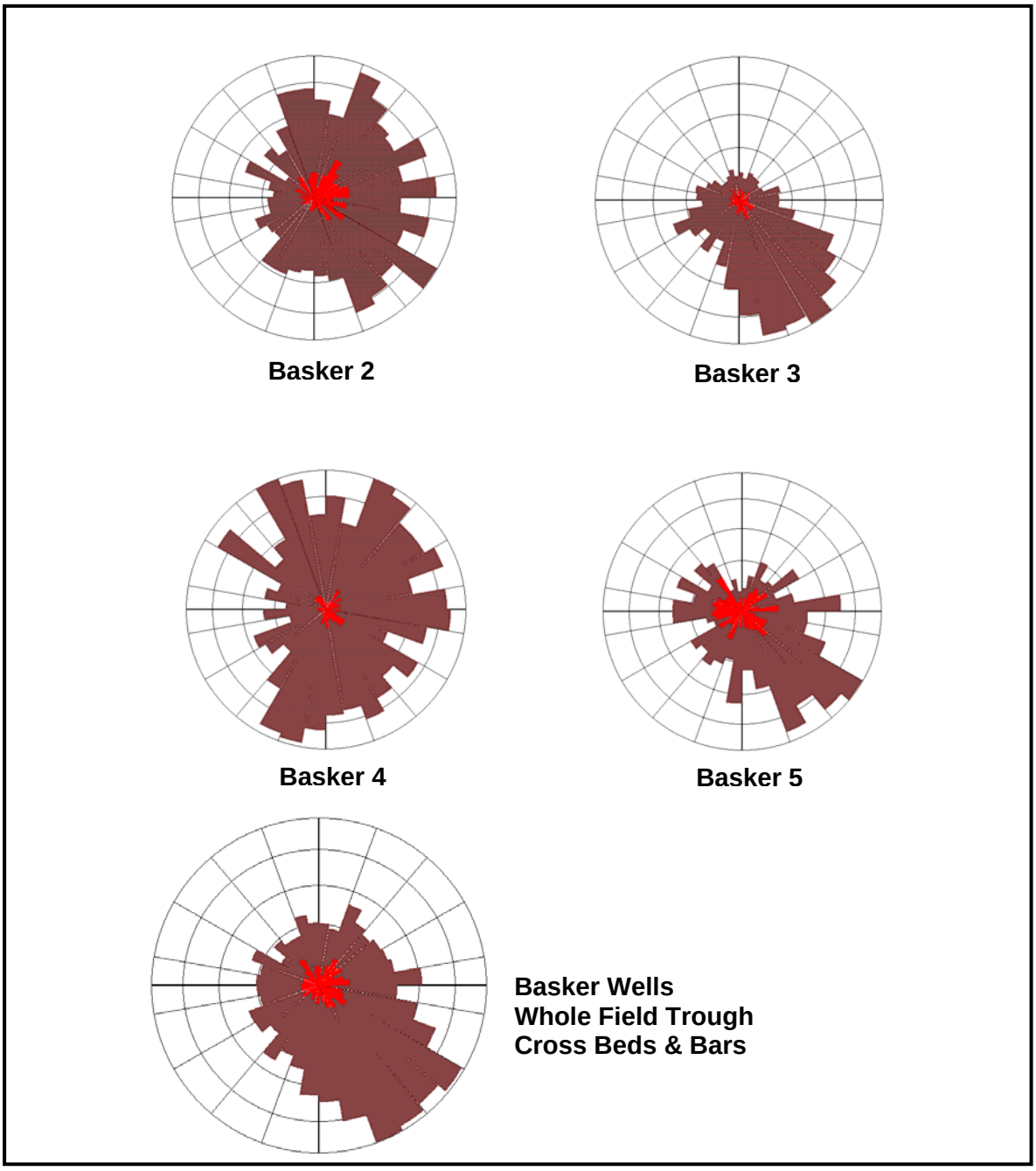

Figure 4.2 Basker Palaeo-transport directions for Basker-2, -3, -4 and -5

The well correlation across the field is presented in Enclosure 1. The pressure data had a significant influence on the well correlation. It indicated which reservoir units were in communication. Other units such as the hydrocarbons encountered in Zone 4, show a more limited areal distribution. The sandstone distribution can be explained by their relative position within a sequence. The major reservoirs are present between Zone 0 and Zone 2. These are interpreted to have been deposited during the late HST with channels migrating across the floodplain resulting in sheet sands greater than 2km in diameter. Hence good connectivity is interpreted in these sand bodies.

The Seahorse unconformity between the Intra-Latrobe Siliclastics (Halibut Subgroup) and the Golden Beach (Bernecker and Partridge, 2005) is near the top of T. lilliei and the base of Lower F. longus. There is little evidence of a major unconformity in the BMG area. The FMI data shows little evidence of structural movement between the Golden Beach and Halibut sub-group at this time. Any hiatus present is likely to be of limited time duration. The QEMSCAN data clearly shows a variation in the mineralogy across the interpreted regional unconformity (Figure 4.3).

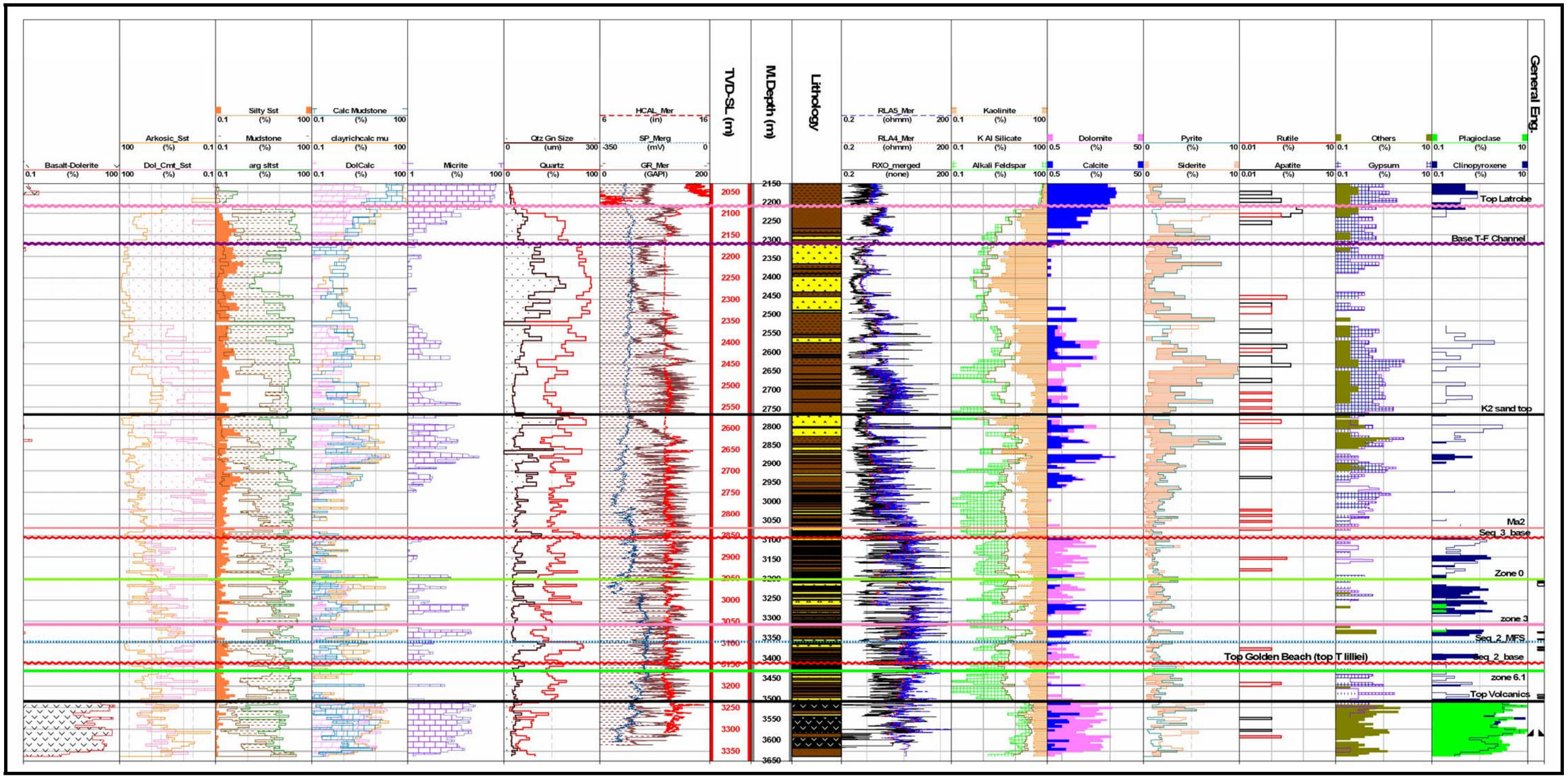

Figure 4.3 Example from Basker-5 showing results of QEMSCAN

Note: The top Golden Beach is a major unconformity to the east. QEMSCAN indicates a significant change in mineralogy across the unconformity.

References

T. Bernecker and A.D. Partridge, 2005, Approaches to Palaeogeographic reconstructions of the Latrobe Group, Gippsland Basin, Southeastern Australia, APPEA Journal, p581-600

Kevin Bohacs and John Suter, 1997, Sequence Stratigraphic Distribution of Coaly Rocks: Fundamental Controls and Paralic Examples, AAPG Bulletin, V81, No. 10 (October), p1612-1639

5. GEOPHYSICAL DISCUSSION

The trap for the Basker Field hydrocarbons is a fault-dependent closure on the downthrown side of a high-angle normal fault (the Basker Fault) which cuts across a south to southwest plunging nose which joins the Basker, Manta and Gummy fields (Figure 5.1).

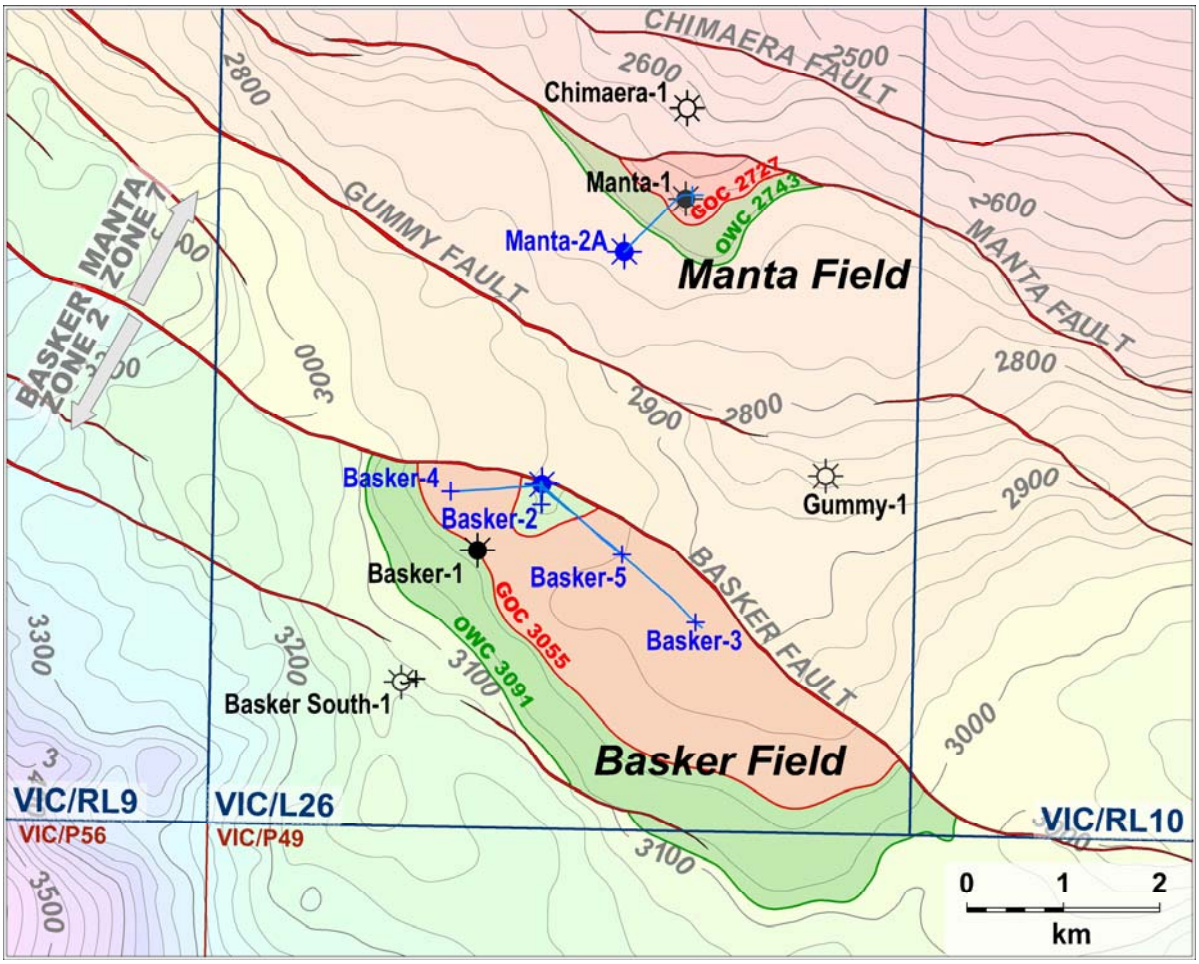

Figure 5.1 Composite Structure Map, Top of Basker Field Zone 2 Reservoir and Top of Manta Field Zone 7 Reservoir (Contour Interval 20m)

Six reservoir mapping seismic horizons (MZN2 and ZC1 to ZC5) have been mapped over the Basker Field, dividing the reservoir section into five intervals. Figure 5.2 (an arbitrary 3D seismic line through the Basker and Manta wells) shows the key Basker reservoirs in relation to the reservoir seismic markers. Enclosure 3 is an arbitrary 3D seismic line along the Basker-4 well path, showing all interpreted seismic horizons.

Seismic coverage for the Basker, Manta and Gummy fields is provided by the 1996 Basker-Manta 3D Seismic Survey. Two processed versions of this survey are presently available: the original 1997 processing by Shell's Melbourne Processing Centre and reprocessing completed by Woodside in 2001, which included both merging with the Kipper 3D and pre-stack depth migration (PSDM). The current reservoir maps were derived from Anzon's interpretation of the 2001 merged and reprocessed Kipper-Basker-Manta PSDM 3D seismic (KBM3D), after scaling from depth back to two-way time.

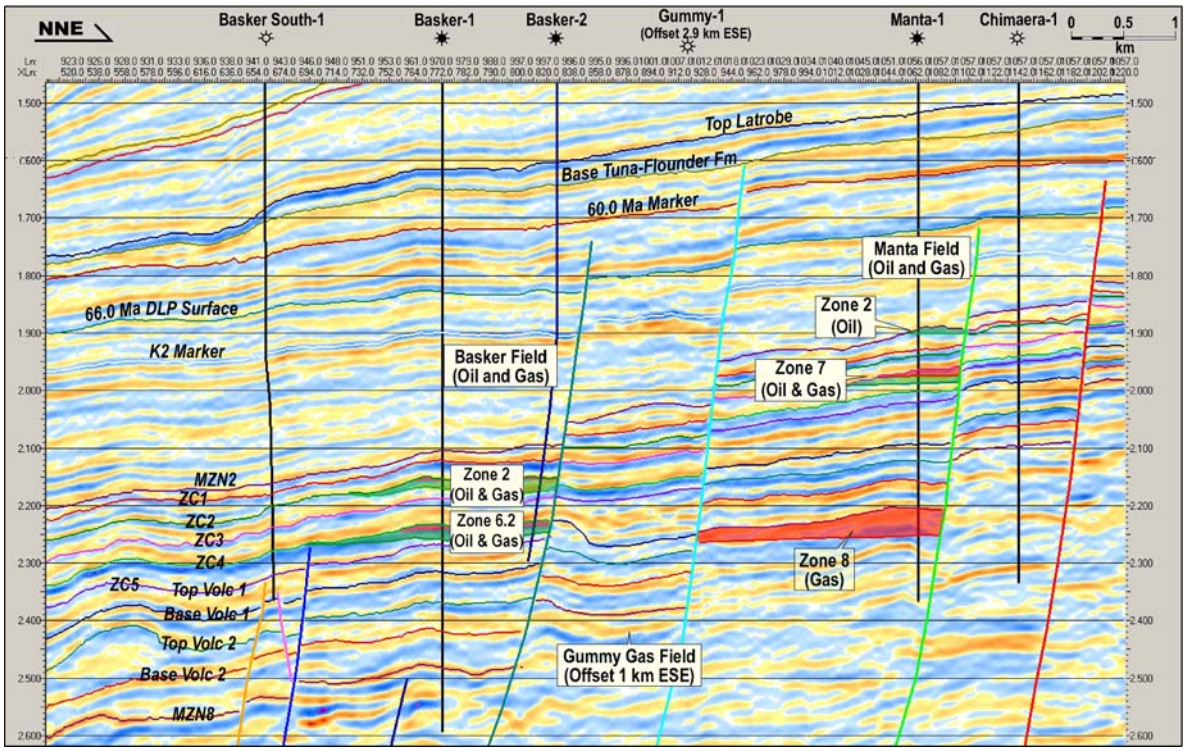

Figure 5.2 Seismic Line through the Basker and Manta Fields, Showing the Reservoir Intervals

The KBM3D seismic is nominally quadrature phase (zero phase with a 90º phase shift) and is displayed with the Australian normal polarity convention (an increase in acoustic impedance displayed as a trough). Hence the marked increase in impedance at the top of Latrobe appears at the zero crossing between a strong trough and peak on the KBM3D seismic (Figure 5.2).

Seismic data quality over the Basker Field is generally good from the surface to about the level of the K2 Marker (Figure 5.2). There is then some degradation in reflector continuity in the section immediately below the K2, probably because of low impedance contrasts at this level and because of interbed multiples sourced from the shallower Latrobe section. Interbed multiples continue to degrade data quality throughout the reservoir section and below. Reflector continuity is generally good across the reservoir interval (the interval between the MZN2 and ZC5 markers) but this continuity appears to be due in part to a contribution from interbed multiples (sourced from the numerous coals which are present within the reservoir section).

Boat-sourced vertical incidence vertical seismic profiles (VIVSPs) were planned for all four of the Basker development wells. The airguns used as the seismic source during a VIVSP are deployed from a workboat so that they can be positioned vertically above the well geophones as they are moved up the hole. VIVSPs were acquired successfully in Basker-2, Basker-3 and Basker-5 but the Basker-4 VIVSP was abandoned after recording at only three levels, because of deteriorating weather conditions. Nevertheless, sufficient data was acquired to facilitate the processing of the Basker-4 VIVSP as a checkshot survey.

Well-to-seismic ties are relatively straightforward for all of the Basker wells, with good agreement between the seismic and the synthetics over most of the logged section. There are however some difficulties with the synthetic ties at the level of the Basker reservoirs, because of interbed multiples. The Basker VIVSPs have demonstrated some multiple contamination for all events through the reservoir section, with the exception of the ZC1 and ZC4 events. Hence only the ZC1 and ZC4 horizons were used for the post-development reservoir mapping.

Within the Intra-Latrobe reservoir interval it is generally difficult to correlate individual sands, shales and coals, both within the Basker Field and between the BMG wells. The gross reservoir correlation was hence derived from the seismic interpretation. Six reservoir seismic markers (MZN2, ZC1, ZC2, ZC3, ZC4 and ZC5) were correlated on the seismic over the reservoir interval, on zero-crossings. Synthetic seismograms were then used to derive the gross well correlations.

Seismic time to depth conversion for the Basker Field is difficult. The combination of the rugose water bottom overlying the Basker Field (Figure 5.3) with rapid shallow lateral velocity variations in the section overlying the Latrobe (due to complex shallow channelling; Enclosure 3) makes accurate depth prediction difficult. Hence, there is an unusually high degree of uncertainty with the depth mapping of the Basker Field reservoirs.

The top of Latrobe was chosen as the key horizon, from which the ZC1 and ZC4 depth conversions were "hung". Six different depth conversion approaches were tested for the top of Latrobe (in order: stacking velocity, PSDM velocity, PSDM velocity slice, layer-cake, velocity function (V0-K) and Dix interval velocity). Two previous depth conversions (by Shell and by Woodside) were also re-visited. A final hand-drawn top Latrobe average velocity map was derived by combining (as top Latrobe average velocity) the output from all of these depth conversions.

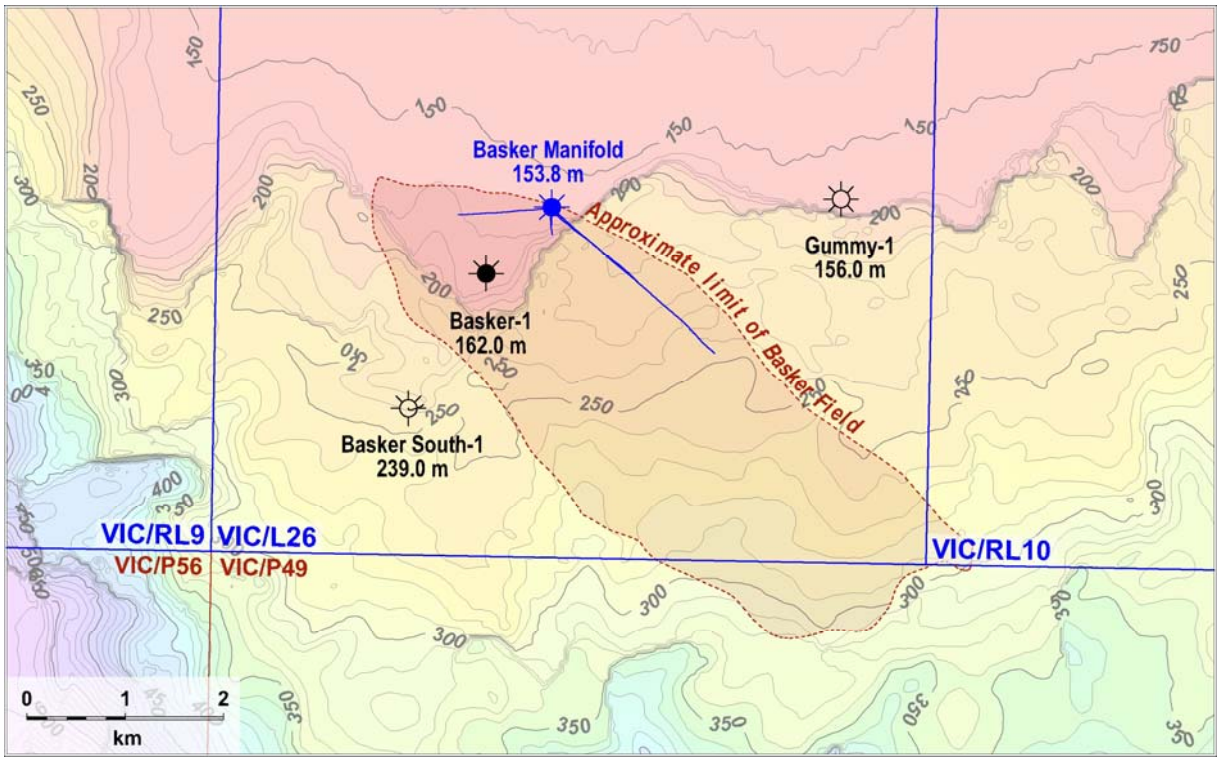

Figure 5.3 Bathymetry Map (Contour Interval 10m), Showing Location of the Basker Field

Average velocity grids for each of the two reservoir mapping horizons (ZC1 and ZC4) were derived from the top of Latrobe average velocity grid, using average velocity difference grids. These difference grids were generated from hand-drawn average velocity difference maps which were based on the well values and the form of maps of the top of Latrobe to ZC1 and ZC4 interval two-way time. Depth conversion for each of the Basker Field reservoirs was then achieved by phantoming from the nearest mapping horizon (ZC1 or ZC4). Reservoir maps for the three key Basker reservoirs are presented as Figures 5.4 to 5.6. In each case it has been mapped at the top of the uppermost sand of the reservoir or its stratigraphic equivalent.

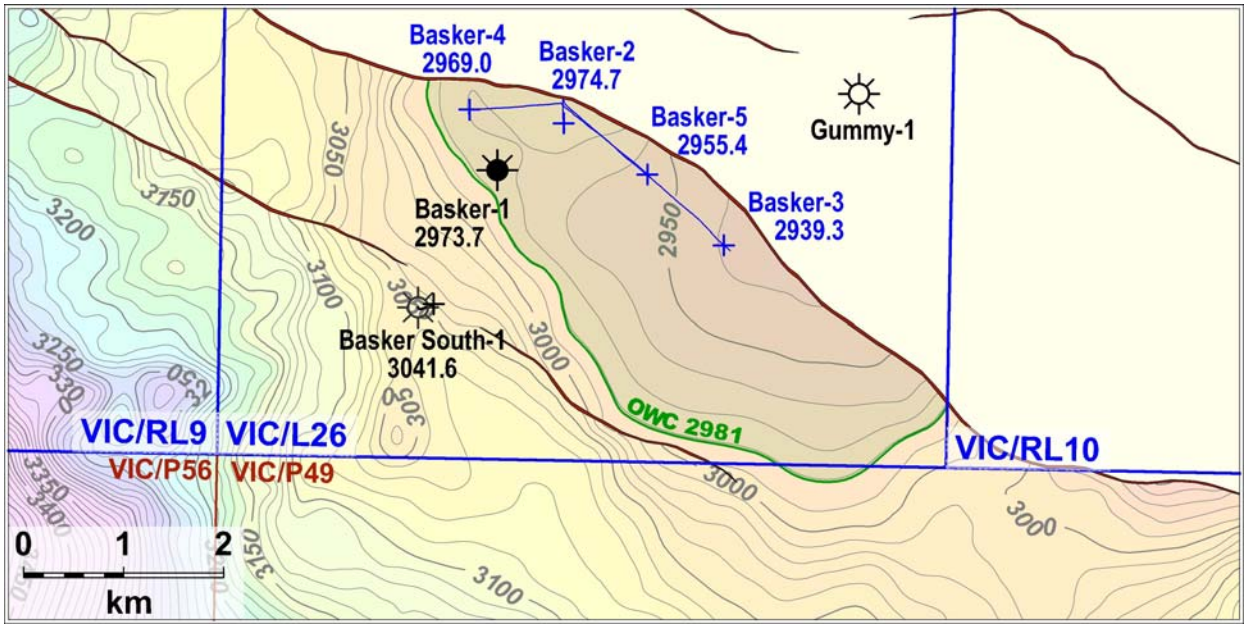

Figure 5.4 Structure Map, Top of Basker Zone 0 Reservoir (Contour Interval 10m)

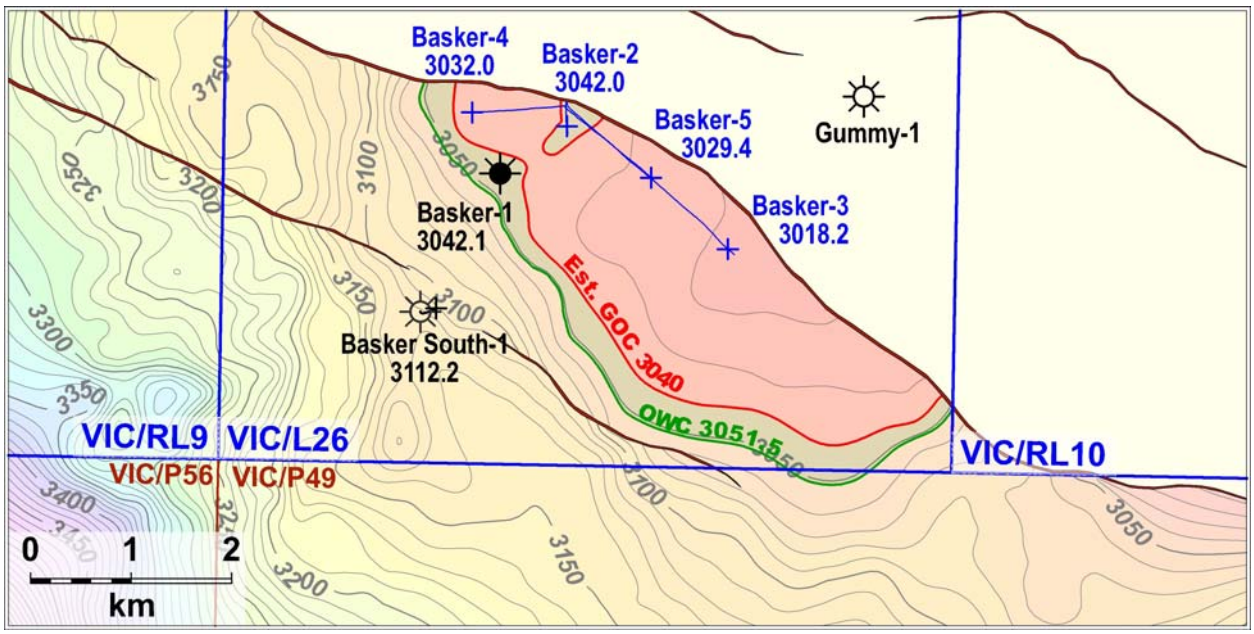

Figure 5.5 Structure Map, Top of Basker Zone 1.2 Reservoir (Contour Interval 10m)

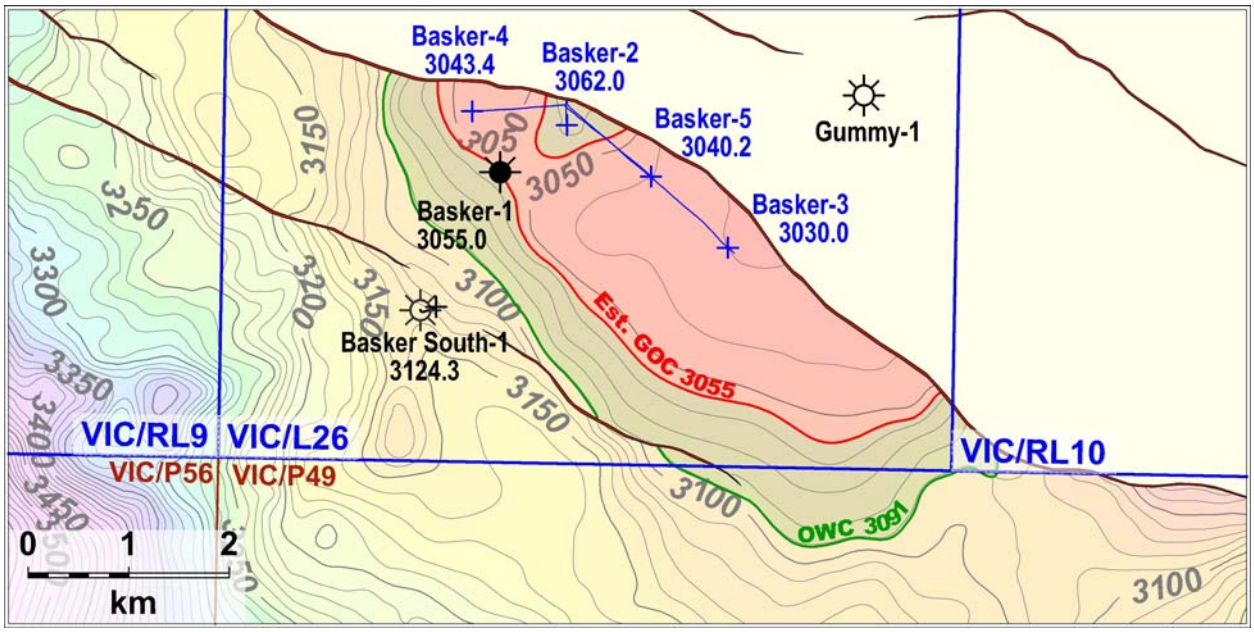

Figure 5.6 Structure Map, Top of Basker Zone 2 Reservoir (Contour Interval 10m)

6. OPEN-HOLE WIRELINE LOG ANALYSIS

Introduction

During drilling, Halliburton Sperry Drilling Services provided LWD tool suite for formation evaluation purposes from 1012-3640mMD. After total depth was reached Schlumberger provided Open-Hole Wireline Logging services with the PEX logging system and data was acquired from 3000-3642mMD (Loggers Depths).

This report presents an evaluation the Schlumberger Open-Hole Wireline Logs from 3000-3642mMD using Crocker Data Processing, Petrolog Complex Lithology Modules.

The results obtained and methods used are summarised in this report. All depths are relative to Schlumberger Gamma Ray Log.

A summary of the results obtained is presented in Table 6.2.

General Information

All depths quoted in this report are m MDKB.

Table 6.1 Open Hole Wireline Log Analysis General Data

Well Name	Basker-5				
Country	Australia				
Company	Anzon Australia Limited				
Location	VIC/RL6				
State	Victoria				
Permanent Datum	MSL				
Elevation of DF (M)	21.5				
Depth to SF (M)	155.5				
Logging Co.	Schlumberger				
Logging Date	28 Mar 2006				
Logs Recorded	FMI-DSI-HRLA-PEX-HNGS MDT-GR MSCT-GR				
Bottom Log Interval (M)		3600.0			
Top Log Interval (M)		3000.0			
Casing shoe (M)		1001.3			
Bit size (inch)		12.25			
Fluid Type		Glydril			
Density g/cc		1.15			
RM (Ohmm) @ TEMP (DegC)		0.097 @21.0			
RMF (Ohmm) @ TEMP (DegC)		0.083 @ 22.0			
RMC (Ohmm) @ TEMP (DegC)		0.131 @ 22.0			
Max Temp (DegC)		101			
Recorded by	S.Kasian/Kyaw Kyaw Aung				

Deviation

The maximum hole deviation at T.D. was 18.89° at 3640.0mMD. Telemetry and directional data from the Sperry Sun LWD run were used as the basis to convert measured depth to true vertical in this interpretation.

Data Acquisition and Quality Control

Although depth offsets occur between LWD curve data and the Schlumberger wireline data, no depth alignments were carried out between the two data sets.

No problems were encountered during Schlumberger wireline operations and quality is acceptable.

The PEX tool was run in high resolution mode; tool string was run eccentered using 1.5" standoff. All curves were recorded in the same run, the caliper log indicates the hole was mostly in-gauge throughout the zones of interest. Digital data received were of acceptable quality, there were no cycle skips observed on the sonic log and no further processing undertaken.

Core Acquisition

An MSCT programme resulted in the recovery of 27 core samples; all samples were submitted to ACS for analysis. The MSCT Test Schedule is presented in Table 6.3, together with the results available for this analysis.

Log Compositing and Editing

The MDT data points (pre-tests and samples) acquired during drilling operations were depth referenced to the Schlumberger wireline GR. All other curves were examined for depth alignment using this reference, no log edits were applied as all log data was sufficiently on depth.

A composite display of input logs is presented together with the results composite plot (Enclosure 4).

Environmental Corrections

Environmental corrections were applied at wellsite.

Logs Used

The primary logs from Suite-1 Run-1 used in the interpretation were GR, RLA3 RLA5, RX08, RH08, HTNP, HDRA, PEF8, SP, DTCO, HTO, HURA, and HFK.

Temperature Gradient

A temperature gradient of 2.49DegC/100m was used in this interpretation.

Hydrocarbon Type Identification

The methodology used to identify hydrocarbon type consisted of a combination of the neutron-density log character, resistivity anomaly, ditch gas readings and hydrocarbon fluorescence shows described in the ditch cuttings.

At Basker-5 the identification of hydrocarbon zones was complex because of relatively low resistivity contrast between the hydrocarbon zones and the water sands due to clay mineral conductivity. Complex mineralogy and detritus e.g. pyrite, within the reservoir units also masked log responses.

An MDT programme was conducted to verify and validate the hydrocarbon type interpreted from the logs. The MDT programme consisted of pretests, fluid analysis using Schlumberger's Down-Hole Fluid Analyser (DFA). Fluid sample recoveries were not attempted in this well.

Using this methodology, several oil and gas zones were identified which are presented in Table 6.2, together with the results of the interpretation. A graphical example is presented in Figure 6.1.

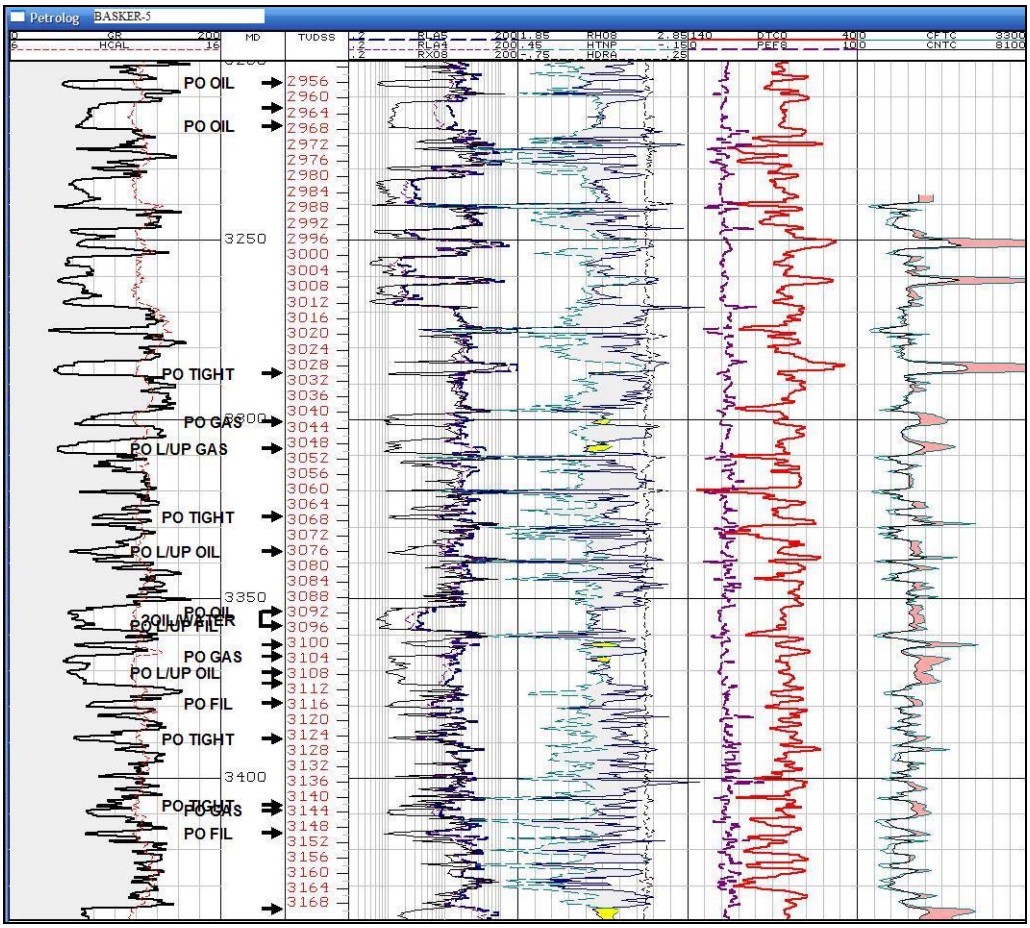

Figure 6.1 Basker-5 Hydrocarbon Type, example of methodology

Petrolog Model Selection

The deterministic Complex Lithology Model (CPX) was selected for the interpretation to compute Vsand, Vclay, Vdolomite, Vcoal, Vvolcanic, Porosity (PHIT and PHIE) and Water Saturation (SWT, SWE).

Complex Lithology

The Complex Lithology Model (CPX) was constructed to use a combination of D-N to compute Vsand, Vclay, Vdolomite, Vcoal, and Vvolcanic.

A colour composite of the Spectral GR displays the relative abundance of Thorium (Th), Uranium (U), Potassium (K), refer Figure 6.2, shows the mineral complexity throughout the section. Although the Th abundance is relatively constant, the K abundance is not uniform indicating changes in clay mineralogy. The high U concentrations indicate increases in organic matter.

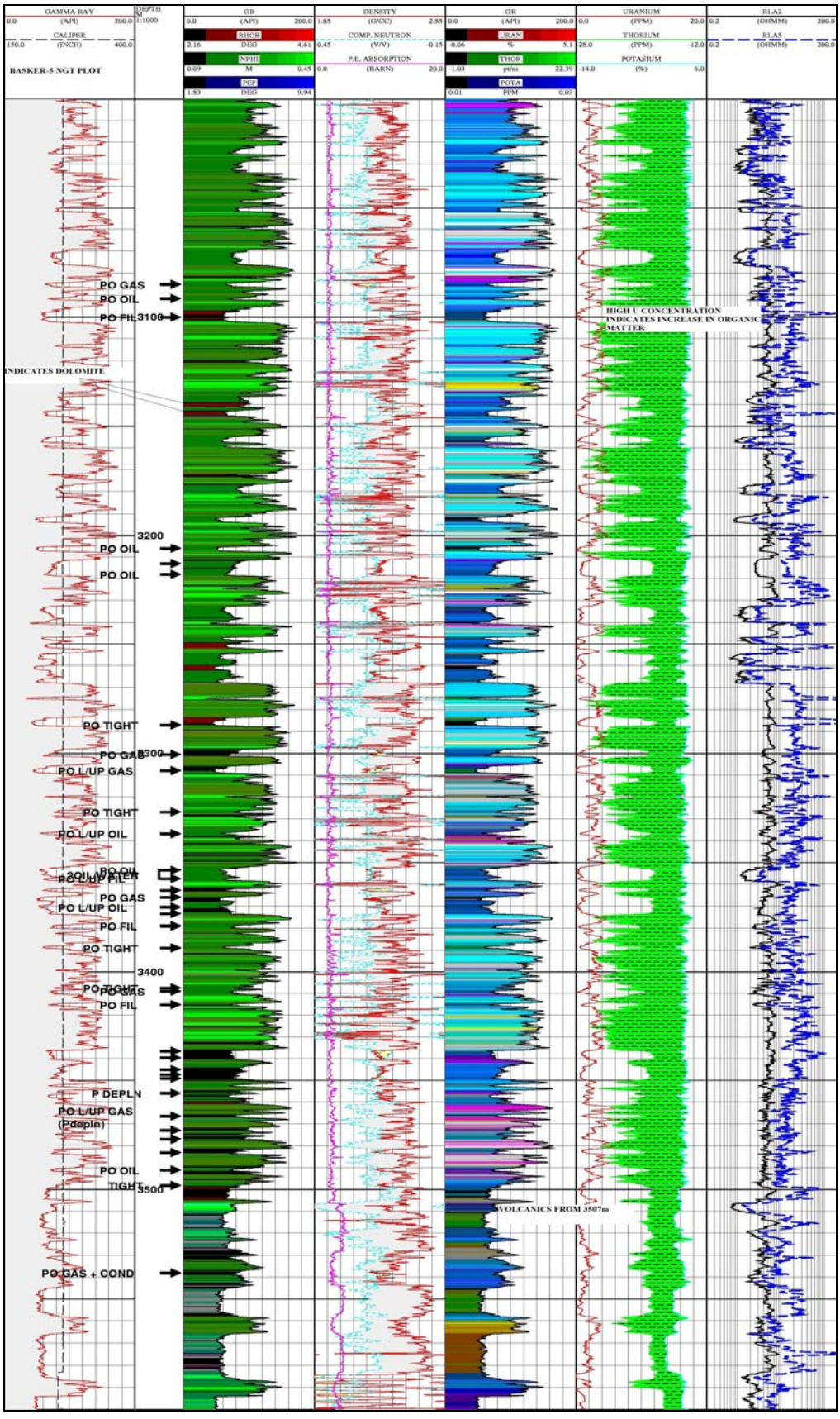

Figure 6.2 Basker-5 NGT Composite Plot

Porosity Determination

Total porosity (PHIT) was calculated using input logs D-N.
Effective porosity (PHIE) was calculated after Vcl determination.
PHIE = PHIT (1-Vcl)

A good match has been achieved between core porosity and log porosity (Figure 6.3).

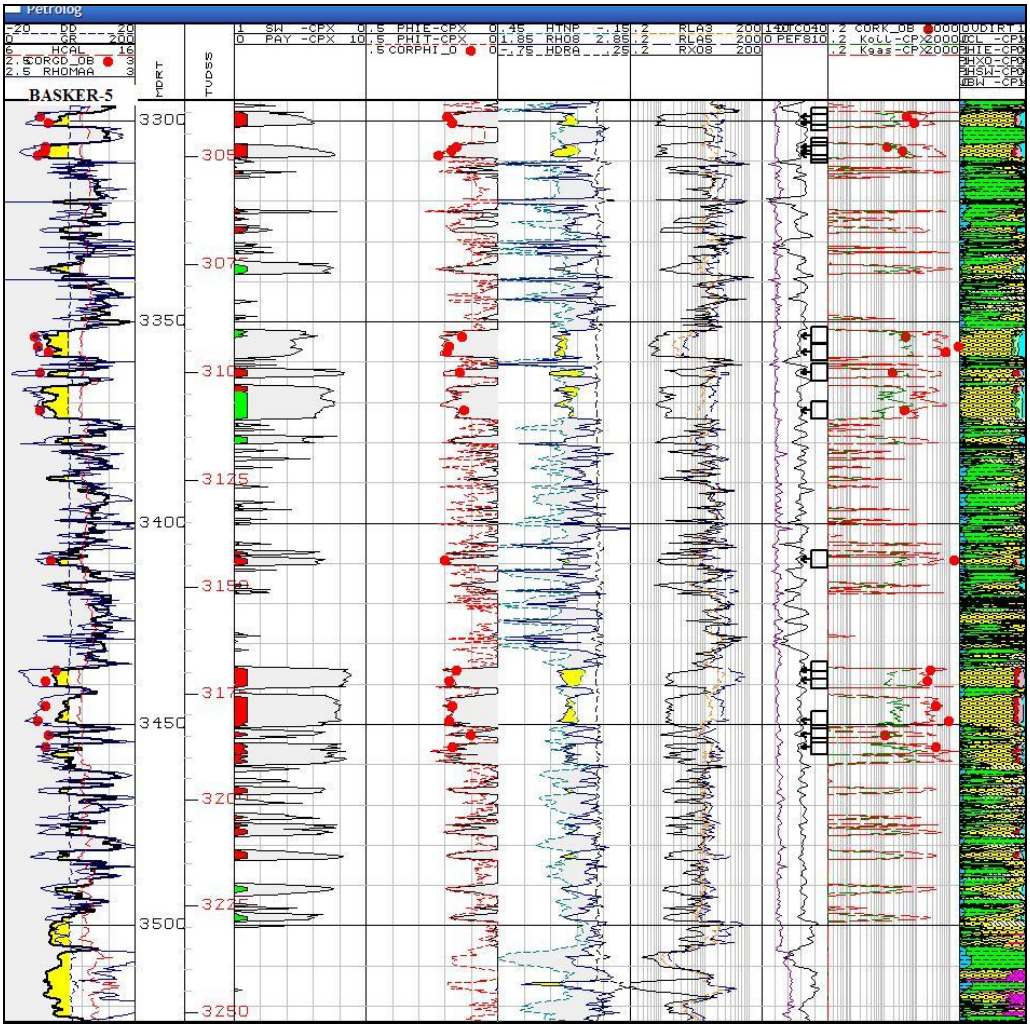

Figure 6.3 Basker-5 Core-Log Comparison

RW Determination

In conventional log analysis, the calculation of hydrocarbon saturation assumes that the formation water salinity in the hydrocarbon zone is the same as that of the underlying water sands. The PHIT-RT crossplots across the water sands in Basker-5 indicate a water salinity of 15,000ppm NaCl equivalent i.e. Figure 6.4. It is considered that this value is inconsistent with salinity values for a near-shore fluvial depositional environment and use of this value would result in pessimistic hydrocarbon saturations.

However, it has been recognised in some regions within the offshore Gippsland Basin a period of meteoric water influx displaced the aquifer without flushing the emplaced hydrocarbons (Kuttan, Kulla and Neumann 1986), resulting in relatively fresh water aquifer underlying hydrocarbon reservoir systems.

As a consequence the assumption that the underlying aquifer is the same salinity as the associated hydrocarbon zones is not always correct. For the purpose of this interpretation a formation water salinity equivalent to 30,000ppm NaCl equivalent has been used to calculate hydrocarbon saturations (Figure 6.5 PHIT-RT crossplot) and 15,000ppm NaCl equivalent for the water zones. Analyses of water samples collected from the test separator during the extended production test support the use of these values.

To reduce the uncertainty of water salinity associated with the hydrocarbon zones, several MSCT samples were submitted for SCAL analysis, in particular capillary pressure measurements. At the time of writing this report the results were not available to verify input parameters and validate the computed hydrocarbon saturations.

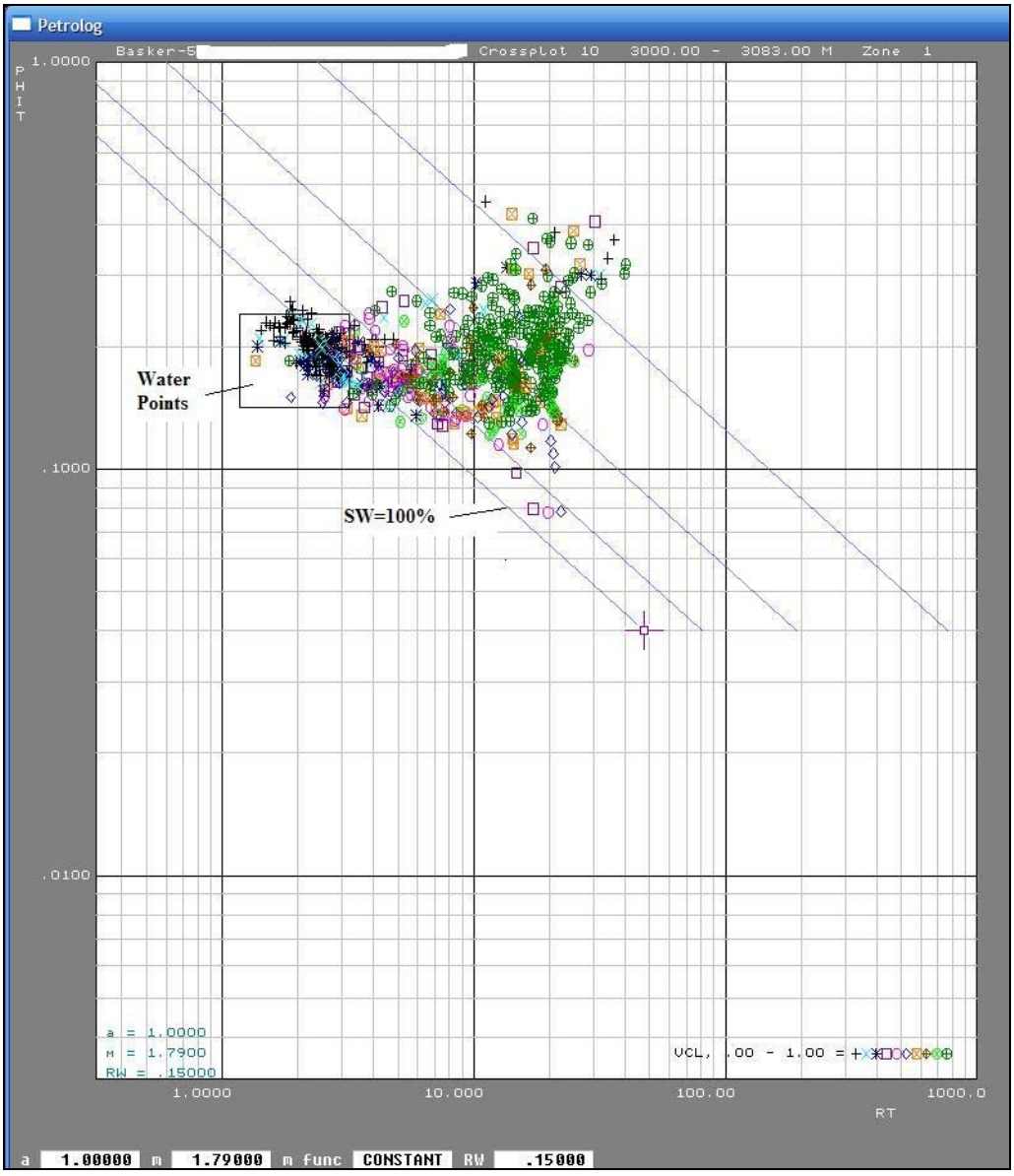

Figure 6.4 Basker-5 PHIT-RT crossplot water sand interval 3000-3083mMD

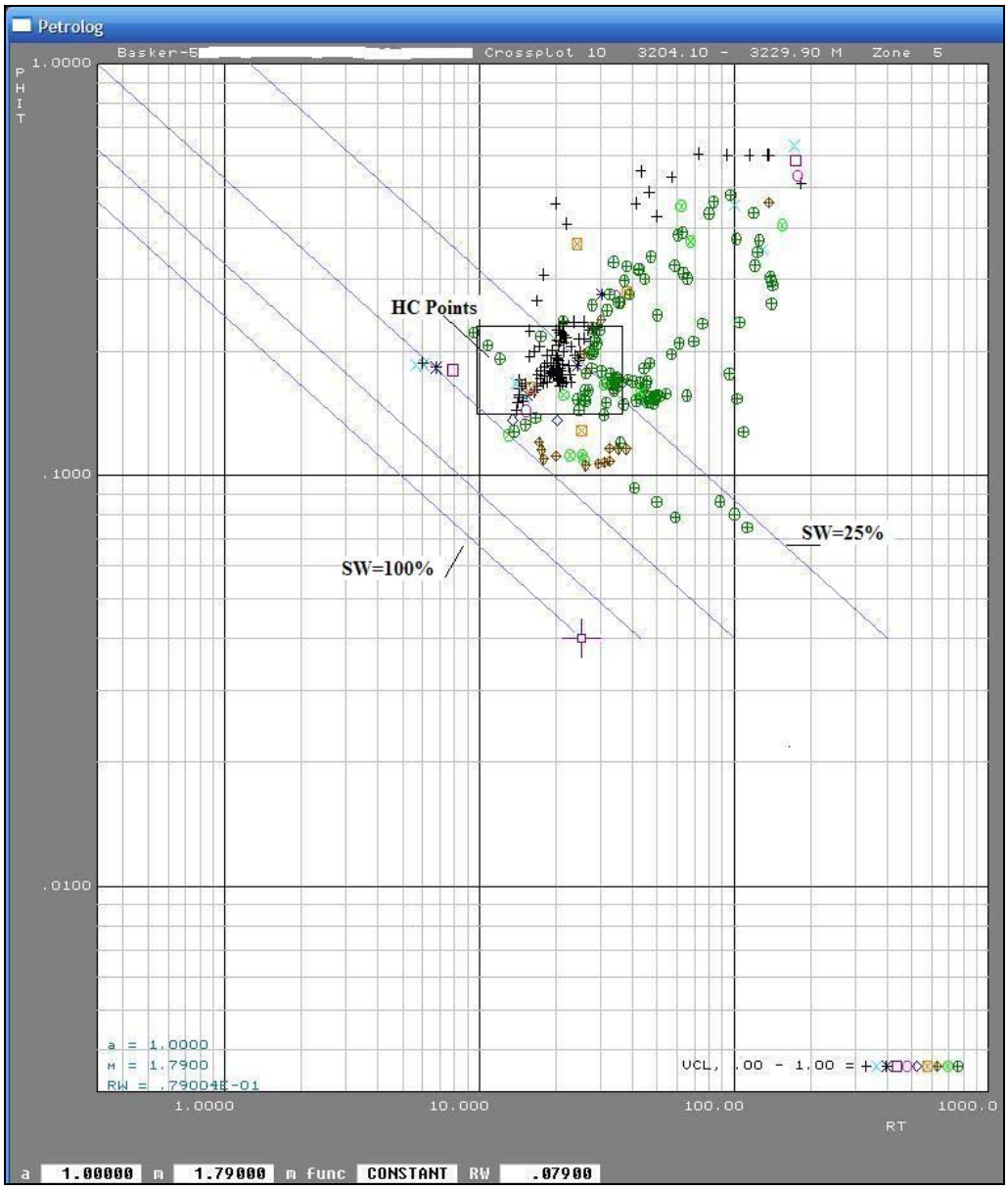

Figure 6.5 Basker-5 PHIT-RT crossplot Hydrocarbon Interval 3204-3230mMD

Determination of Sw, a, m, n

For this interpretation the Simandoux equation was used to compute water saturation (Sw) and is defined as follows:

SWe = (a*Rw/(2.0*PHIE**m))*(SQRT((VCL/RCL)**2.0
+ 4.0*PHIE**m/(a*Rw*RT))-VCL/RCL)

In this interpretation a=1, m= 1.79 and n=1.83

The values a=1, m= 1.79 and n=1.83 were obtained from the Special Core Analysis Report Basker-1. A study of the Capillary Pressure measurements from Basker-1 conventional core was undertaken (refer Anzon Australia Ltd Report September 2005, Determination of Irreducible Water Saturation using the Basker-1 Capillary Pressure Curves by Wong Shau Yee) where an

average capillary pressure curve was converted to a height versus water saturation curve and used to calculate an average water saturation in Basker-1 Zone 2 (PcSw=24%).

A good match was achieved between the Log derived Sw in Basker-1 across zone 2 and the calculated PcSw validated the use of these parameters in Basker-2. Preliminary SCAL results for the Basker-5 MSCT samples also support the use of these values. In Basker-5 the average m=1.77 and preliminary estimates for average n=1.83. The data for Shaly Sand equivalent m* and n* are not yet available.

Results

Table 6.1 lists the results of the interpretation. Based on cut-off parameters PHIE>=10%; Vclay<50% and SWE <=75% a total 24.2m net oil pay and 26.6m net gas pay was intersected by the well.

The PHIE cut-off for net reservoir and net pay determination was established using the core porosity-permeability relationship from Basker-5 MSCT SCAL. The cross-plot indicates that where core porosity @ overburden >10%, permeability (Kinf) @ overburden >1md (Figure 6.6). The SWE cut-off (<=75%) for net pay determination is based on basin knowledge.

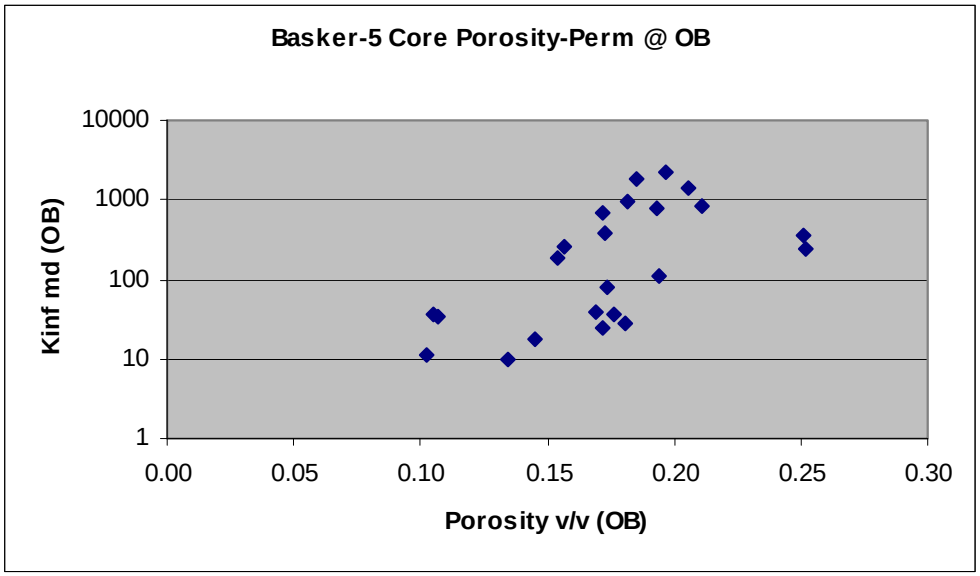

Figure 6.6 Basker-5 Core Porosity-Permeability Crossplot

MSCT Sample Test Schedule and Preliminary results Table 6.3

The analysis parameters are presented in Table 6.4

Schlumberger PEX Log Suite-1 Run-1 information Table 6.5

Log Interpretation Plot 1:200scale presented in Enclosure-4

Table 6.2 Basker-5 Reservoir Summation

top	base	top	base	top	base	reservoir					pay				
md	md	tvdkb	tvdkb	tvdss	tvdss	gross	net res	vcl	phie	swe	net pay	vcl	phie	swe	comments
						tvt	m tvt	%	%	%	mtvt	%	%	%	
3018.0	3018.8	2808.2	2808.9	2786.7	2787.4	0.7	0.7	15.4	16.7	100.0					Water Saturated
3022.8	3025.7	2812.4	2815.0	2790.9	2793.5	2.6	2.6	6.4	17.7	100.0					Water Saturated
3028.6	3032.6	2817.6	2821.2	2796.1	2799.7	3.6	3.6	9.1	17.8	100.0					Water Saturated
3033.0	3034.1	2821.5	2822.5	2800.0	2801.0	1.0	1.0	5.4	20.7	100.0					Water Saturated
3046.4	3048.3	2833.5	2835.2	2812.0	2813.7	1.7	1.3	9.7	19.9	100.0					Water Saturated
3049.5	3052.0	2836.2	2838.5	2814.7	2817.0	2.2	2.2	8.3	18.5	100.0					Water Saturated
3059.4	3060.8	2845.1	2846.3	2823.6	2824.8	1.3	0.8	15.1	17.8	100.0					Water Saturated
3069.3	3076.5	2854.0	2860.4	2832.5	2838.9	6.5	6.5	6.0	17.2	100.0					Water Saturated
3084.2	3087.3	2867.3	2870.1	2845.8	2848.6	2.8	2.0	2.49	21.12	32.91	2.0	2.49	21.12	32.91	MDT PO GAS
3090.8	3092.3	2873.3	2874.7	2851.8	2853.2	1.4	1.4	8.0	20.9	52.6	1.4	8.0	20.9	52.6	MDT PO OIL
3095.5	3096.0	2877.5	2877.9	2856.0	2856.4	0.5	0.5	19.9	14.1	100.0					Water Saturated
3096.6	3097.2	2878.5	2879.0	2857.0	2857.5	0.5	0.5	7.2	18.7	100.0					Water Saturated
3099.3	3100.5	2880.9	2882.0	2859.4	2860.5	1.1	1.1	1.8	13.4	100.0					MDT PO WATER/FILTRATE
3113.0	3114.1	2893.3	2894.3	2871.8	2872.8	1.0	1.0	12.3	16.8	100.0					Water Saturated
3126.8	3127.2	2905.8	2906.1	2884.3	2884.6	0.4	0.4	25.3	10.8	100.0					Water Saturated
3134.4	3136.1	2912.6	2914.2	2891.1	2892.7	1.5	1.1	5.5	18.7	100.0					Water Saturated
3136.2	3138.3	2914.3	2916.2	2892.8	2894.7	1.9	1.9	6.0	16.0	100.0					Water Saturated
3138.5	3139.3	2916.3	2917.1	2894.8	2895.6	0.7	0.7	8.3	13.2	100.0					Water Saturated
3141.1	3141.7	2918.7	2919.2	2897.2	2897.7	0.5	0.5	0.1	16.7	100.0					Water Saturated
3142.3	3143.3	2919.8	2920.7	2898.3	2899.2	0.9	0.9	12.1	13.1	100.0					Water Saturated
3147.4	3148.4	2924.4	2925.3	2902.9	2903.8	0.9	0.9	21.4	13.2	100.0					Water Saturated
3155.0	3155.6	2931.3	2931.8	2909.8	2910.3	0.5	0.5	20.5	14.1	100.0					Water Saturated
3155.8	3158.2	2932.0	2934.2	2910.5	2912.7	2.2	2.1	13.0	19.6	100.0					Water Saturated
3158.9	3159.9	2934.8	2935.7	2913.3	2914.2	0.9	0.9	14.1	19.6	100.0					Water Saturated
3177.0	3177.2	2951.2	2951.4	2929.7	2929.9	0.2	0.2	11.1	11.3	100.0					Water Saturated
3177.3	3178.7	2951.5	2952.8	2930.0	2931.3	1.3	1.3	3.7	18.9	100.0					Water Saturated
3179.3	3180.9	2953.3	2954.8	2931.8	2933.3	1.5	1.5	7.7	16.0	100.0					Water Saturated
3191.4	3194.1	2964.3	2966.8	2942.8	2945.3	2.5	2.5	0.9	22.7	100.0					Water Saturated
3196.4	3197.0	2968.9	2969.4	2947.4	2947.9	0.5	0.6	9.9	16.3	100.0					Water Saturated
3205.1	3207.6	2976.8	2979.1	2955.3	2957.6	2.3	2.1	3.8	22.2	18.5	2.1	3.8	22.2	18.5	MDT PO OIL
3211.3	3218.6	2982.4	2989.1	2960.9	2967.6	6.6	6.6	0.6	17.8	27.4	6.6	0.6	17.8	27.4	MDT PO OIL
3229.5	3230.3	2999.0	2999.7	2977.5	2978.2	0.7	0.7	16.1	15.0	100.0					Water Saturated
3232.6	3239.4	3001.8	3008.0	2980.3	2986.5	6.2	6.2	4.3	17.8	100.0					Water Saturated
3242.4	3242.7	3010.7	3011.0	2989.2	2989.5	0.3	0.3	32.7	21.9	100.0					Water Saturated
3247.0	3248.7	3014.9	3016.4	2993.4	2994.9	1.6	1.6	5.0	17.4	100.0					Water Saturated
3248.8	3249.4	3016.5	3017.1	2995.0	2995.6	0.5	0.6	10.6	13.7	100.0					Water Saturated
3254.8	3259.9	3022.0	3026.6	3000.5	3005.1	4.6	4.6	4.7	18.4	100.0					Water Saturated
3262.5	3265.6	3029.0	3031.8	3007.5	3010.3	2.8	2.8	2.3	19.8	100.0					Water Saturated
3266.0	3267.9	3032.2	3033.9	3010.7	3012.4	1.7	1.7	2.3	21.5	100.0					Water Saturated
3286.6	3287.6	3051.0	3051.9	3029.5	3030.4	0.9	0.9	1.4	18.5	49.7					MDT PO GAS; 568psi P DEPLn
3298.2	3301.4	3061.7	3064.7	3040.2	3043.2	3.0	3.0	0.3	17.3	49.7	3.0	0.2	17.4	48.7	MDT PO GAS
3305.8	3309.1	3068.7	3071.9	3047.2	3050.4	3.2	3.0	1.2	19.2	39.9	3.0	0.1	19.7	36.6	MDT PO GAS
3311.5	3311.8	3074.0	3074.3	3052.5	3052.8	0.3	0.3	21.6	14.5	100.0					Water Saturated
3312.5	3312.9	3074.9	3075.3	3053.4	3053.8	0.4	0.4	12.0	20.3	100.0					Water Saturated
3324.1	3324.7	3085.7	3086.2	3064.2	3064.7	0.6	0.6	17.4	11.4	100.0					Water Saturated
3326.5	3327.7	3087.9	3089.0	3066.4	3067.5	1.1	1.1	7.4	16.2	77.5					MDT PO Tight
3335.9	3337.8	3096.6	3098.1	3075.1	3076.6	1.5	1.5	8.6	17.7	29.6	1.5	8.6	17.7	29.6	MDT PO OIL
3352.2	3353.5	3112.0	3113.5	3090.5	3092.0	1.5	0.9	3.2	19.5	42.0	0.9	3.2	19.5	42.0	MDT PO OIL
3353.5	3358.6	3112.4	3117.0	3090.9	3095.5	4.6	4.6	0.6	20.5	52.3	4.6	0.6	20.5	53.0	MDT PO FILTRATE
3361.7	3363.5	3120.7	3122.4	3099.2	3100.9	1.7	1.7	1.4	19.3	24.6	1.7	1.4	19.3	24.6	Gas
3365.8	3367.5	3124.5	3126.0	3103.0	3104.5	1.5	1.5	1.7	18.2	30.4	1.5	1.7	18.2	30.4	MDT PO GAS GOC @ 3367.5mMD
3367.5	3374.0	3126.1	3132.2	3104.6	3110.7	6.1	5.5	1.8	16.6	32.5	5.5	1.8	16.6	32.5	MDT PO OIL
3378.4	3381.7	3136.3	3139.4	3114.8	3117.9	3.1	1.5	8.9	16.5	45.4					MDT PO FILTRATE, MECH PROBLEMS WITH PROBE
3382.1	3382.4	3139.8	3140.0	3118.3	3118.5	0.3	0.3	25.4	11.2	100.0					Water Saturated
3388.9	3389.1	3146.1	3146.3	3124.6	3124.8	0.2	0.2	18.3	13.1	100.0					MDT PO TIGHT
3396.4	3396.6	3153.2	3153.4	3131.7	3131.9	0.2	0.2	36.2	14.3	100.0					Water Saturated
3408.5	3410.4	3164.5	3166.3	3143.0	3144.8	1.8	1.8	1.5	19.4	34.0	1.8	1.5	19.4	34.0	MDT PO GAS
3414.8	3415.1	3170.4	3170.7	3148.9	3149.2	0.3	0.3	19.7	11.5	100.0					MDT PO WATER/FILTRATE
3415.2	3415.7	3170.8	3171.3	3149.3	3149.8	0.5	0.5	5.0	16.1	100.0					Water Saturated
3436.0	3440.7	3190.4	3194.9	3168.9	3173.4	4.4	4.4	0.5	17.7	15.3	4.4	0.5	17.7	15.3	GAS
3443.2	3449.7	3197.3	3203.4	3175.8	3181.9	6.2	6.2	0.8	18.1	23.2	6.2	0.8	18.1	23.2	GAS
3476.0	3477.3	3228.3	3229.6	3206.8	3208.1	1.2	1.2	5.2	16.8	35.2	1.2	5.2	16.8	35.2	GAS
3481.5	3483.4	3233.5	3235.3	3212.0	3213.8	1.8	1.8	1.7	17.1	28.5	1.8	1.7	17.1	28.5	GAS
3490.2	3491.6	3241.9	3243.3	3220.4	3221.8	1.4	1.4	2.2	18.2	29.2	1.4	2.2	18.2	29.2	MDT PO OIL
3497.4	3498.7	3248.6	3250.1	3227.1	3228.6	1.5	0.3	8.2	15.8	43.0	0.3	8.2	15.8	43.0	MDT PO TIGHT
INTRA VOLCANICS															
3537.0	3538.6	3286.2	3287.7	3264.7	3266.2	1.5	1.5	1.9	16.8	41.6	1.5	1.9	16.8	41.6	MDT PO GAS + CONDENSATE
3538.9	3540.4	3288.0	3289.4	3266.5	3267.9	1.4	1.4	11.4	15.7	58.6	1.0	11.4	15.7	58.6	
3540.5	3542.2	3289.5	3291.1	3268.0	3269.6	1.6	1.6	12.7	16.6	56.3	1.2	12.7	16.6	56.3	

Anzon Australia LIMITED

Table 6.3 MSCT TEST Schedule (Part 1)

TEST SCHEDULE

Client: Anzon Australia Ltd
Well/Project: Basker-5
ACS File No: 0496-08

F = failed
C = cancelled

		Test Sequence																										
					Pre-Study																				Off-Cuts			
Sample	Depth	Sample Trimming	White Light Photography	UV Photography	Cold Solcent Soxhlet Cleaning	Critical Point Dry	Ambient Base Parameters	Warm Solvent Soxhlet Cleaning	Humidity Oven Dry	Ambient Base Parameters	Dean-Stark Fluid Extraction	Oven Dry	Warm Solvent Soxhlet Cleaning	Humidity Oven Dry	Ambient Base Parameters	Overburden Base Parameters	Sample Saturation with 8000 ppm	Sample Saturation with 35000 ppm	Formation Factor	Oil-Brine PcRI Drainage @ OB	Ageing	Brine-Oil Pc Imbibition @ OB	Single Point Pc to Swir	Basic Waterflood	Thin Section	Quemscan	XRD Qualitative Bulk & Clay	Cation Exchenge Capacity
1	3455.5	X	X	X									X	X	X	X		X	X	X	X	X	X	X	X	X	X	X
2	3452.5	X	X	X									X	X	X	X		X	X	X	X	X	X	X				X
3	3449.0	X	X	X							X	X	X	X	X	X		X										
4	3439.0	X	X	X									X	X	X	X		X	X	X	X	X	X	X	X	X	X	X
5	3436.5	X	X	X							X	X	X	X	X	X		X										
6	3409.0	X	X	X							X	X	X	X	X	X		X										
7	3372.0	X	X	X									X	X	X	X		X							X	X	X	
8	3362.5	X	X	X	X	X	X	X	X	X						X		X										
9	3357.5	X	X	X							X	X	X	X	X	X		X										
10	3356.0	X	X	X							X	X	X	X	X	X		X										
11	3353.5	X	X	X									X	X	X	X		X							X	X	X	
12	3308.5	X	X	X							X	X	X	X	X	X		X										
13	3307.5	X	X	X									X	X	X	X		X	X	X	X	X	X	X		X	X	X
14	3306.5	X	X	X									X	X	X	X		X	X	X	X	X	X	X				X
15	3300.5	X	X	X	n-pent extractn added in 200406						X		X	X	X	X		X	X	X	X	X	X	X				X
16	3299.0	X	X	X									X	X	X	X		X							X	X	X	
17	3287.0	X	X	X							X	X	X	X	X	X		X	X									X
18	3267.0	X	X	X									X	X	X	X	X		X						X	X	X	X
19	3251.0	X	X	X									X	X	X	X	X								X	X		
20	3238.0	X	X	X									X	X	X	X	X		X						X	X	X	X
21	3218.0	X	X	X							X	X	X	X	X	X		X										
22	3212.0	X	X	X	X	X	X	X	X	X						X		X										
23	3206.0	X	X	X							X	X	X	X	X	X		X										
24	3192.0	X	X	X									X	X	X	X	X											
25	3097.0	X	X	X									X	X	X	X	X		X									X
26	3085.0	X	X	X									X	X	X	X		X	X									X
	Total	26	26	26	2	2	2	2	2	2	10	9	24	24	24	26	5	21	11	6	6	6	6	6	8	9	8	11

Table 6.3 MSCT TEST Schedule (Part 2)

PRELIMINARY TEST RESULTS

BASE PARAMETERS 26-06-2006

Client : Anzon Australia Ltd

Well : Basker-5

Sample			Ambient		Grain	Overburden 4000psi			Overburden 4250psi			Overburden 4400psi	
Number		Depth	Porosity	Permeability	Density	Porosity	Permeability		Porosity	Permeability		Porosity	Permeability
			(percent)	(milliDarcy's)	(g/cm3)	(percent)	(milliDarcy's)		(percent)	(milliDarcy's)		(percent)	(milliDarcy's)
1		3455.50	20.5	424	2.66							17.3	379
2		3452.50	16.2	13.3	2.67							13.5	11.1
3		3449.00	18.7	921	2.63							17.2	677
4		3439.00	18.5	211	2.66							15.4	183
5		3436.50	17.9	360	2.70							15.7	259
6		3409.00	20.1	1380	2.68							18.2	973
7		3372.00	13.0	41.2	2.64							10.7	34.1
8		3362.50	16.8	26.9	2.64							14.5	18.1
9		3357.50	20.9	957	2.67							19.3	767
10		3356.00	20.4	2160	2.63							18.5	1780
11		3353.50	13.6	45.9	2.62							10.5	36.2
12		3308.50	22.5	2090	2.63							20.6	1380
13		3307.50	20.1	44.2	2.66							17.6	37.3
14		3306.50	15.8	12.4	2.66							13.4	9.9
15		3300.50	19.8	94.8	2.67							17.4	81.9
16		3299.00	19.3	48.4	2.64							16.9	38.2
17		3287.00	3.3	0.04	2.72							2.6	< 0.01
18		3267.00	28.5	287	2.65				25.2	244			
19		3251.00	7.0	2.71	2.69				5.5	0.04			
20		3238.00	19.4	56.4	2.63				17.2	24.9			
21		3218.00	22.6	3150	2.66				19.7	2230			
22		3212.00	19.4	35.8	2.64				18.1	28.0			
23		3206.00	20.7	134	2.70				19.4	110			
24		3192.00	22.1	922	2.64	21.1	845						
25		3097.00	16.6	1.17	2.69	13.3	0.61						
26		3085.00	27.8	398	2.66	25.1	363						

FORMATION RESISTIVITY FACTOR 16-06-06

Client	Anzon Australia Ltd		**Rw of 35000 ppm Brine**	0.17 at 25°C	
Well	Basker-5		**Rw of 8000 ppm Brine**	0.69 at 25°C	
			Overburden		
				Average m	**1.77**

		Permeability		Brine	Formation	Cementation
Sample	Depth	to Air	Porosity	Salinity	Factor	Exponent
Number	(metres)	(milliDarcy's)	(percent)	(ppm)	FF	m
1	3455.50	379	17.3	35000	24.5	1.82
2	3452.50	11.1	13.5	35000	29.6	1.69
4	3439.00	183	15.4	35000	32.8	1.87
13	3307.50	37.3	17.6	35000	23.9	1.83
14	3306.50	9.9	13.4	35000	33.3	1.74
15	3300.50	81.9	17.4	35000	21.8	1.76
17	3287.00	< 0.01	2.6	35000	163	1.40
18	3267.00	244	25.2	8000	10.8	1.73
20	3238.00	24.9	17.2	8000	28.3	1.90
25	3097.00	0.61	13.3	8000	38.5	1.81

Table 6.4 Analysis Parameters (Zones of Interest)

Basker-5		
Input Parameter		**Value**
Analysis Interval (mMD)		3000-3650mMD
Bit Size (inches)		12.25
Method	SW calculation	Simandoux
	Vclay calculation	N-D
	Porosity calculation	N-D
Formation Water Salinity	Rw HC Zone (salinity ppm NaCl equivalent)	30000*
	Rw water Zone (salinity ppm NaCl equivalent)	15000**
Electrical Properties	a	1
	m	1.79***
	n	1.83***
Fluid Properties	RHOH (g/cc)	0.2
	RHOF (g/cc)	1.06
	RHOMA (g/cc)	2.65
Clay Parameters	Rclay (ohm-m)	2
	PHIN clay (v/v)	0.27
	RHOB clay (g/cc)	2.4
	RHOB Dry Clay (g/cc)	2.77
	DT clay (usec/ft)	100
Special Minerals	RHOB dolomite (g/cc)	2.6
	RHOB volcanic (g/cc)	2.92
	RHOB coal (g/cc)	2
Reservoir Summation Cut-offs	VClay (v/v)	<=0.5
	PHIE (v/v)	>=0.1
	SWE (v/v)	N/A****
Temperature	Max Recorded Temp Deg C	84 @ 3217m
* Rw HC Zone	Initially estimated, subsequent water production from Basker Field HC producing zones indicating during extended production test, Fm water salinity measurements range from 30-35Kppm.	
**Rw Water Zone	crossplots (refer text Figure 5)	
*** m & n	Basker-1 SCAL, Basker-5 SCAL	
****RESERVOIR SUMMATION CUT-OFF SWE N/A	Basker-1, Basker-5 Por-Perm Relationship CorePHI>10% has core Kinf >1MD.	

Table 6.5 Schlumberger PEX Log Suite-1 Run1 Main Pass

VERS.	2.0	CWLS Log ASCII Standard – VERSION 2.0
WRAP.	NO	One Line per depth step
PROD.	Schlumberger	LAS Producer
PROG.	DLIS to ASCII 14C0-302	LAS Program name and version
CREA.	2006/03/28 12:54	LAS Creation date {YYYY/MM/DD hh:mm}
DLIS_CREA.	2006-Mar-28 12:45	DLIS Creation date and time {YYYY-MMM-DD hh:mm}
SOURCE.	FMI_DSI_HRLA_TLD_010PUP.DLIS	DLIS File Name
FILE-ID.	FMI_DSI_HRLA_TLD_010PUP	File Identification Number

~WELL INFORMATION

MNEM.UNIT	DATA	DESCRIPTION
STRT M	3650.7420	START DEPTH
STOP .M	2999.5368	STOP DEPTH
STEP M	-0.1524	STEP
NULL .	-999.25	NULL VALUE
COMP	Anzon	COMPANY
WELL .	Basker 5	WELL
FLD	Basker	FIELD
LOC.	VIC/L26	LOCATION
CNTY	Ocean Patriot	COUNTY
STAT .	Victoria	STATE
CTRY	Australia	COUNTRY
API		API NUMBER
UWI		UNIQUE WELL ID
DATE .	28-Mar-2006	LOG DATE {DD-MMM-YYYY}
SRVC .	Schlumberger	SERVICE COMPANY
LATI .DEG	38 17' 59.33" S	LATITUDE
LONG .DEG	148 42' 23.80" E	LONGITUDE
GDAT .		GeoDetic Datum

~PARAMETER INFORMATION

MNEM.UNIT	**VALUE**	**DESCRIPTION**
RUN	1	RUN NUMBER
PDAT .	Mean Sea Lever	Permanent Datum
EPD .M	0.000000	Elevation of Permanent Datum above Mean Sea Level
EPD .M	0.000000	Elevation of tool zero above Mean Sea Level
LMF.	Drill Floor:	Logging Measured From (Name of Logging Elevation Reference)
APD .M	21.500000 :	Elevation of Depth Reference (LMF) above Permanent Datum

~CURVE INFORMATION

#MNEM.UNIT API CODE	DESCRIPTION
DEPT .M	:DEPTH (BOREHOLE) {F10.4}
SP .MV	:SP Shifted {F13.4}
RM_HRLT.OHMM	:HRLT Mud Resistivity {F13.4}
RLA1 .OHMM	:HRLT Borehole Corrected Resistivity 1 {F13.4}
RLA2 .OHMM	:HRLT Borehole Corrected Resistivity 2 {F13.4}
RLA3 .OHMM	:HRLT Borehole Corrected Resistivity 3 {F13.4}
RLA4 .OHMM	:HRLT Borehole Corrected Resistivity 4 {F13.4}
RLA5 .OHMM	:HRLT Borehole Corrected Resistivity 5 {F13.4}
HTHO .PPM	:HNGS Formation Thorium Concentration {F13.4}
HURA .PPM	:HNGS Formation Uranium Concentration {F13.4}
HFK .V/V	:HNGS Formation Potassium Concentration {F13.4}
HSGR .GAPI	:HNGS Standard Gamma Ray {F13.4}
HCGR .GAPI	:HNGS Computed Gamma Ray {F13.4}
GR .GAPI	:Gamma-Ray {F13.4}
HCAL .IN	:HRCC Cal. Caliper {F13.4}
DSO8 .IN	:HRDD High Resolution Density Standoff {F13.4}
HDRA .G/C3	:HRDD Density Correction {F13.4}
PEF8 .	:HRDD High Resolution Formation Photoelectric Factor {F13.4}
RHO8 .G/C3	:HRDD High Resolution Formation Density {F13.4}
RXO8 .OHMM	:MCFL High Resolution Invaded Zone Resistivity {F13.4}
RSO8 .IN	:MCFL High Resolution Resistivity Standoff {F13.4}
EHGR .GAPI	:HiRes Gamma-Ray {F13.4}
HTNP .V/V	:HiRes Thermal Neutron Porosity {F13.4}
DEVI .DEG	:Hole Deviation {F13.4}
ANOR .M/S2	:Acceleration Computed Norm {F13.4}
FNOR .A/M	:Magnetic Field Computed Norm {F13.4}
RB .DEG	:Relative Bearing {F13.4}
C1 .IN	:Caliper 1 {F13.4}
C2 .IN	:Caliper 2 {F13.4}
CDF .N	:Calibrated Downhole Force {F13.4}
DTCO .US/F	:Delta-T Compressional {F13.4}
DTSM .US/F	:Delta-T Shear {F13.4}
PR .	:Poisson's Ratio {F13.4}
VPVS .	:Compressional to Shear Velosity Ratio {F13.4}
DT1 .US/F	:Delta-T Shear - Lower Dipole {F13.4}
DT2 .US/F	:Delta-T Shear - Upper Dipole {F13.4}
DT4P .US/F	:Delta-T Compressional - Monopole P&S {F13.4}
DT4S .US/F	:Delta-T Shear - Monopole P&S {F13.4}
TENS .LBF	:Cable Tension {F13.4}
HDAR .IN	:Hole Diameter from Area {F13.4}

References:

Kuttan, K. Kulla, J.B. & Neumann, R.G.: “Freshwater Influx in the Gippsland Basin: Impact on Formation Evaluation, Hydrocarbon Volumes, and Hydrocarbon Migration.” The APEA Journal 1986.

Basker-5 Well Completion Report, Volume 1, Basic Data, December 2006 Anzon Australia Limited

7. MDT PRESSURE INTERPRETATION, FLUID CONTACTS AND SAMPLING

MDT Pressure Data

A total of 50 MDT stations were picked from well logs and tested. A few of the tests were repeated. The pressure versus depth plot is shown in Figure 7.1 below.

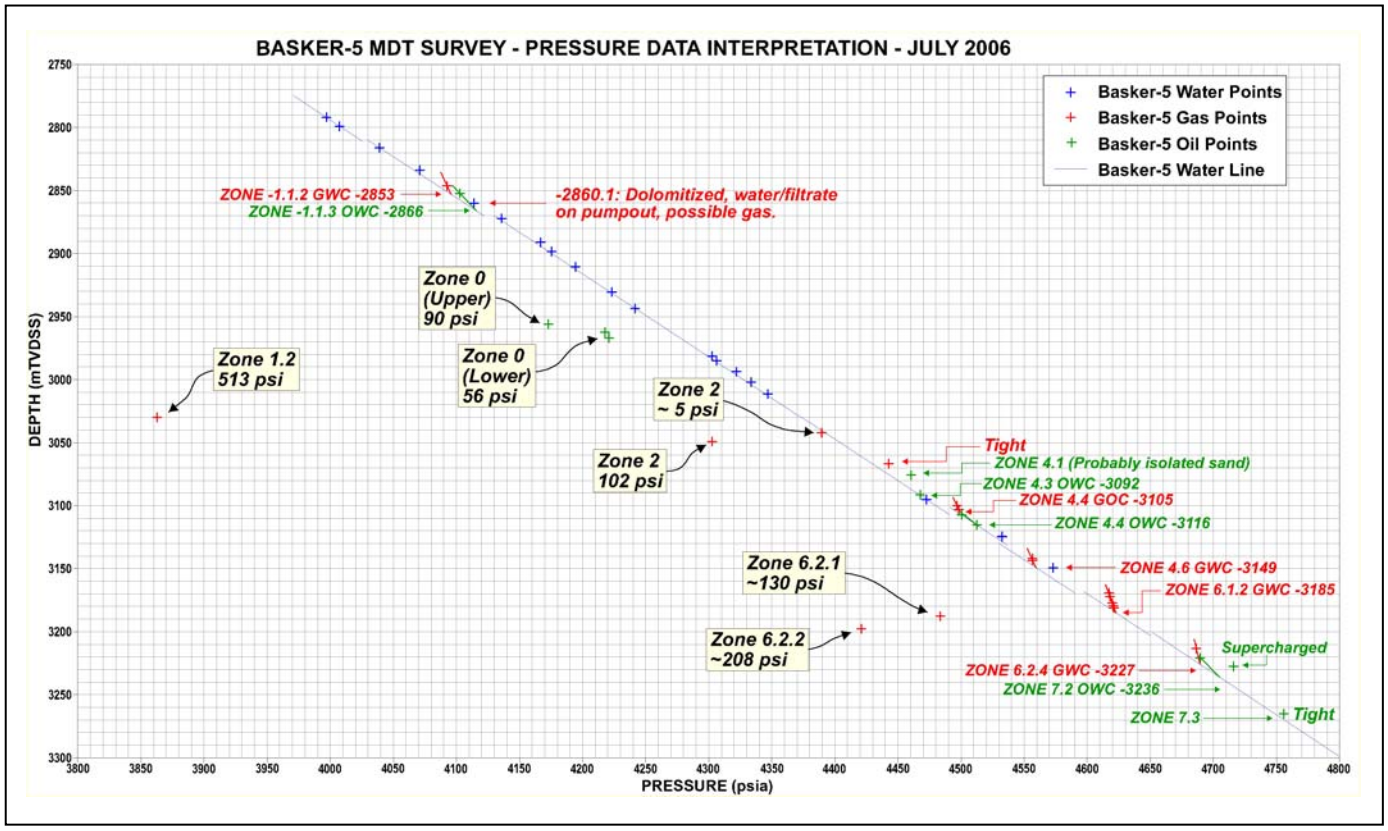

Figure 7.1 Basker-5 MDT Pressure vs Depth Plot

As a result of the Extended Production Test (EPT) in Basker-2 which commenced about six months before Basker-5 was drilled, significant pressure depletion was observed in some of the sands in Basker-5. However, the depletion is not uniform, even between different sand bodies in the same stratigraphic unit, and some of the sands were not connected at all between the two wells. The results are discussed in detail below.

(1) Water Line

Thirteen pre-tests in clean water-bearing sands between 2860 and 3100 mTVDSS lie on a good trend line covering Zone -1 to Zone 4. The pressure gradient of this line, 1.51 psi/m or 0.46 psi/ft, is higher than expected for formation water, but the line virtually coincides with that drawn through the water points in Basker-2. Compared to the original aquifer pressure in Basker-1, the pressure depletion in Basker-5 is ~25 to 40 psi being the same as Basker-2. There were only two water points below 3100 mTVDSS which are on the high side of the trend line.

(2) Pressure Depletion in Oil and Gas Sands

The zones which exhibit significant pressure depletions are the Zone 0 (oil), 1.2 (gas), 2.0 (gas) and 6.2 (gas). Zone 0 is oil in both Basker-2 and -5 and oil was produced in Basker-2 only. Zone 1.2 is gas in Basker-5. Only the lower sand of Zone 2.0 appears to be connected between Basker-2 and -5. Zone 6.2.1 and 6.2.2 were produced for short periods only in the lower completion zone of Basker-2 and yet experienced significant pressure depletion seen in Basker-5. This is believed to be due to gas leakage from the lower into the upper completion zone of Basker-2 during the EPT.

The other sands which lie on or close to the water line are not in communication with Basker-2. This includes Zone 6.1 which was perforated and had produced oil in Basker-2 during the EPT.

The sands which were perforated for oil production from Basker-5 are the Zone 0, 4.1, 4.3, 4.4, 4.5 and 7.

(3) Fluid Contacts

Most of the hydrocarbon-bearing sands have only one single pressure point. The identification of hydrocarbon type from the well logs or MDT is aided by the content of the pump out. Where two or more pressure points are available, the gradients are generally within the range 1.0±0.2 psi/m for oil and 0.3-0.4 psi/m for gas.

The small scale plot shown in Figure 7.1 does not allow any fluid contacts to be determined accurately. Certain parts of the plot were zoomed in on a large scale and the fluid contacts were read off the intersection of the various gradients where possible. Some inaccuracy is also introduced due to the uncertainty of the position of the water line. The following fluid contacts determined from the pressure versus depth plot for Basker-5 should be regarded as approximate estimates only.

Table 7.1 Basker-5 Approximate Fluid Contacts

Zone	Contact	Depth (mTVDSS)
-1.1.2	GWC	2853
-1.1.3	OWC	2866
4.3	OWC	3092
4.4	GOC	3105
4.4	OWC	3116
4.6	GWC	3149
6.1.2	GWC	3185
6.2.4	GWC	3231
7.2	OWC	3236

(4) Sampling

There was no MDT sample taken in this well.

8. SAMPLE ANALYSES USING QEMSCAN

PETROLOGY

of

BASKER-5 MSCT CORE SAMPLES

for

ANZON AUSTRALIA LTD

by

ACS LABORATORIES PTY LTD

5 October, 2006

Anzon Australia Ltd
Suite 504
165 Walker Street
NORTH SYDNEY NSW 2060

Attention: Barry Messent

FINAL REPORT: 0513-01 – BASKER-5

CLIENT REFERENCE:	Service Order BMG-WE-01-0059
MATERIAL:	Fourteen MSCT core samples
LOCALITY:	Basker-5
WORK REQUIRED:	Petrology

Please direct technical enquiries regarding this work to the signatory below under whose supervision the work was carried out.

KEVIN H. FLYNN
Operations Manager

PETROLOGY

of

BASKER-5 MSCT CORE SAMPLES

A report prepared for

ANZON AUSTRALIA LTD

by

JULIAN C. BAKER Ph.D.

October 2006

ACS Laboratories Pty Ltd
ABN: 81 008 273 005

C O N T E N T S

Page

EXECUTIVE SUMMARY 1

1. INTRODUCTION 2

2. ANALYTICAL PROGRAM

2.1 Thin-Section Analysis 2
2.2 X-Ray Diffraction Analysis 2
2.3 Scanning Electron Microscopy 2

3. TEXTURE 4

4. THIN-SECTION COMPOSITION

4.1 Framework Grains 4
4.2 Clays 9
4.3 Cements 11
4.4 Visible Porosity 11

5. X-RAY DIFFRACTION ANALYSES 11

6. DIAGENESIS 13

7. RESERVOIR QUALITY

7.1 General 16
7.2 Samples 23

8. COMPARISON WITH MANTA-1 AND BASKER-1 27

9. SUMMARY AND CONCLUSIONS 29

REFERENCES 30

C O N T E N T S cont.

Page

TABLES

TABLE 1. ANALYSES PERFORMED AND CORE ANALYSES 3

TABLE 2. THIN-SECTION ANALYSES 5

TABLE 3. BULK-ROCK XRD ANALYSES 12

TABLE 4. FINE-FRACTION CLAY MINERALOGY 12

TABLE 5. RESERVOIR QUALITY SUMMARY 25

FIGURES

FIGURE 1. GRAIN SIZE/DEPTH CROSS-PLOT 7

FIGURE 2. QFR COMPOSITIONS 8

FIGURE 3. GRAIN SIZE/CLAY CROSS-PLOT 10

FIGURE 4. DIAGENETIC PARAGENESIS 15

FIGURE 5. POROSITY/PERMEABILITY CROSS-PLOT 17

FIGURE 6. VISIBLE POROSITY/PERMEABILITY CROSS-PLOT 18

FIGURE 7. VISIBLE POR./CLAY + ROCK FRAGS. CROSS-PLOT 19

FIGURE 8. CLAY + ROCK FRAGS./PERMEABILITY CROSS-PLOT 20

FIGURE 9. GRAIN SIZE/PERMEABILITY CROSS-PLOT 21

FIGURE 10. GRAIN SIZE/CLAY + ROCK FRAGMENTS CROSS-PLOT . 22

APPENDICES

1. **X-RAY DIFFRACTION TRACES**
2. **QEMSCAN REPORTS**
3. **PHOTOMICROGRAPHS**

EXECUTIVE SUMMARY

A petrological study was carried out on fourteen MSCT core samples from 3192.0-3449.0m in Basker-5. Analytical techniques used were thin-section analysis, qualitative bulk-rock/fine-fraction X-ray diffraction analysis, and scanning electron microscopy.

Samples are variably sorted, medium to coarse grained subarkoses, lithic arkoses and sublitharenites in which framework grains are mainly quartz, K-feldspar, low-grade metasedimentary rock fragments and siliciclastic sedimentary rock fragments.

Detrital grain assemblages indicate a nearby polymictic provenance dominated by granitic, metasedimentary and sedimentary rocks. Provenance did not change during accumulation of the section, although there were temporal fluctuations in the amount of quartzose detritus and lithic-labile detritus that entered the basin.

Clay content generally increases with decreasing grain size. Clay is mainly authigenic kaolinite and subordinate illite that occur as labile grain decomposition products. Clay minerals detected by XRD are kaolinite, illite and trace chlorite.

Sandstones at 3251.0m and 3287.0m are tightly cemented by late-stage dolomite.

The main diagenetic effects besides authigenic clay formation and localised dolomite cementation include physical compaction, grain contact dissolution, and labile grain dissolution. Quartz overgrowth content does not exceed 3.6%.

Diagenetic effects and paragenesis are identical in water-, oil- and gas-bearing sandstones, suggesting that hydrocarbon entrapment occurred late in the diagenetic history.

Visible porosity is variable, reflecting large differences in authigenic clay, ductile grain and dolomite cement content. Visible porosity is mainly primary and intergranular and also includes scattered secondary pores that result from labile grain dissolution.

Permeability variation (0.04-3150mD) mostly reflects differences in clay + metamorphic/sedimentary rock fragment content and, to a lesser extent, grain size. Low permeability at 3251.0m and 3287.0m results from dolomite cementation.

Sediment composition, diagenetic effects and controls on reservoir quality are similar to those in Manta-1 and Basker-5, although high dolomite contents were recorded only in Basker-5.

1. INTRODUCTION

A petrological study was carried out on fourteen MSCT core samples from 3192.0-3449.0m in Basker-5, Gippsland Basin in order to determine texture, mineralogy, diagenetic effects, and controls on reservoir quality. Basker-5 petrology is compared with Manta-1 and Basker-1 petrology as described by Phillips (2000a,b), and the report also includes reports by Botha & Butcher (2006a,b) that include complementary QEMSCAN data. Sample depths and core analyses are listed in Table 1.

2. ANALYTICAL PROGRAM

2.1 Thin-Section Analysis

Thin-sections were cut in kerosene, impregnated with blue-dyed epoxy resin to aid porosity recognition, and stained with sodium cobaltinitrite to aid feldspar identification. In each thin-section, mineral composition and visible porosity were determined by a count of 400 points, and mean grain size and sorting were estimated with the aid of an eyepiece graticule. Photomicrographs were taken of each thin-section to illustrate texture, composition, diagenetic effects and porosity.

Thin-sections of untreated and Dean-Stark-treated splits of one sample (#21, 3218.0m) were compared in order to determine whether texture and composition have been affected by Dean-Stark analysis. Most petrology samples have been subjected to Dean-Stark analysis.

2.2 X-Ray Diffraction Analysis

Qualitative bulk-rock X-ray diffraction (XRD) analysis was carried out on eight samples using finely ground powders.

Fine-fraction XRD analysis was carried out on the same eight samples in order to precisely determine clay mineralogy. The fine fraction was separated from each sample by disaggregation and settling in distilled water and was air dried on glass discs to produce oriented specimens for XRD analysis. Samples were analysed in air dried condition and also following treatment with ethylene glycol.

2.3 Scanning Electron Microscopy

Scanning electron microscopy (SEM) was carried out on five samples in order to provide information on porosity characteristics and clay morphology/distribution. Analyses were done on freshly exposed surfaces that had been thoroughly washed in shellite to remove volatile hydrocarbons.

TABLE 1. ANALYSES PERFORMED AND CORE ANALYSES

Sample #	Depth (mRT)	Zone	PETROLOGICAL ANALYSES				CORE ANALYSES**		
			MA	XRD	SEM	PM	Por. (%)	Perm. (mD)	GD (g/cm^3)
24	3192.0	water	X	-	-	X	22.1	922	2.64
23	3206.0	oil	X	X	X	X	20.7	134	2.70
22	3212.0	oil	X	-	-	X	19.4	35.8	2.64
21*	3218.0	oil	X	X	X	X	22.6	3150	2.66
19	3251.0	water	X	X	-	X	7.0	2.71	2.69
17	3287.0	gas	X	-	-	X	2.8	0.04	2.72
16	3299.0	gas	X	X	X	X	19.3	48.4	2.64
14	3306.5	gas	X	X	-	X	15.8	12.4	2.66
12	3308.5	gas	X	X	X	X	22.5	2090	2.63
11	3353.5	oil	X	X	-	X	13.6	45.9	2.62
7	3372.0	gas	X	X	X	X	13.0	41.2	2.64
6	3409.0	oil	X	-	-	X	20.1	1380	2.68
4	3439.0	gas	X	-	-	X	18.5	211	2.66
3	3449.0	gas	X	-	-	X	18.7	921	2.63

MA = modal analysis; XRD = qualitative bulk-rock & fine-fraction X-ray diffraction analysis;
SEM = scanning electron microscopy; PM = photomicroscopy

* thin-section examination performed on untreated and Dean-Stark-treated splits

**ambient; horizontal direction

3. TEXTURE

Thin-section texture is given in Table 2, and annotated photomicrographs are presented in Appendix 3. Samples are slightly- to moderately-compacted, grain-supported, variably sorted, medium to coarse grained sandstones with a mean quartz grain size of 0.26-0.85mm. Coarse grained sandstones are restricted to the section at 3212.0-3287.0m and below 3372.0m (Fig. 1). Most sandstones are moderately to moderately-well sorted. Sample #11 (3353.5m) includes a 4mm-wide zone defined by thin, closely-spaced, low-amplitude, stylolitic, argillaceous/carbonaceous laminae. The other sandstones are clean and massive, although #24 (3192.0m) and #16 (3299.0m) include rare, thin, discontinuous, argillaceous/carbonaceous laminae and #17 (3287.0m) includes a single, thin (0.5mm) lamination defined by relatively fine grain size. Samples #19 (3251.0m) and #17 (3287.0m) are tightly cemented by coarsely-crystalline/poikilotopic carbonate, whereas the other sandstones are generally poorly cemented, although some sandstones (e.g., 3218.0m, 3372.0m, 3439.0m) contain common, scattered, fine to coarse, scalenohedral carbonate crystals and coarsely-crystalline carbonate cement patches. Framework grain packing density has been increased by micaceous/argillaceous grain compactional deformation and by grain contact dissolution (pressure solution) to form long, embayed and sutured (including microstylolitic) grain contacts. Common patchy authigenic clay pseudomatrix results from micaceous/argillaceous grain compaction and alteration. Feldspar grains are locally compactionally fractured and crushed. The two deepest samples (#4, 3439.0m; #3, 3449.0m) are largely crushed due to coring. Quartz grains are angular to subrounded (mainly subangular).

4. THIN-SECTION COMPOSITION

Thin-section composition is given in Table 2, and sandstone QFR composition is plotted in Figure 2, which also includes QFR data for Manta-1 and Basker-1 that are discussed in Section 8. Thin-section data are compared with QEMSCAN data for seven samples in Appendix 2.

4.1 Framework Grains

Sandstones are subarkoses, lithic arkoses and sublitharenites with a mean QFR ratio of $Q_{82}F_{10}R_8$ and in which framework grains are mainly quartz, K-feldspar, metasedimentary rock fragments and sedimentary rock fragments. There are no significant depth- and grain-size-related trends in detrital composition.

Detrital quartz content is 49.3-69.3% and averages 61.5%. Most quartz is monocrystalline. Polycrystalline quartz includes recrystallised metamorphic quartz, schistose metamorphic quartz, quartzite, metaquartzite and granitic quartz. Quartz grains are locally thinly enveloped by authigenic quartz overgrowths where interstitial areas are not filled by clay, compacted ductile grains and carbonate cement.

Feldspar content is 2.7-12.4%. Feldspar is entirely granitic K-feldspar (orthoclase, microcline) that is fresh to moderately altered and commonly etched, partly dissolved and compactionally fractured and crushed.

TABLE 2. THIN-SECTION ANALYSES

Sample #	24	23	22	21	19	17	16
Depth (mRT)	3192.0	3206.0	3212.0	3218.0	3251.0	3287.0	3299.0
Zone	water	oil	oil	oil	water	gas	gas
Quartz (monocrystalline)	60.3	60.0	57.8	57.0	46.1	50.4	51.9
Quartz (polycrystalline)	4.3	5.6	3.2	2.5	3.2	9.2	3.3
Quartz overgrowths	1.7	2.2	1.2	1.1	-	-	2.3
Chert	-	0.3	0.3	0.3	0.8	0.3	0.8
K-feldspar	2.7	3.4	12.3	7.5	12.4	3.7	11.4
Plagioclase	-	-	-	-	-	-	-
Granitic rock fragments	-	-	0.7	0.7	0.4	0.7	0.3
Volcanic rock fragments	0.8	0.3	0.9	0.3	0.4	0.3	1.8
Metamorphic rock fragments	2.8	4.0	6.5	4.3	4.0	2.1	7.1
Sedimentary rock fragments	1.6	0.3	1.5	1.3	0.7	-	2.1
Mica	0.3	0.3	1.2	-	0.3	-	1.1
Organic fragments	-	-	-	-	-	-	-
Dolomite	-	-	-	-	30.0	33.0	-
Siderite	0.3	1.0	1.0	1.9	0.3	-	0.3
Anatase/leucoxene	-	-	-	-	-	-	-
Authigenic kaolinite	6.2	6.8	5.0	2.4	1.1	0.3	7.4
Authigenic illite	1.1	1.3	1.3	0.3	0.3	-	1.2
Detrital clay	-	-	-	-	-	-	0.3
Primary porosity	16.2	13.0	6.8	17.2	-	-	6.3
Secondary porosity	1.7	1.5	0.3	3.2	-	-	2.4
Q (quartz + chert)	89.4	89.5	74.0	81.2	73.7	89.9	71.9
F (feldspar)	3.6	4.5	14.6	10.0	18.2	5.5	14.1
R (rock fragments)	7.0	6.0	11.4	8.8	8.1	4.6	14.0
Mean grain size (mm)	0.43	0.26	0.51	0.79	0.85	0.77	0.39
Mean grain size (class)	medium	medium	coarse	coarse	coarse	coarse	medium
Sorting (class)	mod	well	mod	md-well	poor	mod	md-well

TABLE 2. THIN-SECTION ANALYSES (cont.)

Sample #	14	12	11	7	6	4	3
Depth (mRT)	3306.5	3308.5	3353.5	3372.0	3409.0	3439.0	3449.0
Zone	gas	gas	oil	gas	oil	gas	gas
Quartz (monocrystalline)	63.0	63.2	60.4	59.8	54.0	60.2	62.4
Quartz (polycrystalline)	2.4	6.1	1.6	2.0	3.3	3.0	2.7
Quartz overgrowths	1.2	1.1	2.0	2.0	3.6	2.0	2.0
Chert	-	-	0.4	1.0	0.3	0.3	0.3
K-feldspar	11.3	3.2	7.0	9.8	10.0	11.2	7.6
Plagioclase	-	-	-	-	-	-	-
Granitic rock fragments	-	-	-	-	-	-	-
Volcanic rock fragments	0.7	0.7	1.3	1.3	-	-	0.7
Metamorphic rock fragments	5.1	1.2	3.7	4.0	5.2	6.2	6.6
Sedimentary rock fragments	1.6	-	0.6	2.0	0.7	2.0	1.1
Mica	-	-	0.3	0.9	-	0.7	0.3
Organic fragments	-	-	1.6	-	-	-	-
Dolomite	-	-	-	2.9	-	2.4	0.3
Siderite	2.0	1.2	0.3	0.3	-	-	-
Anatase/leucoxene	0.3	-	0.3	-	-	-	0.3
Authigenic kaolinite	8.9	2.3	8.7	6.4	6.4	4.4	5.5
Authigenic illite	2.0	-	0.7	1.2	2.8	-	0.7
Detrital clay	-	-	2.8	-	-	-	-
Primary porosity	1.1	19.8	5.4	4.4	12.1	6.5	8.7
Secondary porosity	0.4	1.2	2.9	2.0	1.6	1.1	0.8
Q (quartz + chert)	78.1	93.3	83.6	79.1	79.3	77.1	80.8
F (feldspar)	13.2	4.2	9.1	12.0	13.0	13.2	9.1
R (rock fragments)	8.7	2.5	7.3	8.9	7.7	9.7	10.1
Mean grain size (mm)	0.31	0.45	0.31	0.43	0.60	0.70	0.82
Mean grain size (class)	medium	medium	medium	medium	coarse	coarse	coarse
Sorting (class)	md-well	md-well	md-well	md-well	md-well	mod	md-well

FIGURE 1. GRAIN SIZE/DEPTH CROSS-PLOT

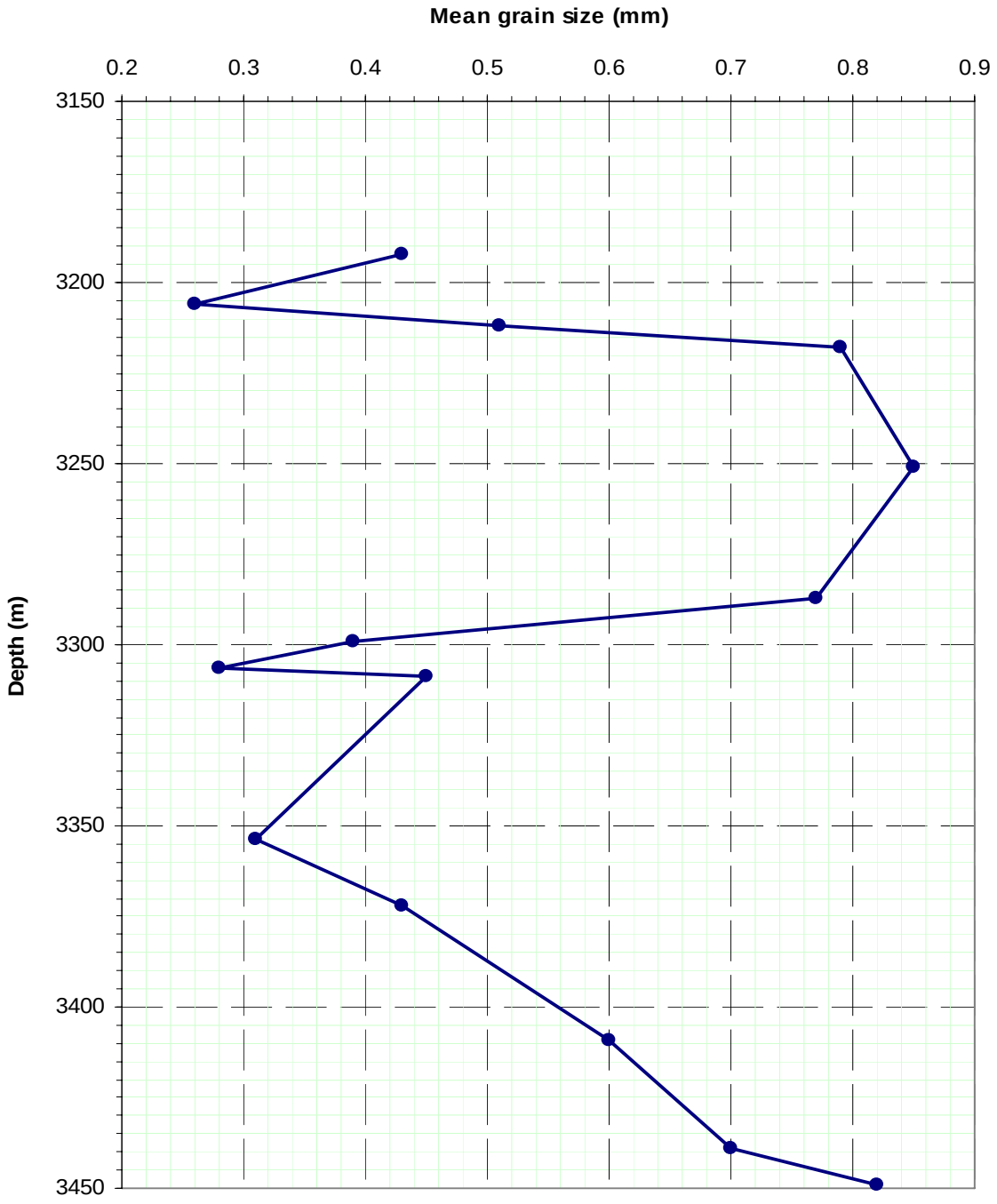

FIGURE 2. QFR COMPOSITIONS

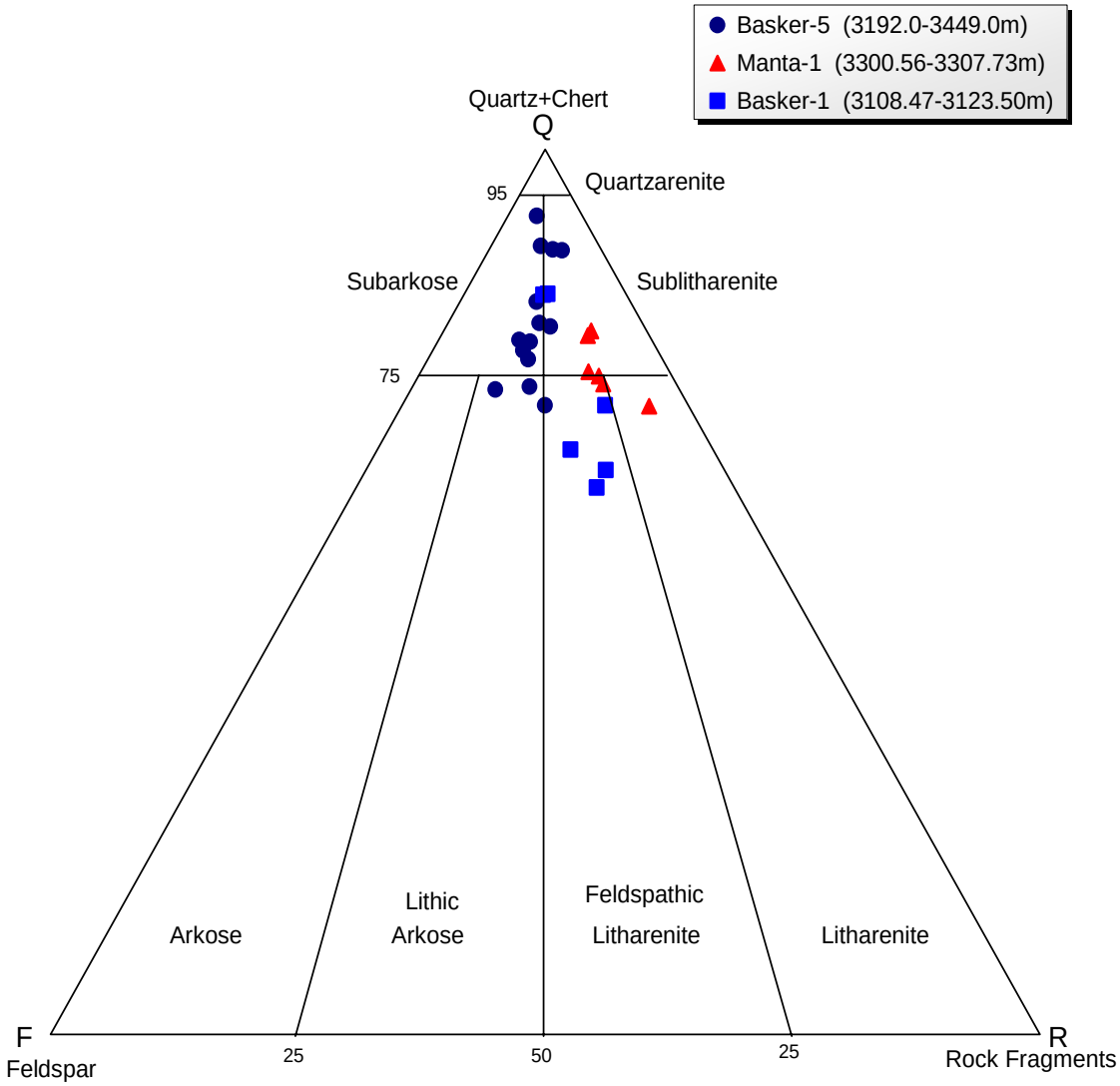

Rock fragment content is 1.9-11.3%. Lithic grains are mainly low-grade metasedimentary rock fragments (illitic meta-argillite, meta-sandstone, phyllite, quartz-muscovite/illite/chlorite schist, micaceous/illitic quartzite) (1.2-7.1%) and also include strongly indurated/silicified siliciclastic sedimentary rock fragments (shale, illitic siltstones, illitic/micaceous sandstones, quartzose sandstones) (<2.2%), cherty silicified felsic and rare intermediate volcanic rock fragments (<1.9%) and granitic rock fragments (micrographically and coarsely intergrown quartz and K-feldspar) (<0.8%). There is complete gradation between sedimentary and metasedimentary rock fragments, making the distinction between the two rock fragment types rather arbitrary. Argillaceous/micaceous rock fragments are commonly compactionally deformed around adjacent rigid grains, and many labile rock fragments have partly altered to illite and kaolinite.

Other framework grains include chert, chalcedony, mica (variably altered biotite, muscovite), organic fragments and accessory heavy minerals (tourmaline, zircon, garnet, anatase, leucoxene). Organic fragments are most common (1.6%) in #11 (3353.5m), where they are concentrated with detrital clay and fine micaceous/illitic grains along thin, localised laminae. Bitumen is absent.

Provenance: Detrital grain assemblages indicate a nearby polymictic provenance dominated by granitic, low-grade metasedimentary and siliciclastic sedimentary rocks and which also included felsic volcanics. The same grain types occur throughout the sampled section, indicating that provenance did not change during accumulation of the section, but differing proportions of the main grain types (unrelated to grain size and diagenesis) indicate that there were temporal fluctuations in the amount of quartzose detritus and lithic-labile detritus that entered the basin.

4.2 Clays

Clay content ranges from 0.3% to 12.2% and generally increases with decreasing grain size (Fig. 3). Clay is mainly authigenic kaolinite, the amount of which ranges from less than 1.2% in the strongly dolomite-cemented sandstones (#19, 3251.0m; #17, 3287.0m) to 8.9%. Authigenic kaolinite forms patchy and dispersed, microporous pseudomatrix and deformed, mica-like grains where mica, micaceous/illitic metasedimentary rock fragments, sedimentary rock fragments and feldspar have altered. Micaceous/illitic grains are commonly partly altered to kaolinite, and illitic remnants of micaceous/illitic precursor grains are commonly associated with kaolinite.

The other authigenic clay is illite, the amount of which ranges up to 2.8%. Authigenic illite occurs as an intermediate decomposition product of micaceous/argillaceous grains and forms patchy and thinly dispersed pseudomatrix that is commonly intimately associated with authigenic kaolinite. There is complete gradation between slightly compacted and illitised metasedimentary/sedimentary rock fragments, illitic clay pseudomatrix and, the final decomposition product, kaolinite.

Sample #11 (3353.5m) contains minor (2.8%) brown detrital clay, all of which is concentrated along localised, thin, argillaceous/carbonaceous laminae. The other sandstones contain little (<0.4%) or no detrital clay.

FIGURE 3. GRAIN SIZE/CLAY CROSS-PLOT

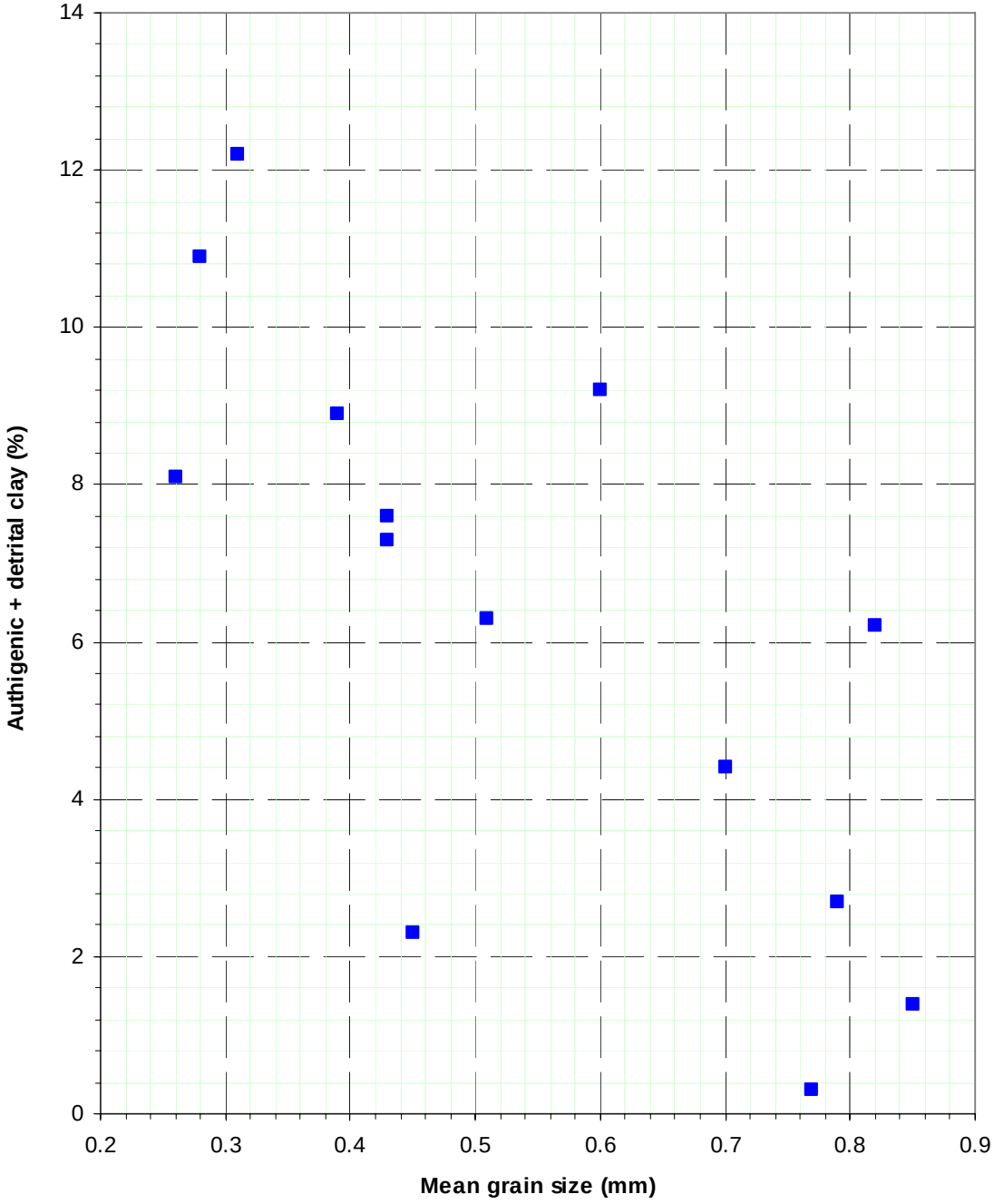

4.3 Cements

Sandstones are generally poorly cemented, except #19 (3251.0m) and #17 (3287.0m), which contain 30-33% coarsely-crystalline/poikilotopic dolomite cement that tightly fills intergranular pores and replaces clay and some argillaceous/fine grained rock fragments. In the other samples, dolomite does not exceed 2.9% and forms scattered, coarsely-crystalline pore-filling and replacive cement patches. Most sandstones lack dolomite.

Siderite occurs in small amounts (<2.0%) throughout most of the section, where it forms scattered fine to coarse scalenohedral crystals and cement patches that occupy intergranular pores and replace clay and altered biotite grains.

Quartz overgrowth content does not exceed 3.6% and is mainly below 2.4%. Even where quartz overgrowth development has not been inhibited by interstitial clay, compacted ductile grains and dolomite cement, quartz overgrowths are thinly developed and thus occlude only a small portion of total available intergranular space.

A single 1.4mm-long pyrite cement patch is included in #21 (3218.0m), and trace fine framboidal pyrite occupies pores in #3 (3449.0m).

4.4 Visible Porosity

Visible porosity is variable, reflecting large differences in authigenic clay, ductile grain and dolomite cement content. Two tightly dolomite-cemented sandstones (#19, 3251.0m; #17, 3287.0m) contain less than 0.3% visible porosity. The other twelve sandstones contain 1.5-21.0% visible porosity, the amount of which varies largely according to clay and metamorphic/sedimentary rock fragment content (see Fig. 7). Visible porosity is mainly primary and intergranular, particularly in the highly macroporous sandstones, and also includes scattered secondary intergranular and intragranular pores that result from partial to complete dissolution of K-feldspar grains and labile rock fragments.

5. X-RAY DIFFRACTION ANALYSES

Qualitative bulk-rock and fine-fraction XRD analyses were carried out on eight sandstones. Qualitative XRD analyses are given in Table 3, clay mineralogy is given in Table 4, and annotated XRD traces are presented in Appendix 1.

Bulk-rock XRD analyses show that quartz is the dominant mineral in all samples except #19 (3251.0m) and #7 (3272.0m), both of which contain major dolomite. Although major dolomite was detected by XRD in #7, thin-section analyses indicate that #7 contains only 2.9% dolomite, which indicates that dolomite is unevenly distributed in this sample. Samples also contain minor K-feldspar and kaolinite and trace to minor illite/mica, siderite and contaminant KCl. Sandstones generally have a consistent mineralogy throughout the section according to bulk-rock XRD analyses.

TABLE 3. BULK-ROCK XRD ANALYSES

Sample #	Depth (mRT)	Zone	Qtz	KF	Ka	I/M	Dol	Sid	KCl
23	3206.0	oil	A	m	m	m	-	m	m
21	3218.0	oil	A	m	m	m	-	m	m
19	3251.0	water	M	m	m	m	M	T	T
16	3299.0	gas	A	m	m	m	-	m	m
14	3306.5	gas	A	m	m	m	-	m	m
12	3308.5	gas	A	m	m	T	-	T	m
11	3353.5	oil	A	m	m	m	-	T	T
7	3372.0	gas	M	m	m	m	M	T	-

Qtz = quartz; KF = K-feldspar; Ka = kaolinite; I/M = illite/mica; Dol = dolomite;
Sid = siderite; KCl = contaminant potassium chloride

TABLE 4. FINE-FRACTION CLAY MINERALOGY

Sample #	Depth (mRT)	Zone	Ka	I/M	I/S	Sm	Chl
23	3206.0	oil	M	m	-	-	-
21	3218.0	oil	M	m	-	-	-
19	3251.0	water	M	m	-	-	-
16	3299.0	gas	M	m	-	-	-
14	3306.5	gas	M	m	-	-	T
12	3308.5	gas	M	m	-	-	-
11	3353.5	oil	M	m	-	-	m
7	3372.0	gas	M	m	-	-	T

Ka = kaolinite; I/M = illite/mica; I/S = mixed-layer illite/smectite; Sm = smectite;
Chl = chlorite

A = abundant; M = major; m = minor; T = trace

Fine-fraction XRD analyses (Table 4) confirm that the clay mineral suite is dominated by kaolinite and subordinate illite throughout the section. Trace to minor chlorite was also detected in the fine fraction of #14 (3306.5m), #11 (3353.5m) and #7 (3372.0m). Smectitic clays are absent.

Detected kaolinite occurs mainly as a labile grain alteration product, whereas detected illite is not only a product of labile grain alteration, but also occurs as fine detrital mica and as an original constituent of micaceous/illitic metasedimentary and sedimentary rock fragments. Detected chlorite occurs as an original constituent of metasedimentary rock fragments.

6. DIAGENESIS

Sandstones have been severely affected by diagenesis, with the main diagenetic processes being authigenic clay (kaolinite, illite) formation, physical compaction, grain contact dissolution/microstylolitisation, labile grain dissolution, and localised dolomite cementation.

In all sandstones, **authigenic clay** is dominated by kaolinite that forms patchy and dispersed, microporous pseudomatrix and deformed, mica-like grains where mica, micaceous/illitic rock fragments and feldspar have altered (Plates 4-7, 9, 13; Plate 15, Fig. 2; Plates 16-18; Plate 19, Fig. 2; Plate 20, Fig. 2; Plates 21-24, 27, 29). Micaceous/illitic grains are commonly partly altered to kaolinite, and illitic remnants of micaceous/illitic precursor grains are commonly associated with kaolinite.

Authigenic illite forms patchy and thinly dispersed pseudomatrix that is commonly intimately associated with authigenic kaolinite (Plates 5, 6, 25, 28, 29). Authigenic illite appears to be an intermediate decomposition product of micaceous/illitic grains, with kaolinite being the final alteration product.

Sandstones were prone to authigenic clay formation on account of containing a large component of micaceous/illitic grains at the time of accumulation. A notable exception is #12 (3308.5m), which, being originally highly quartzose, has not been significantly affected by clay diagenesis (Plates 17, 18, 19).

The generally high content of micaceous/illitic grains at the time of accumulation also made the sandstones susceptible to **physical compaction**. In all sandstones except highly quartzose #12 (3308.5m), these grain types are commonly compactionally deformed and dispersed between adjacent rigid grains, commonly to form pseudomatrix (Plates 2, 6; Plate 8, Fig. 2; Plates 11, 13; Plate 14, Fig. 1; Plates 16, 21, 23, 27, 28, 30). In addition, authigenic clay has compacted to form common patchy and dispersed pseudomatrix that is highly effective in filling intergranular spaces. Strongly compacted carbonaceous fragments are concentrated along localised thin laminae at 3353.5m (#11) (Plate 21), and K-feldspar grains are commonly compactionally fractured and crushed, particularly those feldspar grains that are partly dissolved (Plates 7, 28).

Framework grain packing density has been increased by **grain contact dissolution** to form long, embayed and sutured (including microstylolitic) grain contacts between juxtaposed quartzose and K-feldspar grains (Plates 1, 2, 5, 7, 11, 12, 16-18; Plate 20, Fig. 1; Plates 22-24, 27-31). Some quartz grains have also dissolved where they are in contact with micaceous/illitic rock fragments. Between some grains, grain contact dissolution and microstylolitisation were promoted by thin illitic clay films that are remnants of compactionally deformed and dispersed micaceous/illitic grains. Sandstone at 3353.5m (#11) is cut by thin, stylolitic, argillaceous/carbonaceous laminae (Plate 21).

Sandstones contain up to 2.9% **secondary porosity** that results from partial to complete dissolution of K-feldspar and, of lesser importance, micaceous/illitic grains (Plates 2, 7; Plate 9, Fig. 1; Plates 25, 27, 28, 30). Except in the tightly dolomite-cemented sandstones (#19, 3251.0m; #17, 3287.0m), etched and partly dissolved K-feldspar grains are common, and many secondary pores are partly clogged by kaolinitic and/or illitic remnants of pore-precursor grains.

Sandstones at 3251.0m (#19) and 3287.0m (#17) are tightly cemented by coarsely-crystalline/poikilotopic **dolomite** that fills intergranular pores and replaces clay and some argillaceous/fine grained rock fragments (Plates 10-12). The other samples contain little (Plates 23, 25, 29) or no dolomite.

Other diagenetic effects include minor siderite (Plates 5, 7, 16, 18) and quartz overgrowth (Plates 2-4, 8, 13; Plate 14, Fig. 1; Plate 15; Plate 20, Fig. 1; Plates 23, 24; Plate 26, Fig. 1; Plates 27-31) precipitation and rare pyrite formation. Quartz overgrowths are invariably thinly developed, even where quartz overgrowth cementation was not inhibited by interstitial clay, compacted ductile grains and dolomite cement (e.g., #12, 3308.5m).

Paragenetic timing: The interpreted paragenetic timing of the main diagenetic effects is shown in Figure 4. Long/embayed/irregular grain dissolution contacts occur between quartz and dissolved K-feldspar grains and between quartz and kaolinitised micaceous/illitic grains, indicating that K-feldspar dissolution and authigenic kaolinite postdate at least some grain contact dissolution. Dolomite cement at 3251.0m (#19) and 3287.0m (#17) tightly encloses 1) compactionally-deformed micaceous/illitic grains (Plate 11), 2) compactionally-fractured feldspar grains, and 3) quartz grains with long and slightly embayed grain contacts that result from grain contact dissolution (Plates 11, 12), indicating that dolomite postdates physical compaction and some grain contact dissolution. Dolomite replaces and thus postdates authigenic kaolinite. Framework grains are more tightly packed in the non-dolomite-cemented sandstones than in the tightly dolomite-cemented sandstones, indicating that physical compaction and grain contact dissolution continued after dolomite cementation. Unlike quartz grains in adjacent non-dolomite-cemented sandstones, quartz grains in the tightly dolomite-cemented sandstones lack quartz overgrowths, indicating that dolomite predates quartz overgrowths. There has been little feldspar dissolution in the tightly dolomite-cemented sandstones, suggesting that dolomite inhibited feldspar dissolution and that most feldspar dissolution occurred after dolomite cementation. Siderite encloses quartz grains with welded grain contacts (due to grain contact dissolution) and is enclosed by dolomite, indicating that siderite postdates some grain contact dissolution and predates dolomite. Quartz overgrowths, which generally start to form at temperatures around 80-90ºC, appear to be the latest diagenetic effect.

Sandstone samples are from several water-, oil- and gas-bearing zones according to information supplied by Anzon Australia Ltd. (Table 1). Particular attention was paid to comparing diagenetic effects between sandstones from each zone in order to determine 1) whether diagenesis has advanced further in the water-bearing sandstones, and 2) the relative timing of the hydrocarbon charge based on differences in diagenetic paragenesis between zones.
Diagenetic effects and paragenesis are identical in water-, oil- and gas-bearing sandstones. For example, late-stage dolomite cement is abundant in both water-

bearing sandstone at 3251.0m and gas-bearing sandstone at 3287.0m, and quartz overgrowth content is the same throughout the section, regardless of whether sandstones are water, oil or gas bearing. Accordingly, postdating deep burial diagenetic effects, hydrocarbon entrapment must have occurred late in the diagenetic history, assuming that diagenesis is inhibited or prevented by the presence of hydrocarbons.

FIGURE 4. DIAGENETIC PARAGENESIS

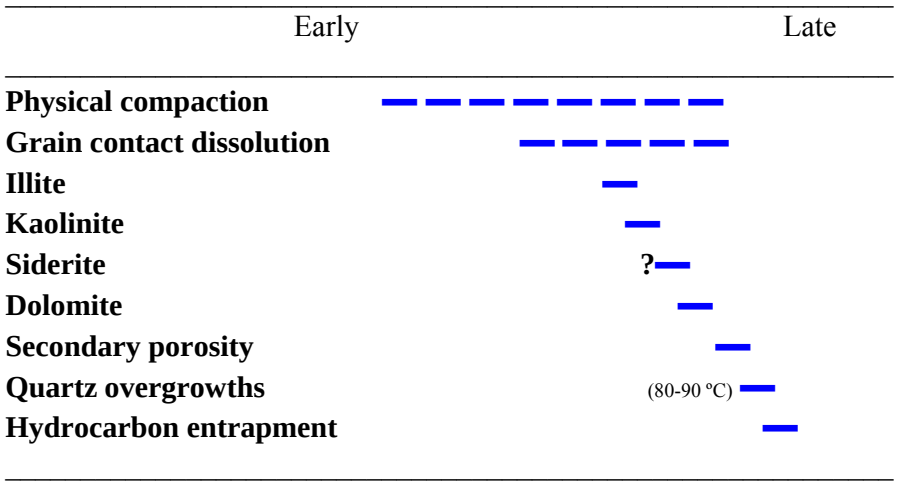

7. RESERVOIR QUALITY

7.1 General

Samples are variably sorted, medium to coarse grained sandstones that have poor to excellent reservoir quality, with measured (He-injection) porosity and permeability ranging from 2.8% to 22.6% and 0.04mD to 3150mD (Table 1; Fig. 5). Permeability values for petrology samples cover the full range of available permeability values for the section between 3085.0m and 3455.5m (Fig. 5).

Visible macroporosity ranges from 0% to 21.0% and is strongly (R^2 = 0.733) positively correlated with permeability (Fig. 6). A strong correlation is expected given that visible macroporosity is conducive to permeability. Discrepancies between visible macroporosity and measured porosity, which are greatest for the less macroporous sandstones, result from the presence of microporosity within authigenic clays, argillaceous rock fragments and etched and slightly dissolved feldspars.

Figure 7 shows that there is a moderate (R^2 = -0.641) negative correlation between visible porosity and clay + metamorphic/sedimentary rock fragment (RF) content if two tightly dolomite-cemented sandstones (#19, 3251.0m; #17, 3287.0m) are excluded. Therefore, since there is a strong positive correlation between visible porosity and permeability (Fig. 6), it is expected that clay + RF content should be negatively correlated with permeability. This is confirmed by Figure 8, which shows that there is a moderate (R^2 = -0.516) negative correlation between clay + RF content and permeability, excluding #19 and #17. Accordingly, clay + RF content is a major control on permeability. Metamorphic and sedimentary rock fragments influence permeability on account of being largely micaceous/illitic and thus prone to compactional deformation and dispersion, commonly to form pseudomatrix.

Figure 9 shows that there is only a weak (R^2 = 0.400) positive correlation between grain size and permeability, excluding #19 and #17. This indicates that the control of grain size on permeability is largely masked by differences in clay + RF content, which is expected given that 1) permeability is influenced by clay + RF content (Fig. 8), and 2) grain size and clay + RF content are poorly (R^2 = 0.267) correlated (Fig. 10). Scatter in the grain size versus permeability cross-plot (Fig. 9) would also result from wide sorting variation (sorting varies from poor to well).

In summary, permeability variation mainly reflects differences in clay + metamorphic/sedimentary rock fragment content and, to a lesser extent, grain size. Grain size only weakly influences permeability because grain size and clay + metamorphic/sedimentary rock fragment content are poorly correlated, which directly reflects temporal fluctuations in the amount of quartzose detritus and lithic-labile detritus that entered the basin. Low permeability at 3251.0m (#19) and 3287.0m (#17) results from localised dolomite cementation.

FIGURE 5. POROSITY/PERMEABILITY CROSS-PLOT

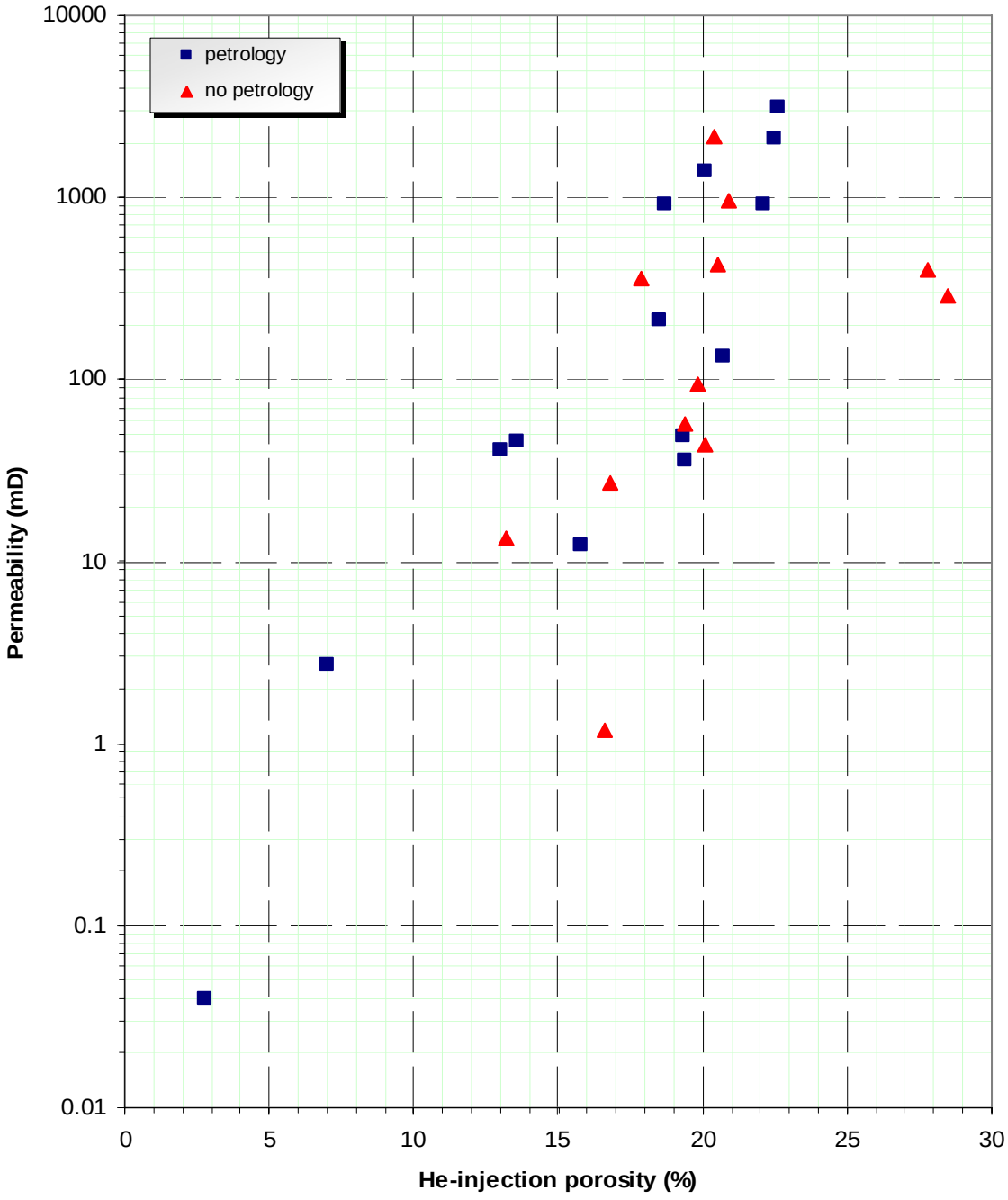

FIGURE 6. VISIBLE POROSITY/PERMEABILITY CROSS-PLOT

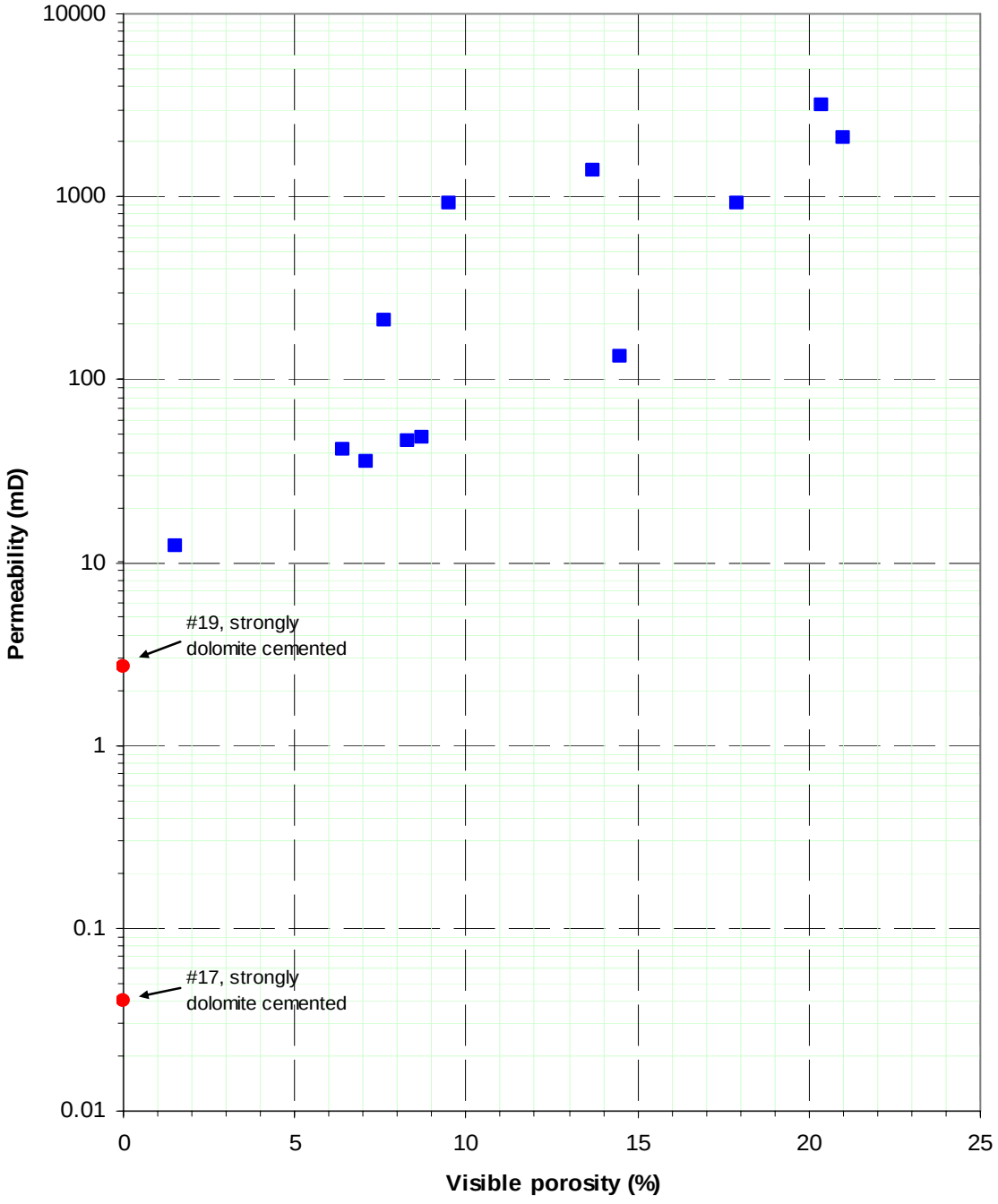

FIGURE 7. VISIBLE POROSITY/CLAY + ROCK FRAGMENTS CROSS-PLOT

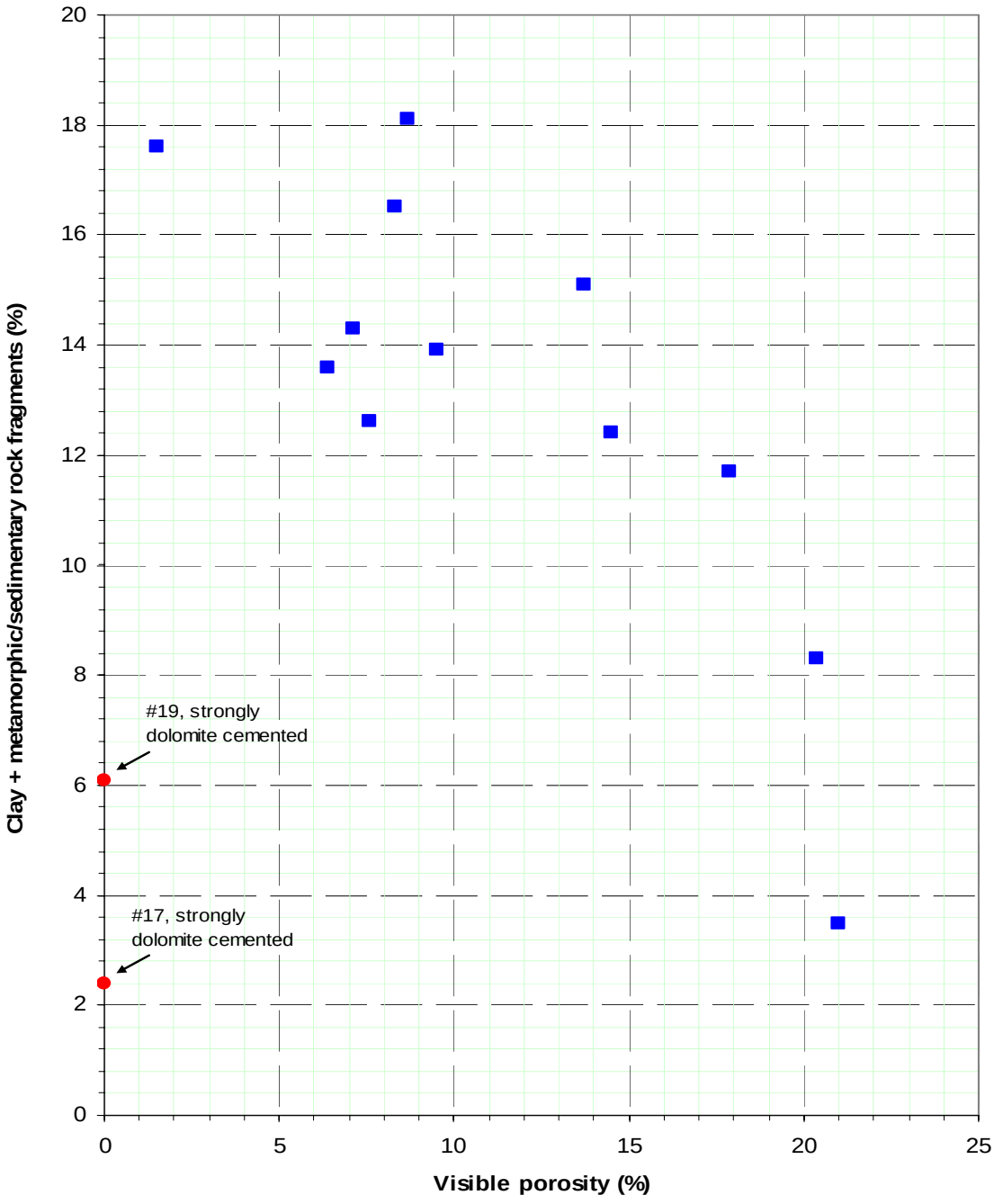

FIGURE 8. CLAY + ROCK FRAGMENTS/PERMEABILITY CROSS-PLOT

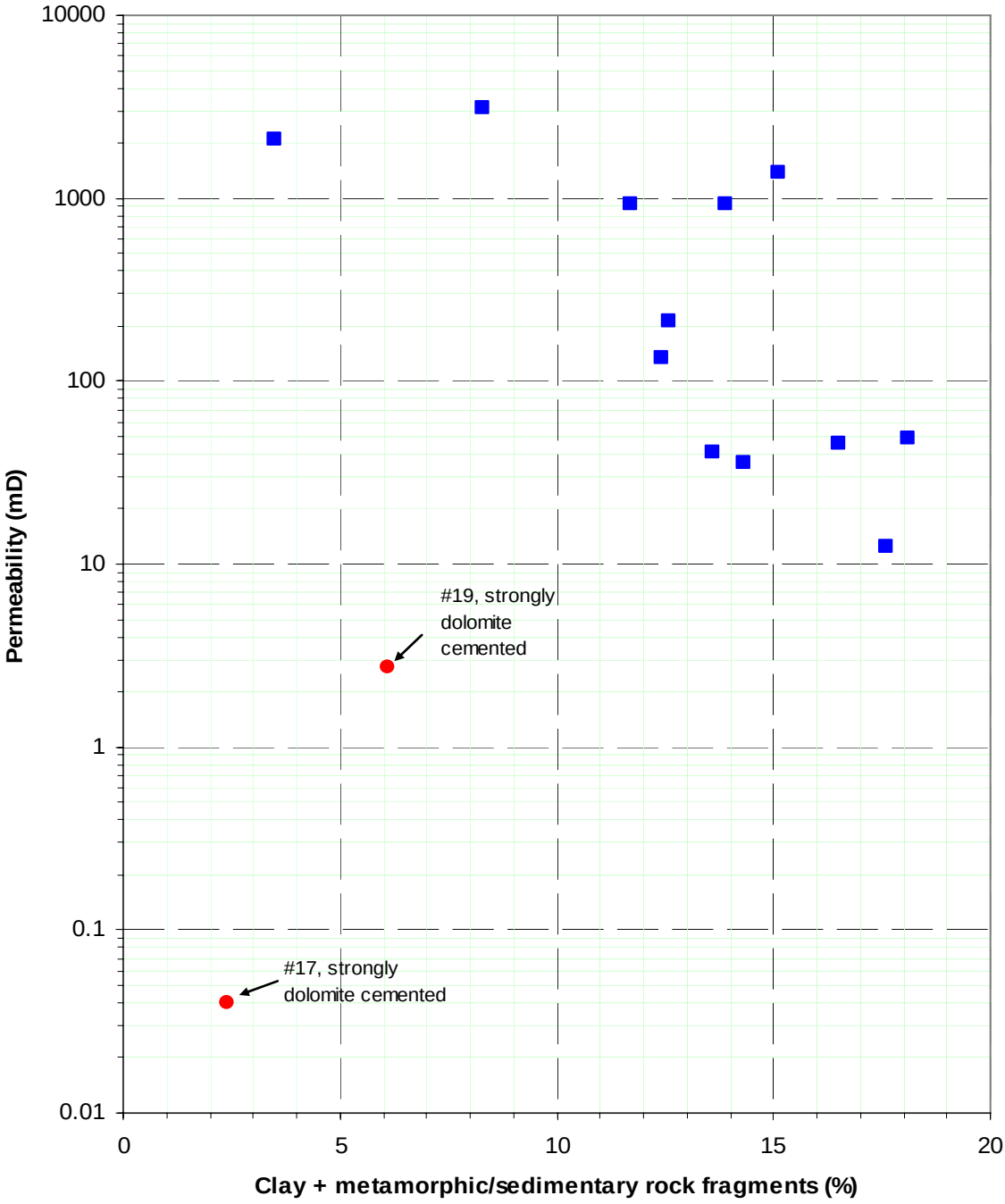

FIGURE 9. GRAIN SIZE/PERMEABILITY CROSS-PLOT

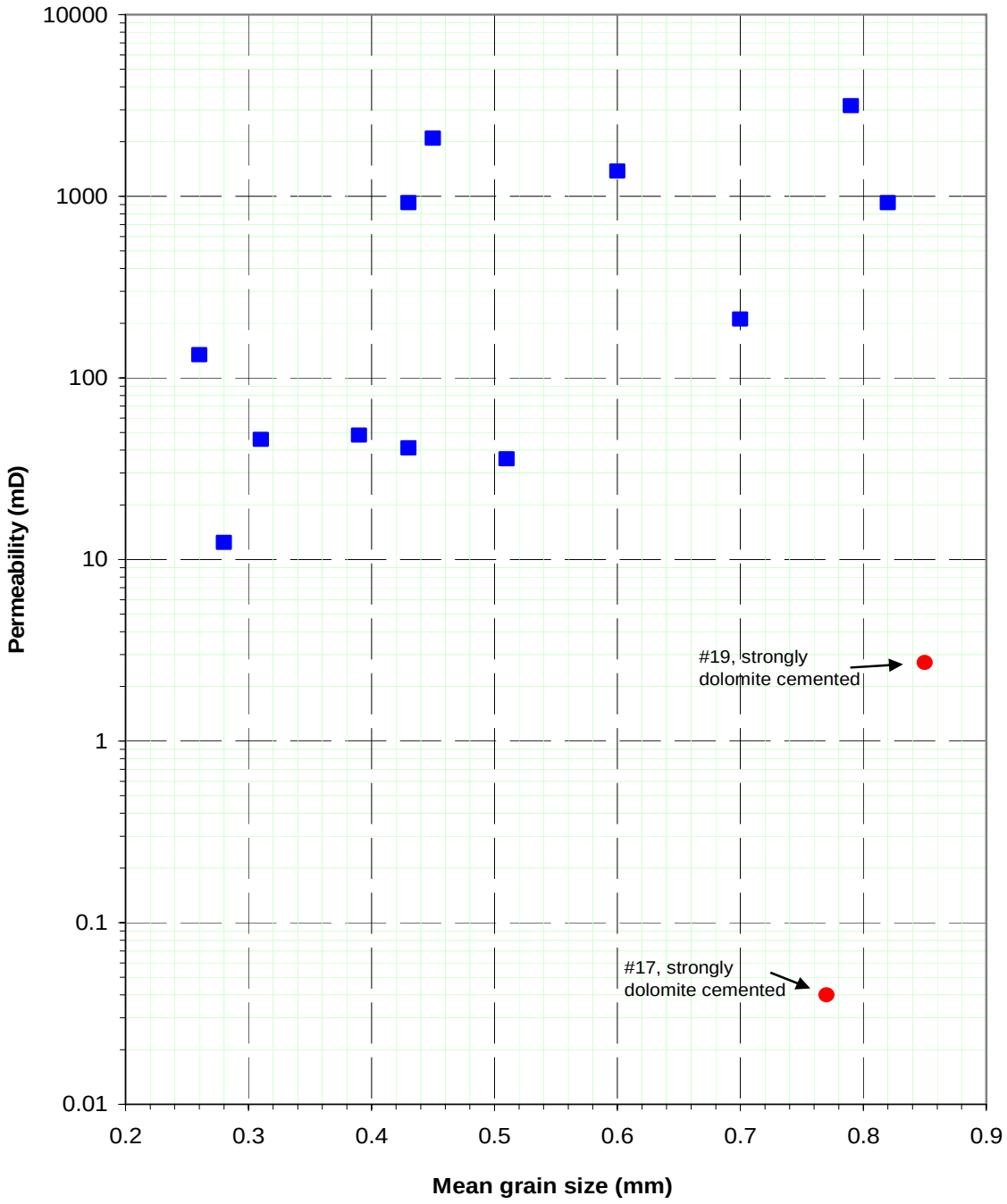

FIGURE 10. GRAIN SIZE/CLAY + ROCK FRAGMENTS CROSS-PLOT

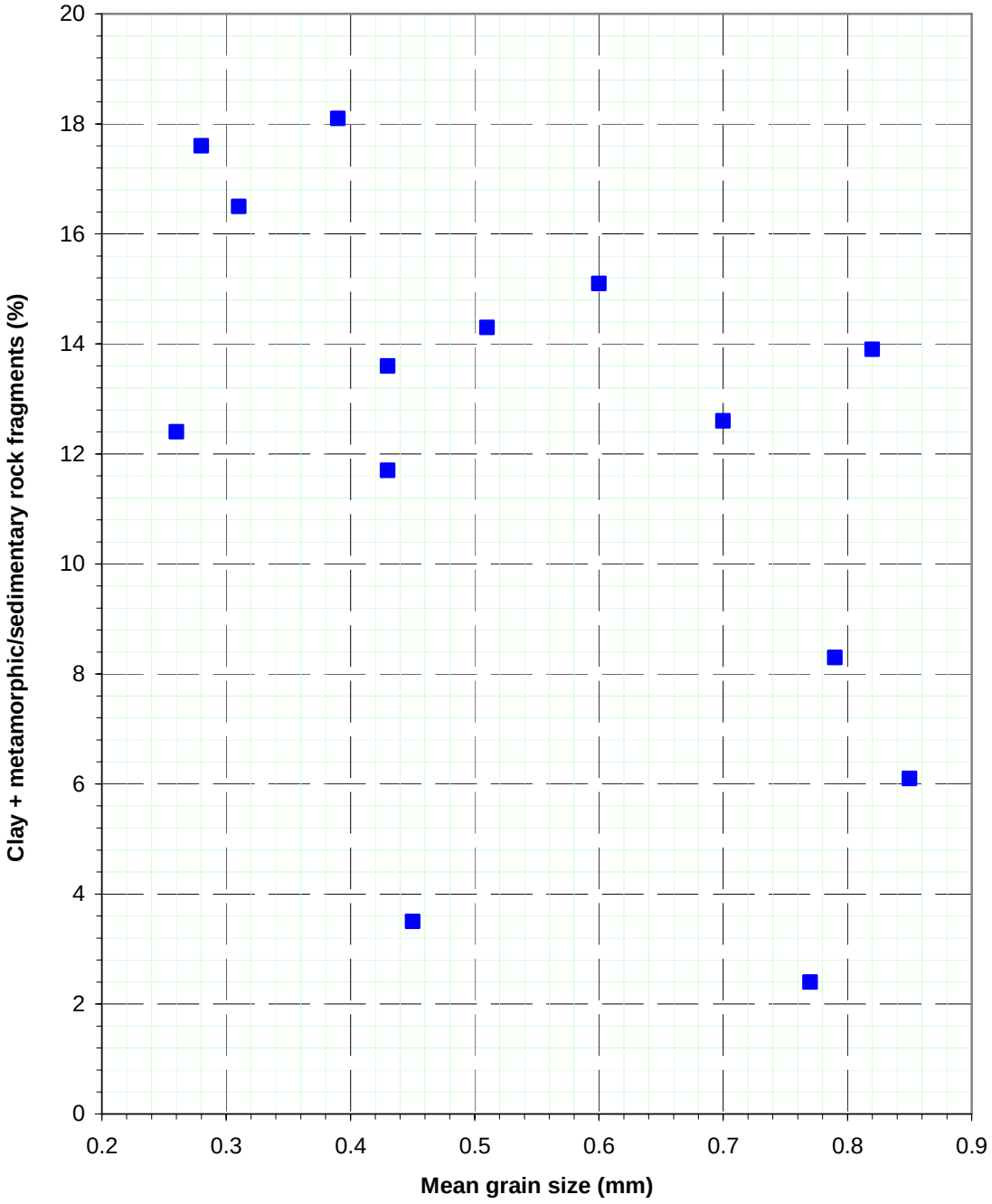

7.2 Samples

Poor reservoir quality: Two samples **(#19, 3251.0m; #17, 3287.0m)** are clean, coarse grained sandstones that have very low (2.71mD, 0.04mD) permeability on account of being tightly cemented by late-stage, coarsely-crystalline/poikilotopic dolomite. Prior to dolomite cementation, the sandstones would have contained good primary intergranular porosity, despite porosity reduction by grain contact dissolution, ductile grain compaction and minor authigenic clay formation.

Marginal reservoir quality: Sample **#14 (3306.5m)** is a lower medium grained sandstone that contains little (1.1%) primary intergranular porosity due to most intergranular areas being completely filled by compacted micaceous/argillaceous grains, authigenic clay (kaolinite, illite) pseudomatrix and very minor siderite and quartz overgrowth cement. Further porosity reduction results from grain contact dissolution/microstylolitisation, particularly where illitic clay films occur between juxtaposed quartz grains. The sandstone contained common micaceous/illitic rock fragments at the time of accumulation, which made it prone to physical compaction and authigenic clay formation. Small primary intergranular pores are widely and erratically scattered and thus have very limited interconnectivity. Most porosity is microporosity associated with clays, rock fragments and etched feldspar grains. Permeability is low (12.4mD).

Fair reservoir quality: Samples **#22 (3212.0m)**, **#16 (3299.0m), #11 (3353.5m)** and **#7 (3372.0m)** are lower medium to lower coarse grained sandstones that contain far more macroporosity (6.4-8.7%) than the previous sandstone (#14), having been less affected by the deleterious diagenetic processes that have eliminated most intergranular porosity in #14. Porosity-reducing diagenetic effects also include patchy dolomite cementation (#7) and stylolitisation along localised, thin, argillaceous/carbonaceous laminae (#11). Although intergranular pores are common, pore interconnectivity is greatly reduced by authigenic clay, compacted ductile grains and, in #7, dolomite cement occupying many intergranular spaces. Permeability is fair (35.8-48.4mD).

Good reservoir quality: Samples **#24 (3192.0m), #23 (3206.0m), #4 (3439.0m)** and **#3 (3449.0m)** are texturally varied, being moderately to well sorted, lower medium to upper coarse grained sandstones. Medium grained sandstones (#24, #23) contain good (17.9%, 14.5%) visible porosity, with many intergranular areas being free of clay and compacted ductile grains, and thus have high (922mD, 134mD) permeability, with #23 having much lower permeability than #24 due to its finer grain size. In contrast, the coarse grained sandstones (#4, #3) contain only modest (7.6%, 9.5%) visible porosity, having been more affected by ductile grain deformation, authigenic clay formation and grain contact dissolution than the medium grained sandstones, but still have high (211mD, 921mD) permeability due to coarse grain size.

Excellent reservoir quality: One uncemented, upper medium grained sandstone **(#12, 3308.5m)** was highly quartzose at the time of accumulation and thus was not prone to physical compaction and authigenic clay formation. Accordingly, despite porosity reduction by grain contact dissolution and localised pore filling by authigenic clay, the sandstone contains abundant (20.4%), evenly distributed, hence well-interconnected macroporosity, most of which is primary and intergranular. Permeability is very high (2090mD).

Samples **#21 (3218.0m)** and **#6 (3409.0m)** are coarse grained sandstones that were relatively quartzose at the time of accumulation, but not as quartzose as #12. Despite porosity reduction by grain contact dissolution, authigenic clay formation, ductile grain deformation and, in #21, minor siderite cementation, the sandstones contain good visible porosity (20.4%, 13.7%) that is mainly primary and intergranular and also includes secondary porosity that results from labile grain dissolution. Sample #21 has the highest permeability (3150mD) of the sample suite, reflecting its very high macroporosity, low clay content and coarse grain size. The lower permeability of #6 (1380mD) compared with #12 and #21 reflects a higher incidence of pore filling by authigenic clay and compacted ductile grains, particularly in finer parts of the sample.

Effect of Dean-Stark Analysis: A comparison of thin-sections made from untreated and Dean-Stark-analysed splits of #21 showed that Dean-Stark analysis had no effect on sandstone texture and composition.

A reservoir quality summary for individual samples is given in Table 5.

TABLE 5. RESERVOIR QUALITY SUMMARY

Sample #	Depth (mRT)	Comments
24	3192.0	Massive, moderately sorted, upper medium grained sublitharenite with good intergranular porosity, despite porosity reduction by grain contact dissolution and authigenic clay formation. Intergranular pores are fairly evenly distributed and thus are well interconnected. K = 922mD
23	3206.0	Massive, well sorted, lower medium grained sublitharenite with good intergranular porosity, despite porosity reduction by authigenic clay formation, grain contact dissolution and ductile grain compaction. Intergranular pores are sufficiently common to be moderately well interconnected, but permeability is limited by relatively fine grain size. K = 134mD
22	3212.0	Massive, moderately sorted, coarse grained lithic arkose in which intergranular spaces are commonly occupied by compacted ductile grains, authigenic clay and very minor siderite. Further porosity reduction results from grain contact dissolution. Intergranular pores are erratically distributed and thus have limited interconnection. K = 35.8mD
21	3218.0	Massive, moderately-well sorted, coarse grained subarkose with good intergranular porosity, despite porosity reduction by grain contact dissolution, authigenic clay formation, ductile grain compaction and very minor siderite cementation. Intergranular pores are evenly distributed and thus are well interconnected. K = 3150mD
19	3251.0	Massive, poorly sorted, coarse grained lithic arkose tightly cemented by dolomite. Negligible visible porosity. K = 2.71mD
17	3287.0	Massive, moderately sorted, coarse grained subarkose tightly cemented by dolomite. No visible porosity. K = 0.04mD
16	3299.0	Massive, moderately-well sorted, medium grained lithic arkose in which intergranular spaces are commonly occupied by authigenic clay and compacted ductile grains. Further porosity reduction results from grain contact dissolution and very minor quartz overgrowths. Intergranular pores are erratically distributed and thus have limited interconnection. K = 48.4mD
14	3306.5	Massive, moderately-well sorted, lower medium grained subarkose with little intergranular porosity due to widespread authigenic clay formation, ductile grain compaction and grain contact dissolution/microstylolitisation. Small primary intergranular pores are widely and erratically scattered and thus have very limited interconnectivity. Highly microporous. K = 12.4mD
12	3308.5	Massive, uncemented, moderately-well sorted, upper medium grained subarkose with good intergranular porosity, despite porosity reduction by grain contact dissolution and localised authigenic kaolinite formation. Sandstone was highly quartzose at the time of accumulation. Intergranular pores are evenly distributed and thus are well interconnected. K = 2090mD
11	3353.5	Moderately-well sorted, medium grained subarkose with localised stylolitic argillaceous/carbonaceous laminae and in which intergranular spaces are commonly occupied by authigenic clay, compacted ductile grains and thinly-developed quartz overgrowths. Common microstylolitic grain contacts. Intergranular pores are erratically distributed and thus have limited interconnection. K = 45.9mD

TABLE 5. RESERVOIR QUALITY SUMMARY (cont.)

Sample #	Depth (mRT)	Comments
7	3372.0	Massive, moderately-well sorted, upper medium grained subarkose in which intergranular spaces are commonly occupied by authigenic clay, compacted ductile grains and patchy dolomite. Further porosity reduction results from grain contact dissolution and thinly-developed quartz overgrowths. Intergranular pores are erratically distributed and thus have limited interconnection. K = 41.2mD
6	3409.0	Massive, moderately-well sorted, coarse grained subarkose with good intergranular porosity, despite porosity reduction by grain contact dissolution, authigenic clay formation, ductile grain compaction and minor quartz overgrowth cementation. Intergranular pores are fairly evenly distributed and thus are well interconnected. K = 1380mD
4	3439.0	Massive, moderately sorted, coarse grained subarkose in which intergranular spaces are commonly occupied by compacted ductile grains, authigenic clay and patchy dolomite. Further porosity reduction results from grain contact dissolution and thinly-developed quartz overgrowths. Intergranular pores are erratically distributed and thus have limited interconnection, but permeability is still moderate due to coarse grain size. K = 211mD
3	3449.0	Massive, moderately-well sorted, coarse grained sublitharenite in which intergranular spaces are commonly occupied by compacted ductile grains and authigenic clay. Further porosity reduction results from grain contact dissolution and thinly-developed quartz overgrowths, but the sandstone still contains modest intergranular porosity, which, together with coarse grain size, results in high permeability. K = 921mD

8. COMPARISON WITH MANTA-1 AND BASKER-1

Basker-5 petrology samples are compared to six samples from the Golden Beach Group in Manta-1 (3300.56-3307.73m) and six samples from the intra-Latrobe Group in Basker-1 (3108.47-3123.50m) that were petrologically analysed by Phillips (2000a,b).

Manta-1 samples are moderately to moderately-well sorted, medium to coarse grained sublitharenites, feldspathic litharenites and a litharenite with a mean grain size between 0.46mm and 0.68mm, whereas Basker-1 samples are poorly to moderately-well sorted, fine to medium grained feldspathic litharenites, a subarkose and a sublitharenite with a mean grain size between 0.21mm and 0.39mm. Basker-5 samples are poorly to well sorted, medium to coarse grained subarkoses, lithic arkoses and sublitharenites with a mean quartz grain size of 0.26-0.85mm and are thus more texturally varied and less lithic labile than the Manta-1 and Basker-1 sandstones (Fig. 1). Basker-1 and -5 sandstones generally contain significantly more feldspar than Manta-1 sandstones. Quartz grains are relatively angular in all three wells.

Framework grain types in Manta-1 and Basker-1 are identical to those in Basker-5, with the main framework grain types in all three wells being quartz, K-feldspar, metamorphic rock fragments and sedimentary rock fragments that are derived from a provenance dominated by granitic, low-grade metasedimentary and siliciclastic sedimentary rocks. Rock fragments in Manta-1 and Basker-1 are largely shale, whereas rock fragments in Basker-5 are mainly low-grade metasediments, but this difference may partly reflect the subjectivity in discriminating highly indurated/illitic shaley sedimentary rock fragments from low-grade meta-argillites and phyllites during point counting. In Manta-1, finer grained sandstones tend to be more lithic labile, but, in Basker-1 and -5, there is no well-defined correlation between grain size and rock fragment content.

Sandstones contain little or no detrital clay. Authigenic kaolinite and illite content in Basker-5 is far higher than in Manta-1 and Basker-1. XRD indicates that clay minerals are consistently dominated by kaolinite and illite and also include trace chlorite.

Diagenetic effects in Basker-5 (see Section 6) are similar to those in Manta-1 and Basker-1, although no Manta-1 and Basker-1 samples are tightly cemented by dolomite like #19 (3251.0m) and #17 (3287.0m) from Basker-5, with dolomite not exceeding 5.4% in Manta-1 and 2.6% in Basker-1. Quartz overgrowth cement content is consistently low, being 2.2-5.6% in Manta-1, 1.0-4.0% in Basker-1 and 0-3.6% in Basker-5. Although diagenetic effects are similar in each well, there is some variation in the interpreted diagenetic paragenesis for each well.

Visible porosity is 8.4-12.4% in Manta-1, 5.8-18.2% in Basker-1 and 0-21.0% in Basker-5. In all three wells, visible porosity is mainly primary and intergranular and also includes secondary intergranular and intragranular porosity that results mostly from labile grain (especially K-feldspar) dissolution.

Permeability does not exceed 100mD in Manta-1 and 200mD in Basker-1 and ranges up to 3150mD in Basker-5. In all three wells, ductile grain + clay content is a major control on reservoir quality. In addition, grain size and permeability are strongly positively correlated in Manta-1 and Basker-1, but are only weakly correlated in Basker-5. Cement (dolomite) significantly impacts reservoir quality only at 3251.0m and 3287.0m in Basker-5.

9. SUMMARY AND CONCLUSIONS

- Samples from 3192.0-3449.0m in Basker-5 are variably sorted, medium to coarse grained subarkoses, lithic arkoses and sublitharenites in which framework grains are mainly quartz, K-feldspar, low-grade metasedimentary rock fragments and siliciclastic sedimentary rock fragments. There are no significant depth- and grain-size-related trends in detrital composition.

- Detrital grain assemblages indicate a nearby polymictic provenance dominated by granitic, metasedimentary and sedimentary rocks and which also included felsic volcanics. Provenance did not change during accumulation of the section, although there were temporal fluctuations in the amount of quartzose detritus and lithic-labile detritus that entered the basin.

- Clay content generally increases with decreasing grain size. Clay is mainly authigenic kaolinite that forms patchy and dispersed, microporous pseudomatrix and deformed, mica-like grains where labile grains have altered. Authigenic clay also includes illite that occurs as an intermediate decomposition product of micaceous/argillaceous grains. Sandstones contain little or no detrital clay. Clay minerals detected by XRD are kaolinite, illite and trace chlorite.

- Sandstones at 3251.0m and 3287.0m are tightly cemented by late-stage dolomite.

- The main diagenetic effects besides authigenic clay formation and localised dolomite cementation include physical compaction, grain contact dissolution, and labile grain dissolution. Quartz overgrowth content does not exceed 3.6%.

- Diagenetic effects and paragenesis are identical in water-, oil- and gas-bearing sandstones, suggesting that hydrocarbon entrapment occurred late in the diagenetic history.

- Visible porosity is variable. Two tightly dolomite-cemented sandstones (3251.0m, 3287.0m) contain less than 0.3% visible porosity. The other sandstones contain 1.5-21.0% visible porosity, the amount of which varies largely according to clay + metamorphic/sedimentary rock fragment content. Visible porosity is mainly primary and intergranular and also includes scattered secondary pores that result from labile grain dissolution.

- Permeability variation (0.04-3150mD) mostly reflects differences in clay + metamorphic/sedimentary rock fragment content and, to a lesser extent, grain size. Grain size only weakly influences permeability because grain size and clay + metamorphic/sedimentary rock fragment content are poorly correlated. Low permeability at 3251.0m and 3287.0m results from dolomite cementation.

- Sediment composition, diagenetic effects and controls on reservoir quality are similar to those in Manta-1 and Basker-5, although high dolomite contents were recorded only in Basker-5.

REFERENCES

Botha, P. and Butcher, A. R., 2006a, QEMSCAN analysis of 7 Side Wall Cores from Basker #5. Report to ANZON Australia Ltd. (Included in Appendix 2 of this report)

Botha, P. and Butcher, A. R., 2006b, QEMSCAN analysis of 8 Cuttings Samples from Basker #5. Report to ANZON Australia Ltd. (Included in Appendix 2 of this report)

Phillips, S. E., 2000a, Petrology report - Manta-1, Gippsland Basin. Report to Woodside Energy Ltd.

Phillips, S. E., 2000b, Petrology report - Basker-1, Gippsland Basin. Report to Woodside Energy Ltd.

(i) Appendix 1 - X-Ray Diffraction Traces

APPENDIX 1

X-RAY DIFFRACTION TRACES

Key to abbreviations:

C = chlorite
Do = dolomite
I = illite/mica
K = kaolinite
KCl = potassium chlorite (contaminant)
KF = K-feldspar
Q = quartz
S = siderite

#23 3206.0m
Bulk rock

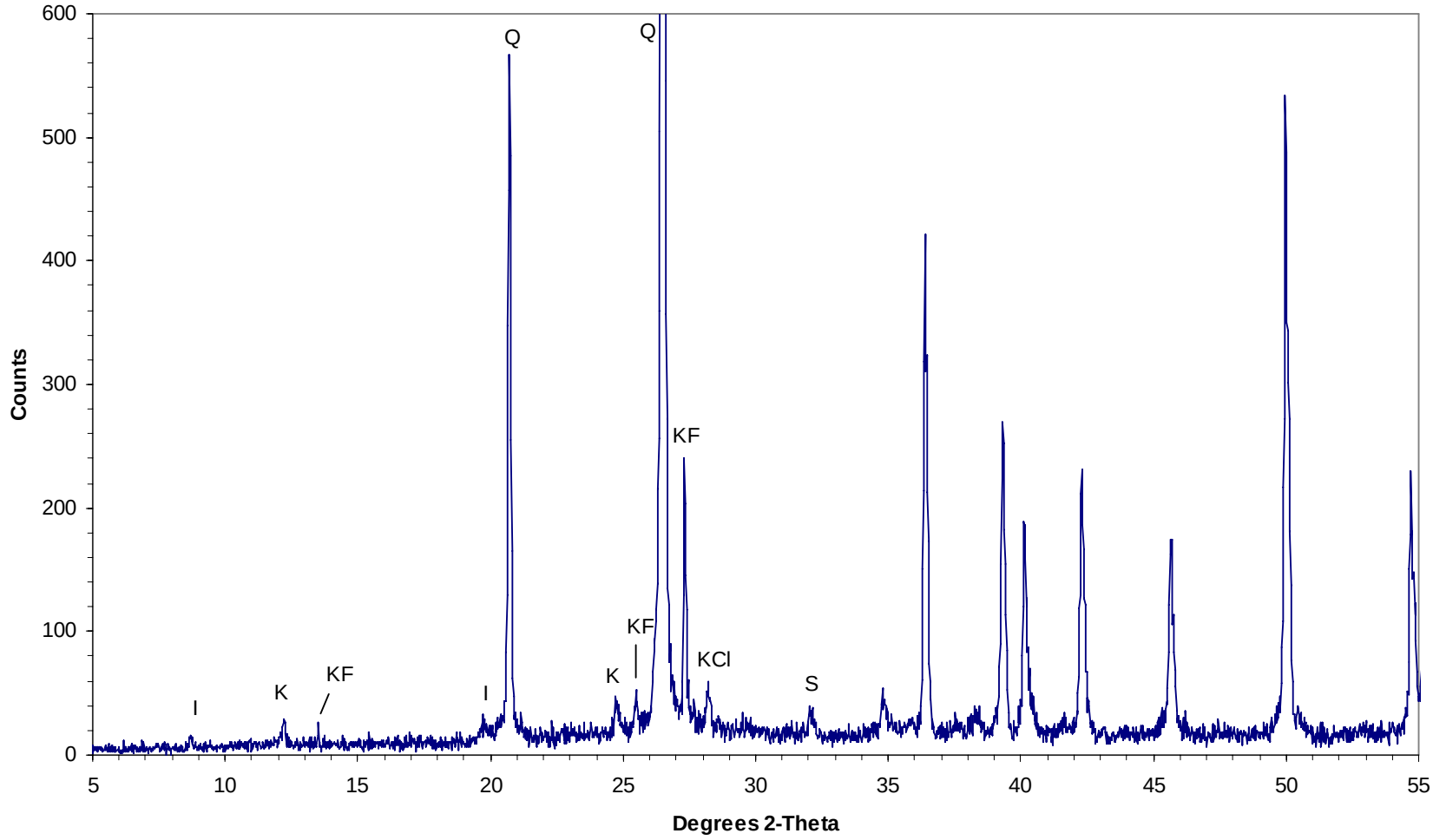

ACS Laboratories Pty Ltd
ABN: 81 008 273 005

#23 3206.0m
Fine fraction

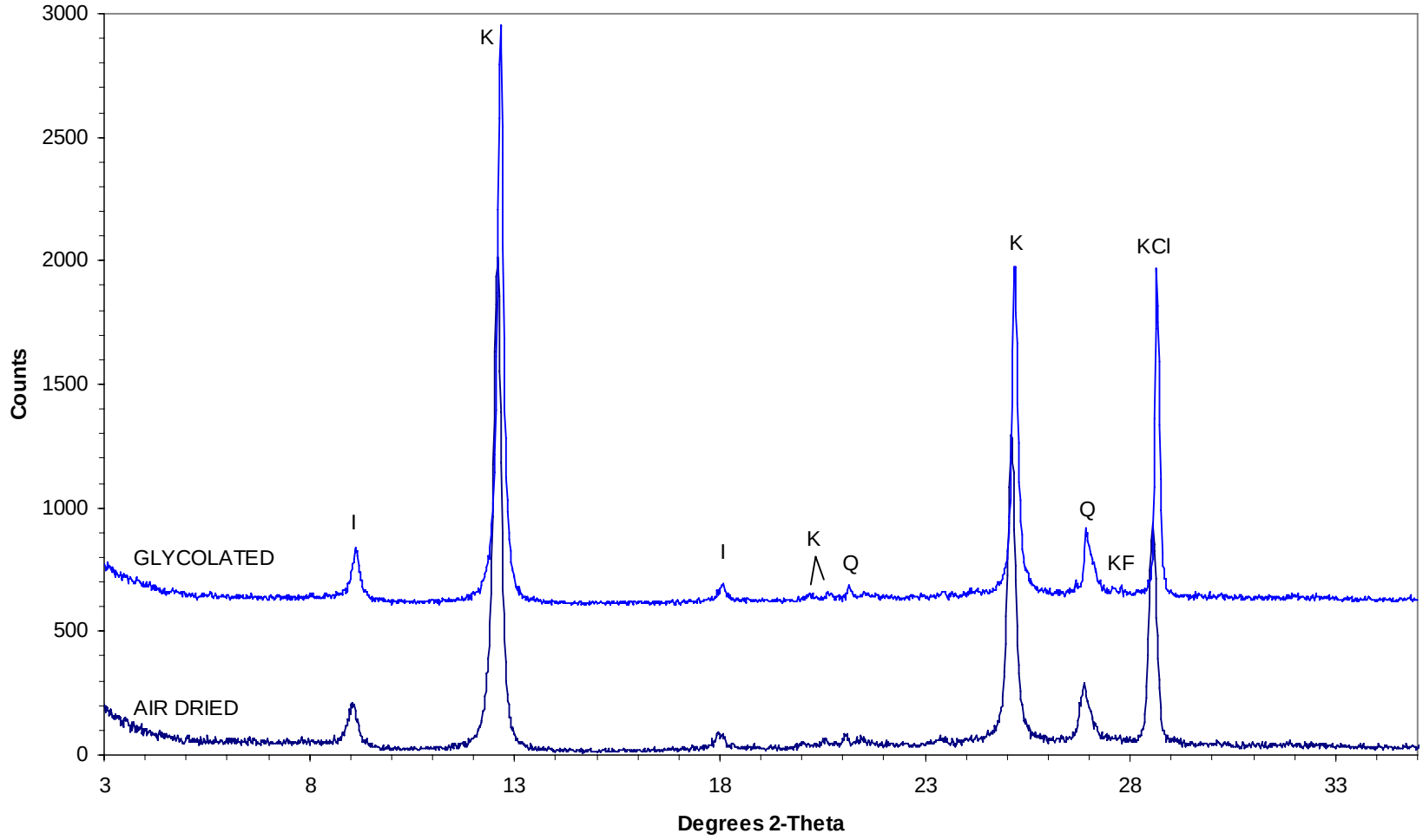

ACS Laboratories Pty Ltd
ABN: 81 008 273 005

#21 3218.0m
Bulk rock

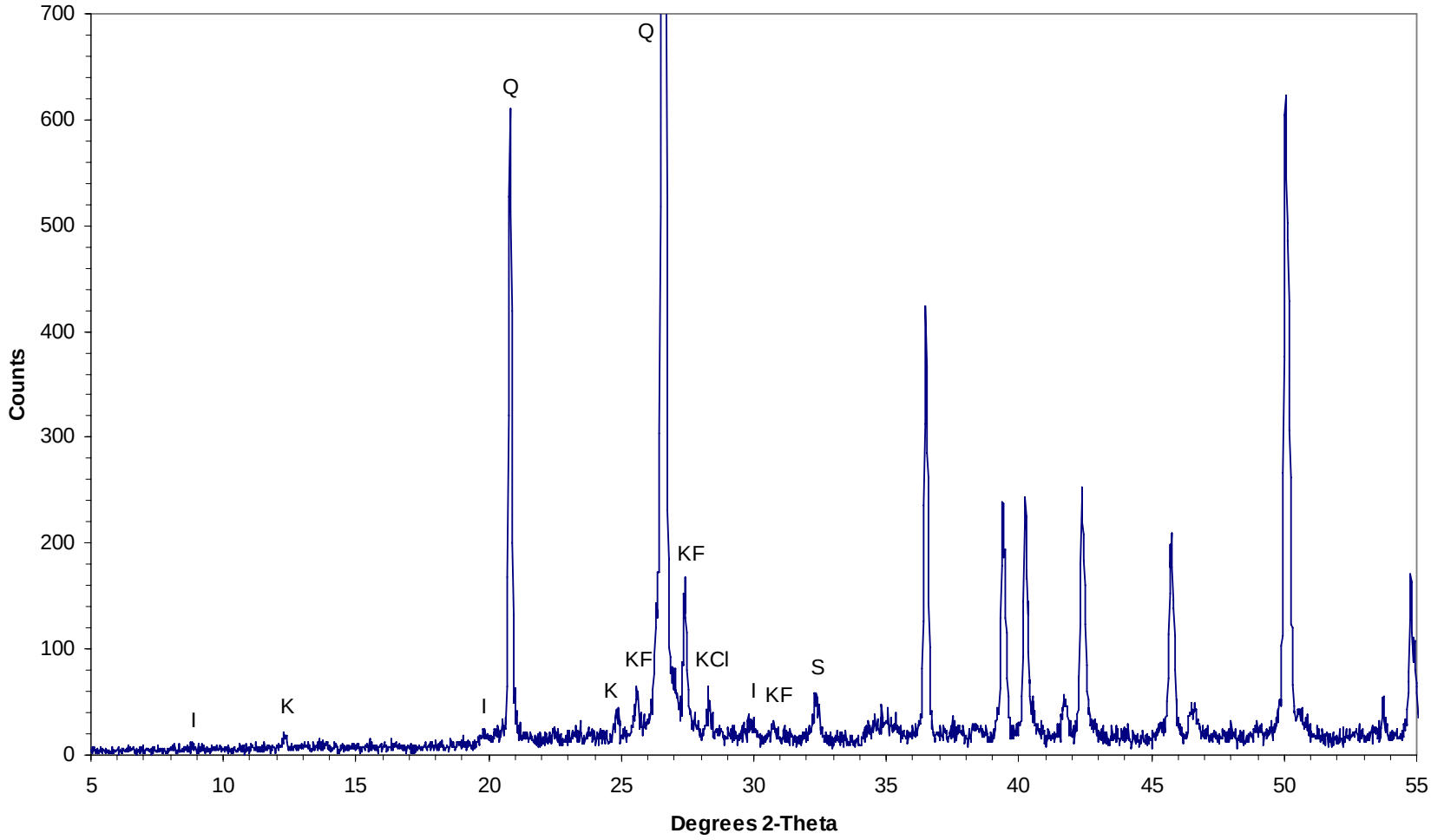

ACS Laboratories Pty Ltd
ABN: 81 008 273 005

#21 3218.0m
Fine fraction

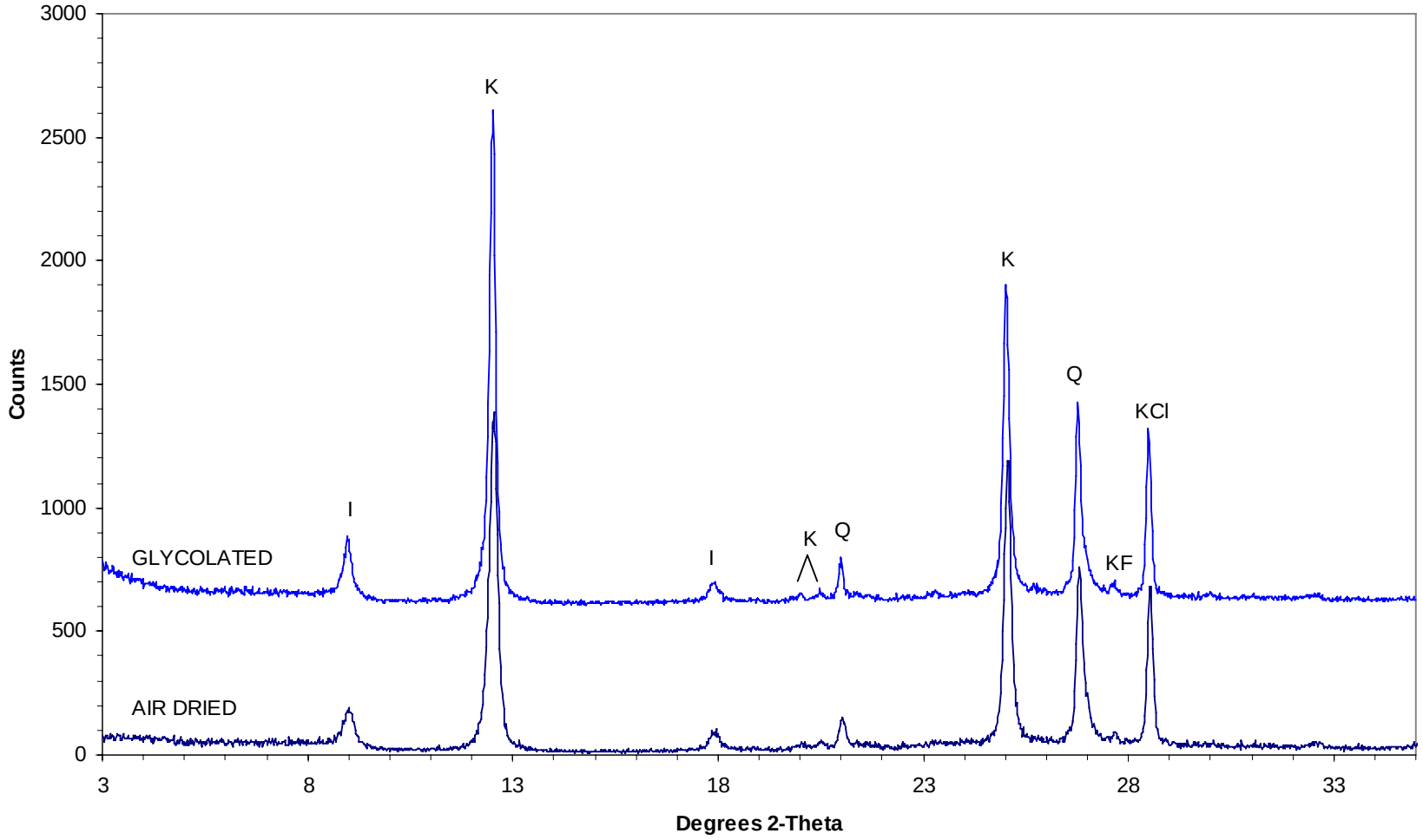

ACS Laboratories Pty Ltd
ABN: 81 008 273 005

#19 3251.0m
Bulk rock

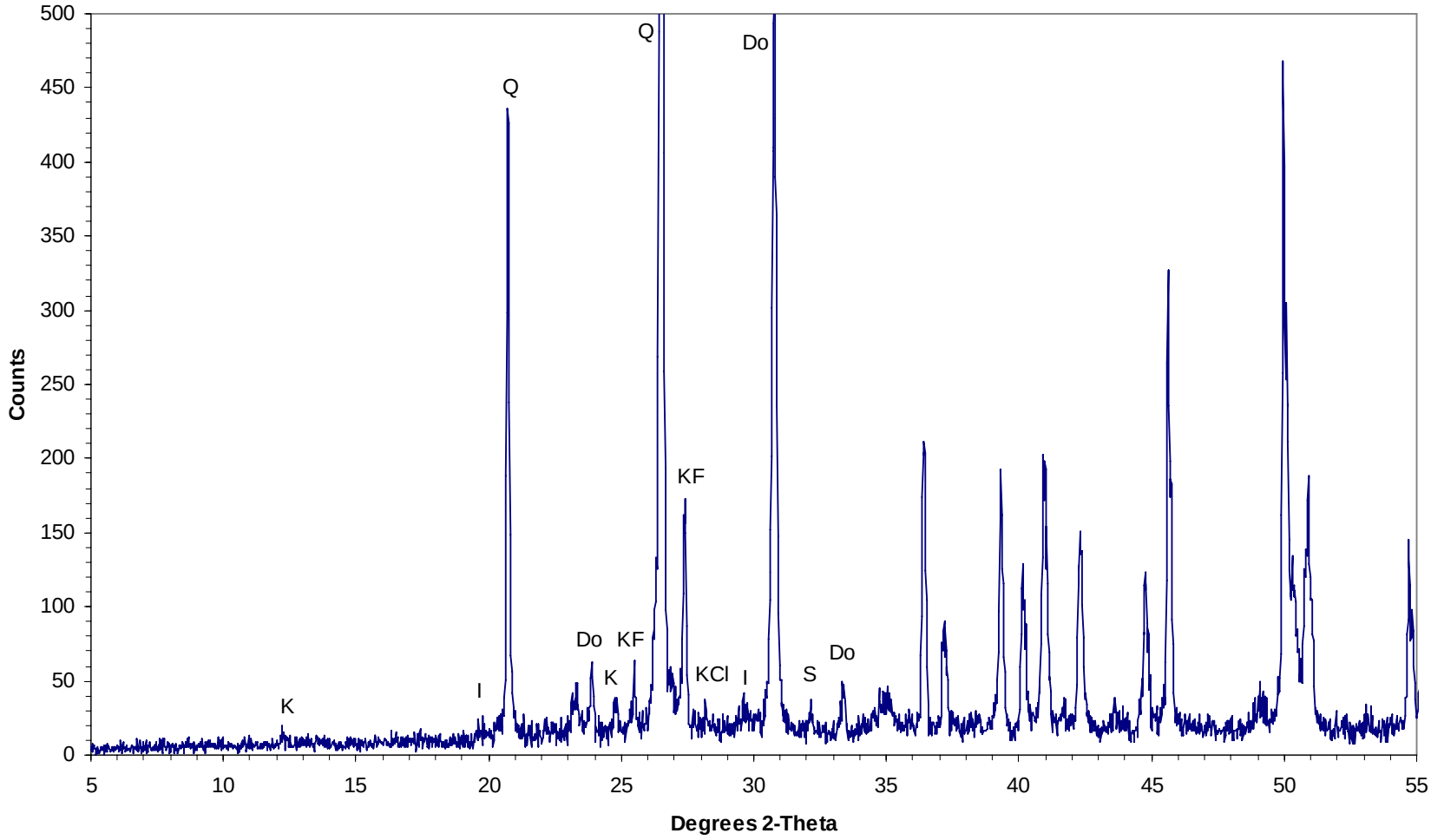

ACS Laboratories Pty Ltd
ABN: 81 008 273 005

#19 3251.0m
Fine fraction

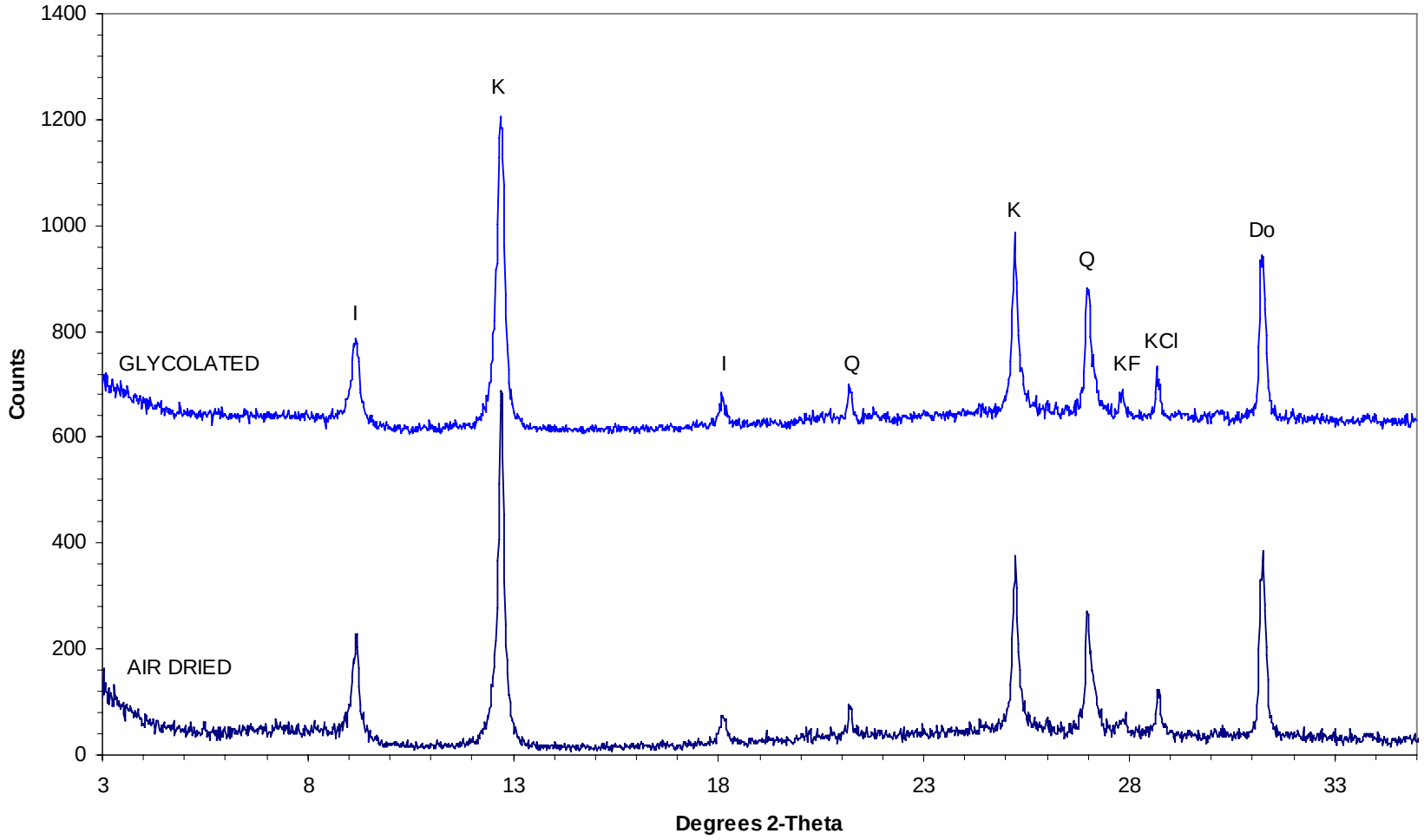

ACS Laboratories Pty Ltd
ABN: 81 008 273 005

#16 3299.0m
Bulk rock

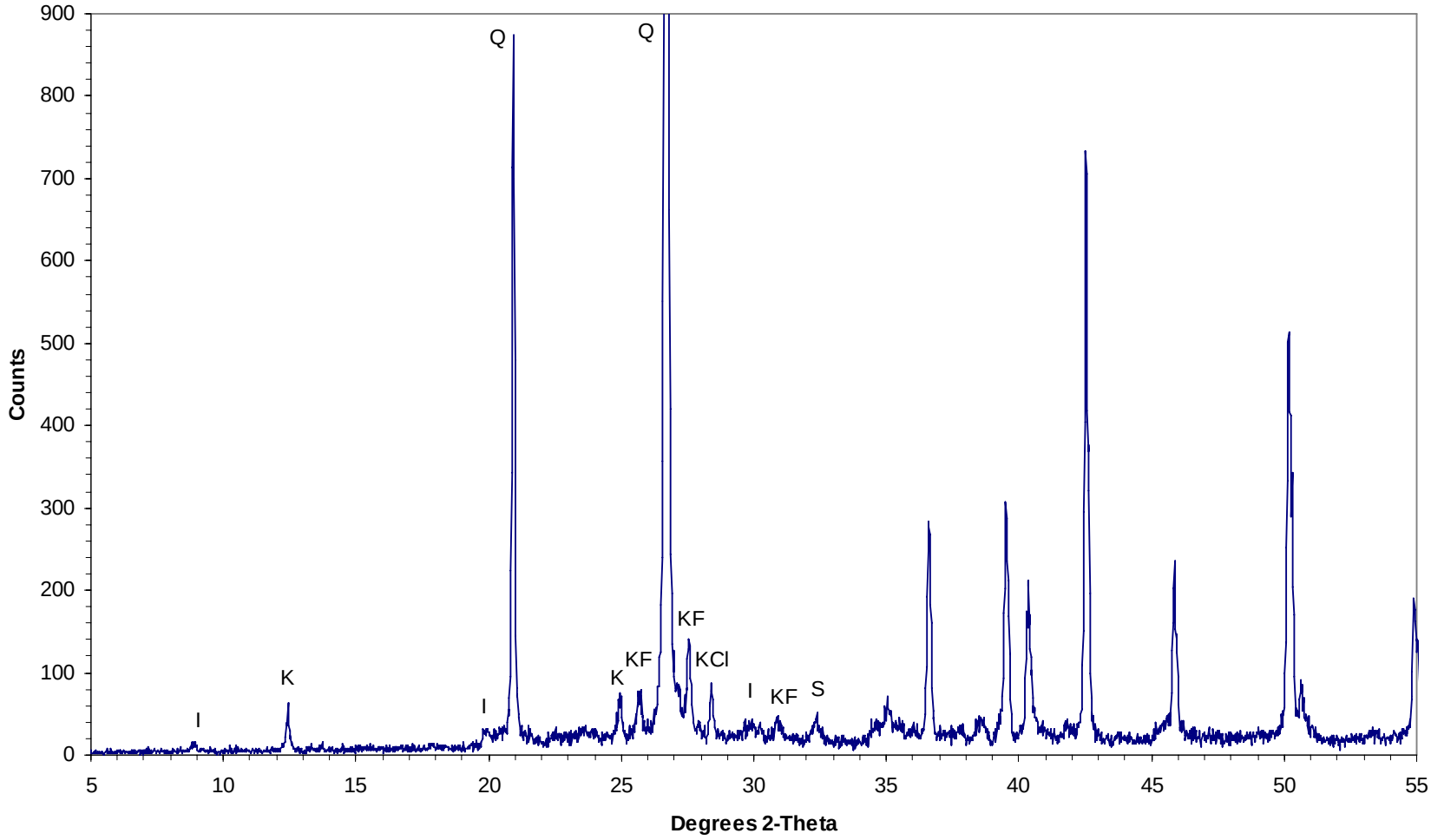

ACS Laboratories Pty Ltd
ABN: 81 008 273 005

#16 3299.0m
Fine fraction

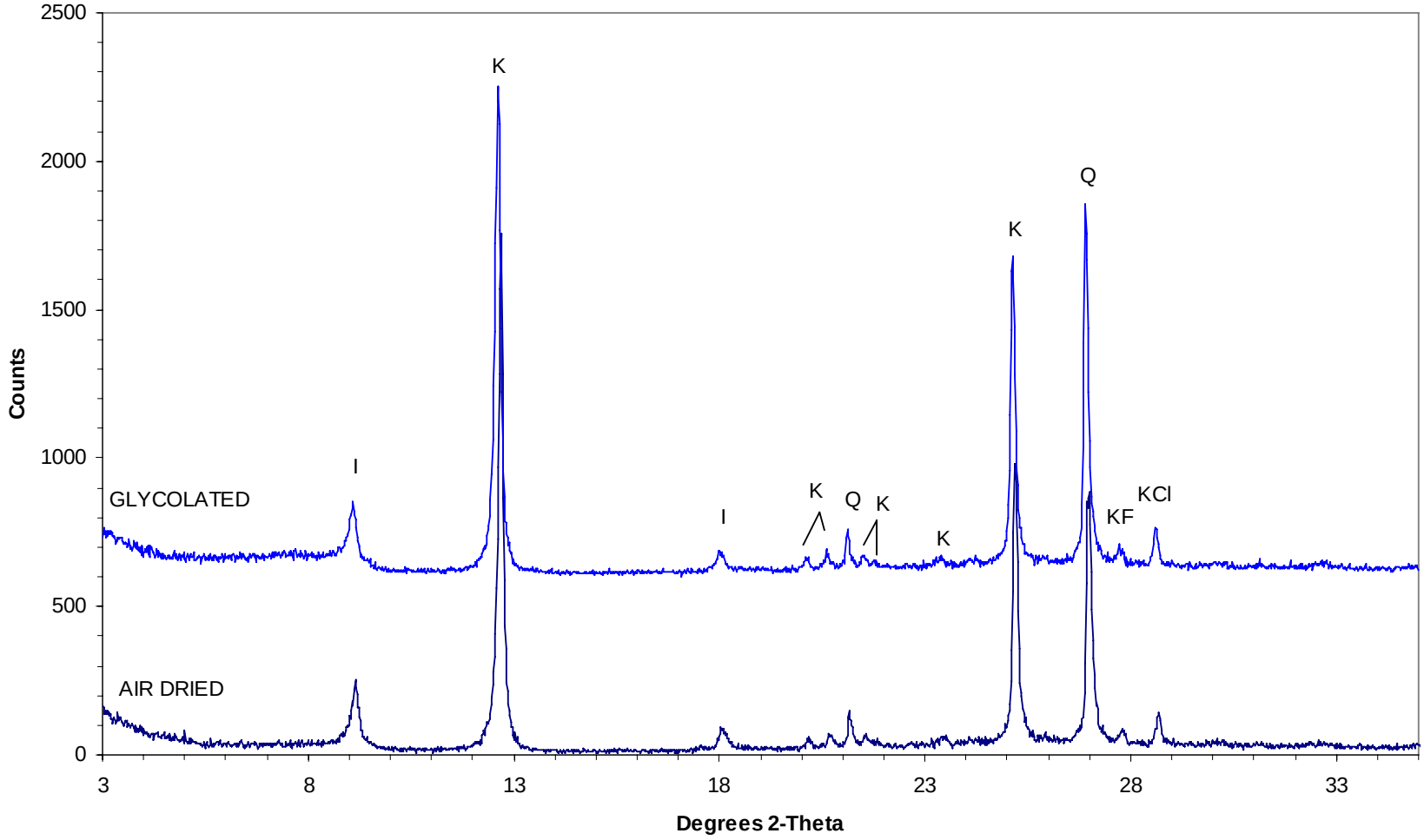

ACS Laboratories Pty Ltd
ABN: 81 008 273 005

#14 3306.5m
Bulk rock

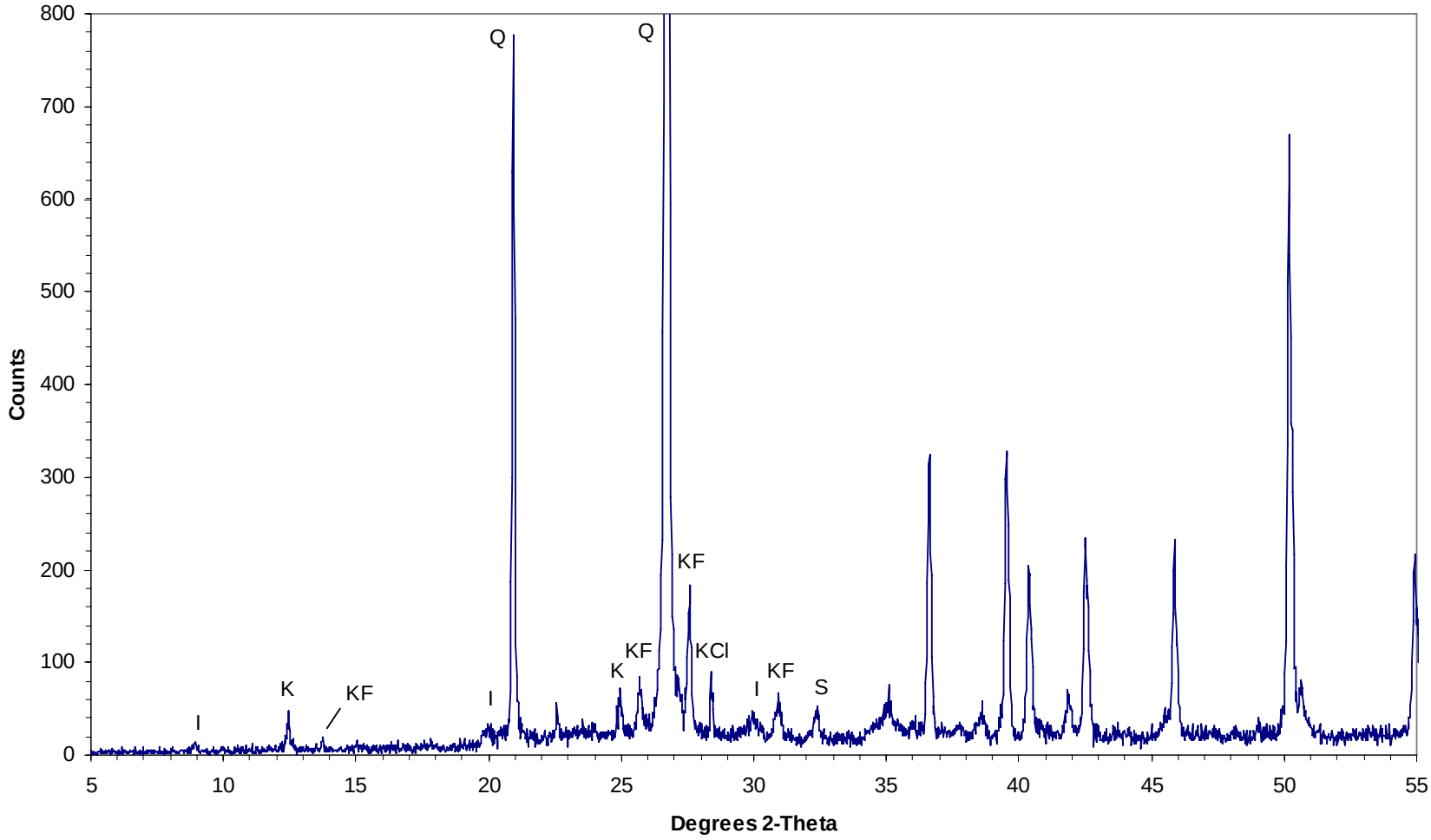

ACS Laboratories Pty Ltd
ABN: 81 008 273 005

#14 3306.5m
Fine fraction

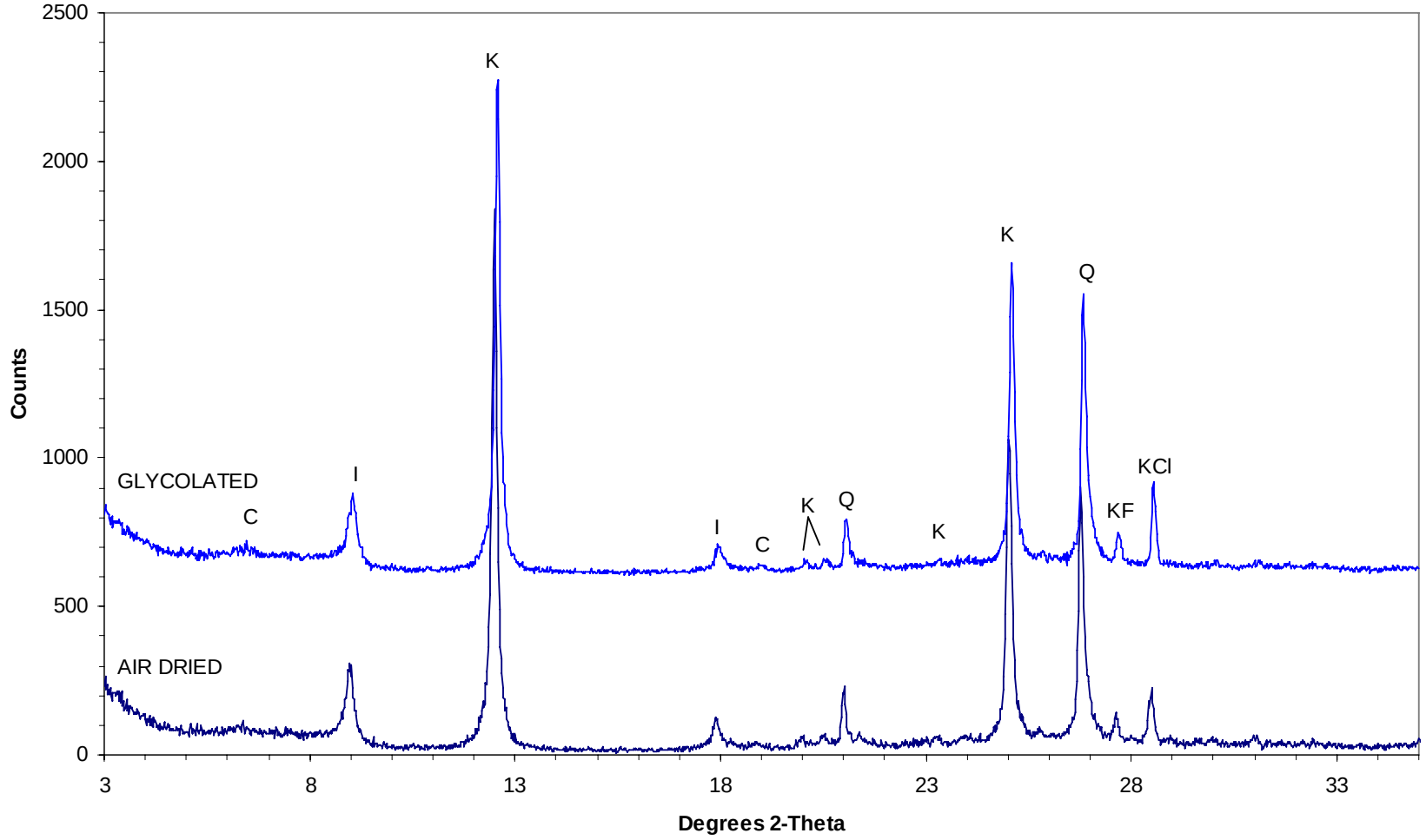

ACS Laboratories Pty Ltd
ABN: 81 008 273 005

#12 3308.5m
Bulk rock

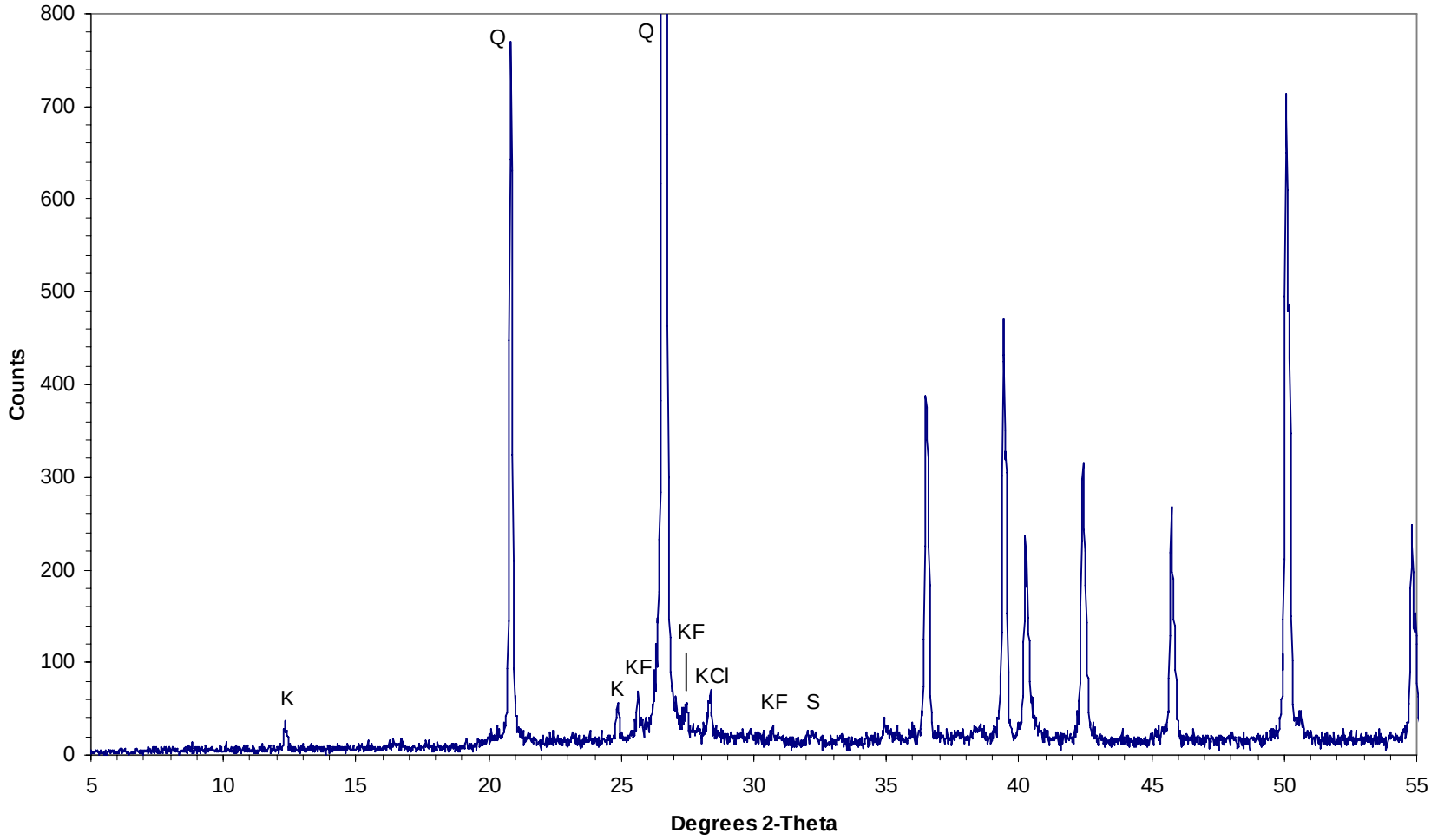

ACS Laboratories Pty Ltd
ABN: 81 008 273 005

#12 3308.5m
Fine fraction

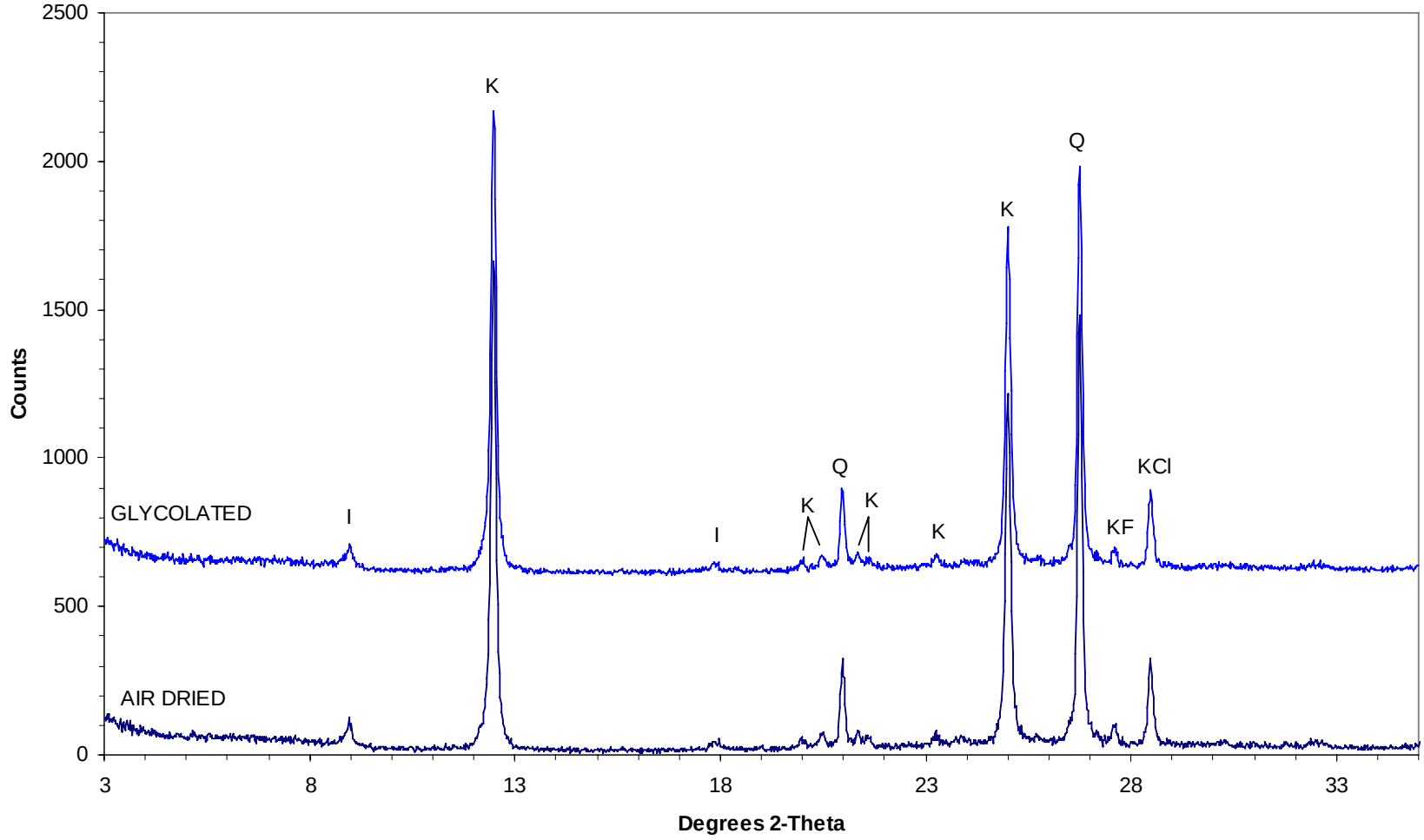

ACS Laboratories Pty Ltd
ABN: 81 008 273 005

#11 3353.5m
Bulk rock

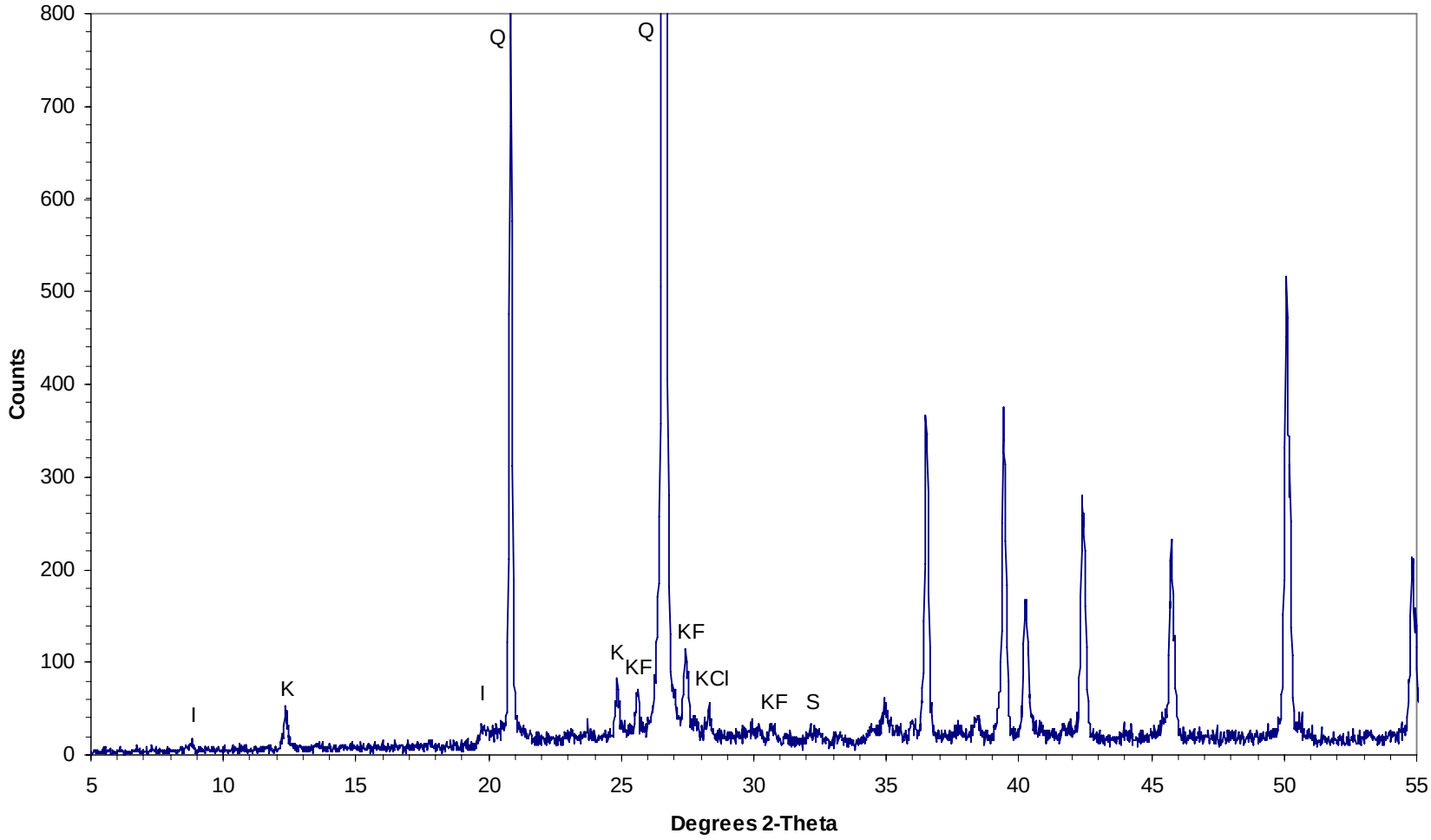

ACS Laboratories Pty Ltd
ABN: 81 008 273 005

#11 3353.5m
Fine fraction

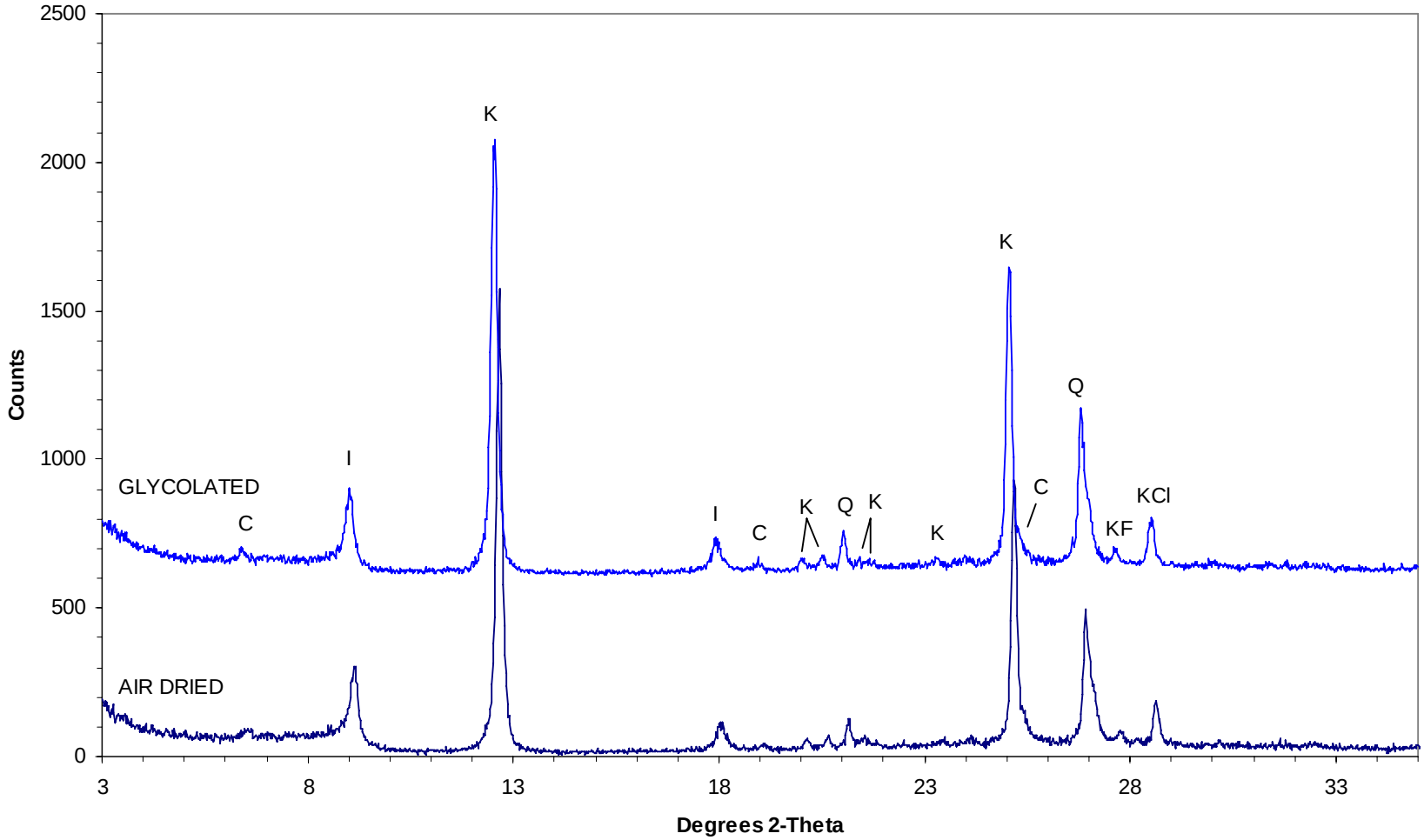

ACS Laboratories Pty Ltd
ABN: 81 008 273 005

#7 3372.0m
Bulk rock

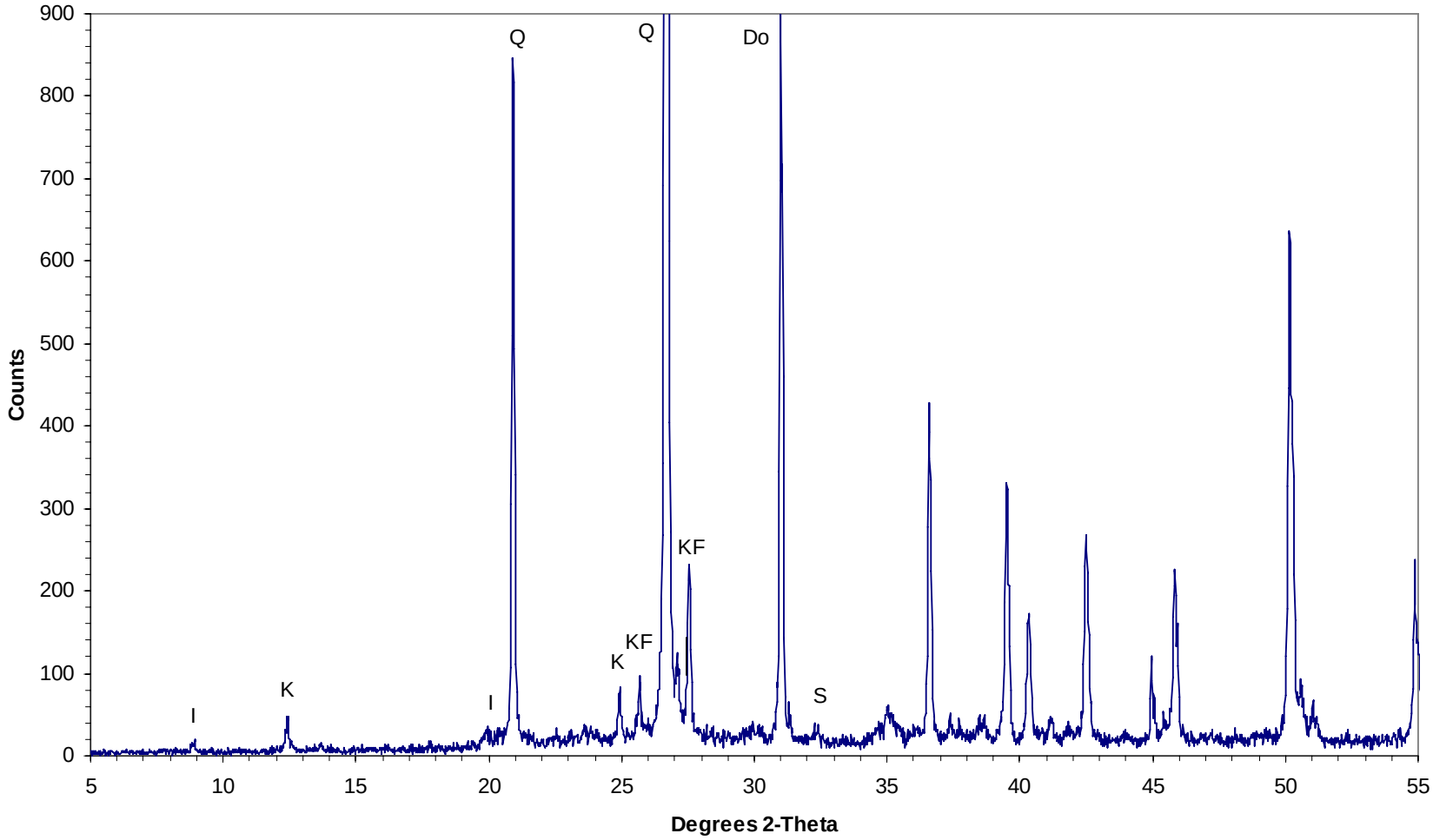

ACS Laboratories Pty Ltd
ABN: 81 008 273 005

#7 3372.0m
Fine fraction

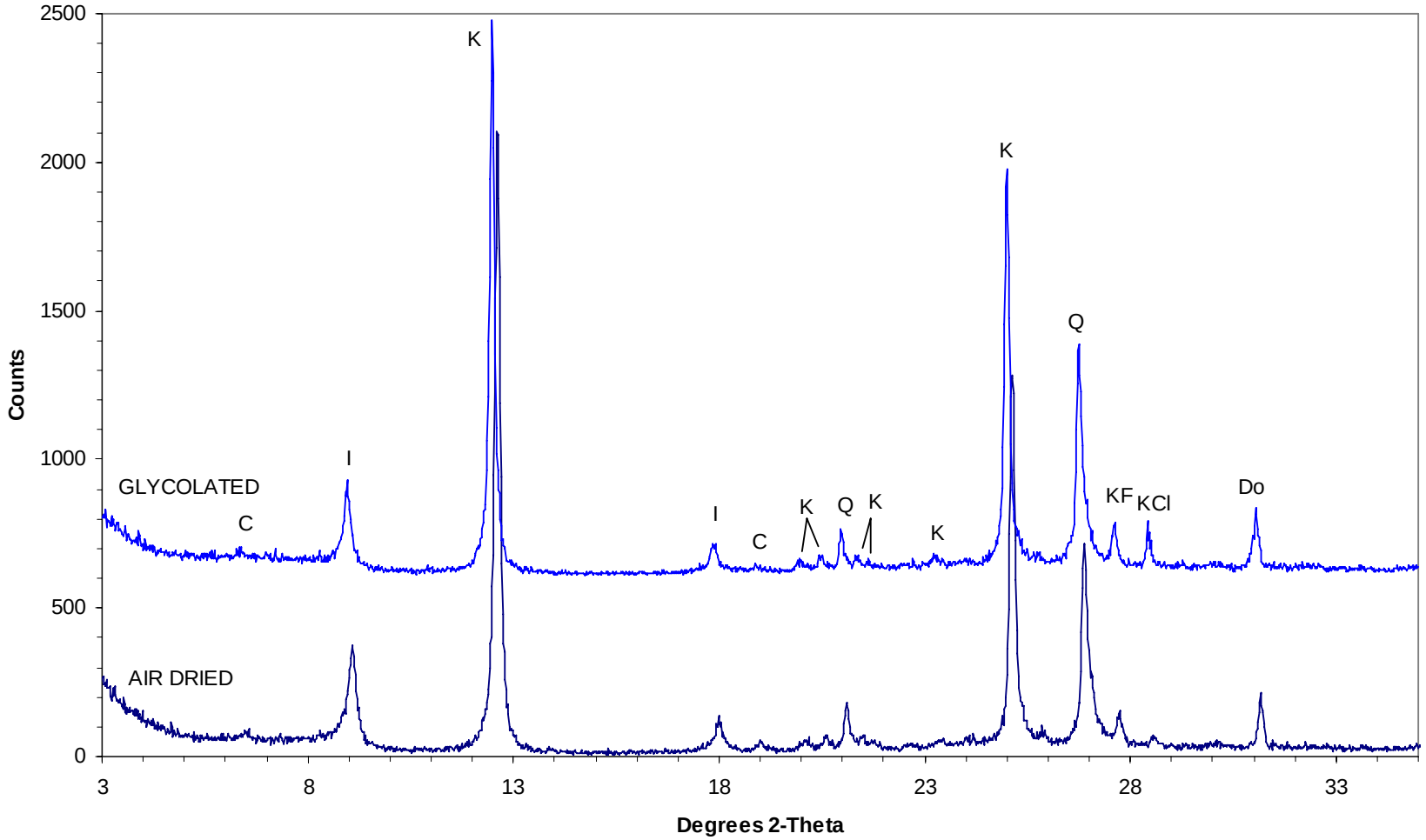

ACS Laboratories Pty Ltd
ABN: 81 008 273 005

(ii) Appendix 2 – QEMSCAN Reports

APPENDIX 2

QEMSCAN REPORTS

Thin-section modal analyses for seven samples analysed in this study are compared to quantitative mineralogical data obtained by Intellection Pty Ltd for the same samples using QEMSCAN. QEMSCAN technique details and QEMSCAN results for the seven samples and for additional cuttings samples from 3350-3500m in Basker-5 are given in Botha & Butcher (2006a,b). Both reports are included in this appendix.

Results are shown for each technique in Table 1. Thin-section analyses are re-calculated to exclude visible porosity since QEMSCAN analyses exclude porosity.

For one highly quartzose sandstone (#12, 3308.5m), there is excellent agreement between thin-section and QEMSCAN analyses. For the other samples, there is good correspondence between analyses for some minerals (K-feldspar, kaolinite, mica/illite, siderite), but there are significant differences between analyses for quartz and, in the case of #19 (3251.0m), dolomite.

Discrepancies (2.8-19.7%) between quartz analyses are largely due to the presence of common quartzose rock fragments, which are counted in the "others" category in the thin-section analyses and as their individual mineral constituents in the QEMSCAN analyses.

It is likely that the large discrepancy (17.6%) between thin-section and QEMSCAN dolomite analyses for #19 results from dolomite being unevenly distributed through the sample, with a repeat thin-section point count analysis of #19 confirming the accuracy of the dolomite thin-section analysis for this sample.

It is concluded that QEMSCAN is an excellent complementary technique for not only characterising and quantifying reservoir sandstone mineralogy, but also for providing clear, detailed images (mineral maps) showing texture and mineral/porosity distribution over relatively large (centimetre scale) areas. It appears that porosity can also be measured quite accurately with QEMSCAN (see last table in Botha & Butcher, 2006a) provided that care is taken to recognise and exclude artifact porosity that results from grain/clay plucking during sample preparation.

TABLE 1. MODAL ANALYSES COMPARISON (%)

Sample #	Depth (mRT)	Technique	Qtz	KF	Ka	M/I	Do	Sid	Cal	Oth
23	3206.0	thin-section	79.6	4.0	8.0	1.9	-	1.2	-	5.3
		QEMSCAN	86.7	4.1	6.4	1.0	-	0.7	-	1.0
21	3218.0	thin-section	76.5	9.4	3.0	0.4	-	2.4	-	8.3
		QEMSCAN	79.3	12.2	3.6	1.2	-	2.8	-	0.9
19	3251.0	thin-section	50.1	12.4	1.1	0.6	30.0	0.3	-	5.5
		QEMSCAN	69.8	12.7	2.9	1.1	12.4	0.2	0.3	0.5
16	3299.0	thin-section	63.9	12.5	8.1	2.5	-	0.3	-	12.7
		QEMSCAN	76.7	13.3	7.3	1.2	-	0.6	-	0.8
12	3308.5	thin-section	89.1	4.1	2.9	-	-	1.5	-	2.4
		QEMSCAN	91.5	4.1	3.1	0.5	-	0.4	-	0.6
11	3353.5	thin-section	70.2	7.6	9.5	1.1	-	-	-	11.6
		QEMSCAN	80.3	8.7	7.9	1.7	-	0.2	-	1.0
7	3372.0	thin-section	69.2	10.5	6.8	2.2	3.1	0.3	-	7.9
		QEMSCAN	77.5	12.5	6.7	1.1	0.9	0.1	0.3	0.8

Qtz = quartz; KF = K-feldspar; Ka = kaolinite; M/I = mica/illite; Do = dolomite; Sid = siderite; Cal = calcite: Oth = others (mainly rock fragments in the case of the thin-section analyses)

Intellection Pty Ltd
2/27 Mayneview Street Milton Qld 4064
PO Box 1636 Milton Qld 4064 Australia
Tel +61 7 3512 9100 Fax +61 7 3512 9199
ABN 58 105 166 354
www.intellection.com.au

Report #: AD AATA/5325

September 2006

Anzon Australia Ltd,
Suite 504, 165 Walker St,
North Sydney, 2060,
NSW, Australia

QEMSCAN Analysis of 7 Side Wall Cores from Basker #5

Client:

Barry Messent

Anzon Australia Ltd

Authors:

Pieter Botha

Dr Alan R. Butcher

Intellection Pty Ltd

Table of contents

1. Introduction 3
2. Samples 4
3. QEMSCAN Measurement 5
4. Results 6
4.1 Mineral Key 6
4.2 Sample # 23: 3206.0 m 7
4.3 Sample # 21: 3218.0 m 9
4.4 Sample # 19: 3251.0 m 11
4.5 Sample # 16: 3299.0 m 13
4.6 Sample # 12: 3308.5 m 15
4.7 Sample # 11: 3353.5 m 17
4.8 Sample # 7: 3372.0 m 19
Summary 21

1. Introduction

Intellection was supplied with 7 side wall core samples taken from Basker # 5 for analysis by QEMSCAN. The aim of the study was to use QEMSCAN to measure the core samples and gather quantitative data on the mineralogy and texture of the rocks.

QEMSCAN is an automated SEM-based (Scanning Electron Microscope) system that uses a combination of Energy Dispersive X-Ray (EDX) spectra and Backscattered Electrons (BSE) to identify the minerals present and produce false-colour digital mineral maps of cuttings, or cores. These digital images are used for quantitative analysis of textural information, such as grain size and mineral association, as well as providing the modal abundance of minerals. For further information on QEMSCAN, the reader is referred to www.intellection.com.au or the authors of this report.

Initial results were discussed during a meeting between Dr Julian Baker (Reservoir Solutions and consultant to ACS Laboratories) and the authors on 11 September 2006 at Intellection's offices in Milton, Brisbane, Australia.

2. Sample Presentation Details

Standard sample preparation procedures were followed, with the sample being first mounted in epoxy resin, cut back and polished using Struers polishing equipment, before being carbon coated to establish electrical conductivity. Details of the samples are provided below (Table 1).

Table 1. Details of the samples supplied, their depth and the QEMSCAN reference code.

Sample #	Depth (m)	QEMSCAN Code
23	3206	AATA G0A
21	3218	AATA F0A
19	3251	AATA E0A
16	3299	AATA D0A
12	3308.5	AATA C0A
11	3353.5	AATA B0A
7	3372	AATA A0A

3. QEMSCAN Measurement

All seven samples were measured using identical measurement parameters in FieldImage mode of QEMSCAN measurement. This method places a series of frames (the size of which are determined by the operator) across the surface of the sample. Each frame is measured on a grid of points, with an EDX spectra and BSE value being collected and saved from each point, allowing an individual mineral or phase identification to be made for each. The distance between each measurement point (pixel spacing) is determined by the operator prior to the start of a measurement in microns. Every pixel seen in the final image represents an individual measurement and therefore mineral or phase identification. Each frame is measured in this manner sequentially, and all are then stitched together using iDiscover software to create a mosaic composite image of the entire area.

All 7 samples were measured using a field size of 3000 µm and a point spacing of 15 µm.

4. QEMSCAN Analysis Results

These data are presented on a sample-by-sample basis, followed by a summary comparison of all samples. Mosaic FieldImage mineral maps, along with the quantification of the modal mineralogy and textural information are also provided. The shape of the mosaic created by a FieldImage is a result of the individual frames being stitched together.

4.1 Mineral Key to Mineral Maps

The minerals and phases reported here are shown in Figure 1. Where a mineral name is given, the mineral has been positively identified based on its unique chemical composition and BSE brightness. Groups with names based on their chemical composition contain phases found that may have non-unique chemical compositions. *Others* contain other minerals and phases occurring in trace amounts.

Figure 1. Mineral and phase key to QEMSCAN mineral maps in this report.

4.2 Sample # 23: 3206.0 m

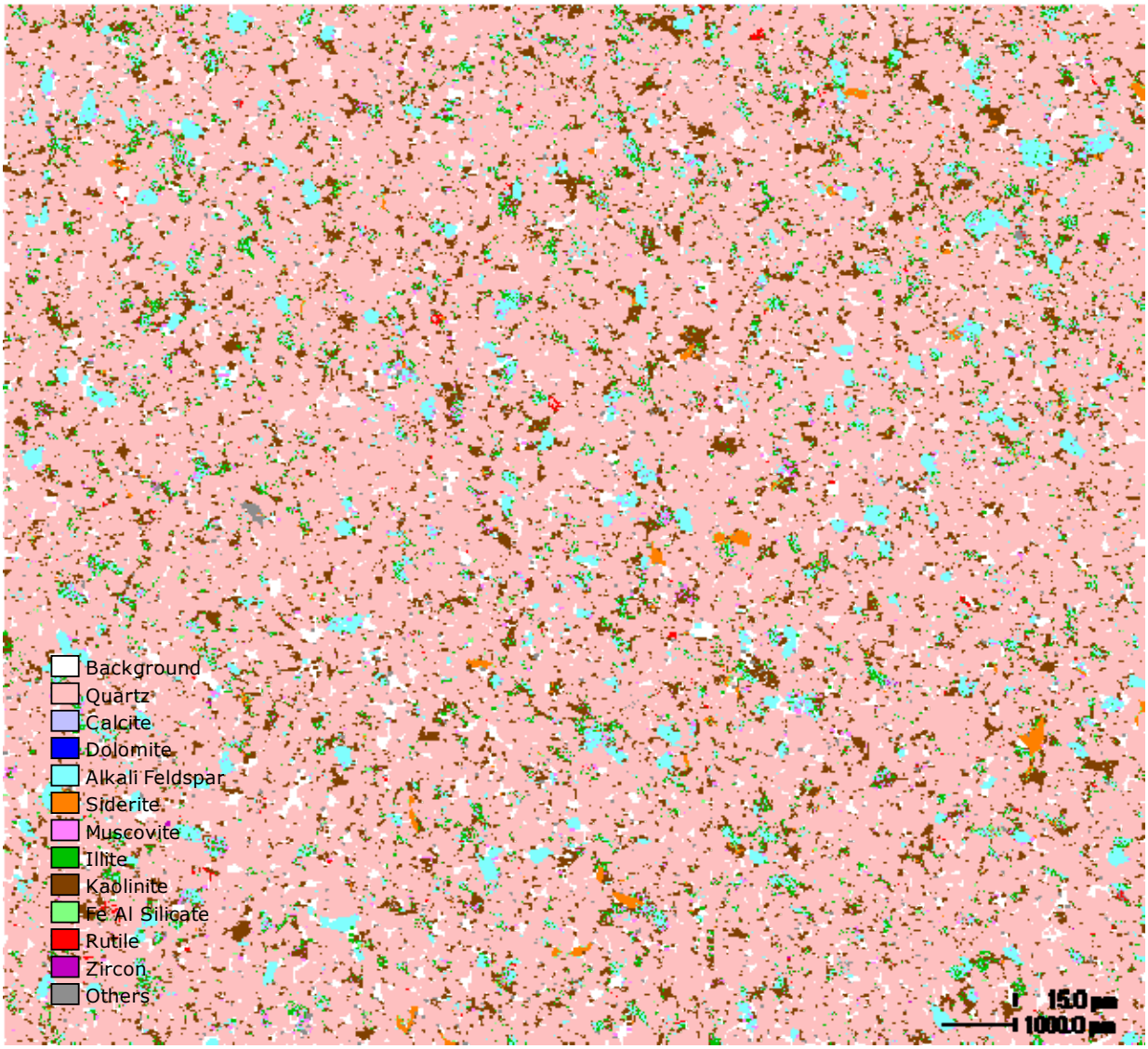

Figure 2. QEMSCAN mineral map of Sample # 23, 3206.0 m.

Table 2: Table showing the modal proportions of minerals as determined by QEMSCAN in Sample # 23, 3206.0 m.

Mineral	Sample
	Basker-5 (23) 3206m
Quartz	86.7
Calcite	0.0
Dolomite	0.0
Alkali Feldspar	4.1
Siderite	0.7
Muscovite	0.9
Illite	0.1
Kaolinite	6.4
Fe Al Silicate	0.5
Rutile	0.0
Zircon	0.0
Others	0.5

4.3 Sample # 21: 3218.0 m

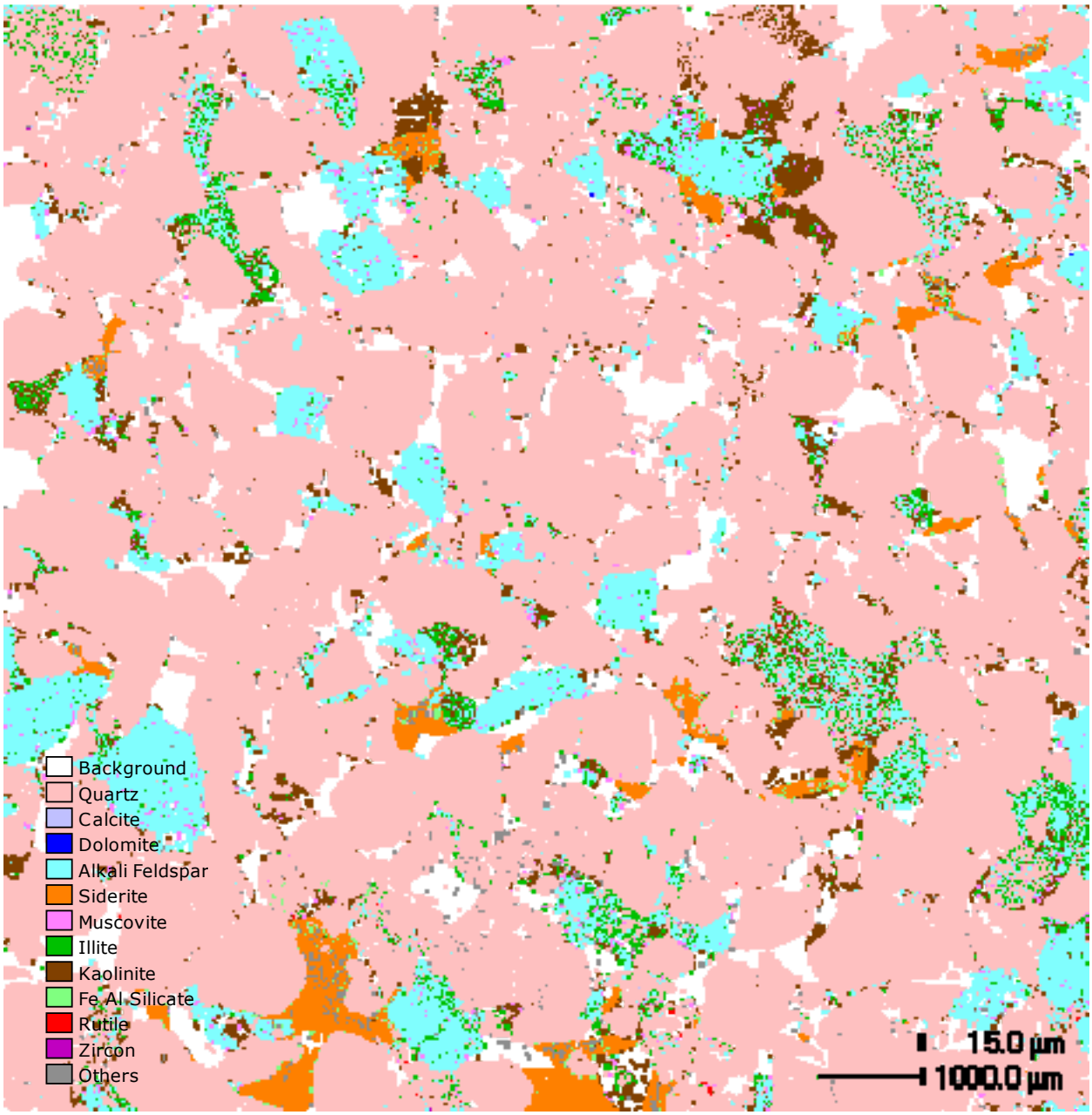

Figure 3. QEMSCAN mineral map of Sample # 21: 3218.0 m.

Table 3. Table showing the modal proportions of minerals as determined by QEMSCAN in Sample # 21: 3218.0 m.

Minerals	Sample
	Basker-5 (21) 3218m
Quartz	79.3
Calcite	0.0
Dolomite	0.0
Alkali Feldspar	12.2
Siderite	2.8
Muscovite	1.0
Illite	0.2
Kaolinite	3.6
Fe Al Silicate	0.3
Rutile	0.0
Zircon	0.0
Others	0.6

4.4 Sample # 19: 3251.0 m

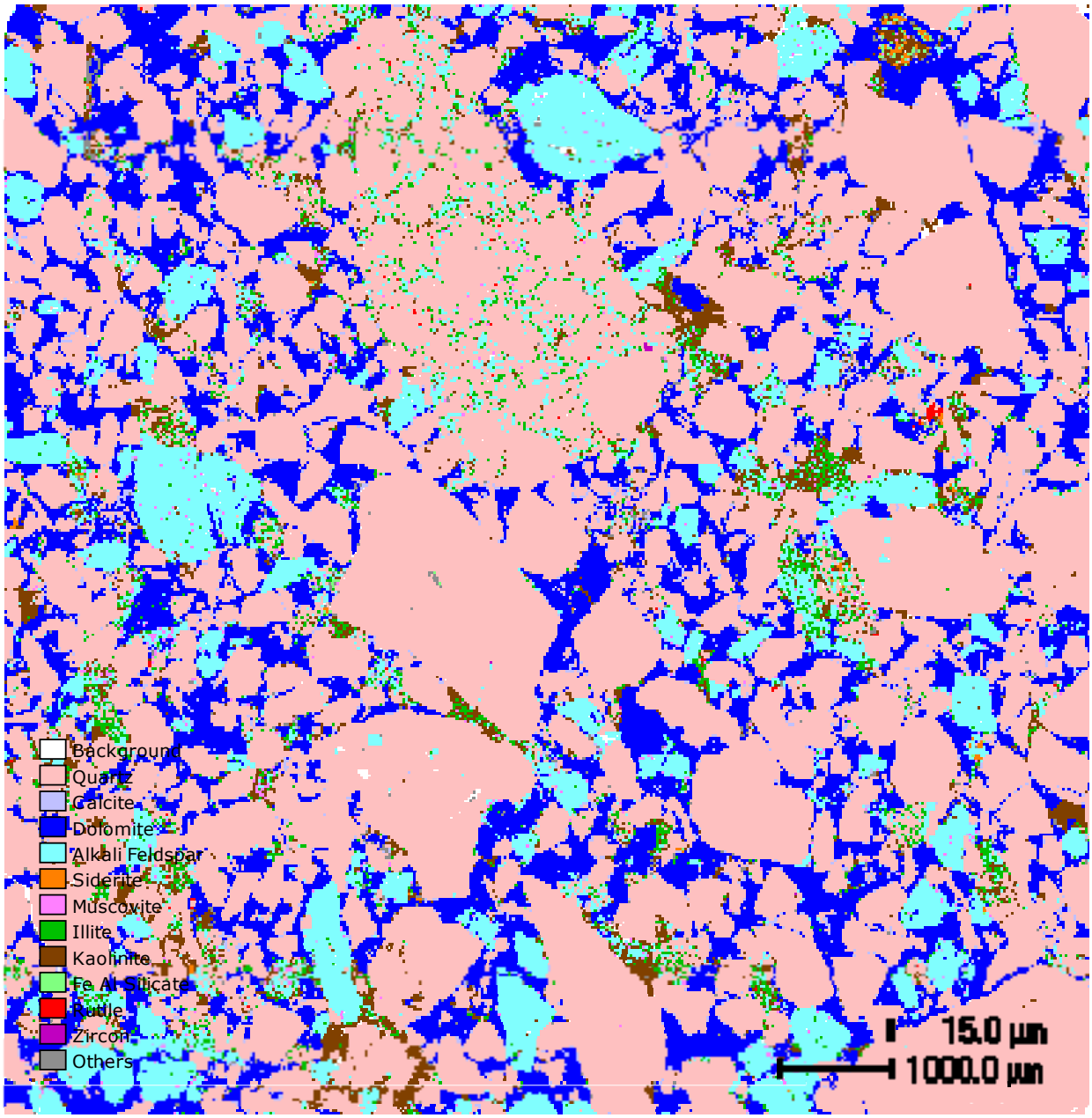

Figure 4. QEMSCAN mineral map of Sample # 19: 3251.0 m.

Table 4. Table of modal proportions of minerals determined by QEMSCAN for Sample # 19: 3251.0 m.

Minerals	Sample
	Basker-5 (19) 3251m
Quartz	69.8
Calcite	0.3
Dolomite	12.4
Alkali Feldspar	12.7
Siderite	0.2
Muscovite	0.7
Illite	0.4
Kaolinite	2.9
Fe Al Silicate	0.1
Rutile	0.0
Zircon	0.0
Others	0.4

4.5 Sample # 16: 3299.0 m

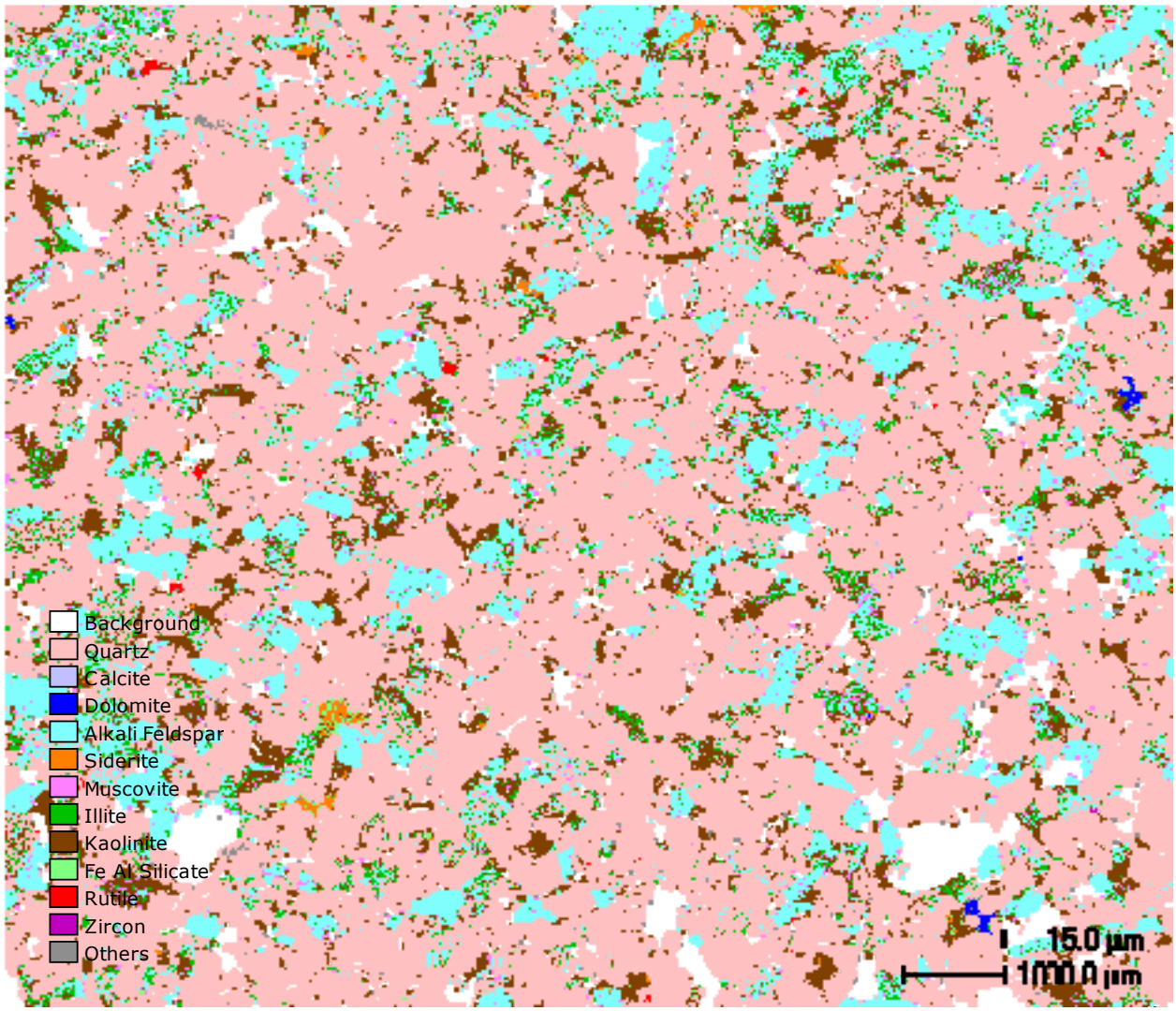

Figure 5. QEMSCAN mineral map of Sample # 16: 3299.0 m.

Table5. Table of modal proportions of minerals determined by QEMSCAN for Sample # 16: 3299.0 m.

Minerals	Sample
	Basker-5 (16) 3299m
Quartz	76.7
Calcite	0.0
Dolomite	0.0
Alkali Feldspar	13.3
Siderite	0.6
Muscovite	1.1
Illite	0.1
Kaolinite	7.3
Fe Al Silicate	0.4
Rutile	0.0
Zircon	0.0
Others	0.4

4.6 Sample # 12: 3308.5 m

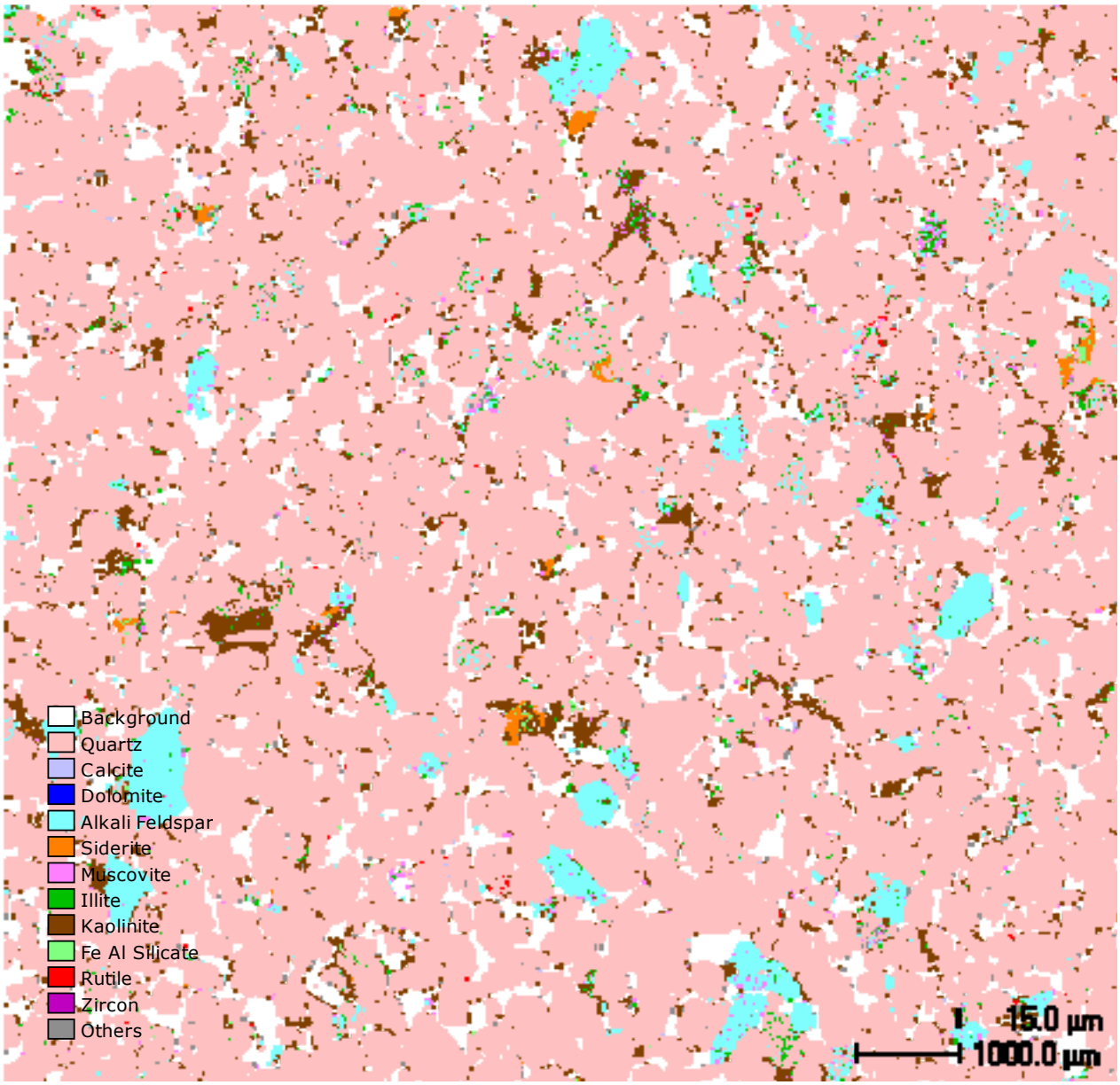

Figure 6. QEMSCAN mineral map of Sample # 12: 3308.5 m.

Table 6. Table of modal proportions of minerals determined by QEMSCAN for Sample # 12: 3308.5 m.

Minerals	Sample
	Basker-5 (12) 3308.5m
Quartz	91.5
Calcite	0.0
Dolomite	0.0
Alkali Feldspar	4.1
Siderite	0.4
Muscovite	0.4
Illite	0.1
Kaolinite	3.1
Fe Al Silicate	0.1
Rutile	0.0
Zircon	0.0
Others	0.5

4.7 Sample # 11: 3353.5 m

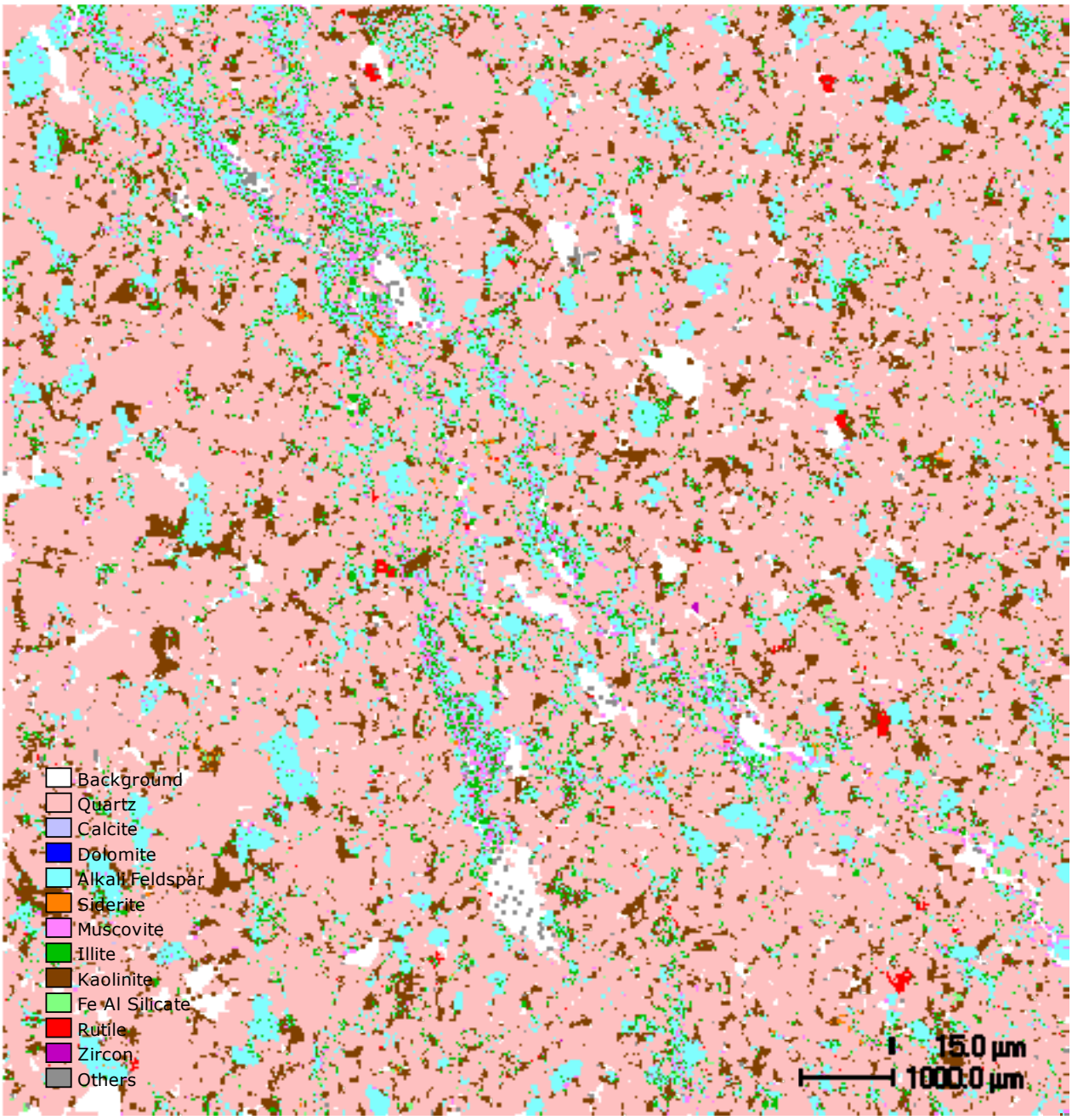

Figure 7 QEMSCAN mineral map of Sample # 11: 3353.5 m.

Table7. Table of modal proportions of minerals determined by QEMSCAN for Sample # 11: 3353.5 m.

Minerals	Sample
	Basker-5 (11) 3353.5m
Quartz	80.3
Calcite	0.0
Dolomite	0.0
Alkali Feldspar	8.7
Siderite	0.2
Muscovite	1.4
Illite	0.3
Kaolinite	7.9
Fe Al Silicate	0.5
Rutile	0.1
Zircon	0.0
Others	0.4

4.8 Sample # 7: 3372.0 m

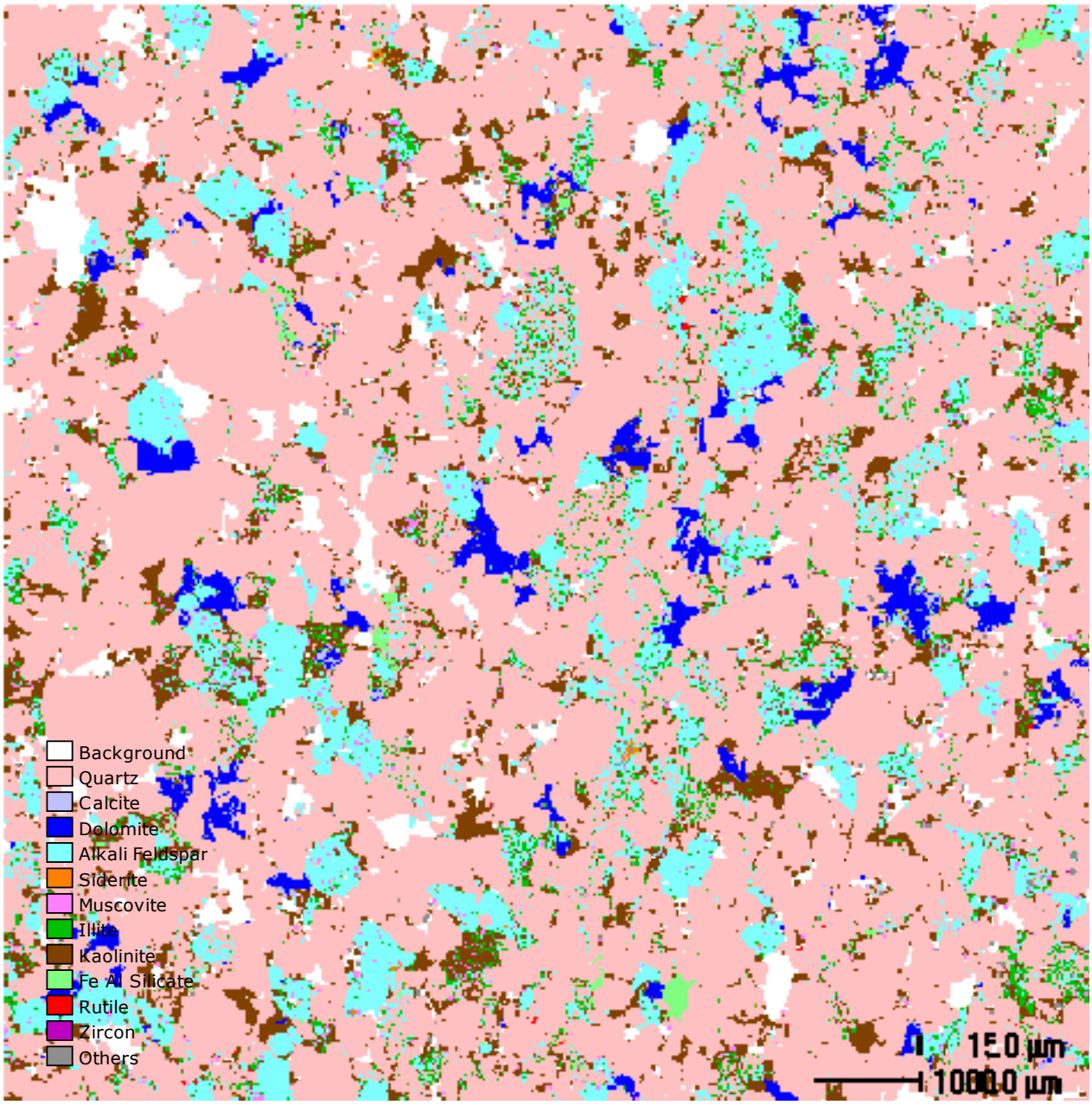

Figure 8. QEMSCAN mineral map of Sample # 7: 3372.0 m.

Table 8. Table of modal proportions of minerals determined by QEMSCAN for Sample # 7: 3372.0 m.

Minerals	Sample
	Basker-5 (7) 3372m
Quartz	77.5
Calcite	0.3
Dolomite	0.9
Alkali Feldspar	12.5
Siderite	0.1
Muscovite	1.0
Illite	0.1
Kaolinite	6.7
Fe Al Silicate	0.4
Rutile	0.0
Zircon	0.0
Others	0.4

Summary Comparison of all Samples

Figure 9 illustrates the modal mineralogy of all seven samples in one chart; Figure 10 the estimated grain size of quartz; Table 9 defines the terms and sizes for clastic sedimentary rocks; and Figure 11 thumbnail mosaics of the total measured area of the side wall cores.

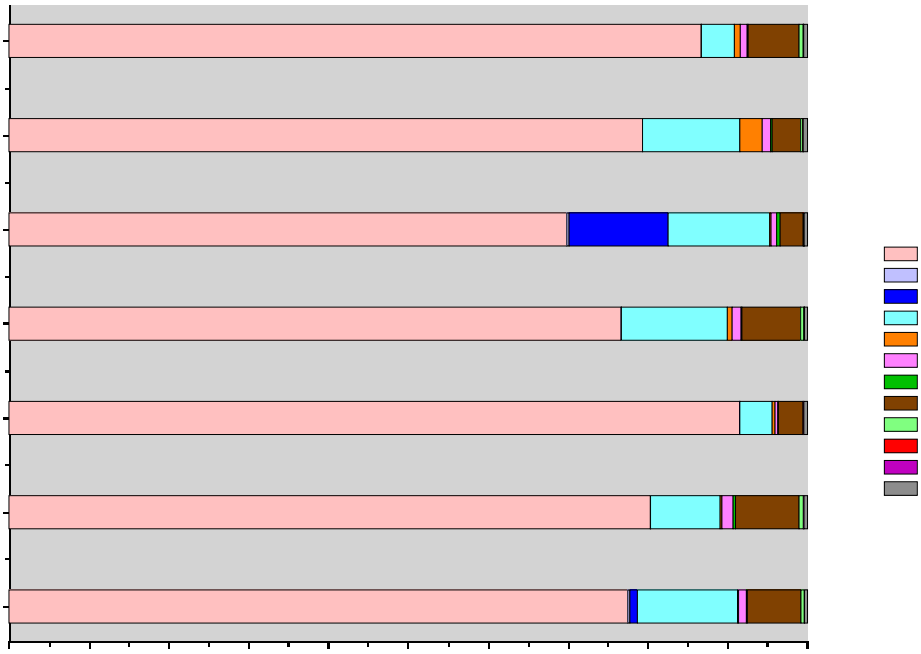

Figure 9. The modal mineralogy as determined by QEMSCAN for all seven samples.

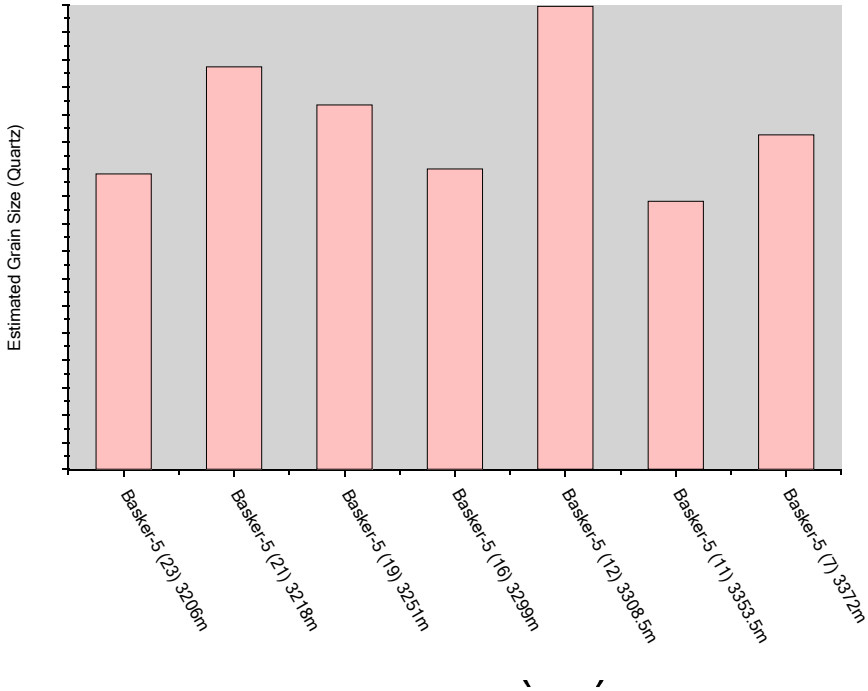

Figure 10. Grain size estimates of quartz grains for all seven samples.

Terms and Sizes for Clastic Sediments and Clastic Sedimentrary Rock Types		Millimeter	Micrometers
Gravel	**Boulder**	4,096	
	Cobble	256	
	Pebble	64	
	Granule	4	4000
		2	2000
Sand	**Very Coarse Sand**	1	1000
	Coarse Sand	0.5	500
	Medium Sand	0.25	250
	Fine Sand	0.125	125
	Very Fine Sand	0.062	62
Mud	**Coarse Silt**	0.031	31
	Medium Silt	0.016	16
	Fine Silt	0.008	8
	Very Fine Silt	0.004	4
	Clay		

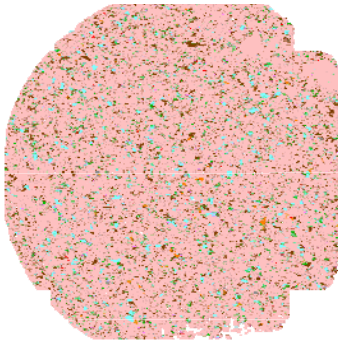

Sample # 23: 3206.0 m

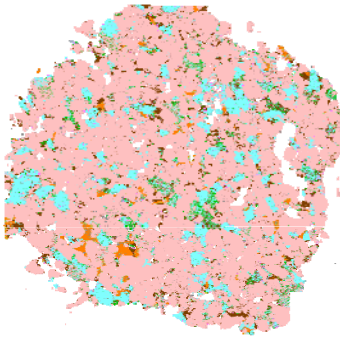

Sample # 21: 3218.0 m

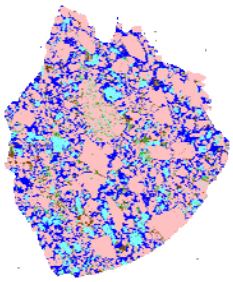

Sample # 19: 3251.0 m

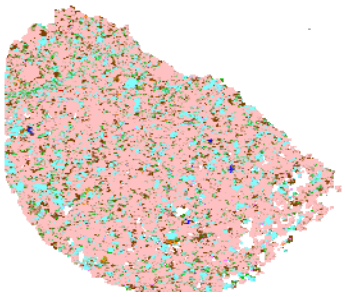

Sample # 16: 3299.0 m

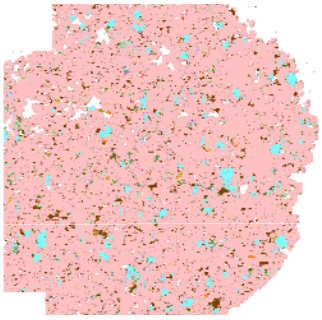

Sample # 12: 3308.5 m

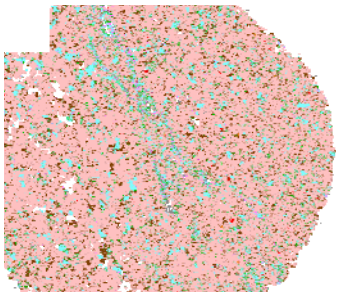

Sample # 11: 3353.5 m

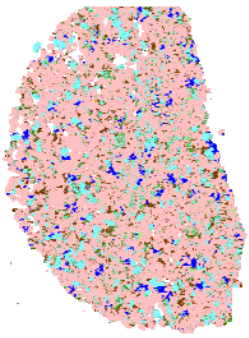

Sample # 7: 3372.0 m

Sample nr.	Porosity % (As provided by Anzon)	Permeability (mD)	QEMSCAN Estimated Porosity %
23	20.7	134	20.5
21	22.6	3150	20.0
19	7.0	3	0.6
16	19.3	48	17.6
12	22.5	2090	25.0
11	13.6	46	15.9
7	13.0	41	13.8

Figure 11. Thumbnail QEMSCAN mosaics illustrating the total area measured in each of the seven side wall core samples, and a table with the Porosity % and Permeability, as determined by Anzon, and the QEMSCAN Calculated Porosity %.

Intellection Pty Ltd
2/27 Mayneview Street Milton Qld 4064
PO Box 1636 Milton Qld 4064 Australia
Tel +61 7 3512 9100 Fax +61 7 3512 9199
ABN 58 105 166 354
www.intellection.com.au

Report #: AAPB/IPL 001 AD

Date: 18th October 2006

Anzon Australia Ltd,
Suite 504, 165 Walker St,
North Sydney, 2060,
NSW, Australia

QEMSCAN Analysis of 8 Cuttings Samples from Basker #5

Client:

Barry Messent

Anzon Australia Ltd

Authors:

Pieter WSK Botha

Dr Alan R Butcher

Intellection Pty Ltd

Table of contents

1. Executive Summary 3
2. Introduction 4
3. Sample Presentation Details 5
4. QEMSCAN Measurement 6
5. QEMSCAN Analysis Results 7
5.1 Mineral Key to Mineral Maps 7
6. Summary Comparison of all Samples 8
6.1 Modal Composition 8
6.2 Quantitative Micro-Lithotyping 9
6.3 Example Images of Micro-fossils 11
6.4 Summary Petrographic Data 13
7. Appendix 14
7.1 Sample A (3350-3355 m) 15
7.2 Sample B (3355-3360m) 17
7.3 Sample C (3360-3365m) 19
7.4 Sample D (3365-3370m) 21
7.5 Sample E (3370-3375m) 23
7.6 Sample F (3445-3450m) 25
7.7 Sample G (3480-3485m) 27
7.8 Sample H (3495-3500m) 29

1. Executive Summary

Eight cuttings samples from Basker #5 well, representing depths 3350 – 3500 m (re-labeled A-H by Intellection), have been analyzed by QEMSCAN. Given the nature of the material (the cuttings were delivered wet and unsized) it was necessary to first air dry them, followed by dry sieving. Only cuttings ranging in size from -1180µm/+38µm were investigated, and follows normal QEMSCAN analysis procedures.

The results show that the sequence represented by the eight samples comprises: a lower siltstone sequence (samples H, G, and F), overlain by a sandstone-dominated sequence (samples E, D, and C), which in turn is overlain by a return to siltstone (samples B and A). Micro-fossils were found only in the sandstone sequence. Based on mineralogy and micro-lithotyping, the average Specific Gravity for each sample has been calculated. Porosity estimates, based on the area percent voids measured in each cutting sample, are also reported.

2. Introduction

Intellection was supplied with 8 cuttings samples, taken from Basker # 5, for measurement by QEMSCAN. The aim of the study was to gather quantitative data on the modal mineralogy, mineral textures, and estimated porosity of each cuttings sample.

QEMSCAN is an automated SEM-based (Scanning Electron Microscope) system that uses a combination of Energy Dispersive X-Ray (EDX) spectra and Backscattered Electrons (BSE) to identify the minerals present and produce false-colour digital mineral maps of cuttings and cores. The resulting digital images are used for quantitative analysis of textural information, such as grain size and mineral association, as well as providing the modal abundance of minerals.

3. Sample Presentation Details

Details of the samples are summarized in Table 1.

The samples were received wet and contained a large range of cutting diameters (sub-millimeter to centimeter). Experience has shown that samples with large ranges of particle sizes should ideally be sized into sub-samples for analysis. It was subsequently decided to use metal sieves to size each sample into the following fractions, following air drying:

- +1180 µm,
- -1180 µm /+38 µm, and
- -38 µm.

Standard sample preparation procedures were followed for each size fraction, with the sample being first split into representative aliquots, mounted in epoxy resin, cut back, and polished, before being carbon coated.

Table 1. Details of Basker #5 samples, their depth and the QEMSCAN reference code.

Sample Label	Sample Depth (m)	QEMSCAN Code
A	3350-3355	**AAPBA**
B	3355-3360	**AAPBB**
C	3360-3365	**AAPBC**
D	3365-3370	**AAPBD**
E	3370-3375	**AAPBE**
F	3445-3450	**AAPBF**
G	3480-3485	**AAPBG**
H	3495-3500	**AAPBH**

4. QEMSCAN Measurement

The following measurement modes were used:

- BMA – Line Scans to produce modal mineralogy data;
- PMA – Particle Scans to produce textural data; and
- PMA (BSE Only) – BSE-only Particle Scans for estimated porosity data.

Identical measurement parameters were used for each measurement mode on all samples within a particular size fraction.

5. QEMSCAN Analysis Results

The data are presented first in summary form and then on a sample-by-sample basis in the Appendix. Example particle mineral maps, along with the quantification of the modal mineralogy and textural information, are provided. Results are reported for the intermediate size fraction (-1180/+38 µm) only, in keeping with normal QEMSCAN operating procedures.

5.1 Mineral Key to Mineral Maps

The minerals and phases reported here are summarized in Figure 1. Where a mineral name is given, the phase has been positively identified based on its unique chemical composition and BSE brightness (e.g. quartz, dolomite, calcite, kaolinite, siderite, pyrite, and barite). The K Al Silicates group, on the other hand, contain both muscovite and illite, whilst the Fe Al Silicate grouping encompasses chlorite and garnet. The term Micrite is used specifically in this report to classify fine-grained silicate-bearing limestone. The grouping "Others" includes all remaining minerals and phases.

Figure 1. Mineral and phase key to QEMSCAN particle mineral maps in this report.

6. Summary Comparison of all Samples

6.1 Modal Composition

Figure 2 illustrates the modal mineralogy of all eight samples in one chart. The estimated quartz grain size is shown in Figure 3.

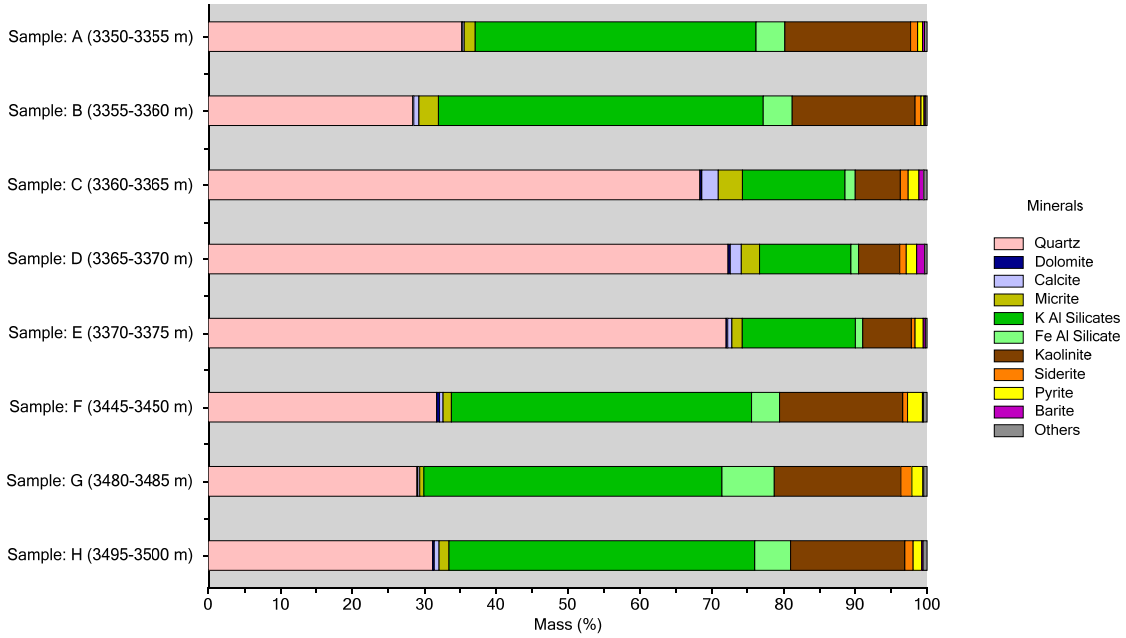

Figure 2. The modal mineralogy as determined by QEMSCAN for all eight samples.

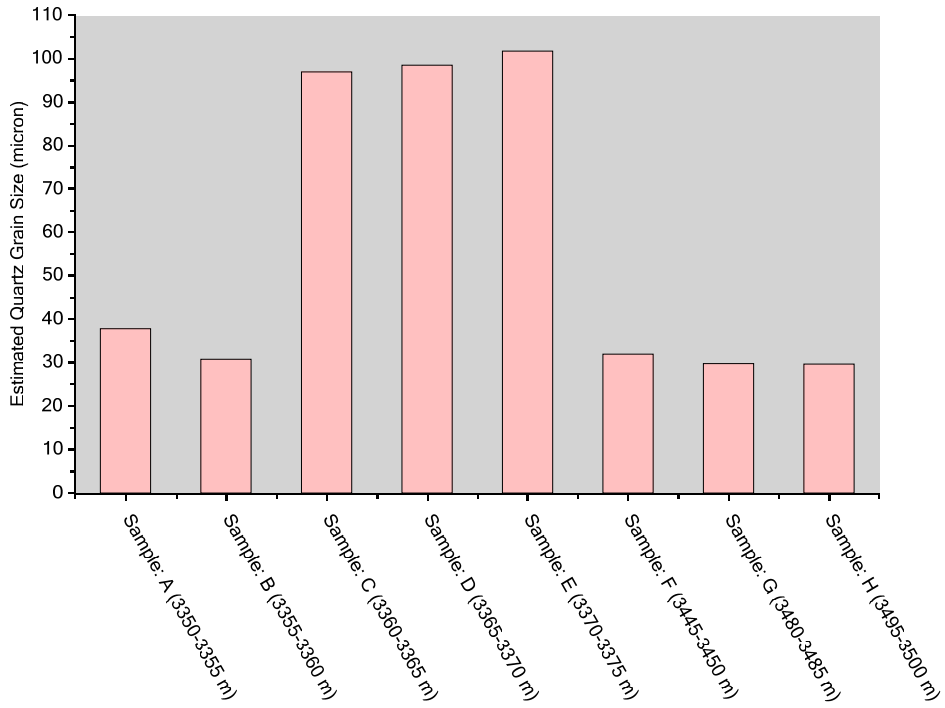

Figure 3. Grain size estimates of quartz (in micron) for all eight samples.

6.2 Quantitative Micro-Lithotyping

Cuttings can be classified into micro-lithotype groups based on their composition and texture. Table 2 provides the detail of the micro-lithotypes and each classification criteria (based on grain size estimate of quartz, in micron, and percentage clay present in each cutting). Figure 4 is an Image Grid illustrating which rock types are present in each cuttings sample. The interested reader is referred to the Appendix for Table 13, which defines the terms and sizes of clastic sediments and clastic sedimentary rocks according to international convention.

Table 2. Lithotypes and their classification criteria.

Micro-Lithotype	Classification Criteria
Micro-fossils	AreaPercent **Calcite** >=35
Free Qtz	AreaPercent **Quartz** >= 75
Sandstone	Size Quartz >60 and Size **Quartz** <= 2000 and AreaPercent **Quartz** > 10 and AreaPercent **K Al Silicates** <= 50
Siltstone	Size **Quartz** > 8 and Size **Quartz** <= 45 and AreaPercent **Quartz** > 0 and AreaPercent **K Al Silicates** < 75
Mudstone	AreaPercent **K Al Silicates** <= 100

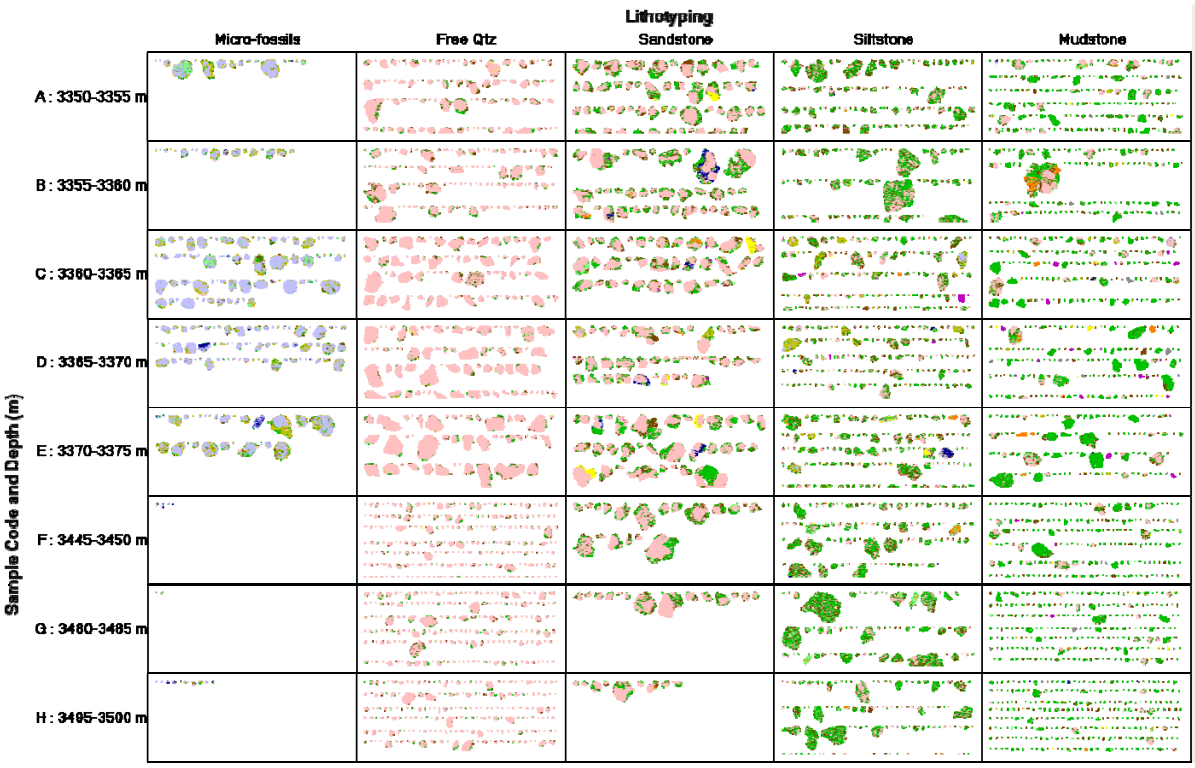

Figure 4. Example cuttings from each sample classified into micro-lithotype groupings.

Figure 5 illustrates how each lithotype can be plotted stratigraphically, and Table 3 tabulates these data.

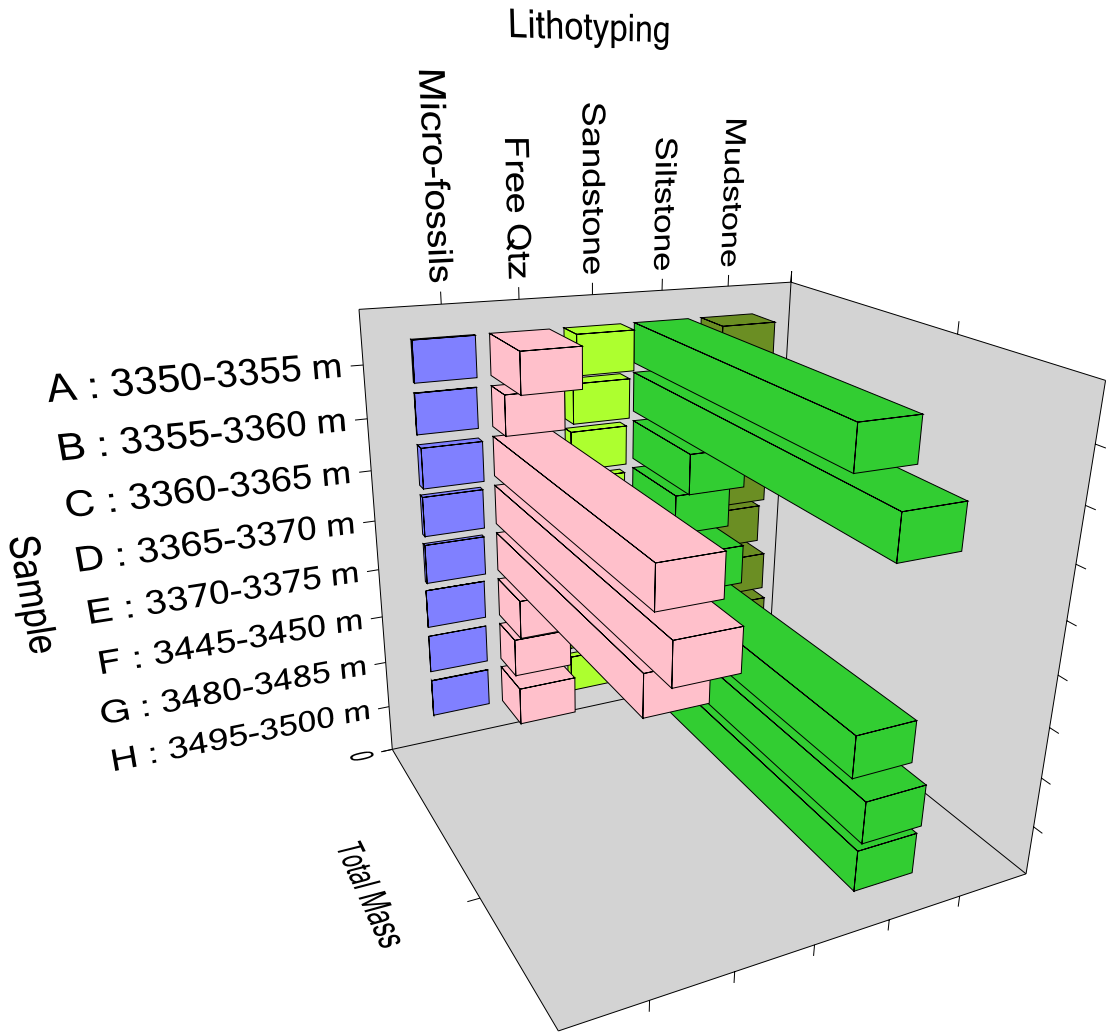

Figure 5. Quantification of micro-lithotype groups for each sample.

Table 3. Mass % of micro-lithotype groupings in each sample.

Sample	Total Mass					Total
	Micro-fossils	Free Qtz	Sandstone	Siltstone	Mudstone	
A : 3350-3355 m	0.7	14.6	5.7	70.7	8.2	100
B : 3355-3360 m	0.2	6.7	4.0	82.1	6.9	100
C : 3360-3365 m	2.3	65.1	2.8	22.9	7.0	100
D : 3365-3370 m	1.4	70.8	2.2	17.9	7.7	100
E : 3370-3375 m	1.0	61.9	7.3	23.7	6.1	100
F : 3445-3450 m	0.0	11.4	3.0	76.8	8.8	100
G : 3480-3485 m	0.0	8.1	1.5	80.6	9.9	100
H : 3495-3500 m	0.2	10.1	1.7	79.8	8.3	100

6.3 Example Images of Micro-fossils

The following images are examples of calcite-rich cuttings, mostly comprised of micro-fossil fragments. It is noted that samples C, D, and E, which contain the highest proportions of "free quartz", also have the highest micro-fossil content (see Figure 6 and inset).

- **Sample A (3350-3355 m):**

- **Sample B (3355-3360m):**

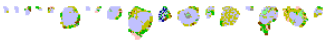

- **Sample C (3360-3365m):**

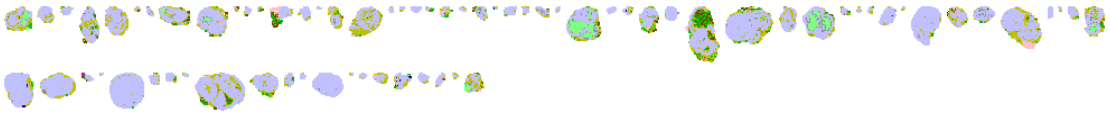

- **Sample D (3365-3370m):**

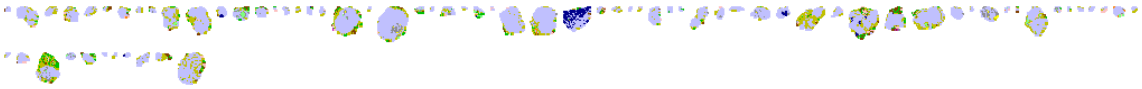

- **Sample E (3370-3375m):**

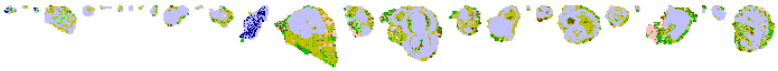

- **Sample F (3445-3450m):**

- **Sample G (3480-3485m):**

- **Sample H (3495-3500m):**

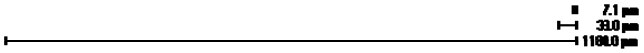

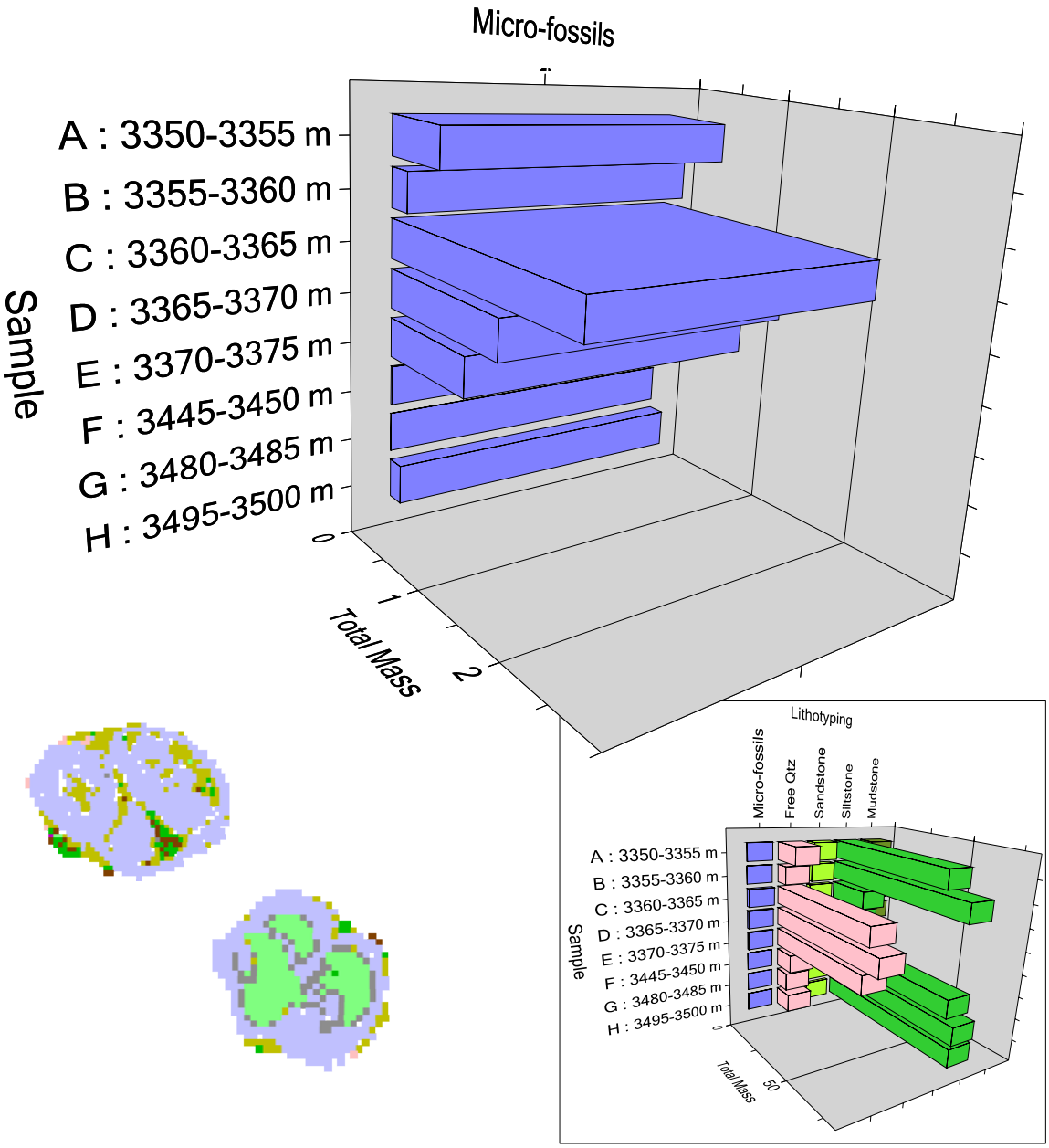

Figure 6. More detailed fossil-bearing cuttings plotted stratigraphically (re-scaled for ease of illustration); overall micro-lithotyping graph shown with inset; two detailed cutting images, containing micro-fossils showing clear morphology and structure, from sample C (3360-3365m).

6.4 Summary Petrographic Data

Table 4 provides summary information on the micro-lithotypes in each sample, estimated quartz grain size, average density, and estimated porosity of each sample.

Table 4. Summary petrographic information. Sample: details as supplied by Anzon Australia; **Micro-Lithotypes** and **Estimated Quartz Grain Size:** calculated from QEMSCAN cuttings images; **Average SG:** calculated from quantitative modal mineralogy; and **Estimated Porosity:** Calculated/Estimated from BSE-only scans.

	Micro-Lithotype (Total Mass)								
Sample	**Micro-fossils**	**Free Qtz**	**Sst**	**Siltst**	**Mudst**	***Total***	**Estimated Quartz Grain Size (micron)**	**Average SG**	**Estimated Porosity (Area %)**
A : 3350-3355 m	0.7	14.6	5.7	**70.7**	8.2	*100*	38	2.69	4.1
B : 3355-3360 m	0.2	6.7	4.0	**82.1**	6.9	*100*	31	2.70	4.0
C : 3360-3365 m	2.3	**65.1**	2.8	22.9	7.0	*100*	97	2.70	1.3
D : 3365-3370 m	1.4	**70.8**	2.2	17.9	7.7	*100*	98	2.70	1.1
E : 3370-3375 m	1.0	**61.9**	7.3	23.7	6.1	*100*	102	2.69	2.4
F : 3445-3450 m	0.0	11.4	3.0	**76.8**	8.8	*100*	32	2.71	3.5
G : 3480-3485 m	0.0	8.1	1.5	**80.6**	9.9	*100*	30	2.72	6.5
H : 3495-3500 m	0.2	10.1	1.7	**79.8**	8.3	*100*	30	2.71	4.9

7. Appendix

Sample-by-Sample Modal Results and Example QEMSCAN Cuttings Mineral Maps

7.1 Sample A (3350-3355 m)

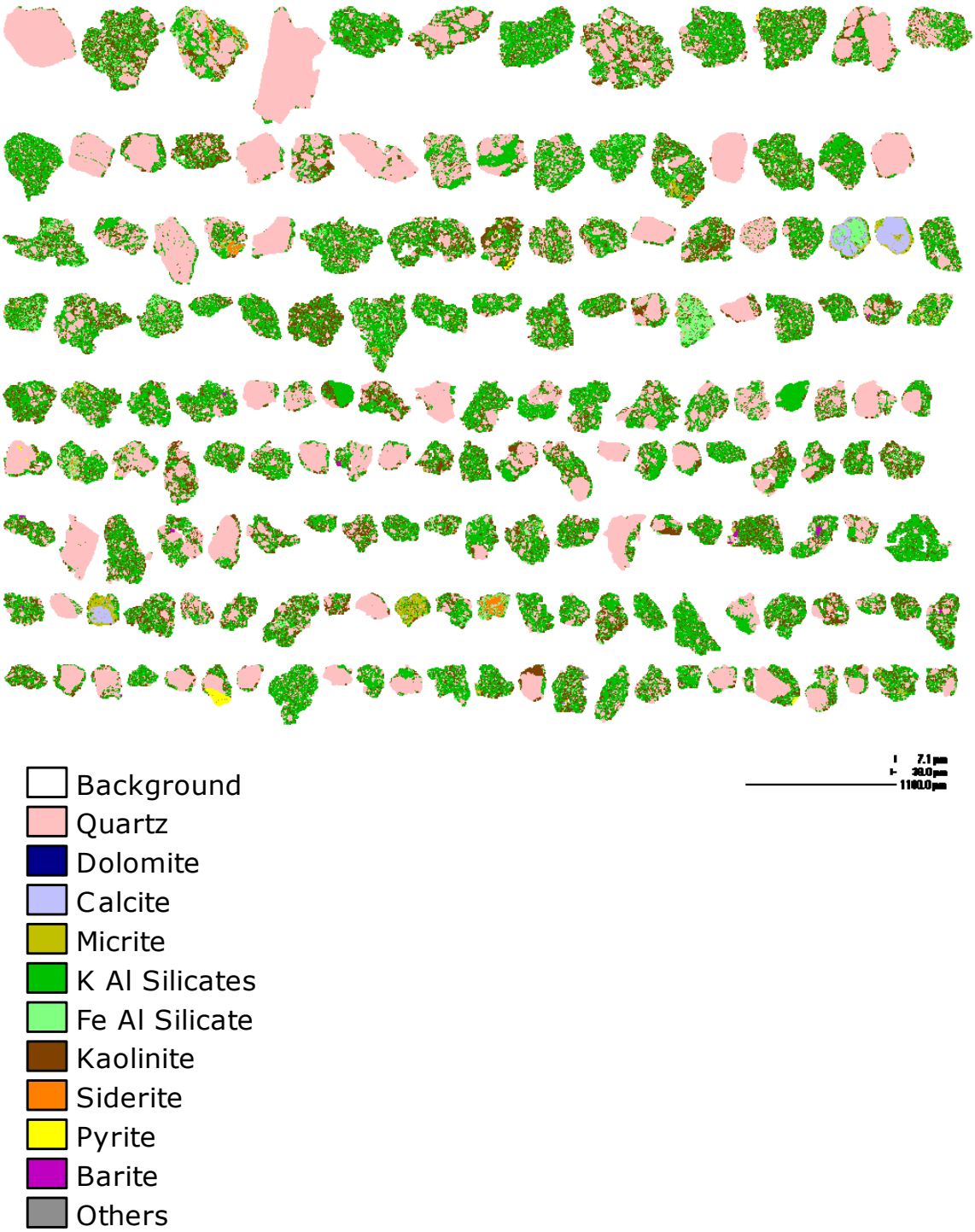

Figure 7. Example QEMSCAN particle mineral maps from Sample A (3350–3355m).

Table 5. Modal proportions of minerals in Sample A (3350-3355m).

Mineral	Sample A 3350-3355m
Quartz	35.3
Dolomite	0.0
Calcite	0.3
Micrite	1.5
K Al Silicates	39.1
Fe Al Silicate	4.0
Kaolinite	17.5
Siderite	1.0
Pyrite	0.7
Barite	0.3
Others	0.3
Total	100.0

7.2 Sample B (3355-3360m)

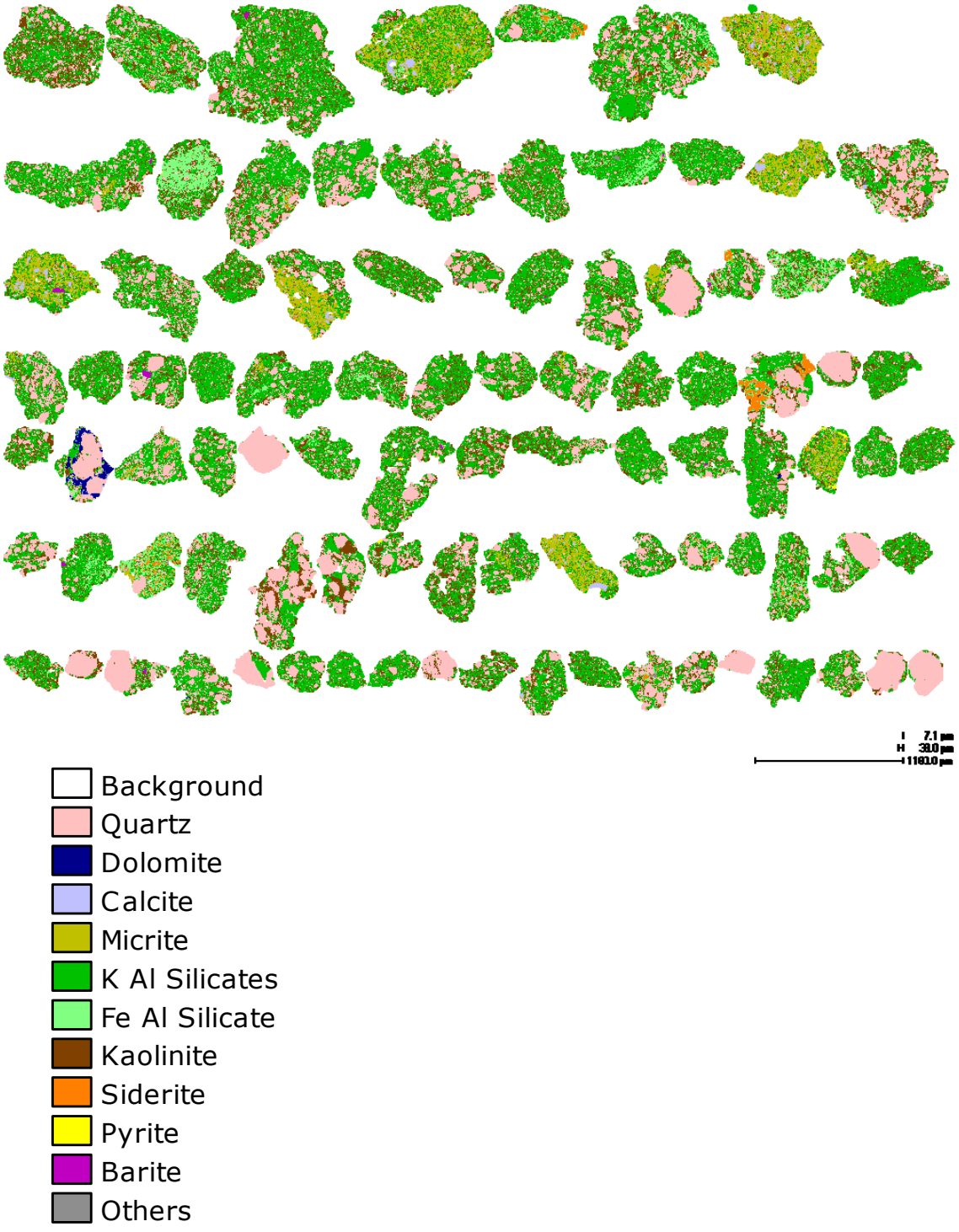

Figure 8. Example QEMSCAN particle mineral maps from Sample B (3355-3360m).

Table 6. Modal proportions of minerals in Sample B (3355-3360m).

Mineral	Sample B 3355-3360m
Quartz	28.5
Dolomite	0.1
Calcite	0.7
Micrite	2.7
K Al Silicates	45.2
Fe Al Silicate	4.0
Kaolinite	17.1
Siderite	0.8
Pyrite	0.4
Barite	0.2
Others	0.2
Total	100.0

7.3 Sample C (3360-3365m)

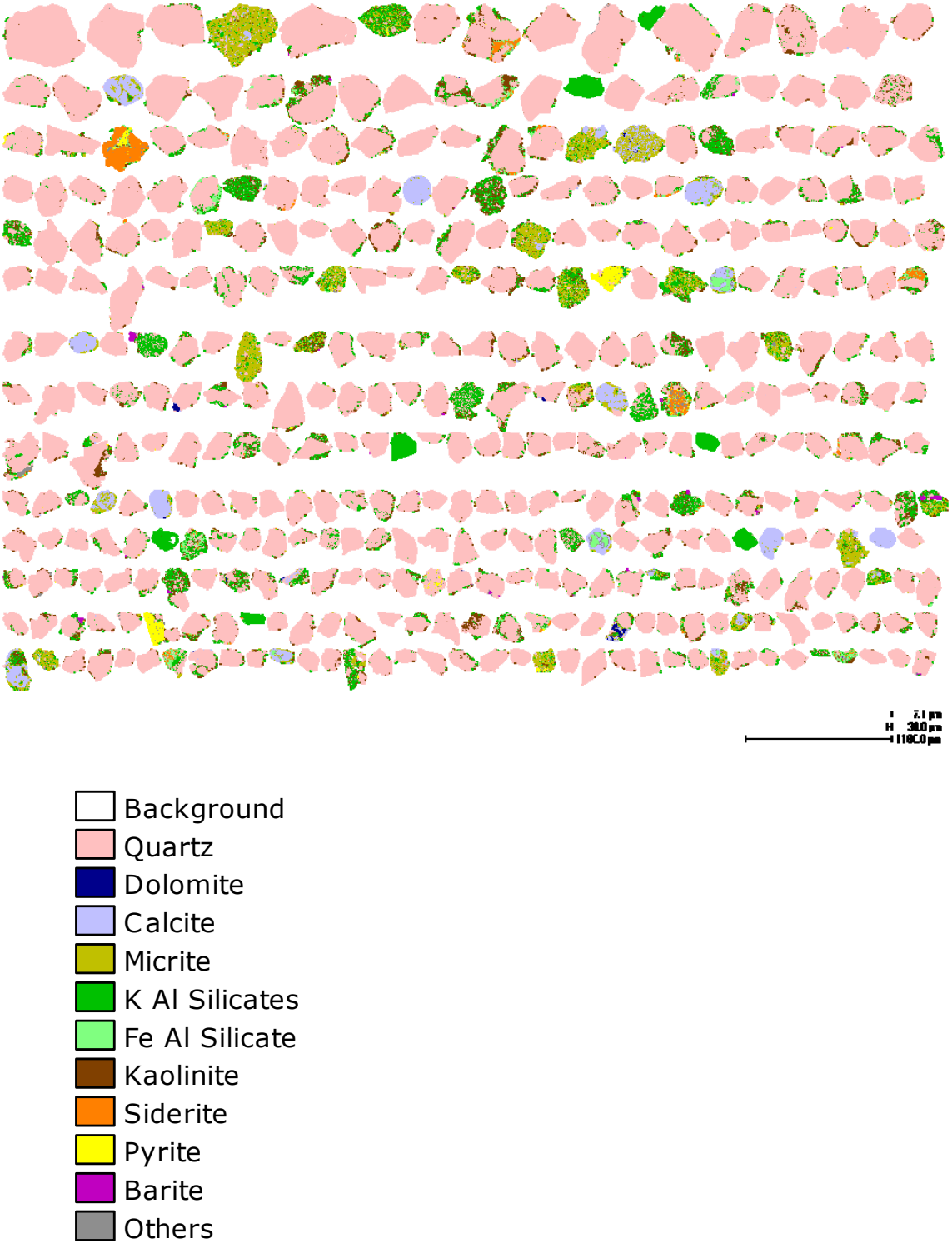

Figure 9. Example QEMSCAN particle mineral maps from Sample C (3360-3365m).

Table 7. Modal proportions of minerals in Sample C (3360-3365m).

Mineral	Sample C 3360-3365 m
Quartz	68.4
Dolomite	0.3
Calcite	2.3
Micrite	3.4
K Al Silicates	14.2
Fe Al Silicate	1.4
Kaolinite	6.3
Siderite	1.1
Pyrite	1.5
Barite	0.7
Others	0.4
Total	100.0

7.4 Sample D (3365-3370m)

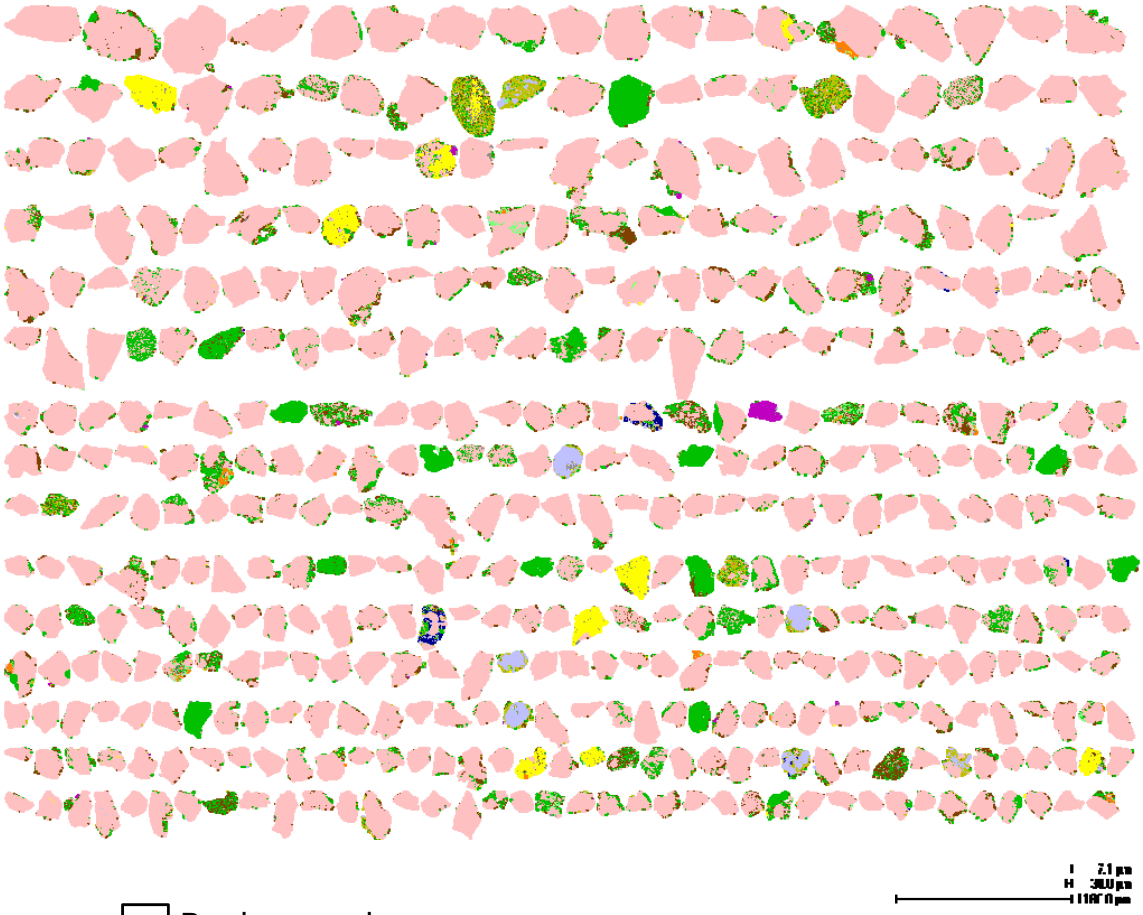

Figure 10. Example QEMSCAN particle mineral maps from Sample D (3365-3370m).

Table 8. Modal proportions of minerals in Sample D (3365-3370m).

Mineral	Sample D 3365-3370 m
Quartz	72.3
Dolomite	0.3
Calcite	1.6
Micrite	2.5
K Al Silicates	12.7
Fe Al Silicate	1.1
Kaolinite	5.7
Siderite	0.9
Pyrite	1.4
Barite	1.1
Others	0.3
Total	100.0

7.5 Sample E (3370-3375m)

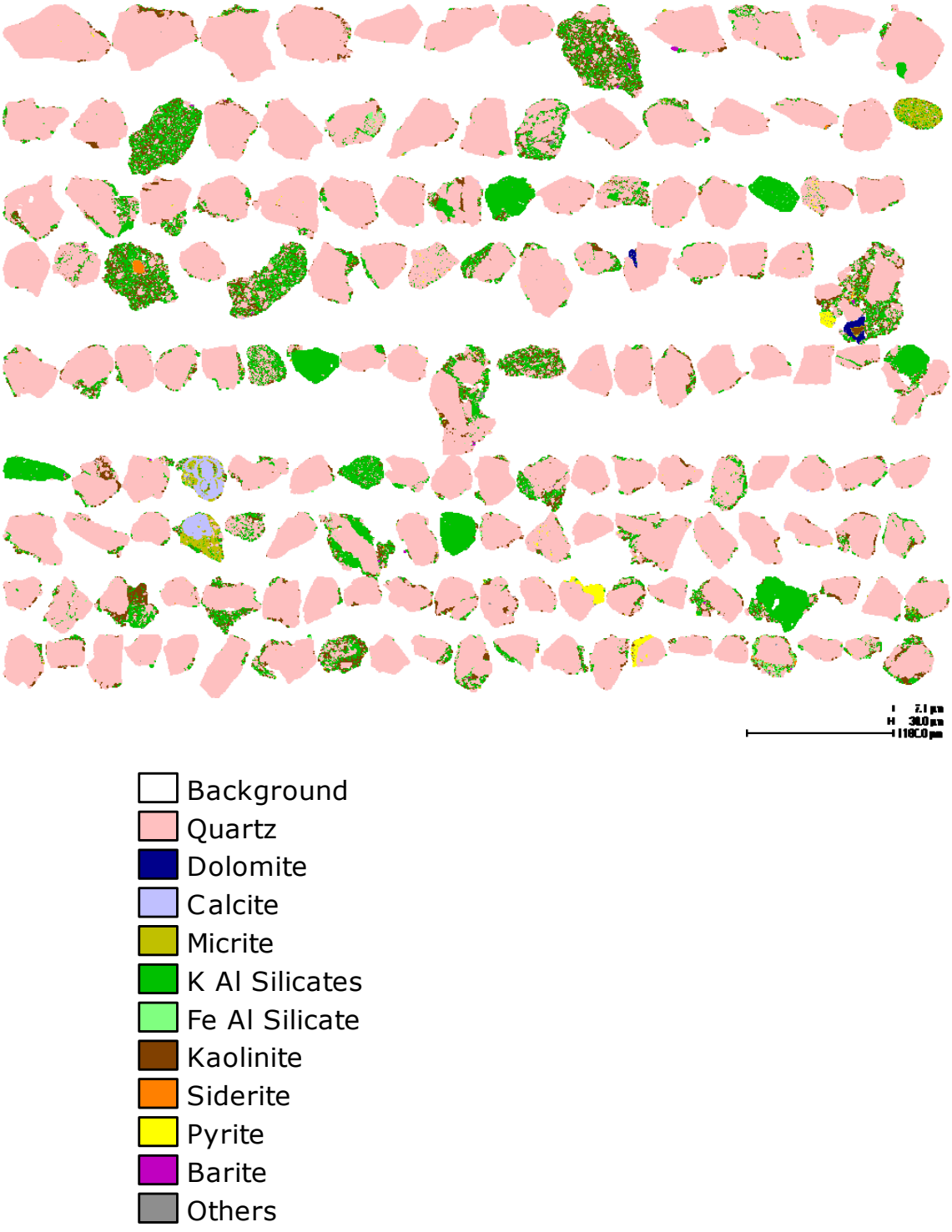

Figure 11. Example QEMSCAN particle mineral maps from Sample E (3370-3375m).

Table 9. Modal proportions of minerals in Sample E (3370-3375m).

Mineral	Sample E 3370-3375 m
Quartz	72.0
Dolomite	0.2
Calcite	0.6
Micrite	1.4
K Al Silicates	15.7
Fe Al Silicate	1.0
Kaolinite	6.8
Siderite	0.5
Pyrite	1.1
Barite	0.3
Others	0.2
Total	100.0

7.6 Sample F (3445-3450m)

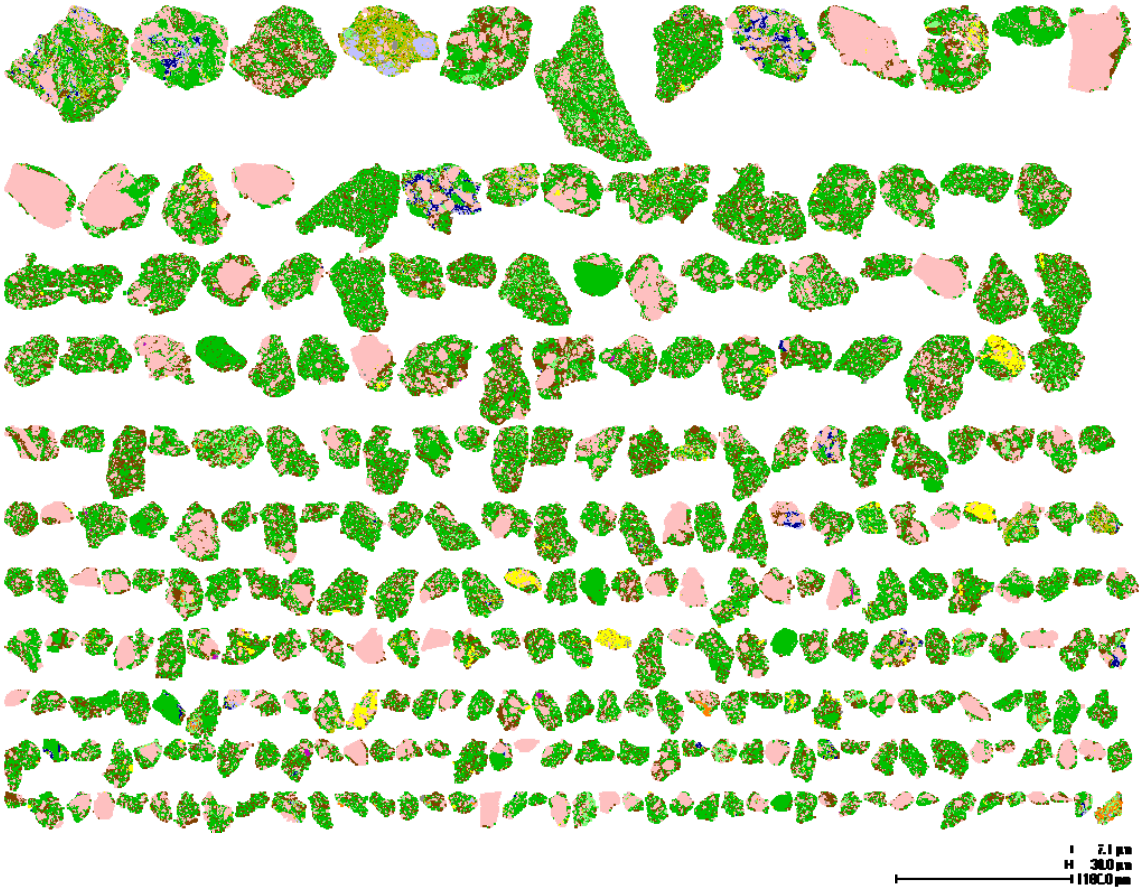

Figure 12. Example QEMSCAN particle mineral maps from Sample F (3445-3450m).

Table 10. Modal proportions of minerals in Sample F (3445-3450m).

Mineral	Sample F 3445-3450 m
Quartz	31.8
Dolomite	0.4
Calcite	0.5
Micrite	1.2
K Al Silicates	41.7
Fe Al Silicate	3.9
Kaolinite	17.1
Siderite	0.7
Pyrite	2.1
Barite	0.1
Others	0.5
Total	100.0

7.7 Sample G (3480-3485m)

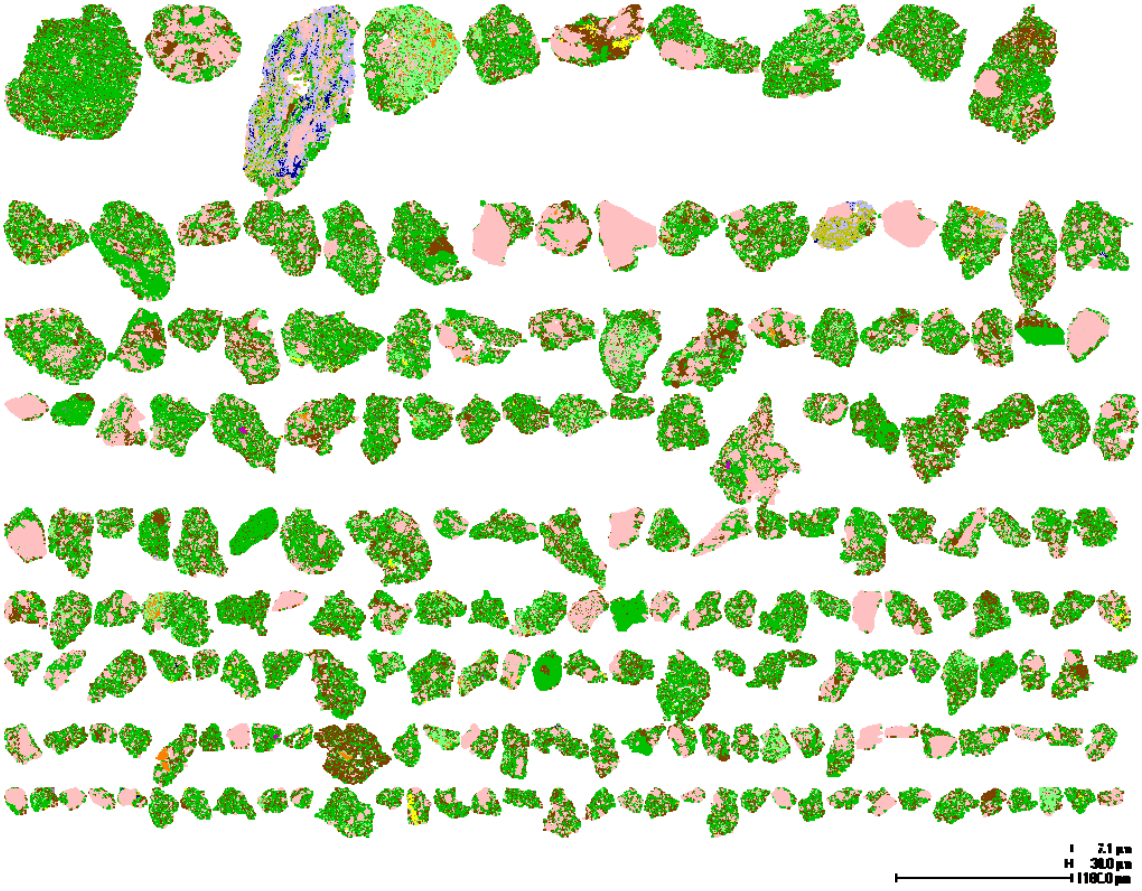

Figure 13. Example QEMSCAN particle mineral maps from Sample G (3480-3485m).

Table 11. Modal proportions of minerals in Sample G (3480-3485m).

Mineral	Sample G 3480-3485 m
Quartz	29.0
Dolomite	0.1
Calcite	0.3
Micrite	0.6
K Al Silicates	41.5
Fe Al Silicate	7.3
Kaolinite	17.6
Siderite	1.5
Pyrite	1.6
Barite	0.1
Others	0.5
Total	100.0

7.8 Sample H (3495-3500m)

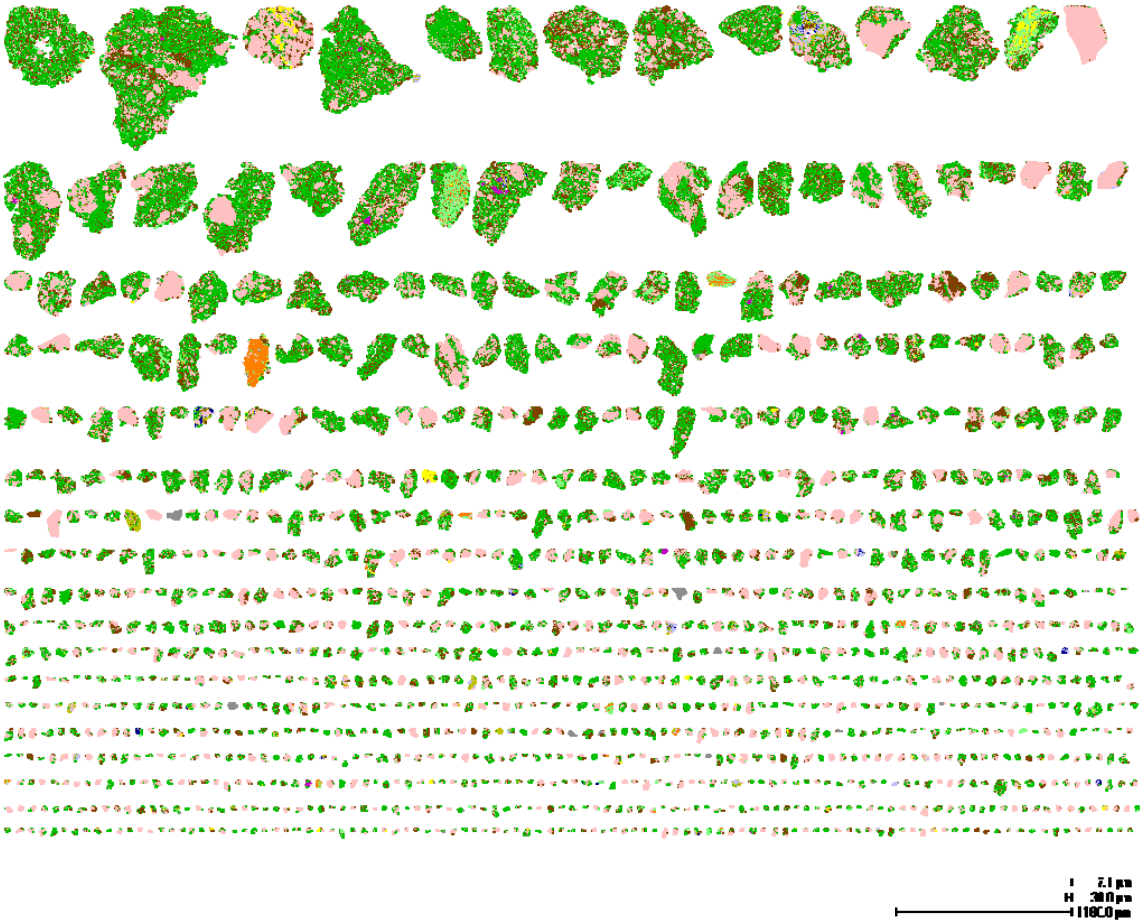

Figure 14. Example QEMSCAN particle mineral maps from Sample H (3495-3500m).

Table 12. Modal proportions of minerals in Sample H (3495-3500m).

Mineral	Sample H 3495-3500 m
Quartz	31.2
Dolomite	0.2
Calcite	0.7
Micrite	1.4
K Al Silicates	42.5
Fe Al Silicate	5.0
Kaolinite	15.9
Siderite	1.2
Pyrite	1.2
Barite	0.2
Others	0.6
Total	100.0

Table 13. Terms and sizes for clastic sediments and sedimentary rock types.

Terms and Sizes for Clastic Sediments and Clastic Sedimentrary Rock Types		Millimeter	Micrometers
Gravel	**Boulder**	4,096	
	Cobble	256	
	Pebble	64	
	Granule	4	4000
		2	2000
Sand	**Very Coarse Sand**	1	1000
	Coarse Sand	0.5	500
	Medium Sand	0.25	250
	Fine Sand	0.125	125
	Very Fine Sand	0.062	62
Mud	**Coarse Silt**	0.031	31
	Medium Silt	0.016	16
	Fine Silt	0.008	8
	Very Fine Silt	0.004	4
	Clay		

(iii) Appendix 3 - Photomicrographs

APPENDIX 3

PHOTOMICROGRAPHS

KEY TO PLATES IN APPENDIX 3

Sample #	Depth (mRT)	Plate #
24	3192.0	1
23	3206.0	2, 3*, 4*
22	3212.0	5, 6
21	3218.0	7, 8*, 9*
19	3251.0	10, 11
17	3287.0	12
16	3299.0	13, 14*, 15*
14	3306.5	16
12	3308.5	17, 18, 19*, 20*
11	3353.5	21, 22
7	3372.0	23, 24, 25, 26*
6	3409.0	27
4	3439.0	28, 29
3	3449.0	30, 31

* SEM micrographs

PLATE 1 #24 3192.0m

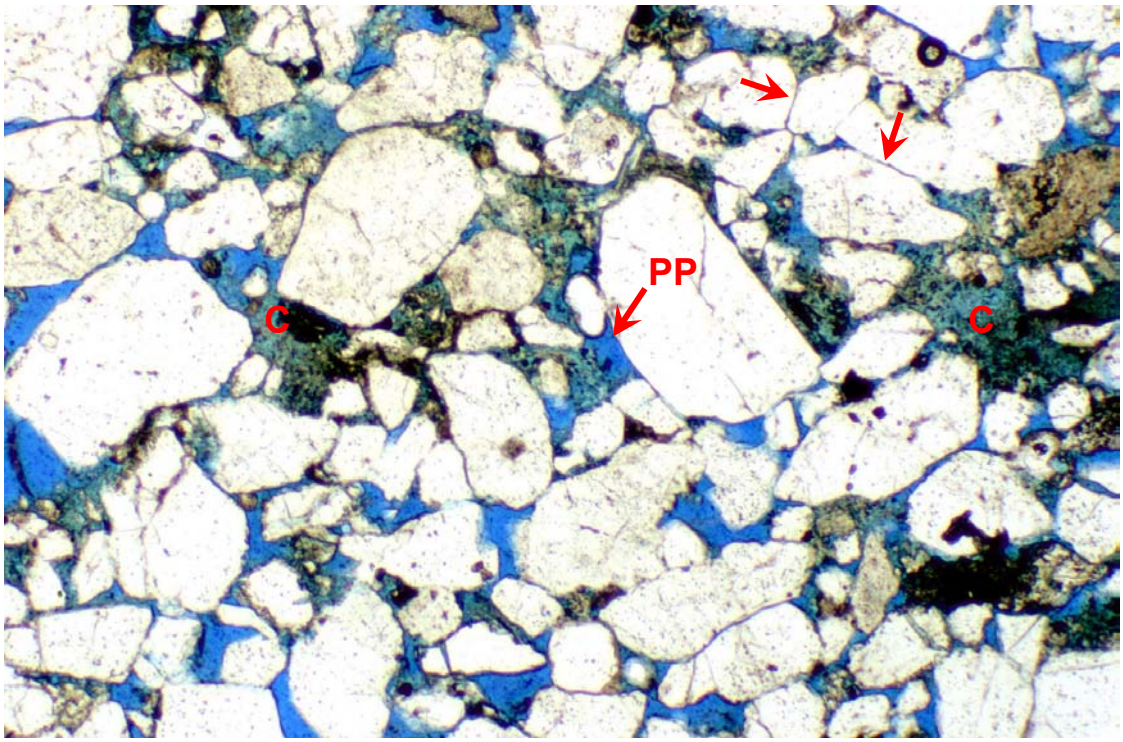

FIGURE 1 Plane polarised light
FIGURE 2 Crossed polarisers

0.4 mm

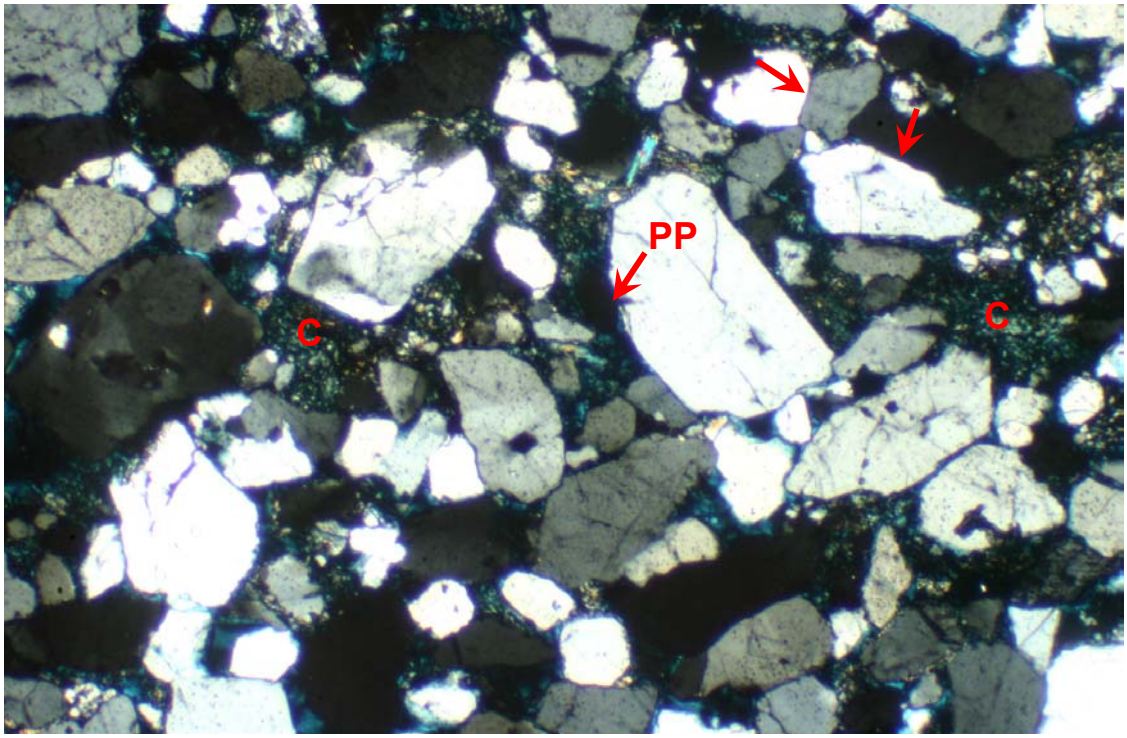

Medium grained sublitharenite in which abundant primary intergranular porosity (PP) is preserved between slightly compacted and weakly quartz overgrowth-cemented framework grains. Porosity reduction results mainly from minor grain contact dissolution to form long grain contacts (arrows) and micaceous/argillaceous rock fragment alteration to form patchy authigenic illitic and kaolinitic clay (C). Quartz overgrowths are too small to be clearly visible in the micrographs. K = 922mD

ACS Laboratories Pty Ltd
ABN: 81 008 273 005

PLATE 2 #23 3206.0m

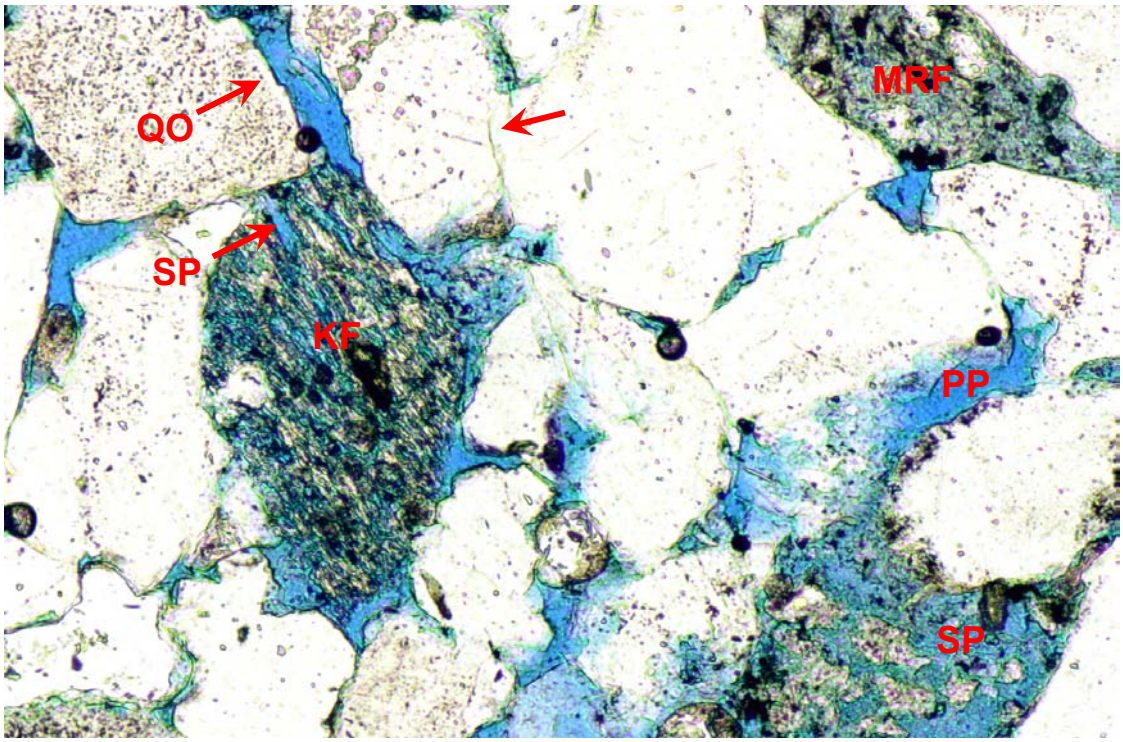

FIGURE 1 Plane polarised light

FIGURE 2 Crossed polarisers

0.2 mm

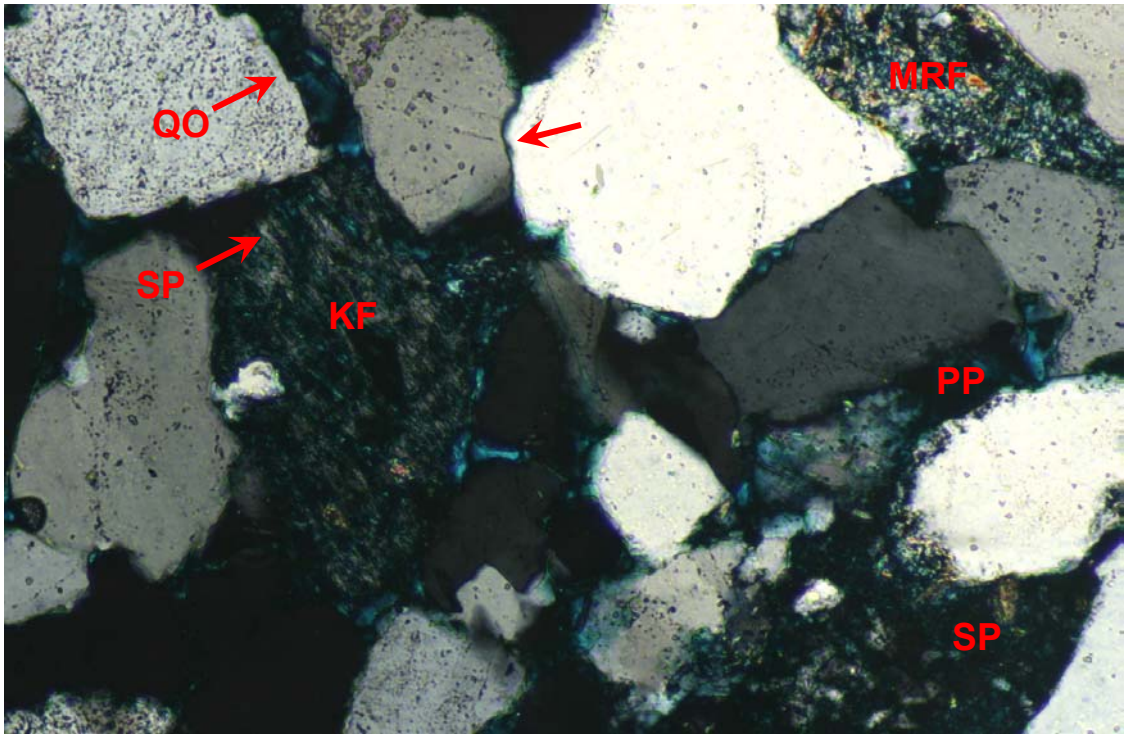

Grain contact dissolution (arrow) and compaction of an illitic low-grade metasedimentary rock fragment (MRF) have reduced intergranular porosity, but the sandstone still contains good primary intergranular porosity (PP) that is supplemented by secondary porosity (SP) that results from K-feldspar (KF) and labile rock fragment dissolution. Quartz overgrowths (QO) are insufficiently well developed to significantly impact reservoir quality. K = 134mD

PLATE 3 #23 3206.0m (cont.)

FIGURE 1

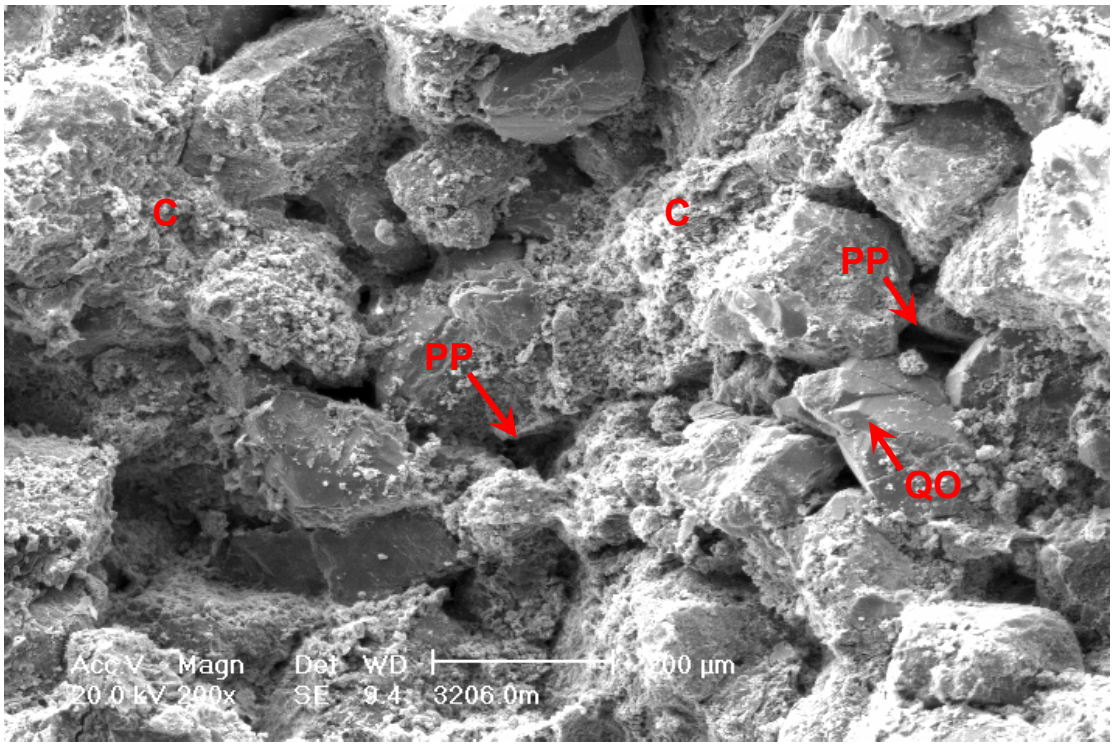

Interconnection between primary pores (PP) is reduced by clogging of intergranular spaces by authigenic clay (C) that is a micaceous/argillaceous grain decomposition product. Quartz overgrowths (QO) are thinly developed and thus only ever partly occlude intergranular pores. (SEM micrograph)

FIGURE 2

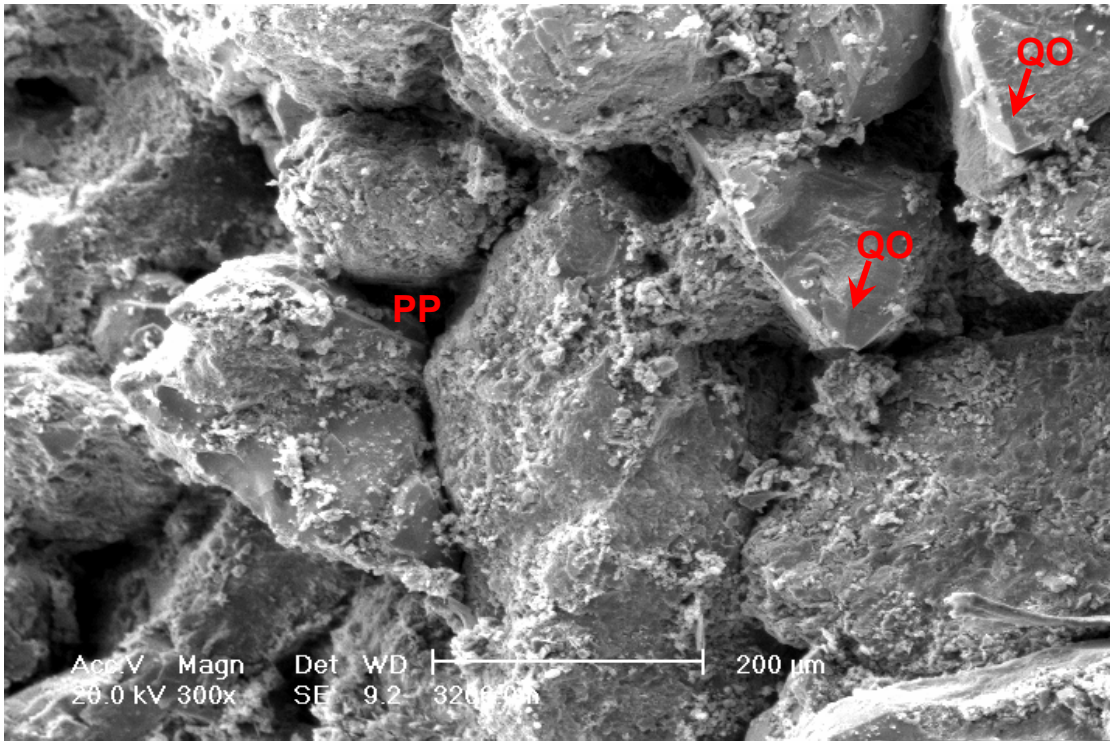

Good primary intergranular porosity (PP) is preserved between poorly compacted and essentially uncemented rigid framework grains. Quartz grains are locally thinly enveloped by quartz overgrowths (QO) that do little to reduce the volume of adjacent intergranular pores. (SEM micrograph)

PLATE 4 #23 3206.0m (cont.)

FIGURE 1

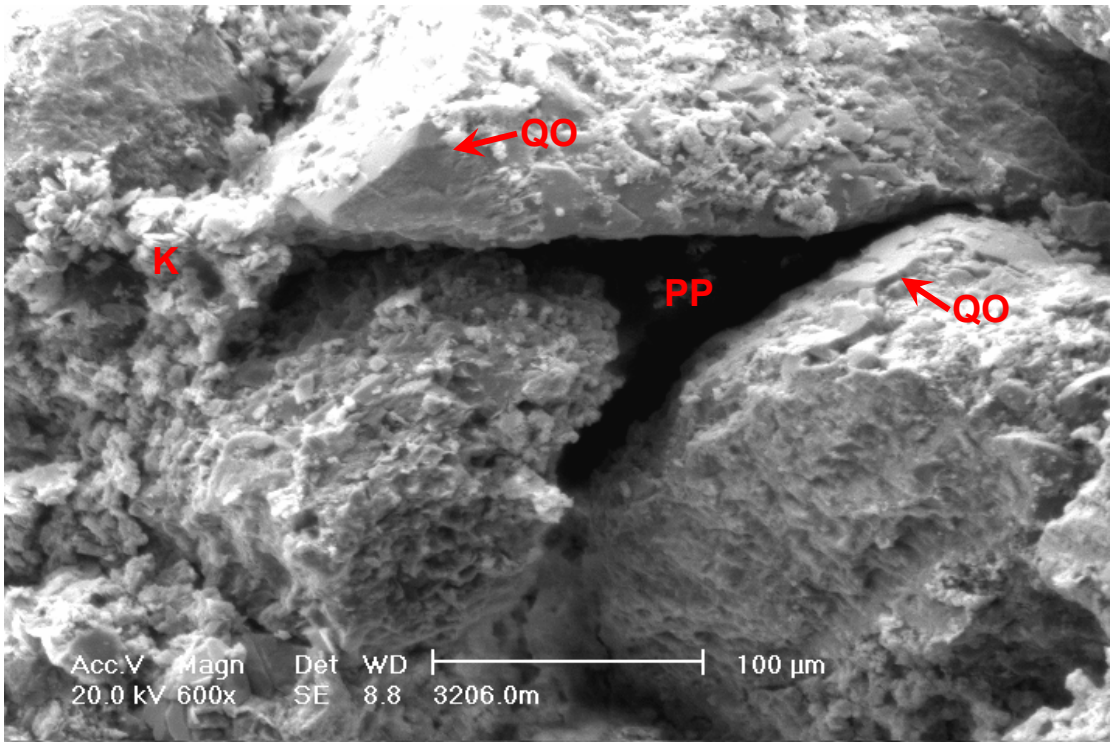

Detail of a typical primary intergranular pore (PP) that is preserved between poorly compacted quartz grains. Intergranular pore interconnectivity is reduced by authigenic kaolinite pseudomatrix (K) that results from micaceous grain alteration. Poorly developed quartz overgrowths (QO) are also marked. (SEM micrograph)

FIGURE 2

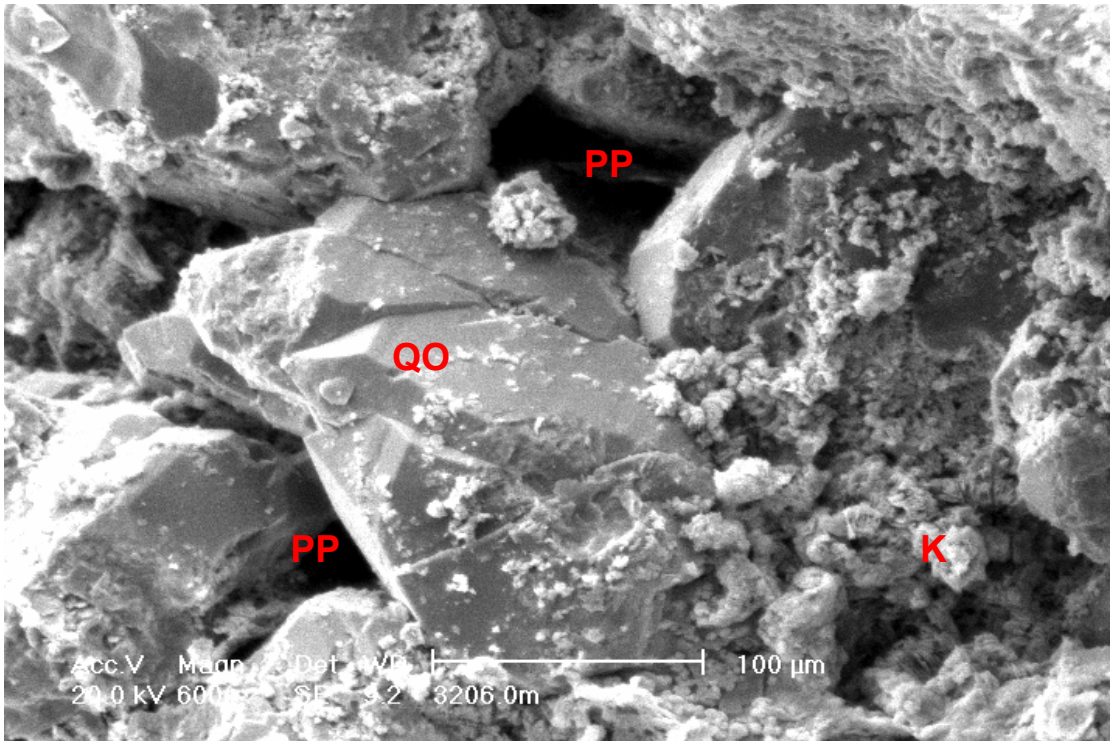

Authigenic kaolinite (K) is effective in completely plugging intergranular pores, whereas quartz overgrowths (QO), being thinly developed, only partly occlude primary intergranular pores (PP). (SEM micrograph)

PLATE 5 #22 3212.0m

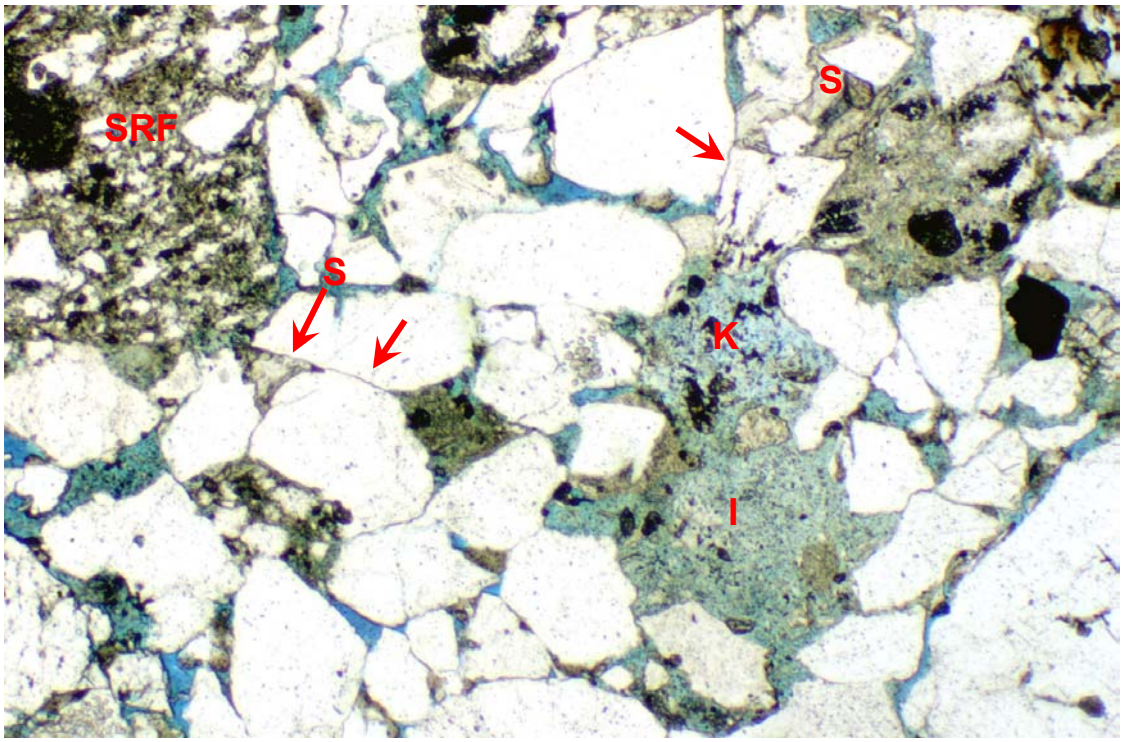

FIGURE 1 Plane polarised light
FIGURE 2 Crossed polarisers

0.4 mm

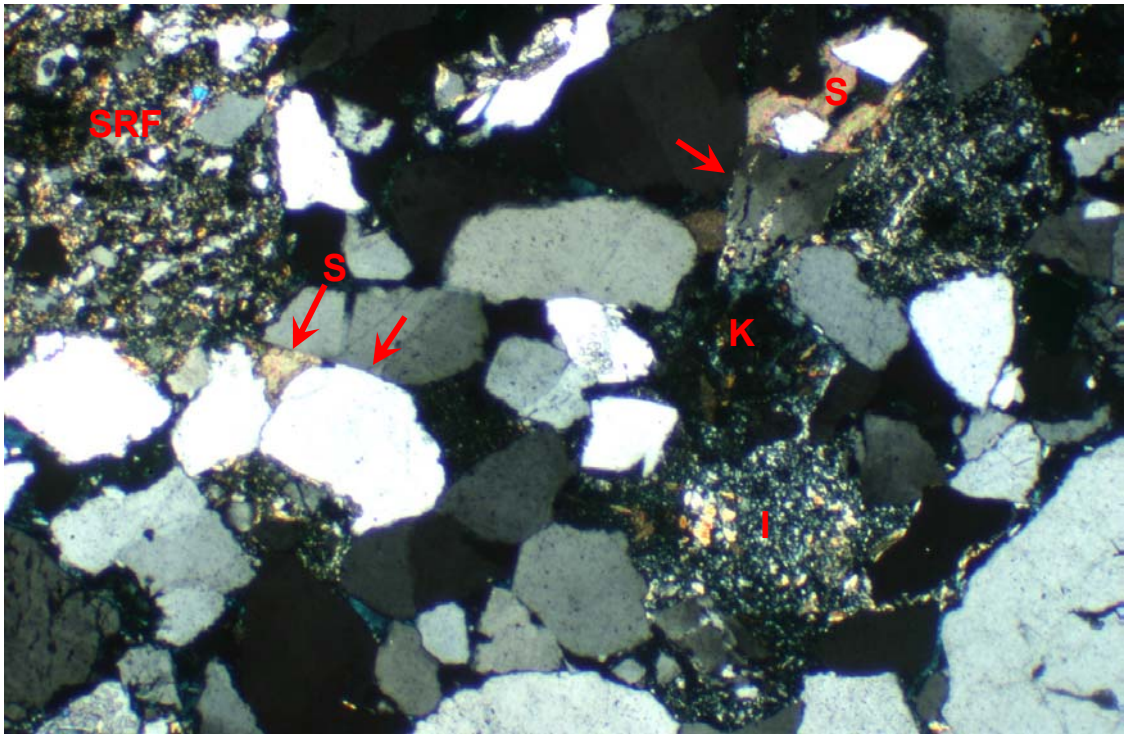

Porosity reduction in this lithic arkose results from pore filling by illitic (I) and kaolinitic (K) pseudomatrix that results from compaction and alteration of micaceous/argillaceous rock fragments. Further porosity loss results from grain contact dissolution (arrows) and minor siderite (S) cementation. Modest primary intergranular porosity (blue) is preserved between juxtaposed quartz grains. A large fine grained sandstone fragment (SRF) is also marked. Detail is shown in Plate 6. K = 35.8mD

ACS Laboratories Pty Ltd
ABN: 81 008 273 005

PLATE 6 #22 3212.0m (cont.)

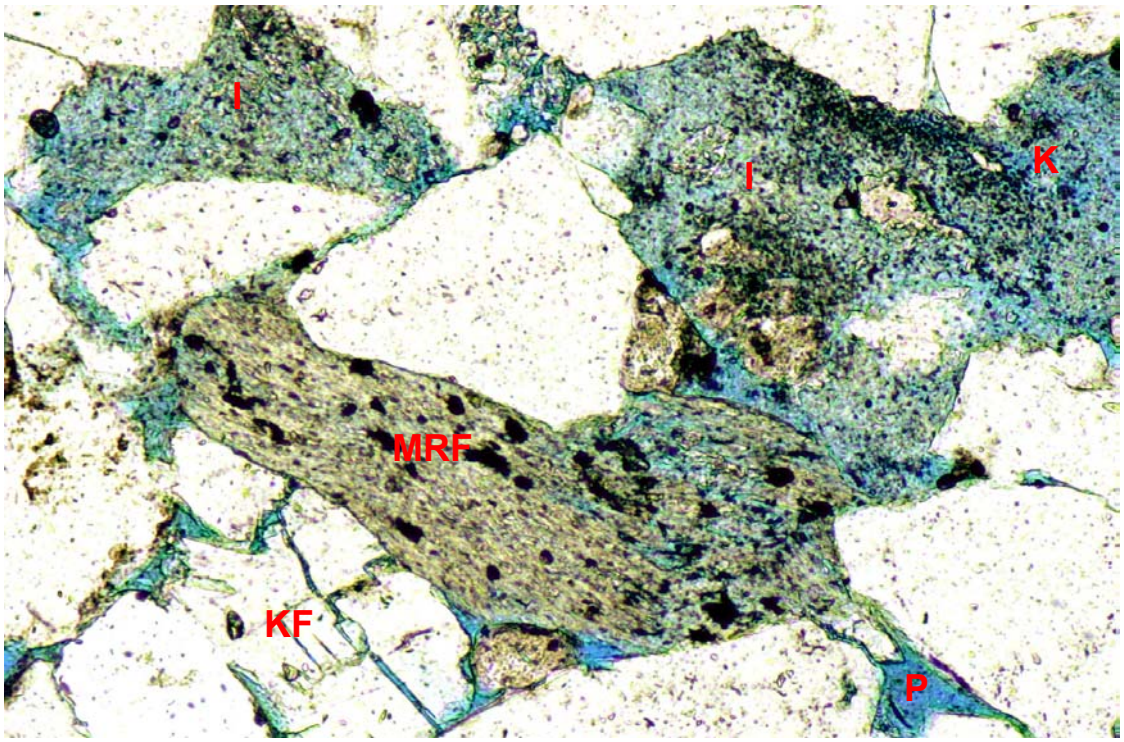

FIGURE 1 Plane polarised light

FIGURE 2 Crossed polarisers

0.2 mm

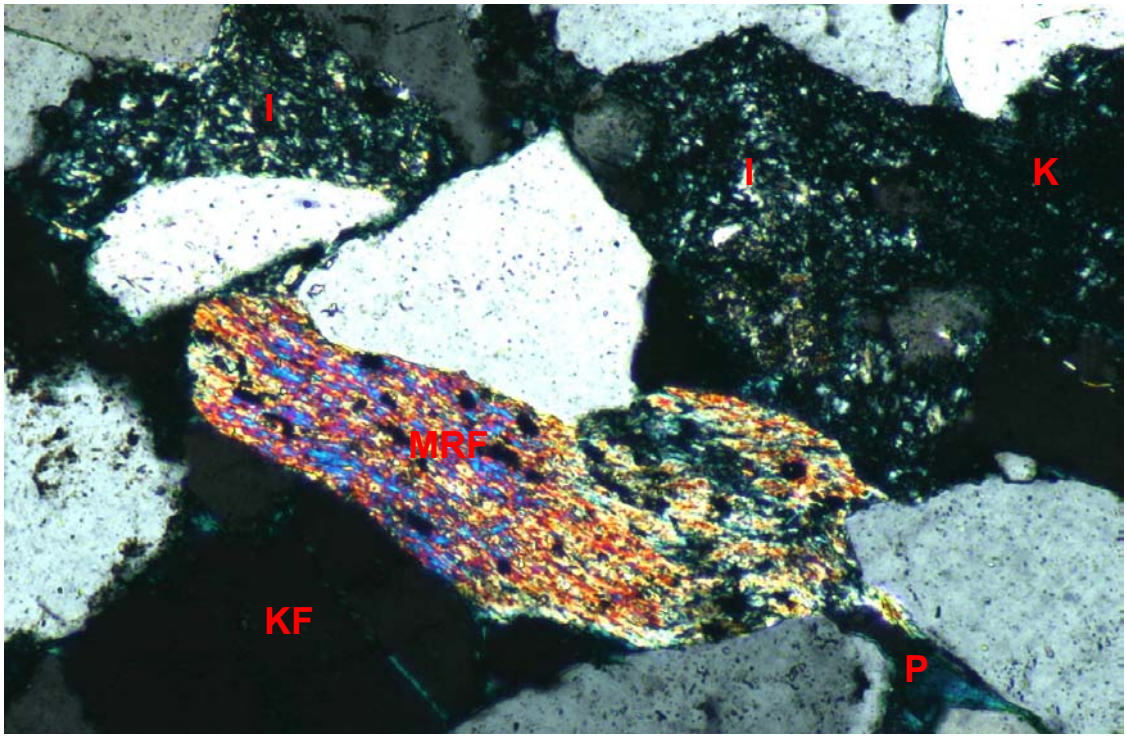

Illitic (I) and kaolinitic (K) clay pseudomatrix and a compacted micaceous metamorphic rock fragment (MRF) greatly reduce interconnectivity between intergranular pores (P) that are preserved between juxtaposed quartz and K-feldspar (KF) grains. K = 35.8mD

PLATE 7 #21 3218.0m

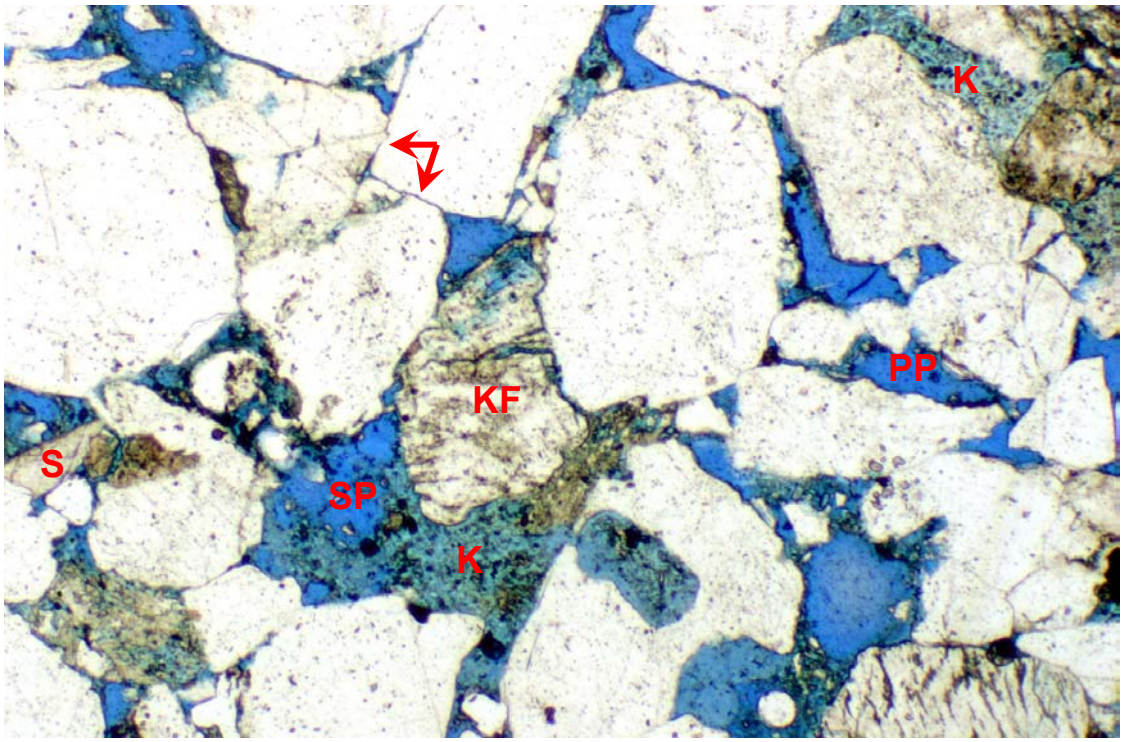

FIGURE 1 Plane polarised light
FIGURE 2 Crossed polarisers

0.4 mm

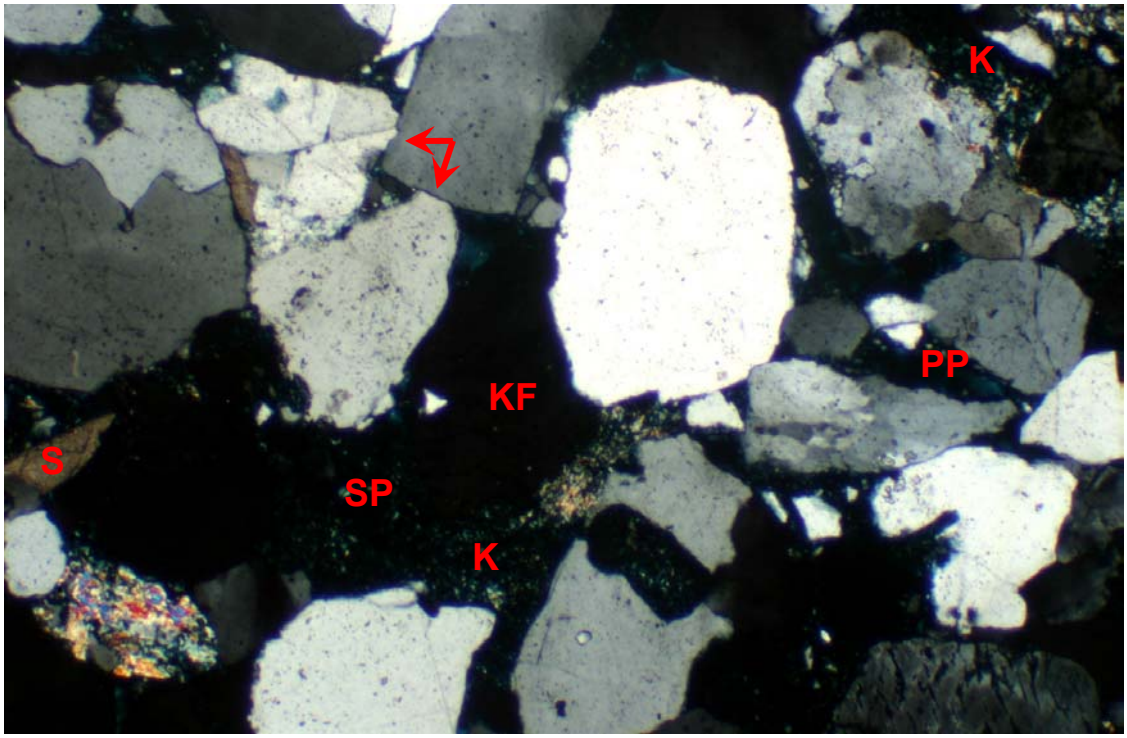

This coarse grained subarkose contains a system of well-interconnected primary intergranular pores (PP) and subordinate secondary labile grain dissolution pores (SP). Good primary intergranular porosity is preserved despite porosity reduction by authigenic kaolinite (K) formation and grain contact dissolution (arrows). Siderite (S) forms scattered, pore-filling, scalenohedral crystals and cement patches that are insufficiently common to impact reservoir quality. Compactionally-fractured K-feldspar (KF) is also marked. K = 3150mD

PLATE 8 #21 3218.0m (cont.)

FIGURE 1

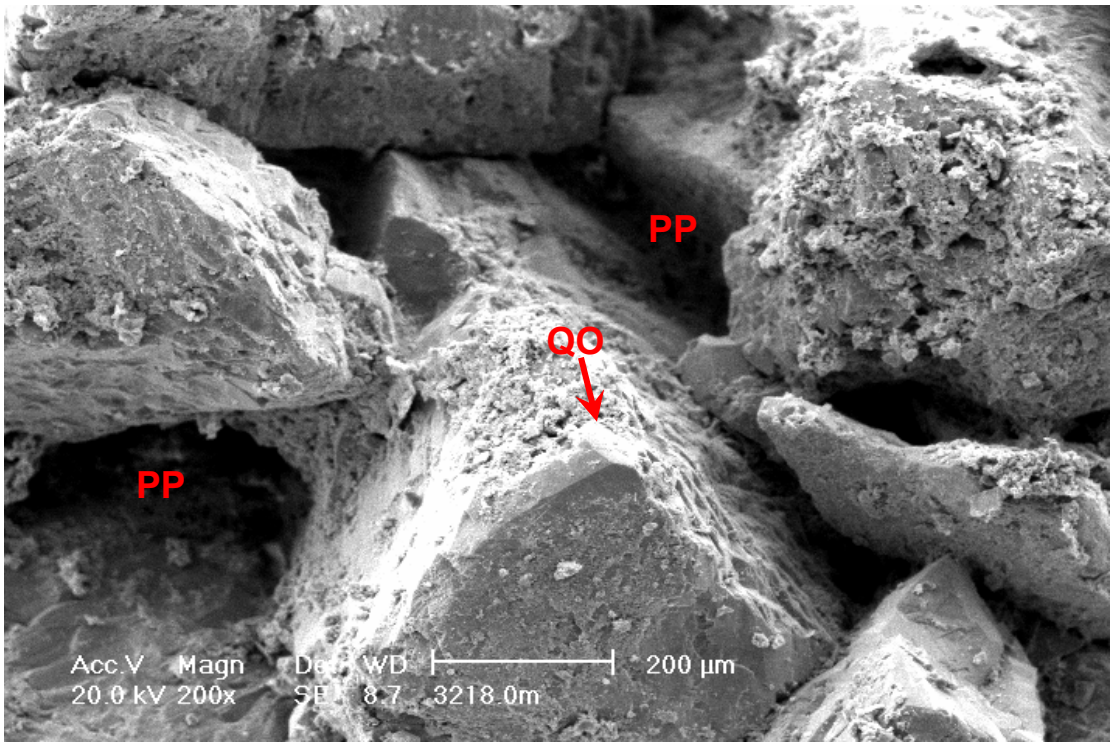

Large primary intergranular pores (PP) are preserved between poorly compacted and essentially uncemented quartz grains. Quartz overgrowths (QO) are poorly developed and thus do little to reduce intergranular porosity. (SEM micrograph)

FIGURE 2

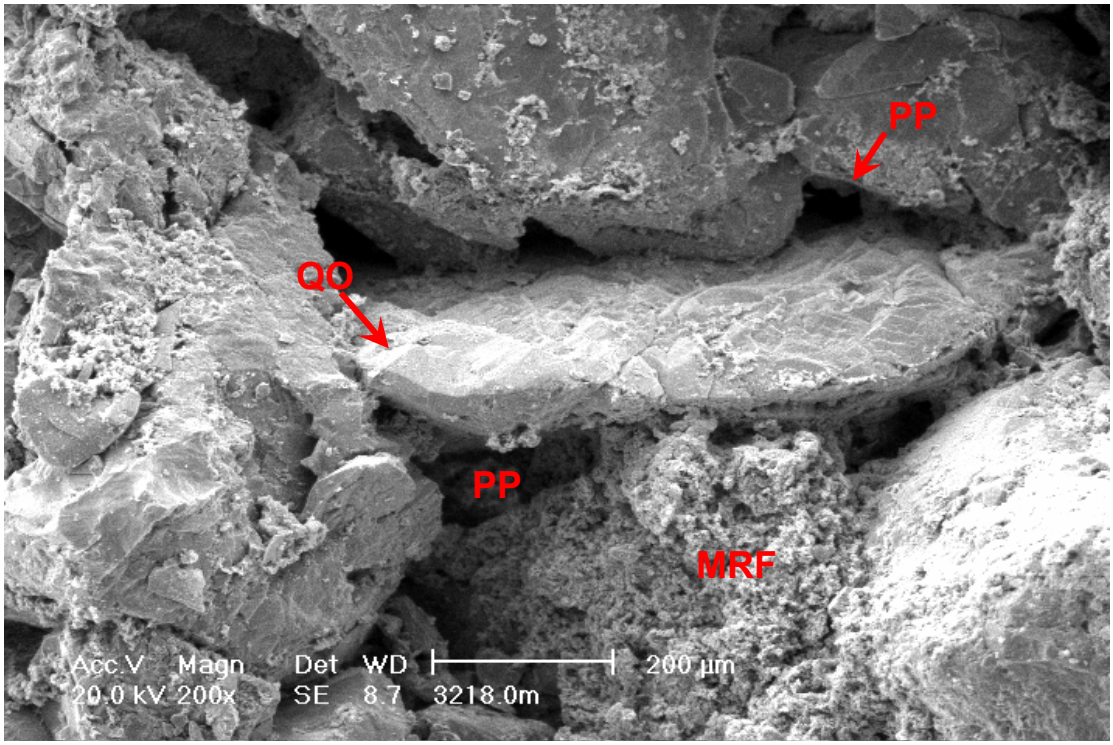

Intergranular spaces are locally filled by compacted/altered micaceous rock fragments (MRF), but the sandstone still contains abundant primary porosity (PP) and is thus highly (3150mD) permeable. Thin quartz overgrowths (QO) envelop one quartz grain. (SEM micrograph)

PLATE 9 #21 3218.0m (cont.)

FIGURE 1

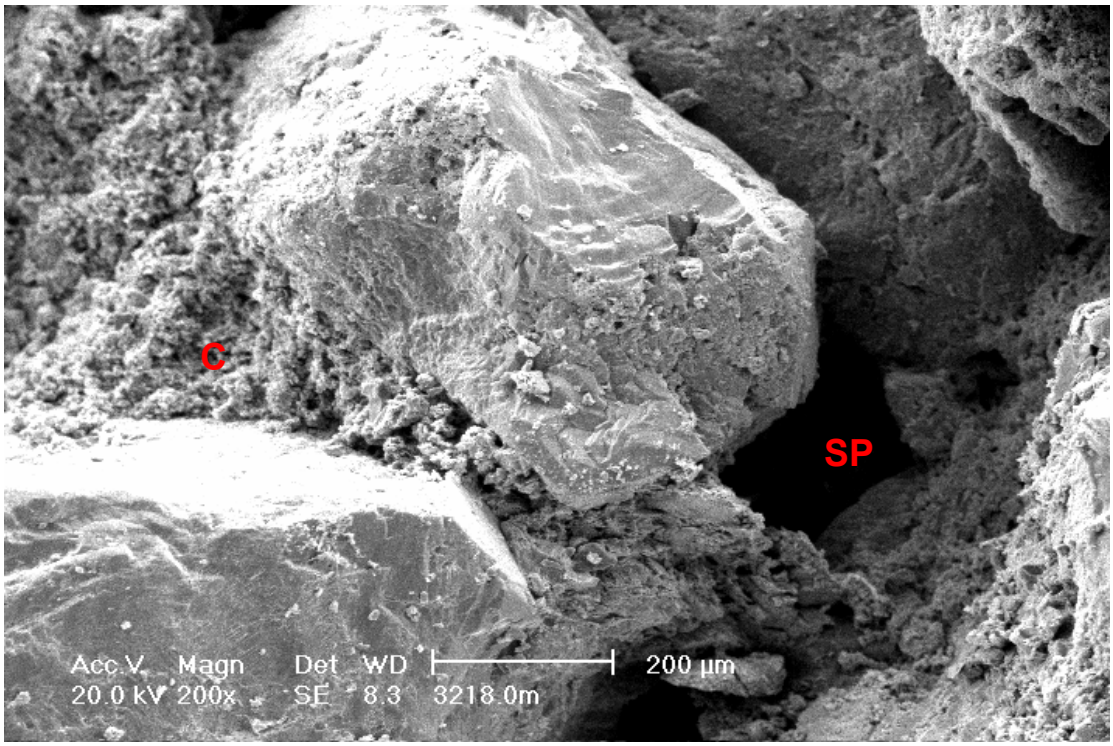

Connectivity between a large secondary pore (SP) and macropores in its vicinity is reduced by authigenic clay pseudomatrix (C) that results from compaction and alteration of a micaceous/argillaceous rock fragment. (SEM micrograph)

FIGURE 2

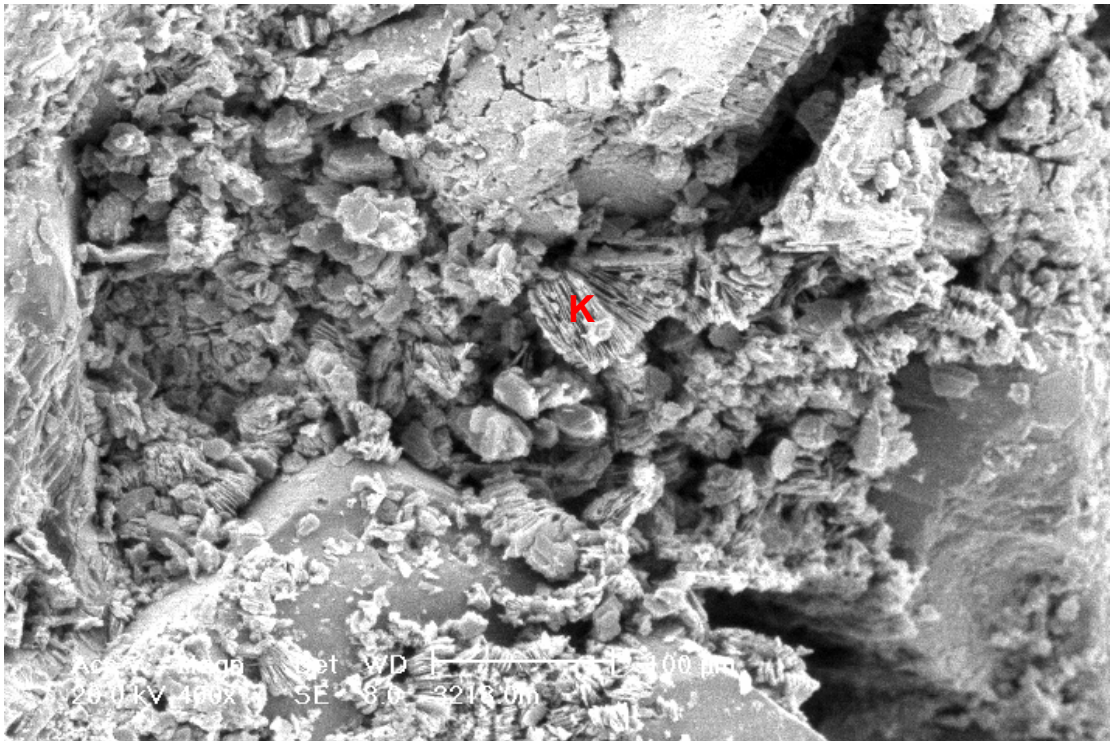

Loosely packed, highly microporous authigenic kaolinite pseudomatrix (K) fills an intergranular space where a micaceous grain has altered. Permeability reduction mainly results from pore filling by authigenic clay and compacted ductile grains. (SEM micrograph)

PLATE 10 #19 3251.0m

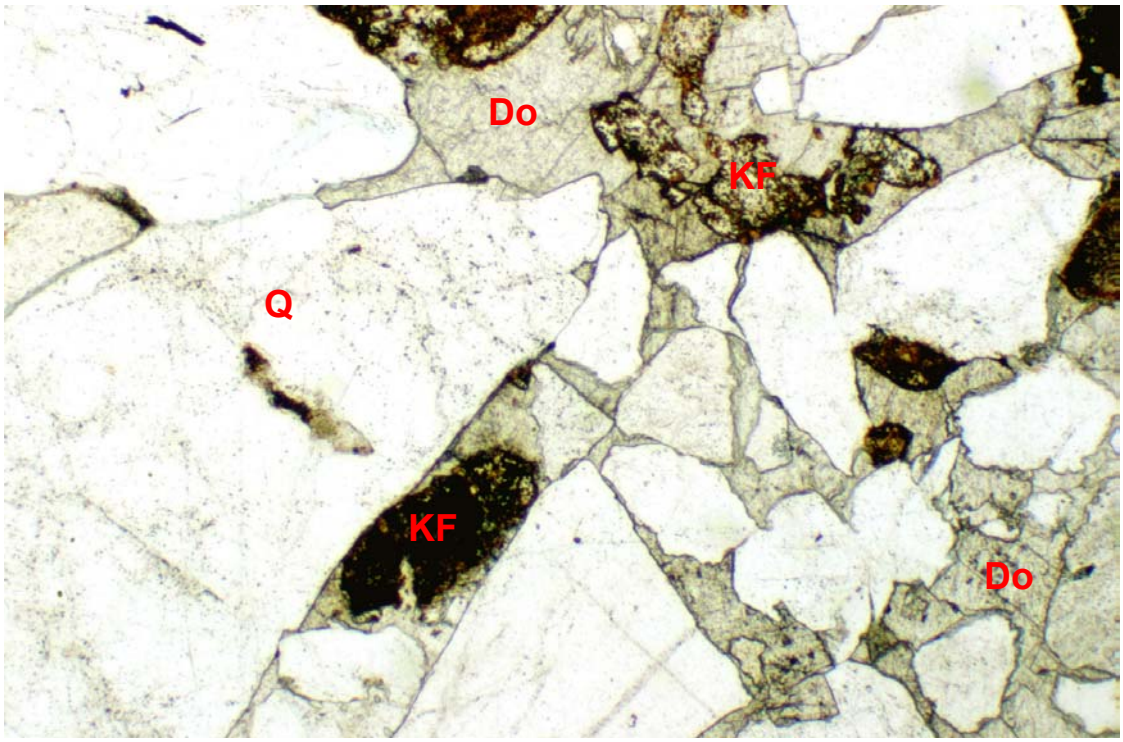

FIGURE 1 Plane polarised light
FIGURE 2 Crossed polarisers

0.4 mm

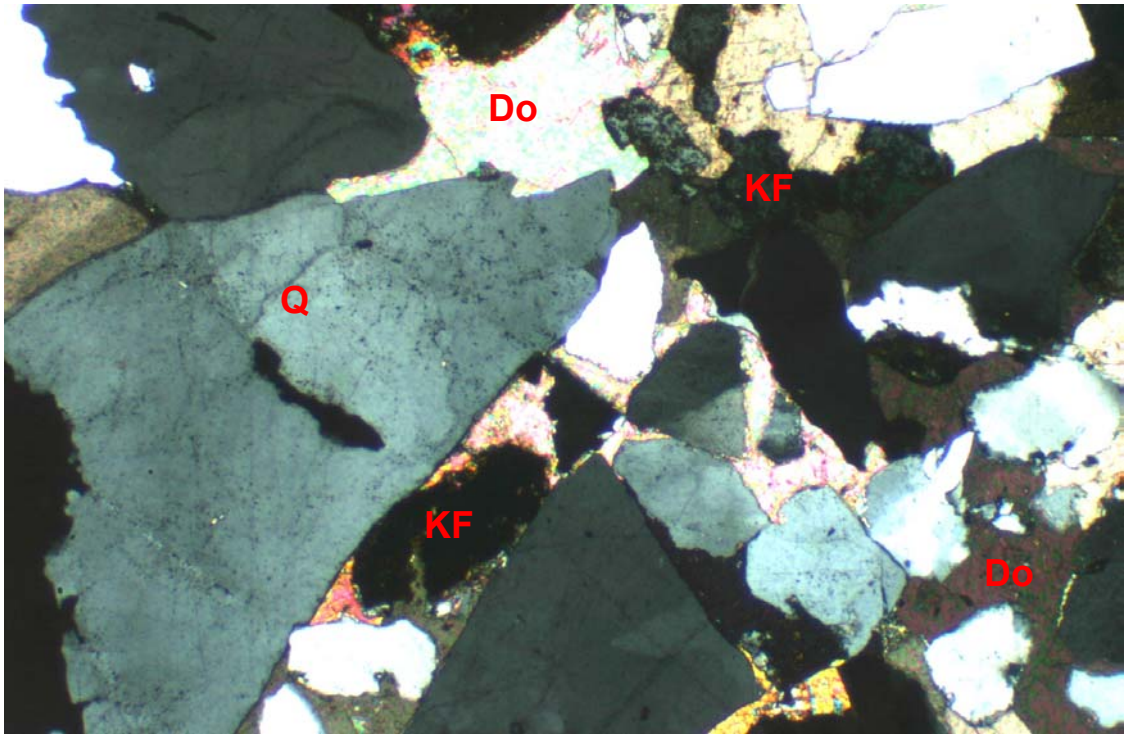

Tight, poorly sorted, coarse grained lithic arkose in which all intergranular spaces between quartz (Q) and K-feldspar (KF) (stained brown) grains are filled by late-stage, coarsely-crystalline dolomite cement (Do). Detail is shown in Plate 11. K = 2.71mD

PLATE 11 #19 3251.0m (cont.)

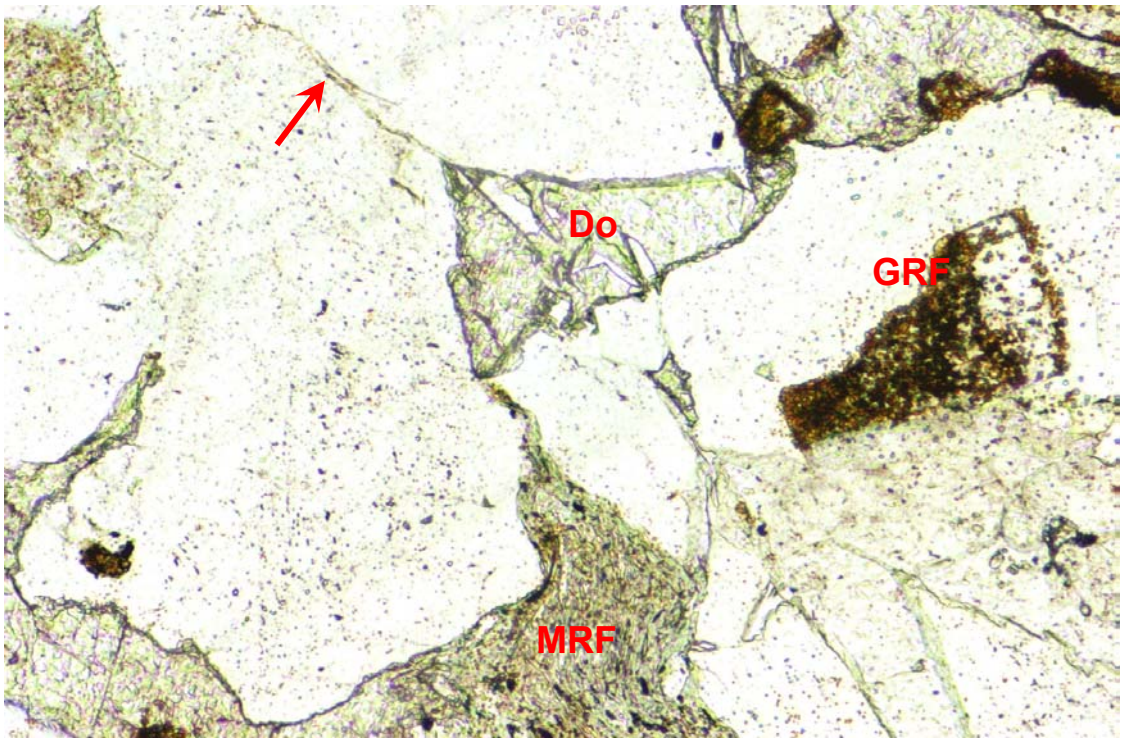

FIGURE 1 Plane polarised light

FIGURE 2 Crossed polarisers

0.2 mm

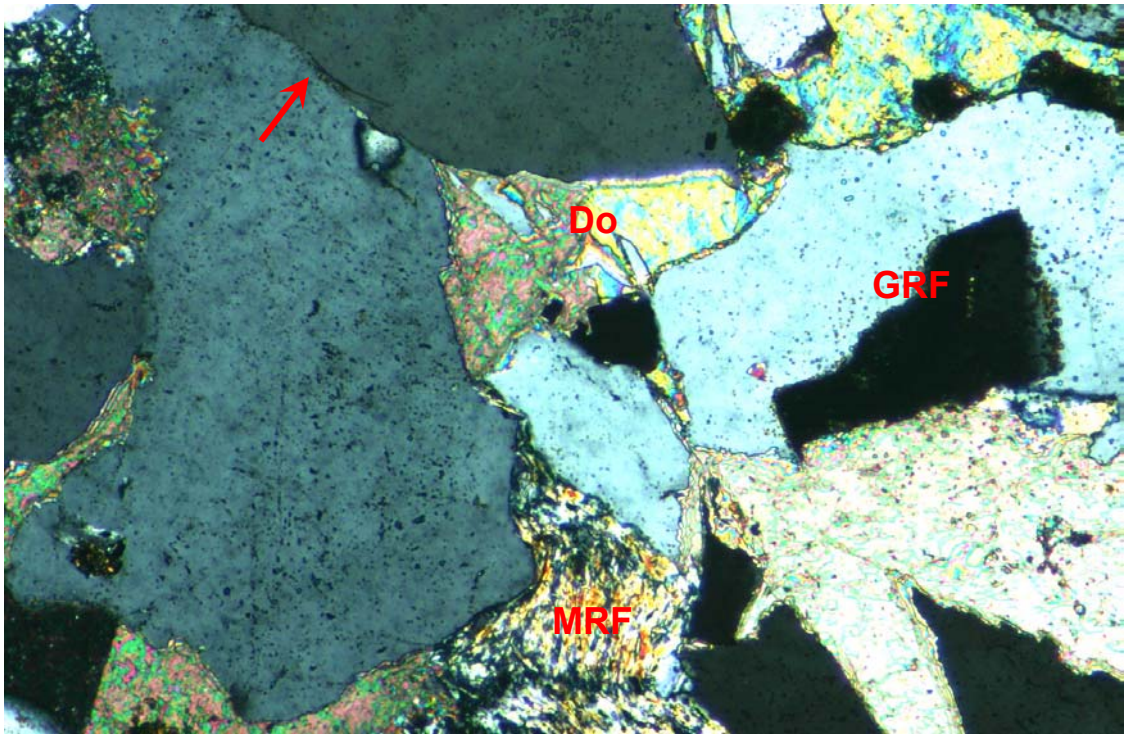

Low permeability (2.71mD) reflects the presence of abundant dolomite cement (Do). Dolomite-cemented micaceous metamorphic rock fragments (MRF) are compactionally deformed, and quartz grains have welded grain contacts resulting from grain contact dissolution (arrow), indicating that dolomite postdates physical compaction and some grain contact dissolution. Framework grains include a granitic rock fragment (coarsely intergrown quartz and stained K-feldspar) (GRF).

PLATE 12 #17 3287.0m

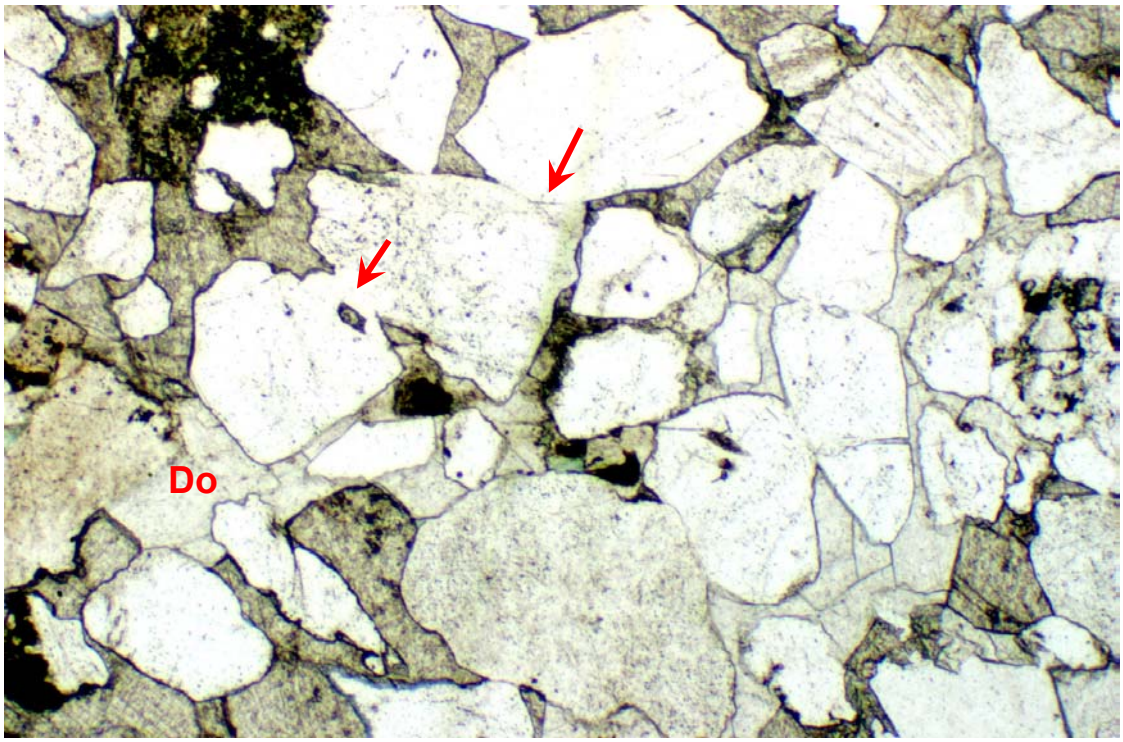

FIGURE 1 Plane polarised light
FIGURE 2 Crossed polarisers

0.4 mm

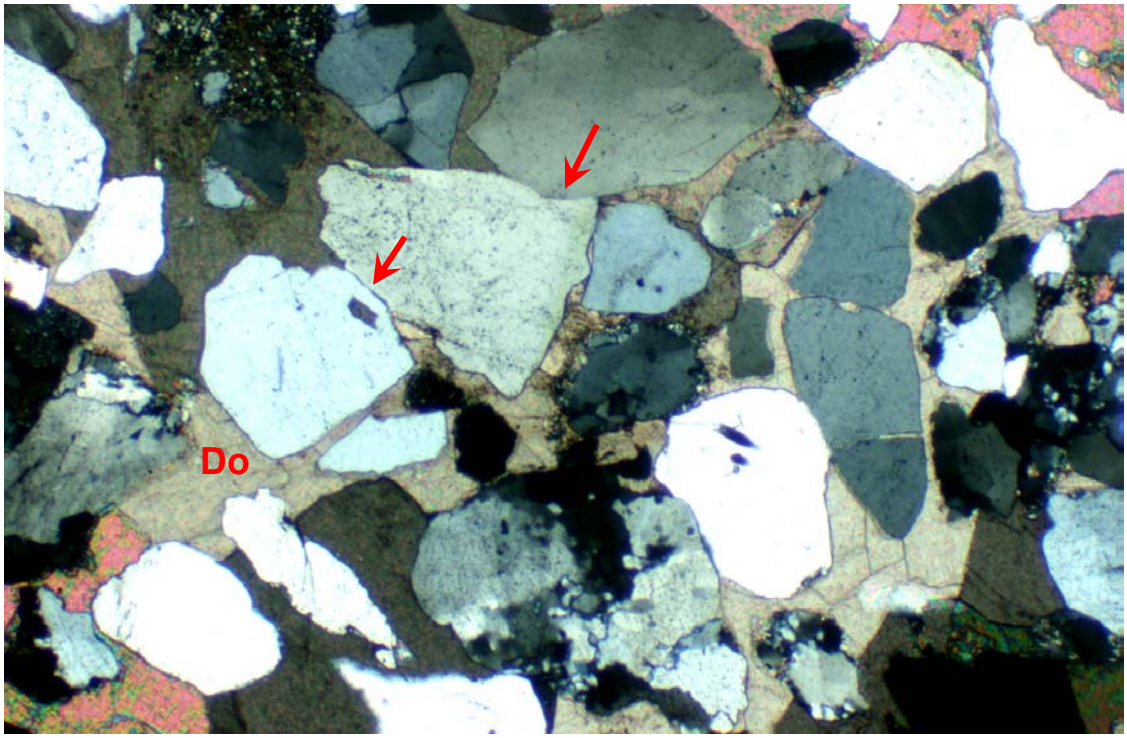

Like the previous sample, this sandstone is tightly cemented by late-stage, coarsely-crystalline dolomite (Do). Grain contact dissolution to form welded grain contacts (arrows) occurred prior to dolomite cementation. K = 0.04mD

PLATE 13 #16 3299.0m

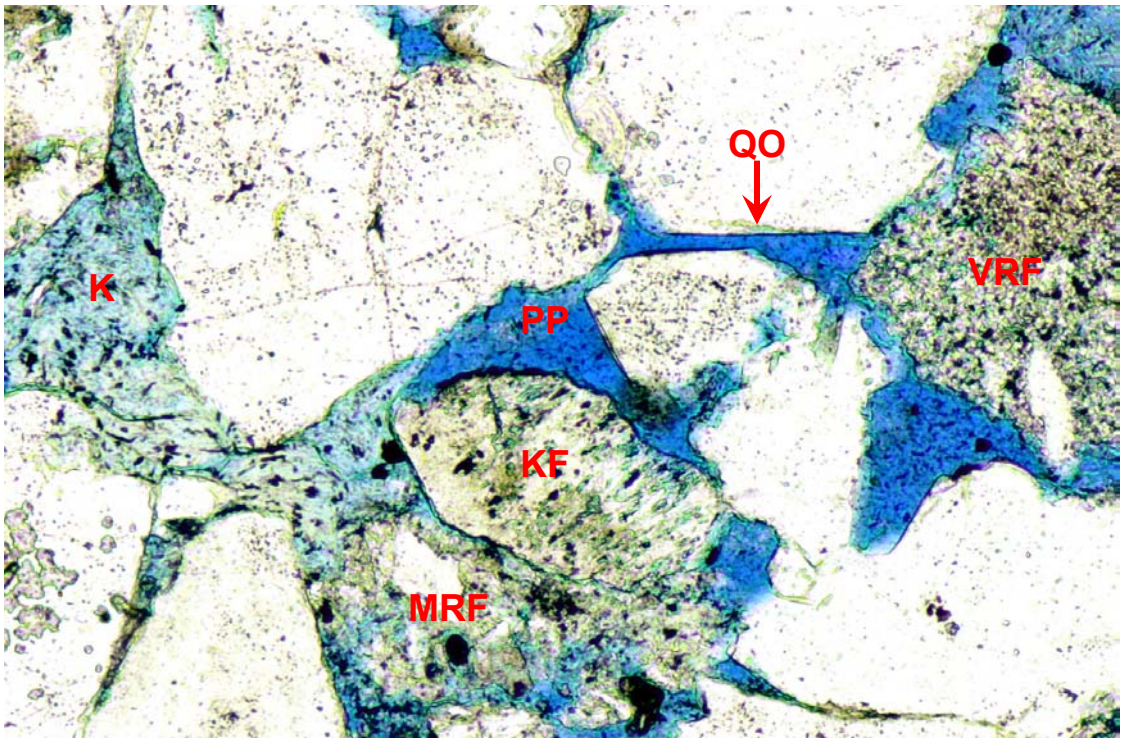

FIGURE 1 Plane polarised light

FIGURE 2 Crossed polarisers

0.2 mm

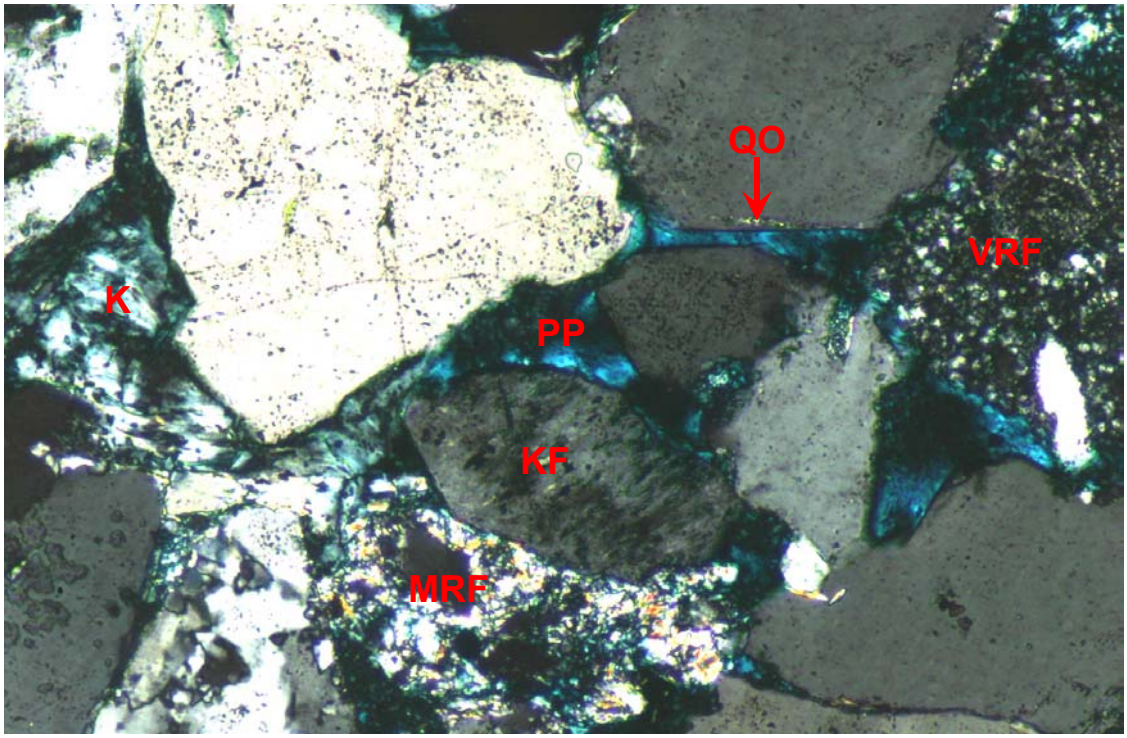

In this medium grained lithic arkose, good primary intergranular porosity (PP) is preserved between juxtaposed quartz and K-feldspar (KF) grains and a silicified volcanic rock fragment (VRF), but pore interconnectivity is significantly reduced by authigenic kaolinite pseudomatrix (K) that results from mica compaction and alteration. Compaction of a micaceous low-grade metasedimentary rock fragment (MRF) has also reduced intergranular porosity. Pores are bounded by thinly developed quartz overgrowths (QO). K = 48.4mD

PLATE 14 #16 3299.0m (cont.)

FIGURE 1

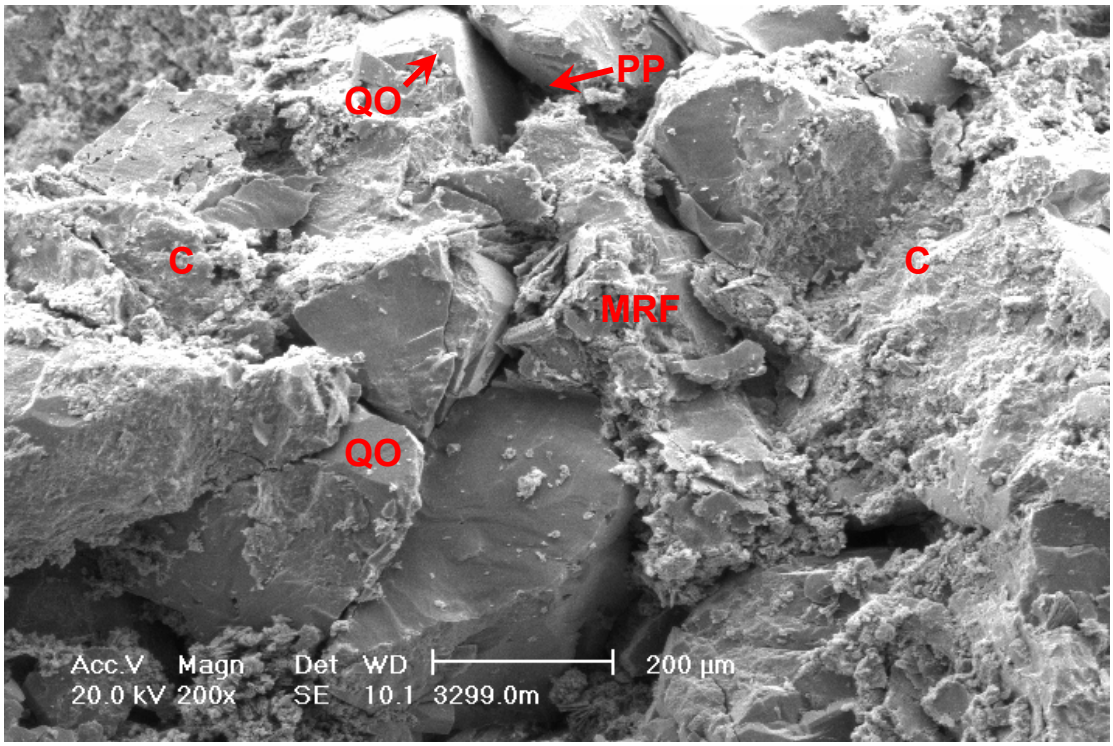

Interconnection between quartz overgrowth (QO)-bounded primary intergranular pores (PP) is reduced by micaceous rock fragment (MRF) compaction and alteration to form clay pseudomatrix (C). (SEM micrograph)

FIGURE 2

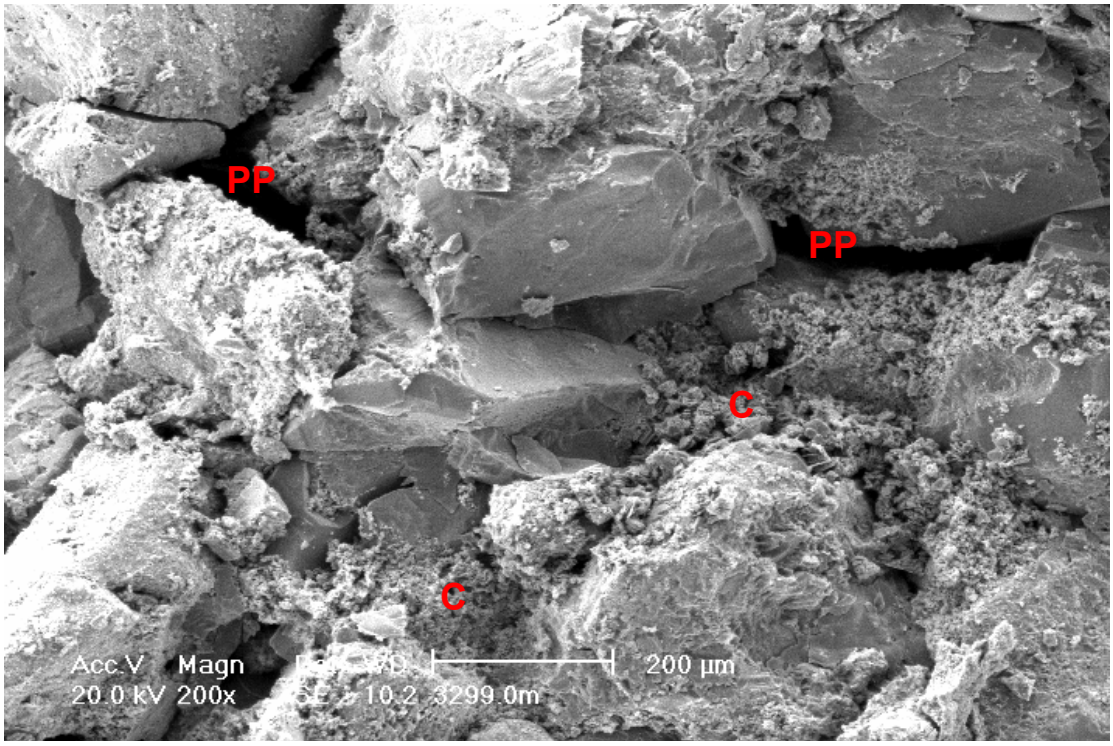

Clay pseudomatrix (C) is effective in completely filling intergranular spaces. Large primary intergranular pores (PP) are preserved where rigid grains are juxtaposed. (SEM micrograph)

PLATE 15 #16 3299.0m (cont.)

FIGURE 1

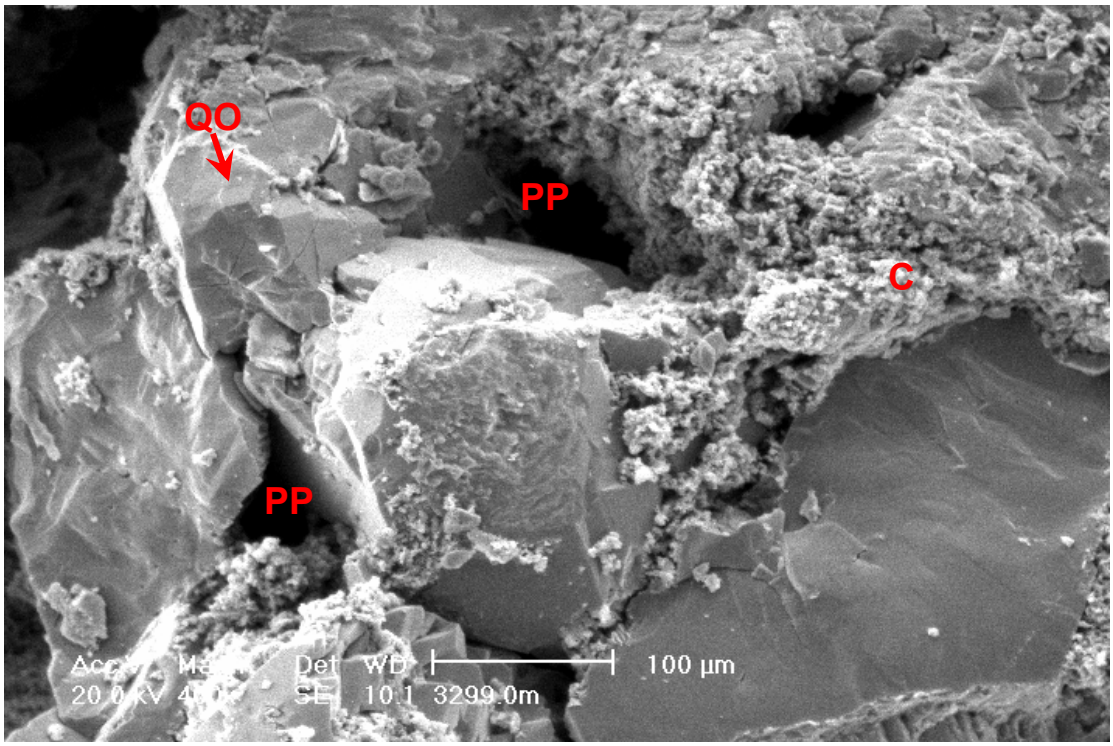

Quartz overgrowths (QO), being thinly developed, only partly occlude primary intergranular pores (PP), whereas authigenic clay pseudomatrix (C) and compacted ductile grains are highly effective in completely clogging intergranular spaces and reducing permeability. (SEM micrograph)

FIGURE 2

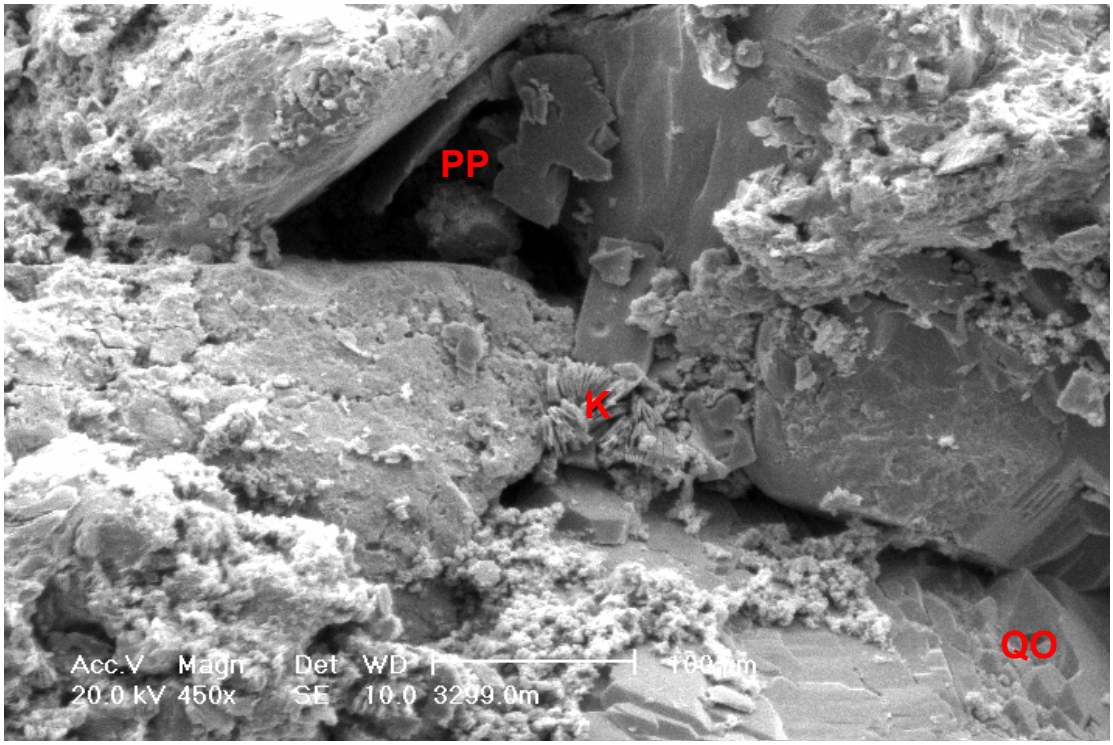

Detail of a typical primary intergranular pore (PP) that is preserved where rigid framework grains are juxtaposed. Clay is largely authigenic kaolinite (K) that results from labile grain alteration. Quartz grains are thinly enveloped by quartz overgrowths (QO). (SEM micrograph)

PLATE 16 #14 3306.5m

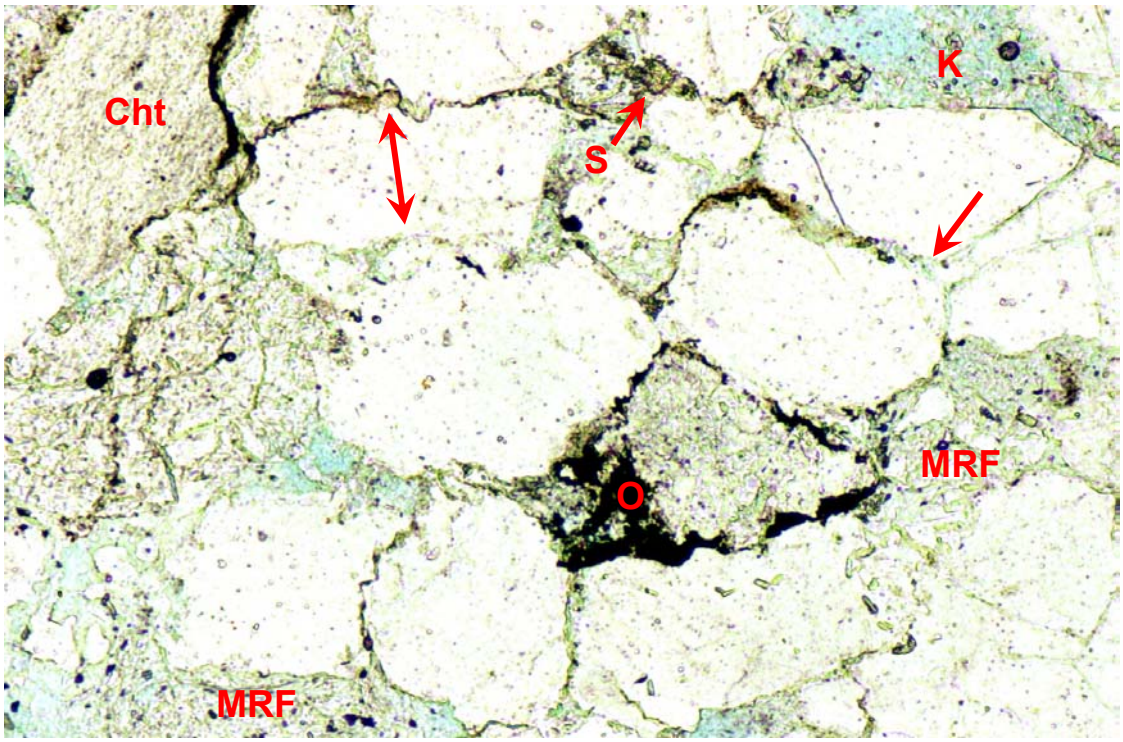

FIGURE 1 Plane polarised light

FIGURE 2 Crossed polarisers

0.2 mm

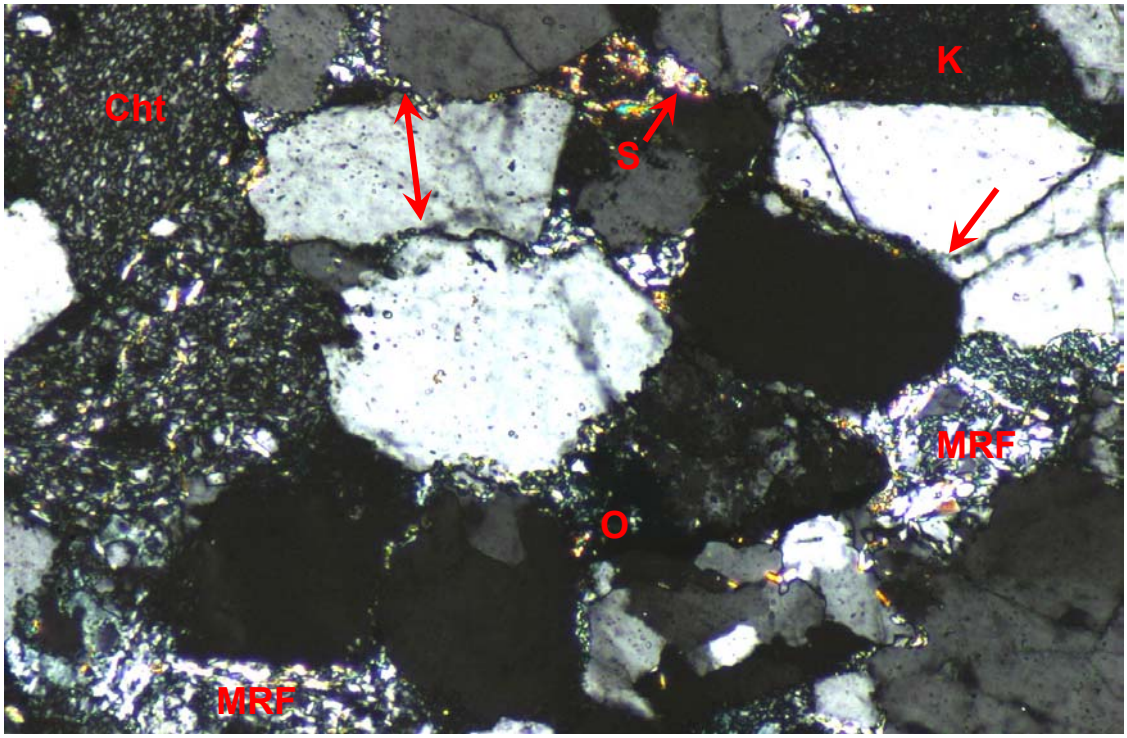

Intergranular porosity is absent in this medium grained sandstone due to the combined effect of authigenic kaolinite (K) formation, altered micaceous/illitic metasedimentary rock fragment (MRF) compaction, and grain contact dissolution/microstylolitisation (arrows). Fine siderite (S) locally replaces clay. Opaques (O) are anatase. Framework grains include chert (Cht). The sandstone was susceptible to authigenic clay formation and compaction on account of containing common micaceous/illitic grains at the time of accumulation. K = 12.4mD

PLATE 17 #12 3308.5m

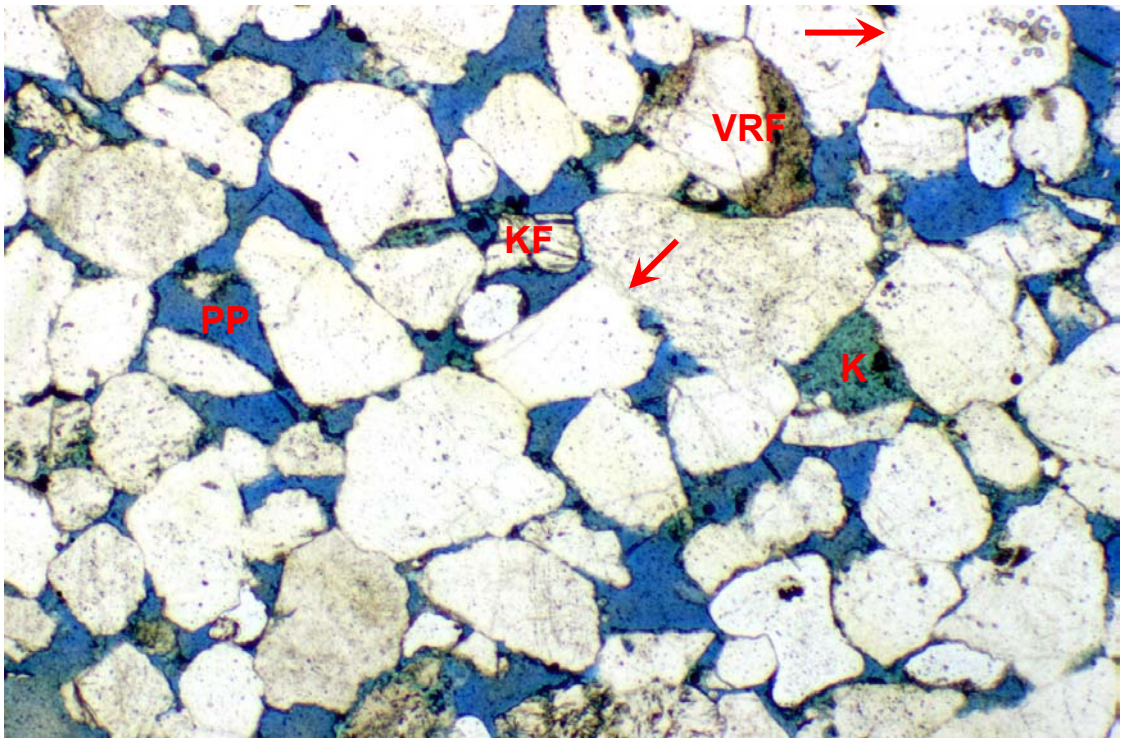

FIGURE 1 Plane polarised light
FIGURE 2 Crossed polarisers

0.4 mm

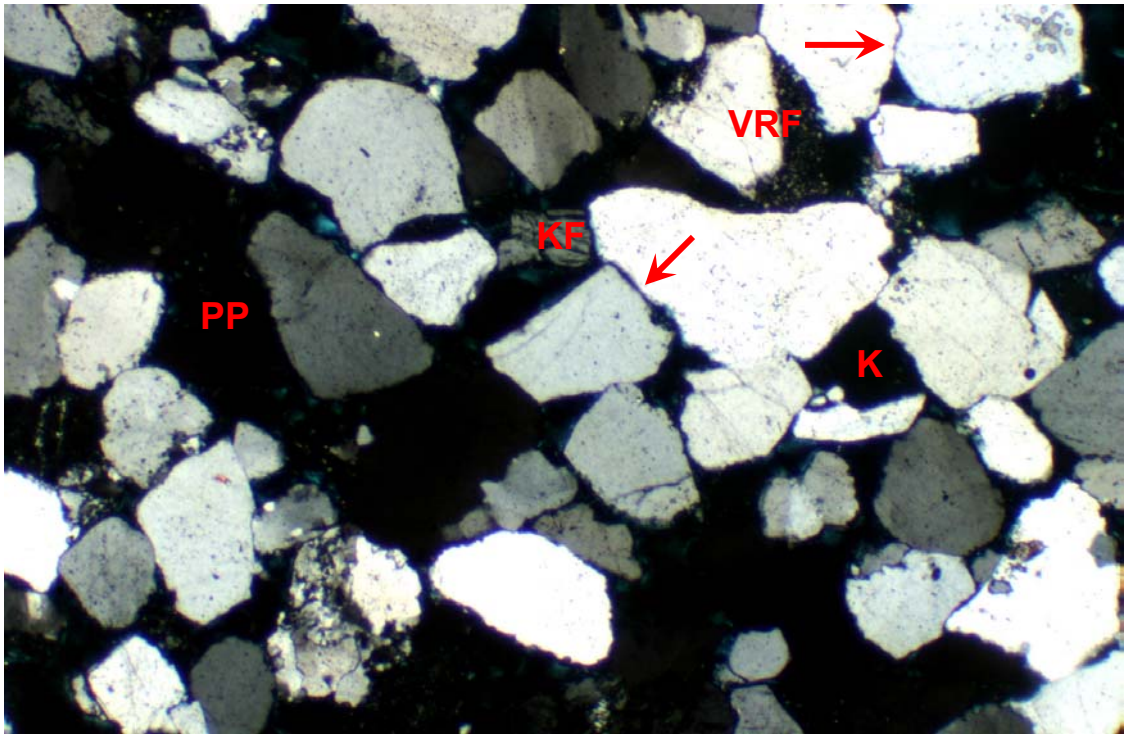

In contrast to the previous sample, this subarkose was highly quartzose at the time of accumulation and consequently now contains little authigenic kaolinite (K) and few compacted ductile grains. Abundant, evenly distributed, hence well-interconnected primary intergranular porosity (PP) is preserved in the sandstone, despite grain welding by grain contact dissolution (arrows). Framework grains include granitic K-feldspar (KF) and a silicified volcanic rock fragment with a quartz phenocryst (VRF). Detail is shown in Plate 18. K = 2090mD

PLATE 18 #12 3308.5m (cont.)

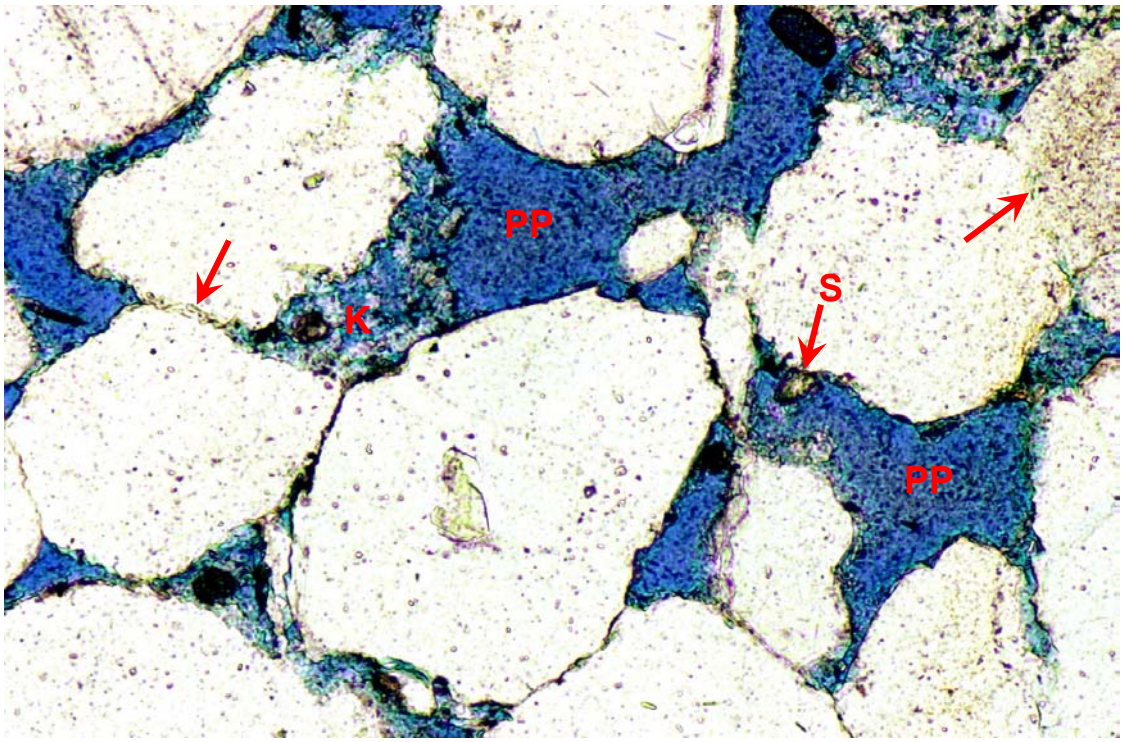

FIGURE 1 Plane polarised light

FIGURE 2 Crossed polarisers

0.2 mm

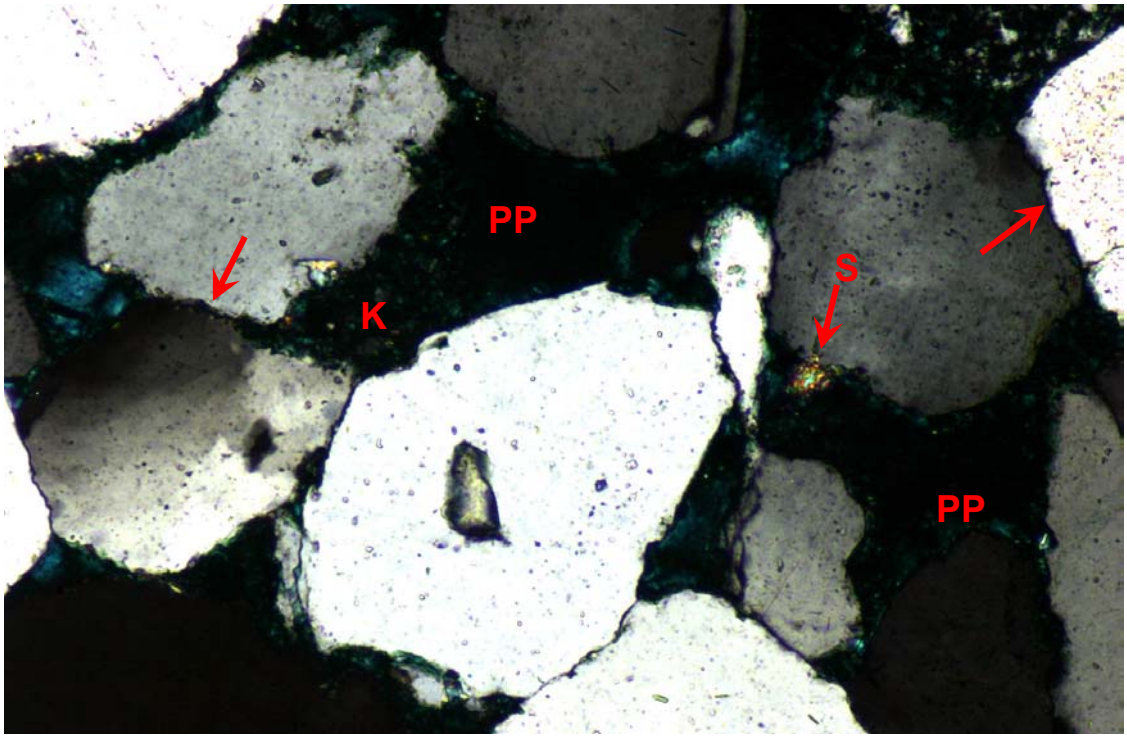

Framework grain packing density has been increased by grain contact dissolution (arrows), but the sandstone still contains abundant primary intergranular porosity (PP). Authigenic kaolinite (K) and siderite (S) are insufficiently common to significantly impact reservoir quality. K = 2090mD

PLATE 19 #12 3308.5m (cont.)

FIGURE 1

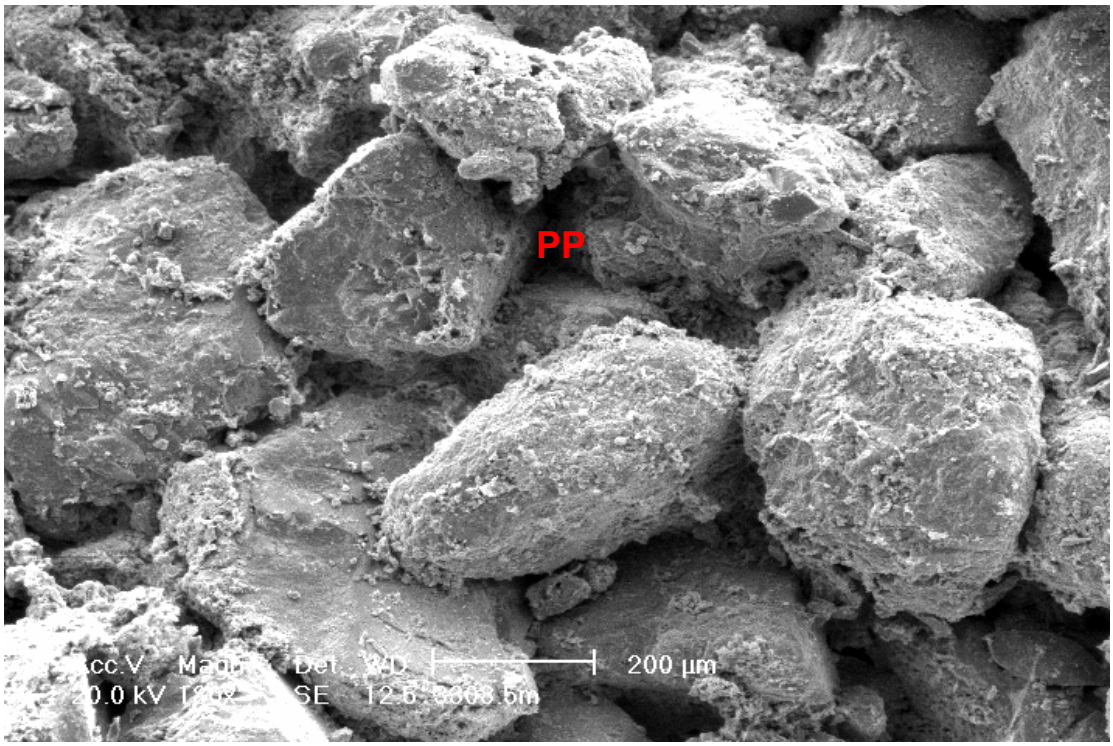

Representative area in which abundant primary intergranular porosity (PP) is preserved between slightly compacted and uncemented framework grains. (SEM micrograph)

FIGURE 2

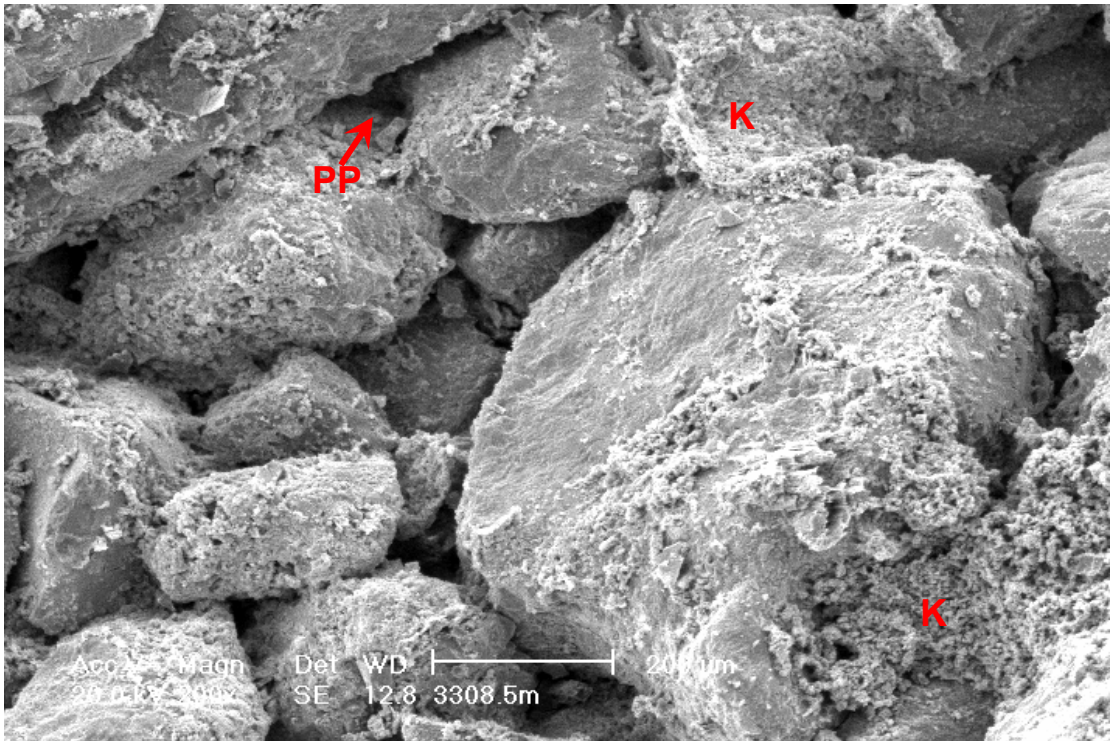

Sporadic patches of authigenic kaolinite (K) that result from micaceous/argillaceous grain and feldspar decomposition are insufficiently common to greatly reduce interconnectivity between primary intergranular pores (PP). Quartz overgrowths are absent on most quartz grains. (SEM micrograph)

PLATE 20 #12 3308.5m (cont.)

FIGURE 1

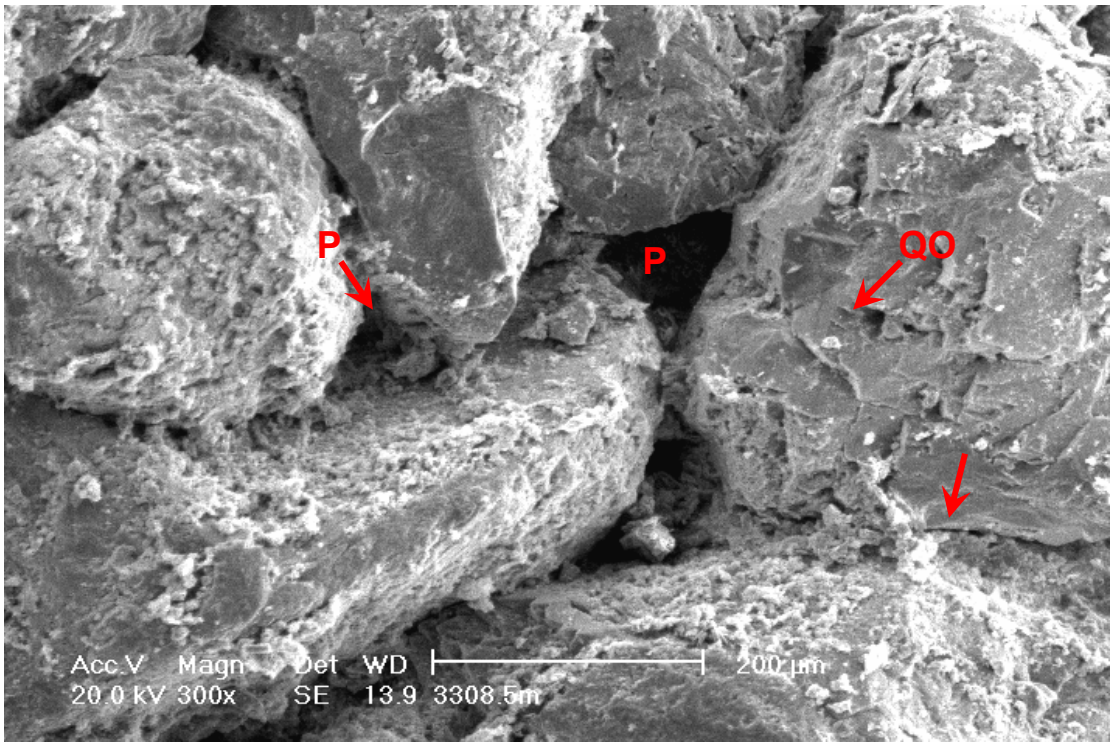

Localised quartz overgrowths (QO) are thinly developed and thus do little to reduce the volume of adjacent intergranular pores (P). Minor porosity loss results from grain welding by grain contact dissolution (arrow). (SEM micrograph)

FIGURE 2

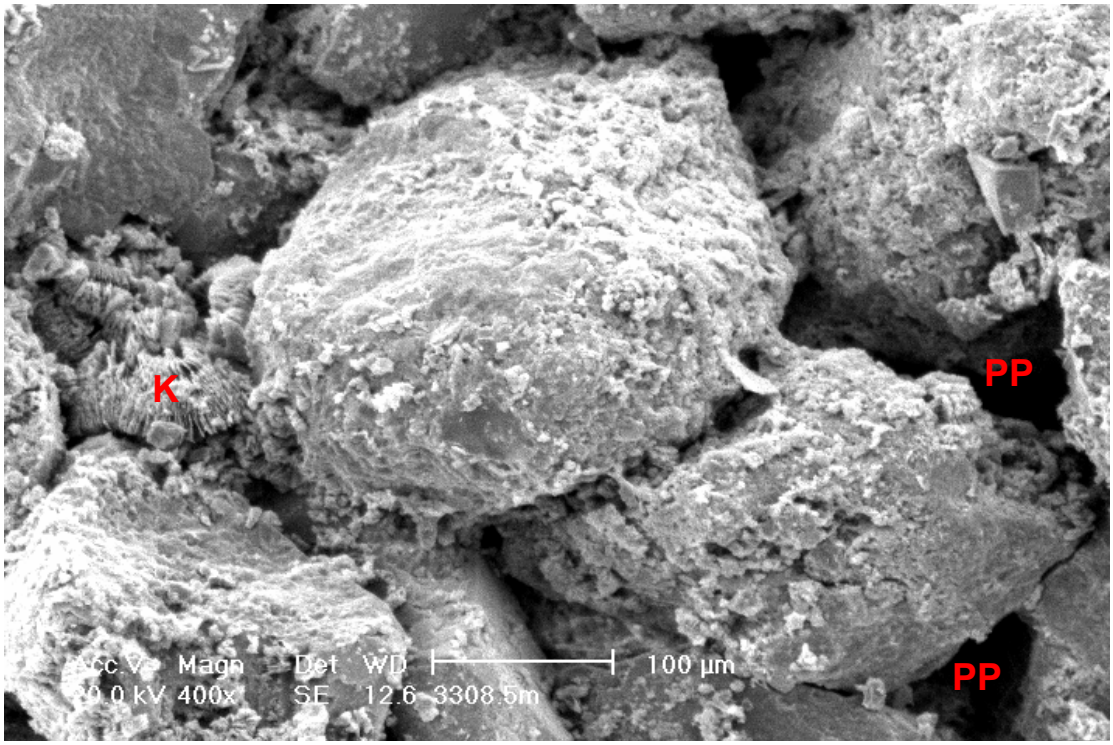

Large, well-interconnected primary intergranular pores (PP) are preserved between most grains, despite porosity loss by grain contact dissolution. Clay is mainly authigenic kaolinite (K) that forms scattered patches where labile grains have altered. The sandstone is essentially uncemented. (SEM micrograph)

PLATE 21 #11 3353.5m

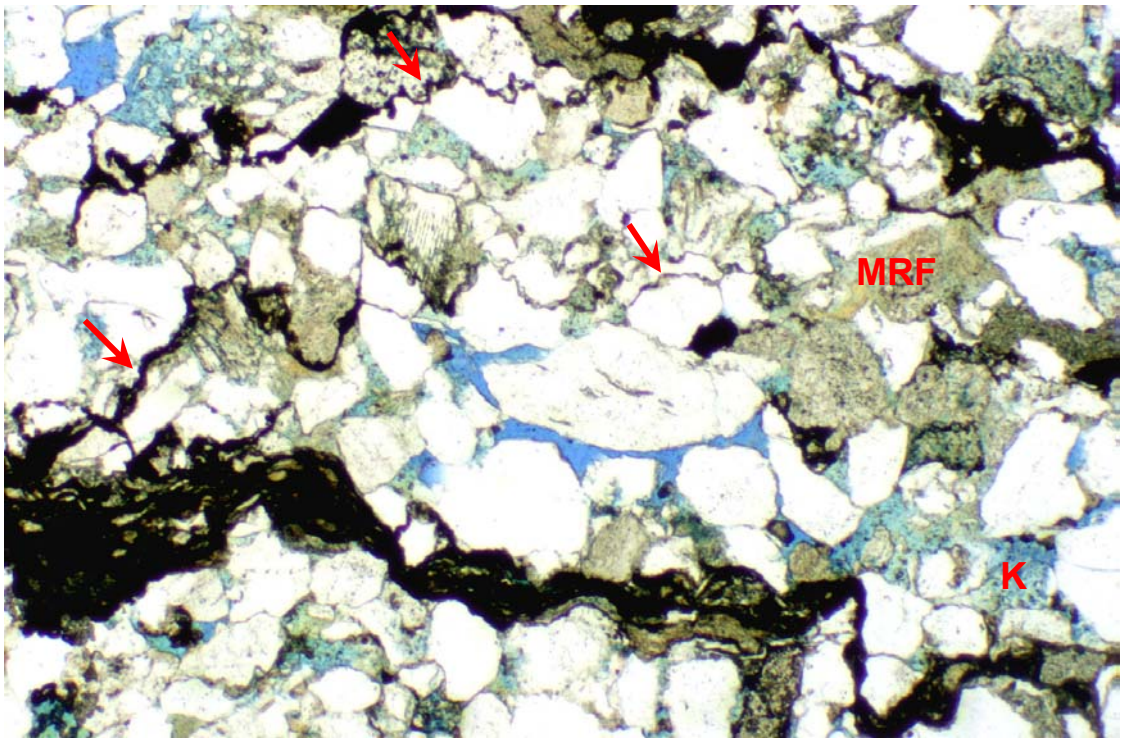

FIGURE 1 Plane polarised light
FIGURE 2 Crossed polarisers

0.4 mm

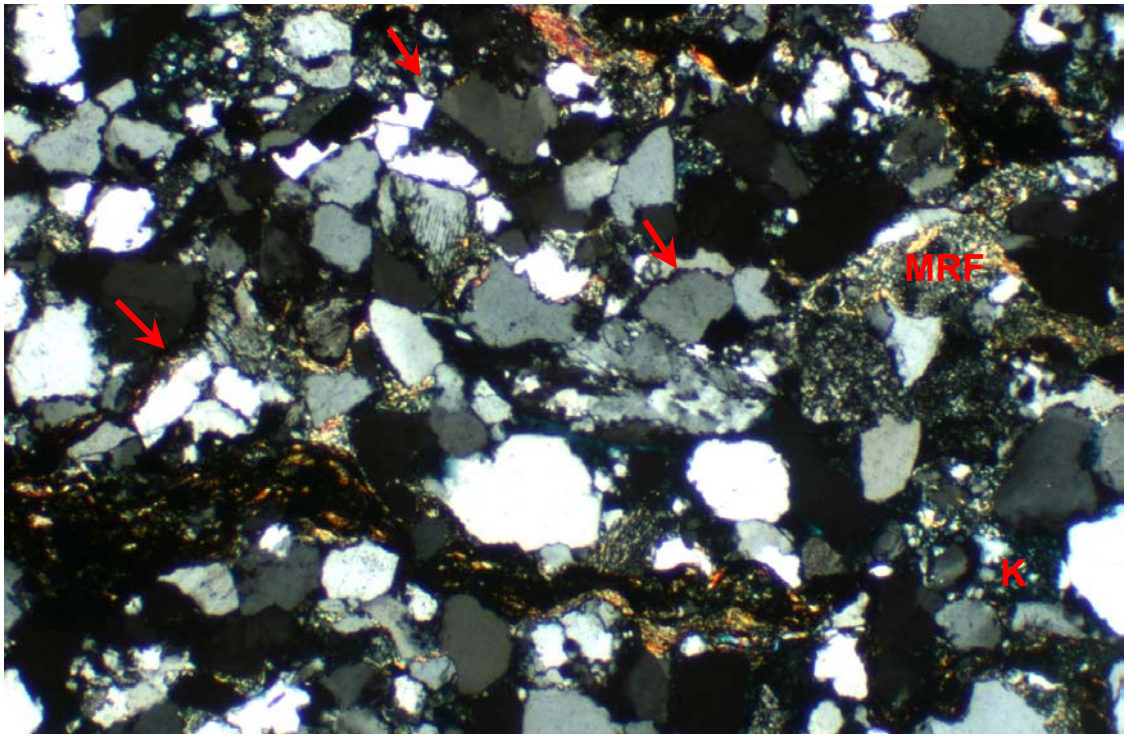

Low magnification micrographs showing general texture of a medium grained sandstone that is cut by tight, stylolitic, argillaceous/carbonaceous laminae (arrows). Between laminae, intergranular porosity (blue) is reduced by micaceous metamorphic rock fragment (MRF) compaction and authigenic kaolinite (K) formation. Detail is shown in Plate 22. K = 45.9mD

PLATE 22 #11 3353.5m (cont.)

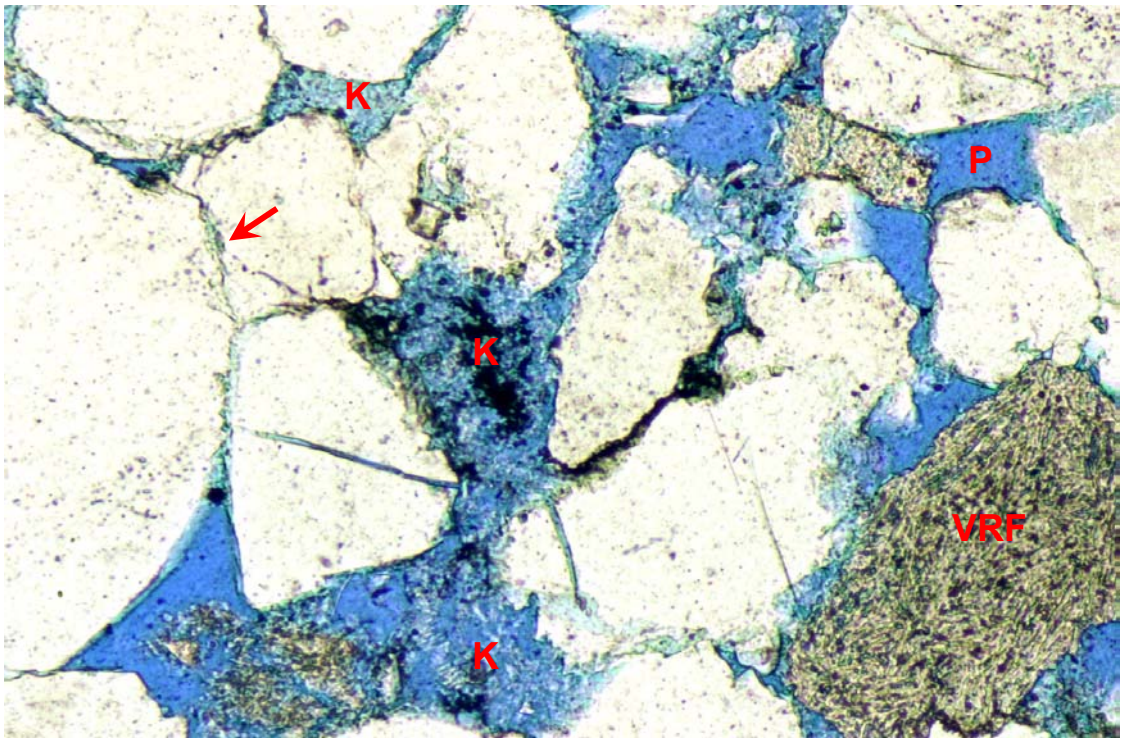

FIGURE 1 Plane polarised light

FIGURE 2 Crossed polarisers

0.2 mm

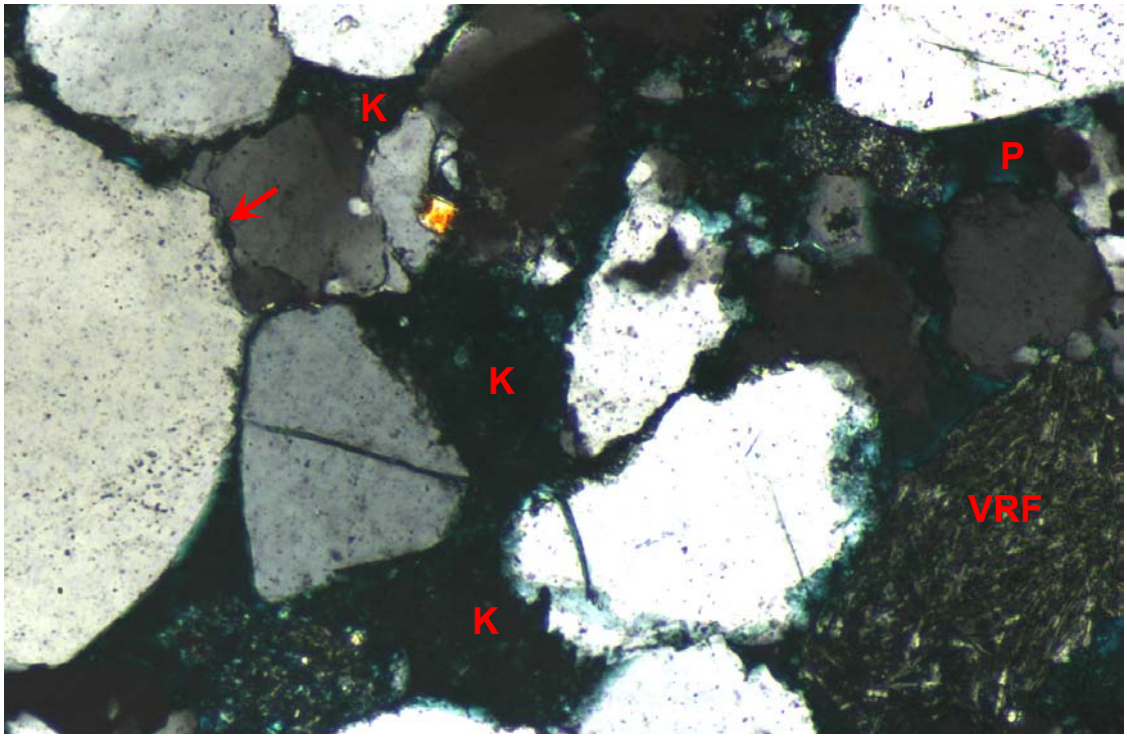

Away from the stylolitic laminae shown in Plate 21, interconnectivity between intergranular pores (P) is reduced by loosely packed authigenic kaolinite (K). Further porosity reduction results from grain contact dissolution (arrow). Framework grains include an intermediate volcanic rock fragment (VRF). K = 45.9mD

PLATE 23 #7 3372.0m

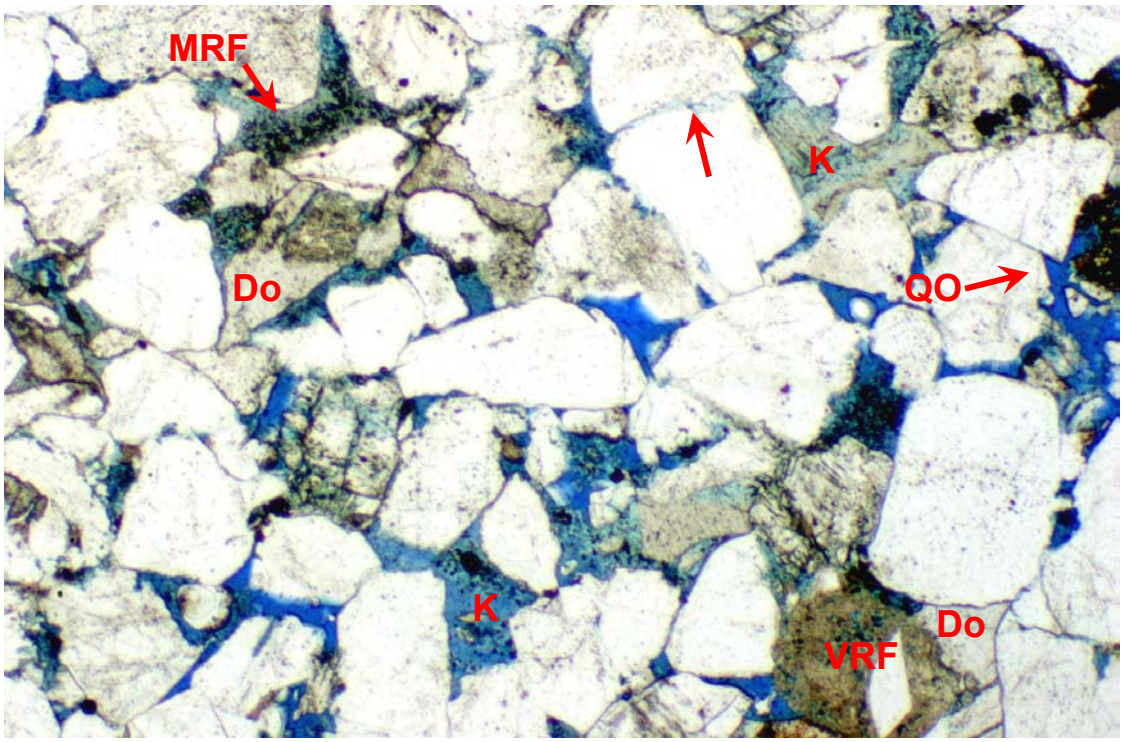

FIGURE 1 Plane polarised light
FIGURE 2 Crossed polarisers

0.4 mm

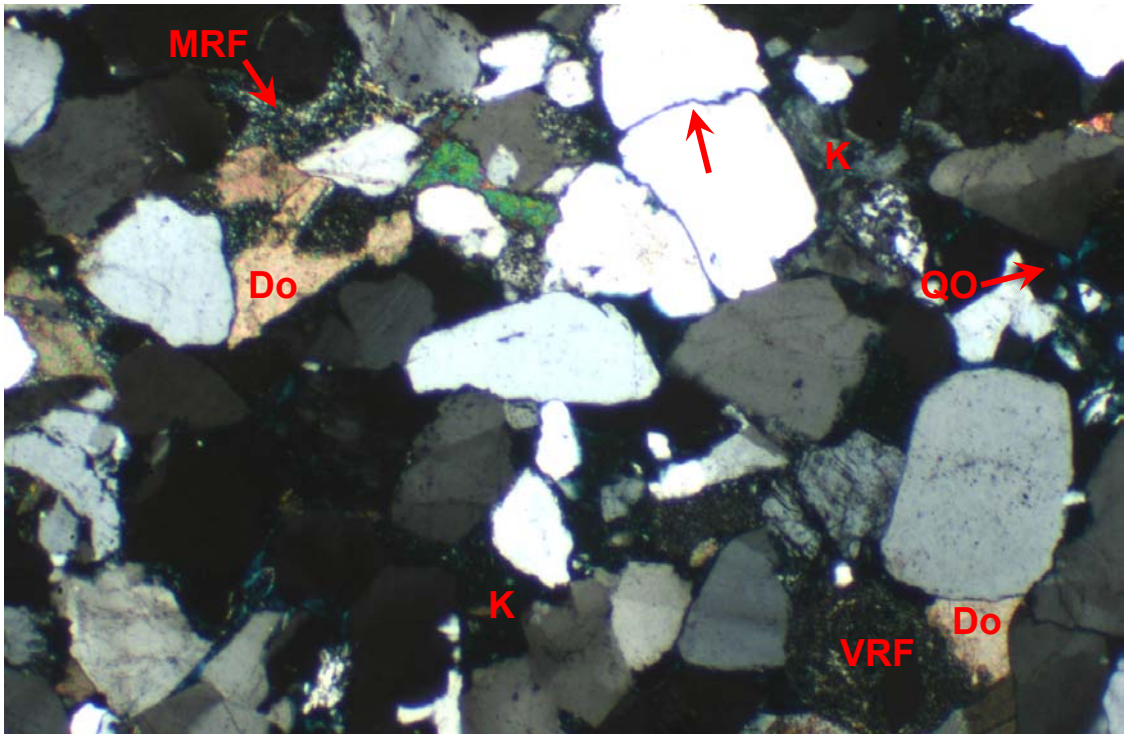

Low magnification micrographs showing general texture of a medium grained sandstone in which connection between intergranular pores (blue) is significantly reduced by authigenic kaolinite (K) formation, illitic metasedimentary rock fragment (MRF) compaction, grain contact dissolution (arrow) and patchy dolomite (Do) cementation. Quartz overgrowths (QO) can barely be seen in the micrographs. A felsic volcanic rock fragment with a quartz phenocryst (VRF) is also marked. Detail is shown in Plates 24 and 25. K = 41.2mD

PLATE 24 #7 3372.0m (cont.)

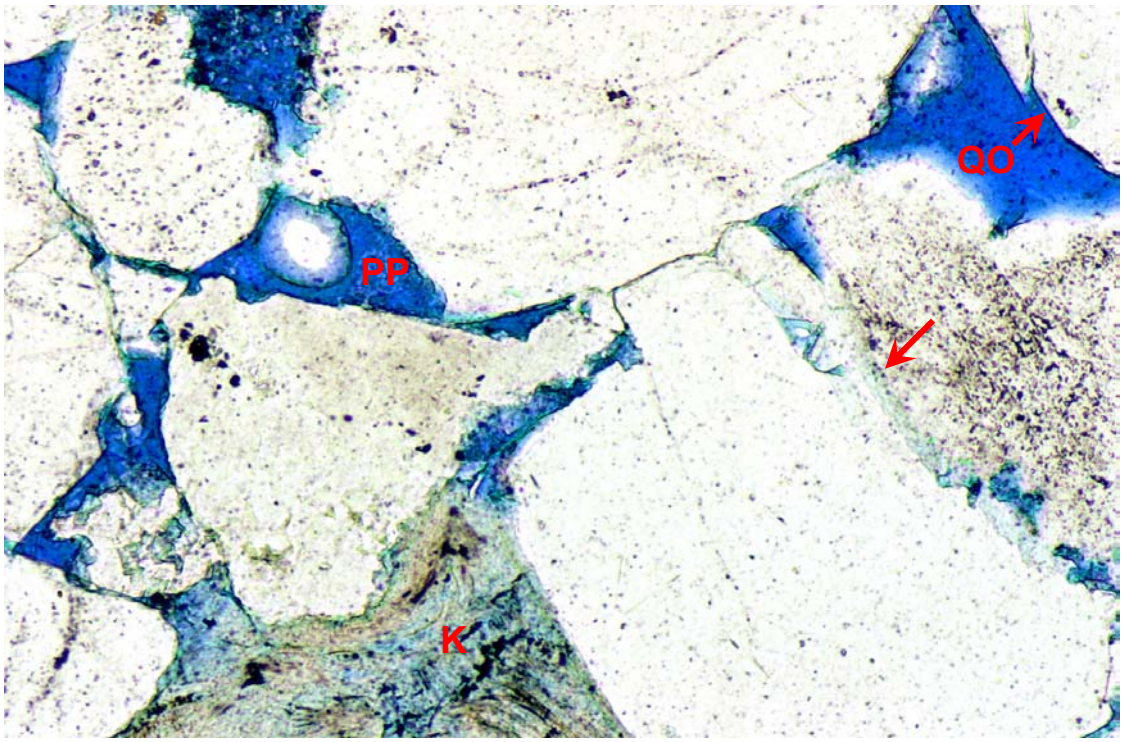

FIGURE 1 Plane polarised light

FIGURE 2 Crossed polarisers

0.2 mm

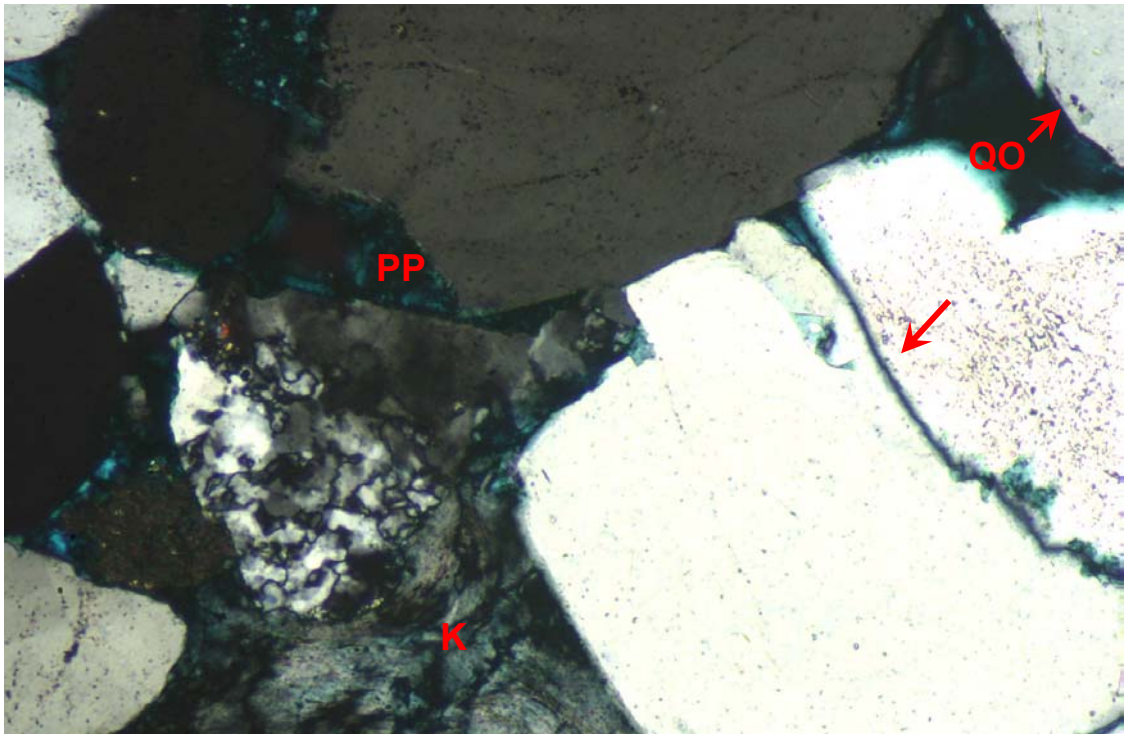

Good primary intergranular porosity (PP) is preserved between juxtaposed quartz grains, despite porosity reduction by grain contact dissolution (arrow) and quartz overgrowth (QO) precipitation, but pore interconnectivity is significantly reduced by plugging of intergranular spaces by authigenic kaolinite pseudomatrix (K) that results from micaceous grain compaction and alteration. K = 41.2mD

PLATE 25 #7 3372.0m (cont.)

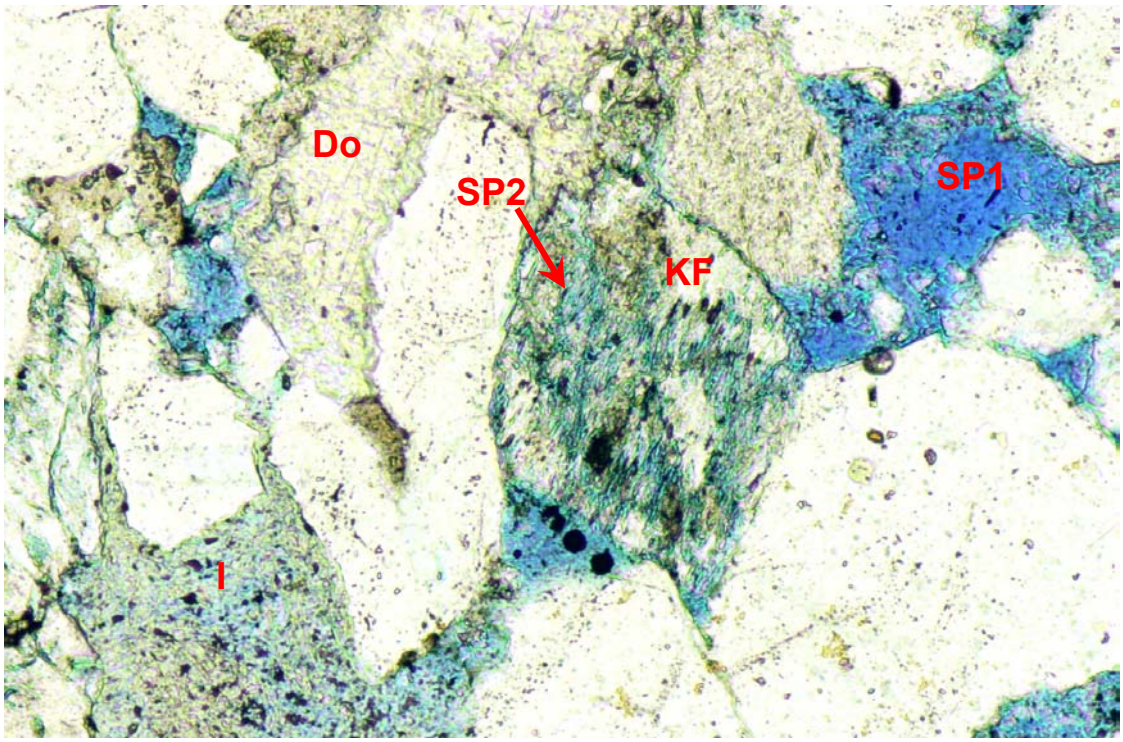

FIGURE 1 Plane polarised light

FIGURE 2 Crossed polarisers

0.2 mm

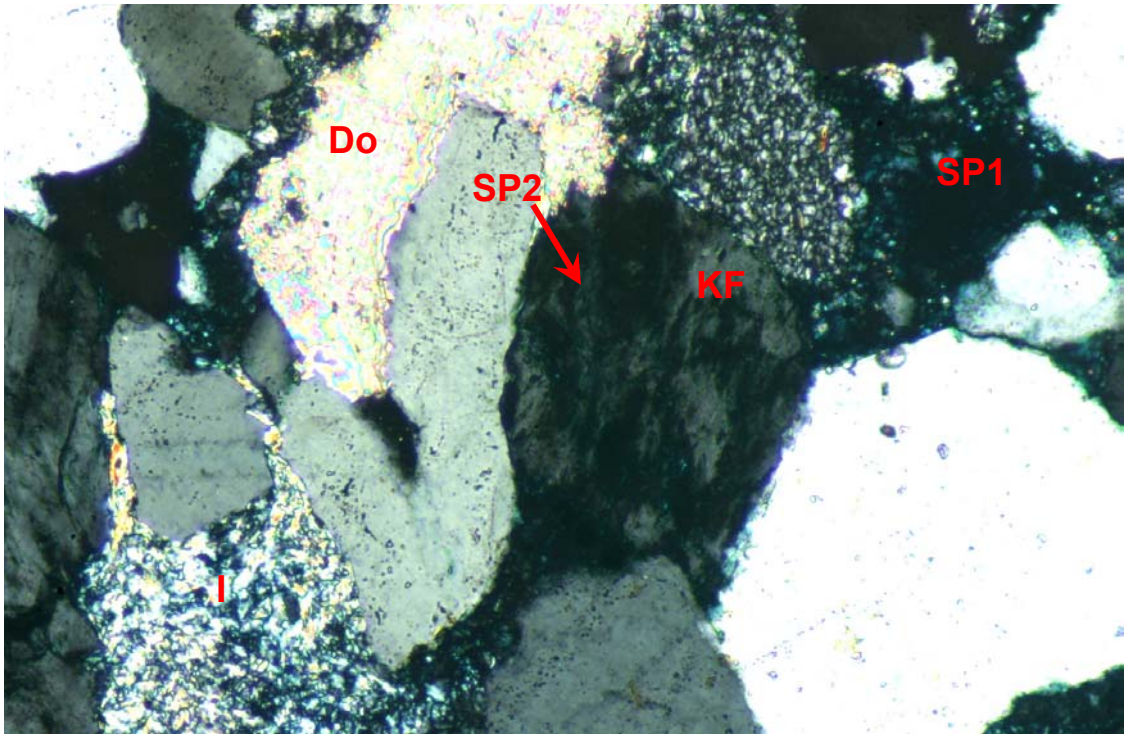

Other causes of porosity reduction besides authigenic kaolinite formation, grain contact dissolution and quartz overgrowth cementation (see Plate 24) include patchy dolomite (Do) cementation and the compaction and alteration of micaceous metamorphic rock fragments to form illite pseudomatrix (I). Visible porosity includes secondary intergranular porosity (SP1) that results from labile grain dissolution and secondary intragranular porosity (SP2) that is associated with the skeletal remnants of a partly dissolved K-feldspar grain (KF). K = 41.2mD

PLATE 26 #7 3372.0m (cont.)

FIGURE 1

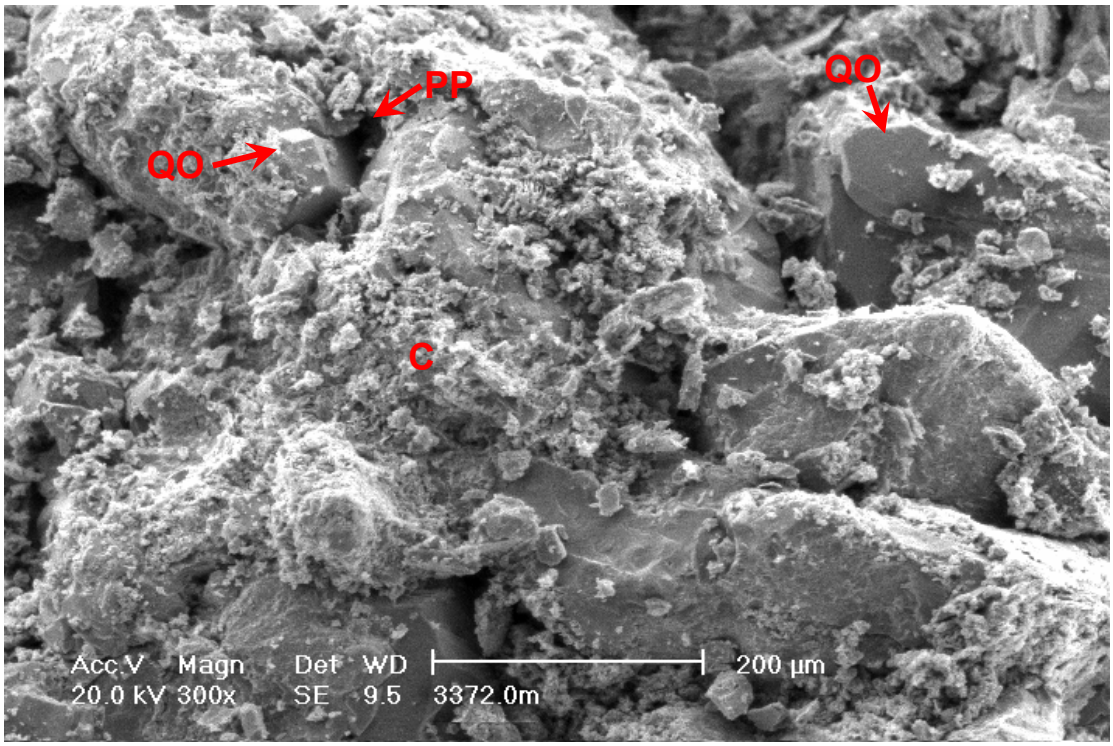

Interconnectivity between primary pores (PP) is greatly reduced by plugging of intergranular spaces by clay pseudomatrix (C) that results from compaction and alteration of micaceous/argillaceous grains. Quartz overgrowths (QO) are thinly developed and thus only partly occlude intergranular pores. (SEM micrograph)

FIGURE 2

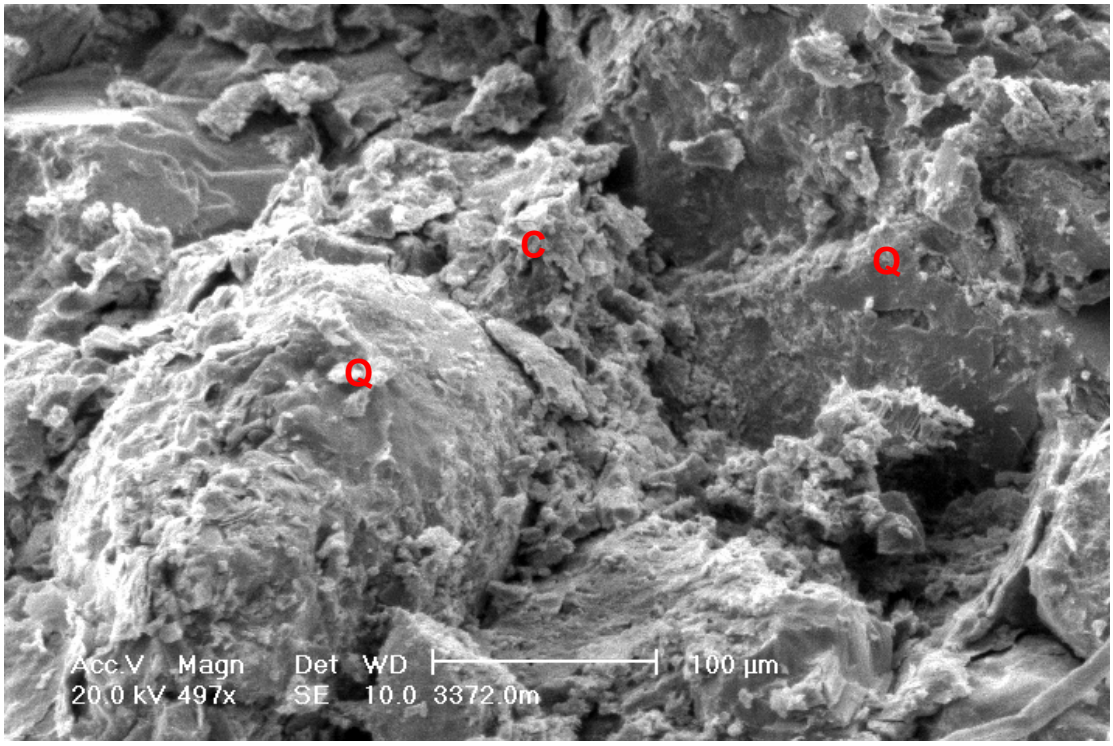

Detail of clay pseudomatrix (C) that plugs an intergranular space between quartz grains (Q). Relatively low permeability (41.2mD) reflects the presence of clay pseudomatrix and compacted micaceous/argillaceous grains in many intergranular pores. (SEM micrograph)

PLATE 27 #6 3409.0m

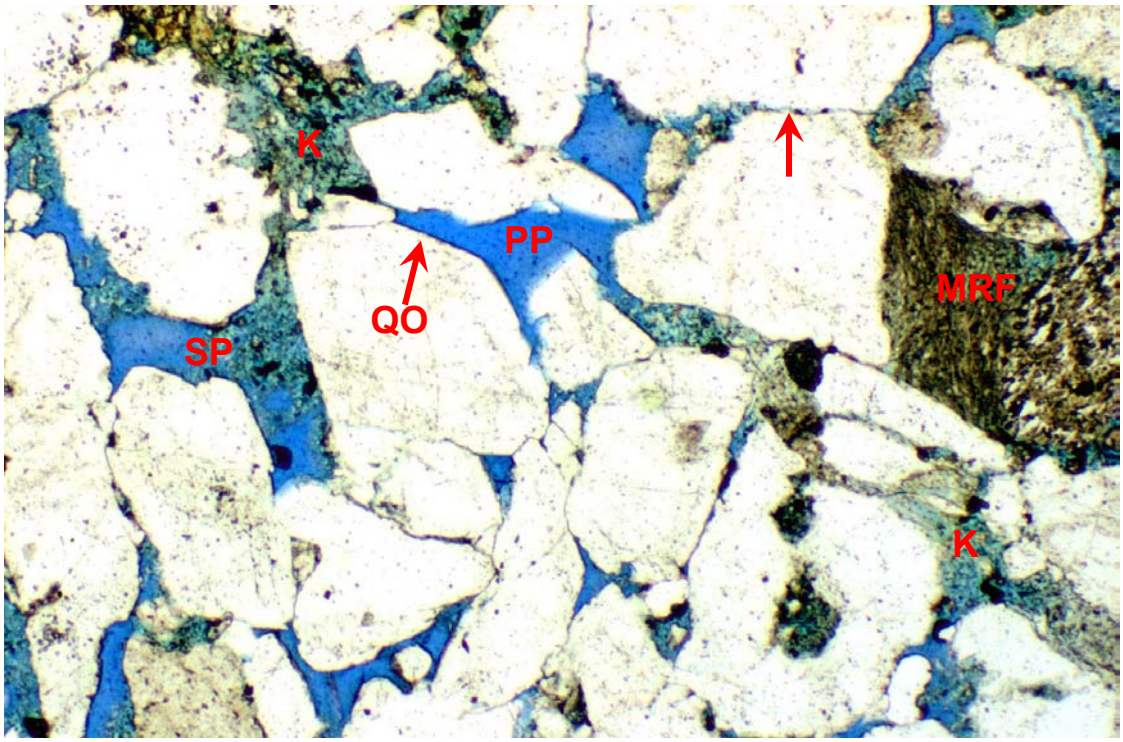

FIGURE 1 Plane polarised light
FIGURE 2 Crossed polarisers

0.4 mm

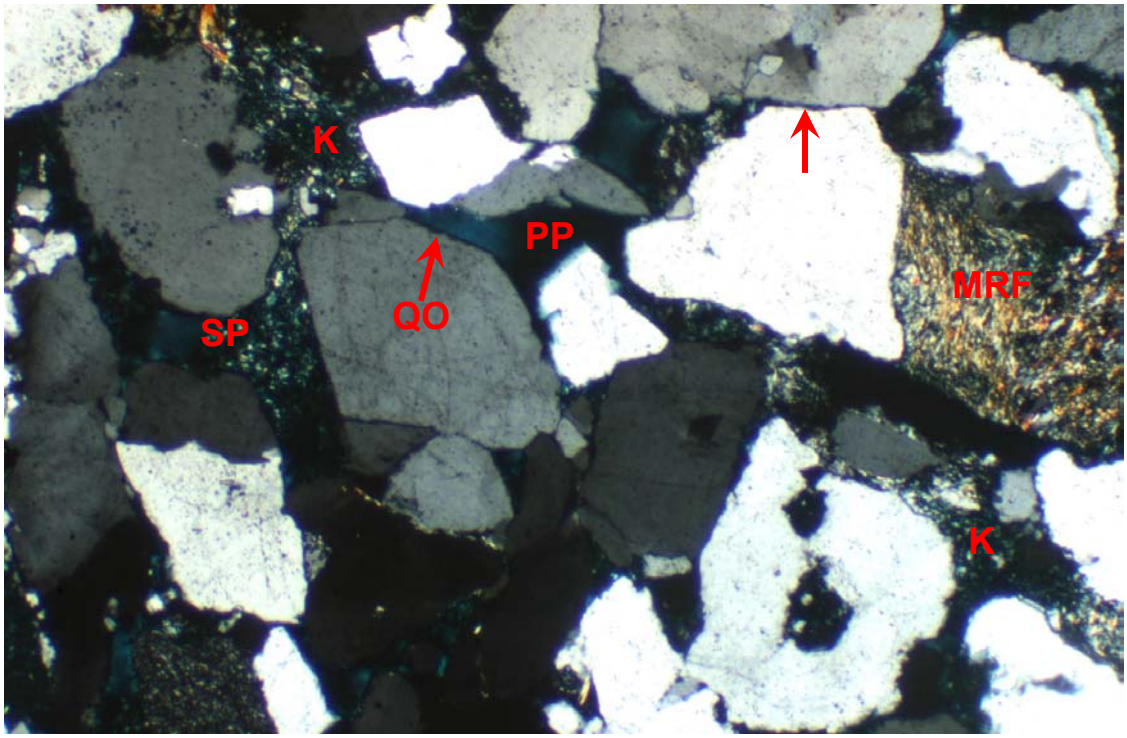

This coarse grained subarkose contains a system of well-interconnected primary intergranular pores (PP) and subordinate secondary labile grain dissolution pores (SP). Good primary intergranular porosity is preserved despite porosity reduction by authigenic kaolinite (K) formation, grain contact dissolution (arrow) and compactional deformation of illitic/micaceous, low-grade metasedimentary rock fragments (MRF). Thinly-developed quartz overgrowths (QO) have little impact on reservoir quality. K = 1380mD

PLATE 28 #4 3439.0m

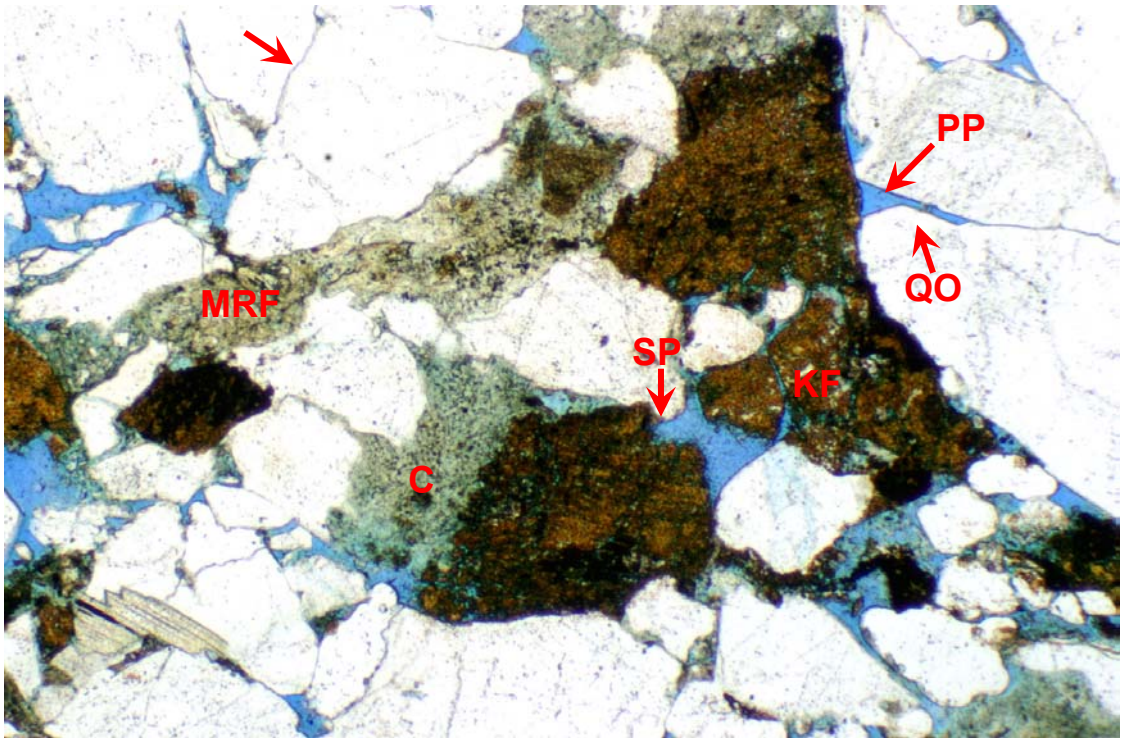

FIGURE 1 Plane polarised light
FIGURE 2 Crossed polarisers

0.4 mm

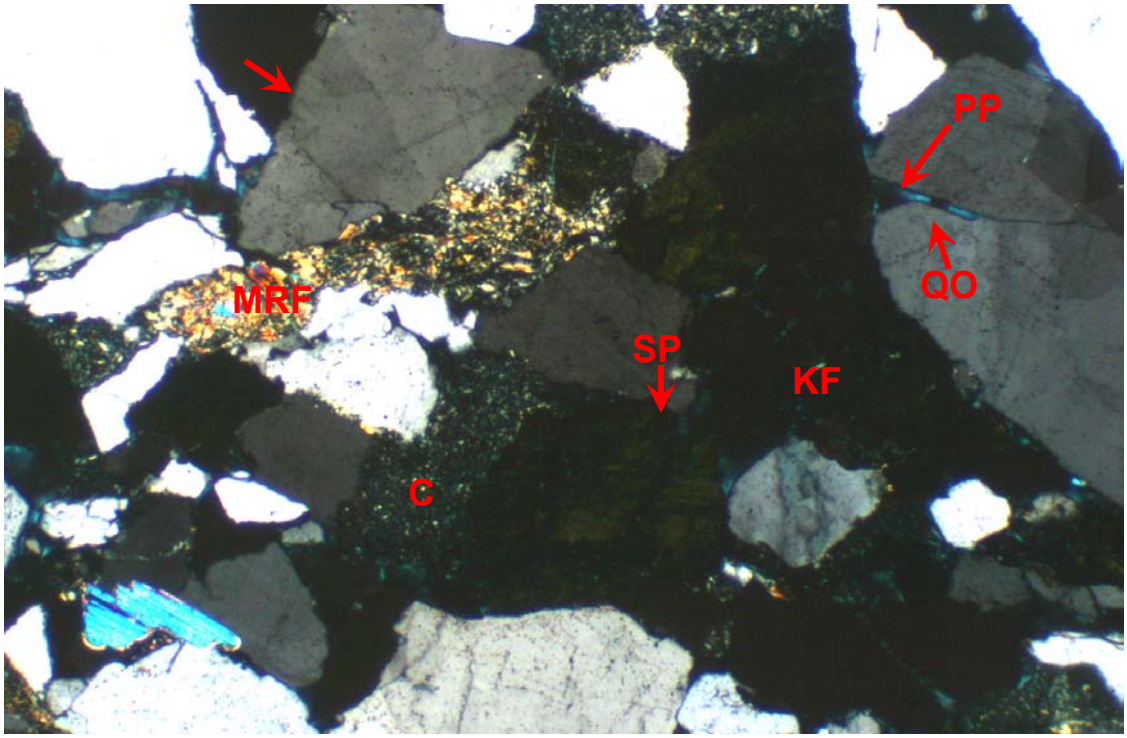

Coarse grained subarkose in which interconnectivity between primary intergranular pores (PP) is greatly reduced by authigenic kaolinitic/illitic clay (C) and compacted micaceous metamorphic rock fragments (MRF). Porosity reduction also results from grain contact dissolution (arrow) and very minor quartz overgrowth (QO) cementation. Granitic K-feldspar (KF) (stained dark brown) is compactionally fractured and has dissolved to form minor secondary porosity (SP). Detail is shown in Plate 29. K = 211mD

PLATE 29 #4 3439.0m (cont.)

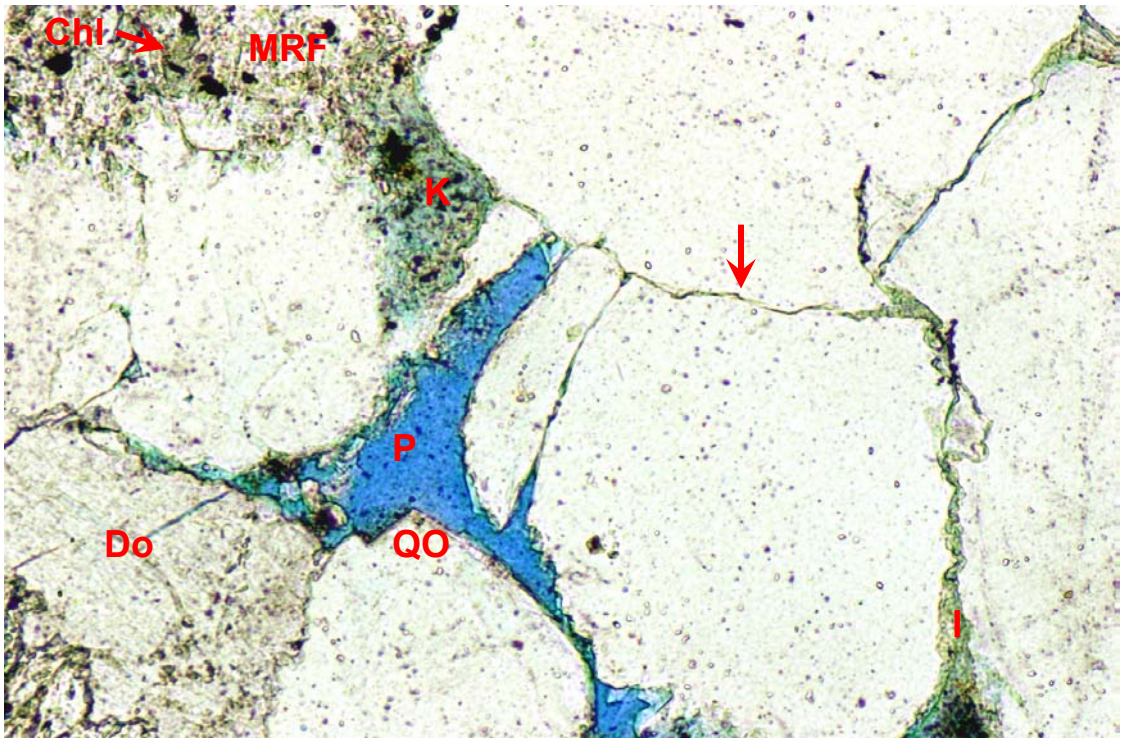

FIGURE 1 Plane polarised light

FIGURE 2 Crossed polarisers

0.2 mm

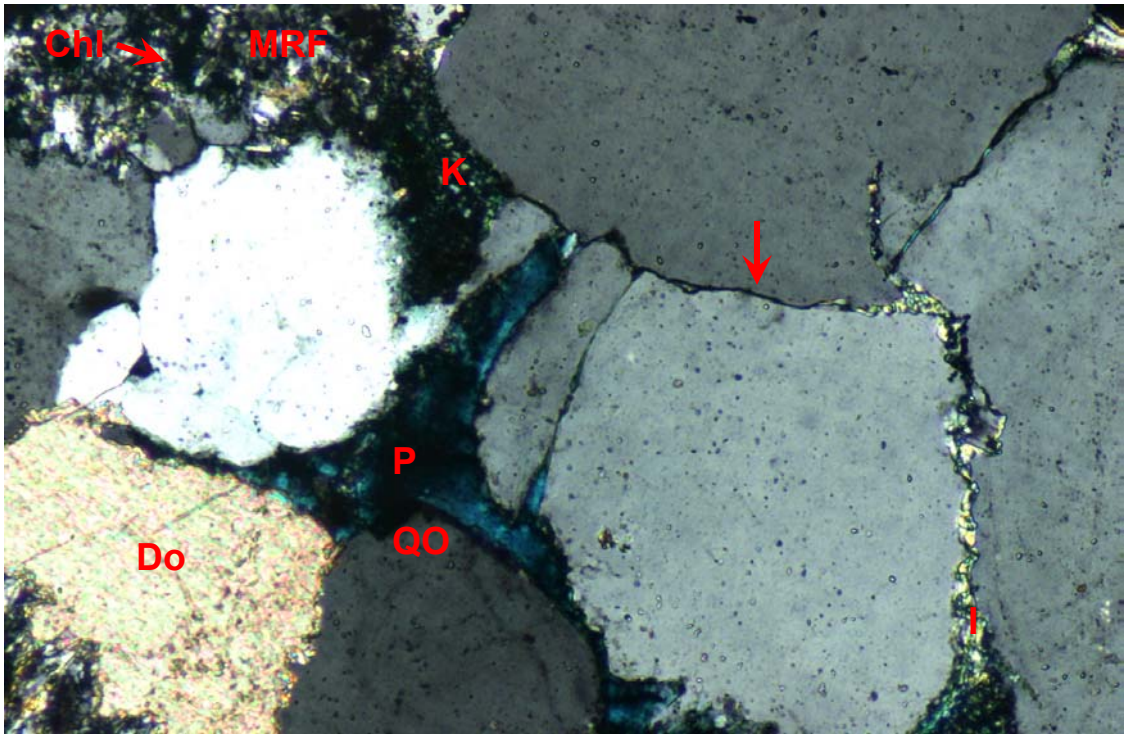

Tight grain welding between quartz grains (arrow) results from grain contact dissolution that was promoted by illitic clay films (I) that are the altered and dispersed remnants of micaceous/illitic grains. Intergranular porosity (P) reduction also results from minor dolomite (Do) and quartz overgrowth (QO) cementation and authigenic kaolinite (K) formation. A chlorite (Chl)-bearing metasedimentary rock fragment (MRF) is also marked. K = 211mD

PLATE 30 #3 3449.0m

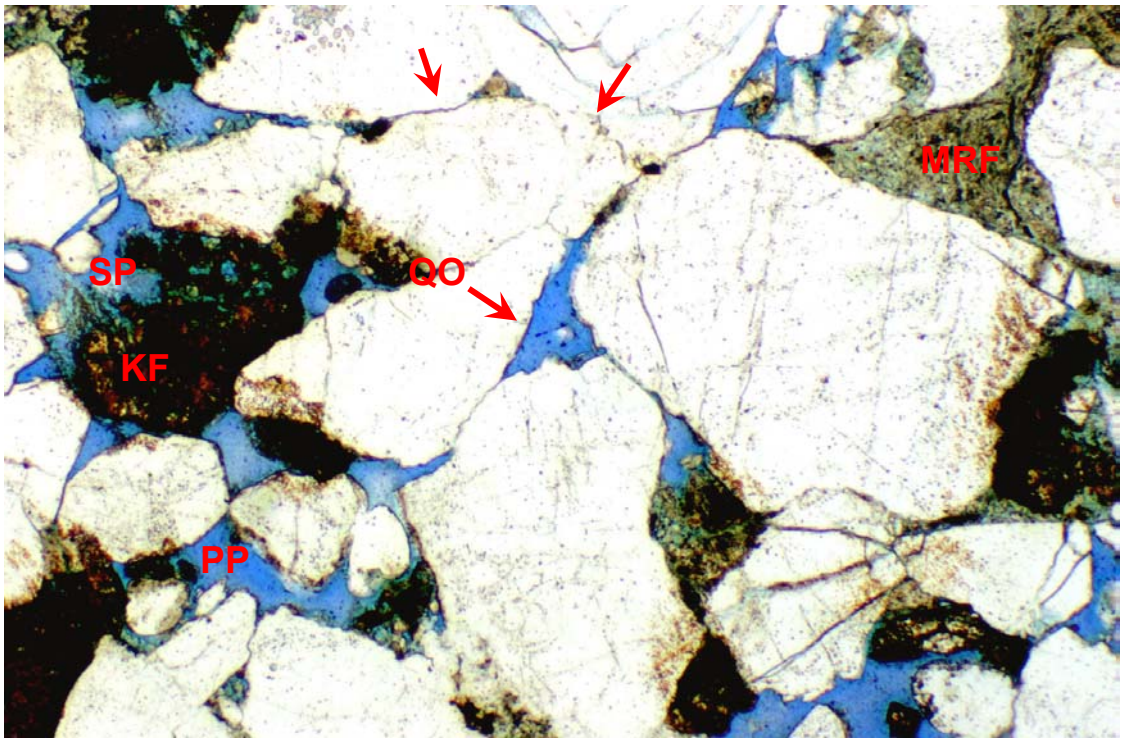

FIGURE 1 Plane polarised light
FIGURE 2 Crossed polarisers

0.4 mm

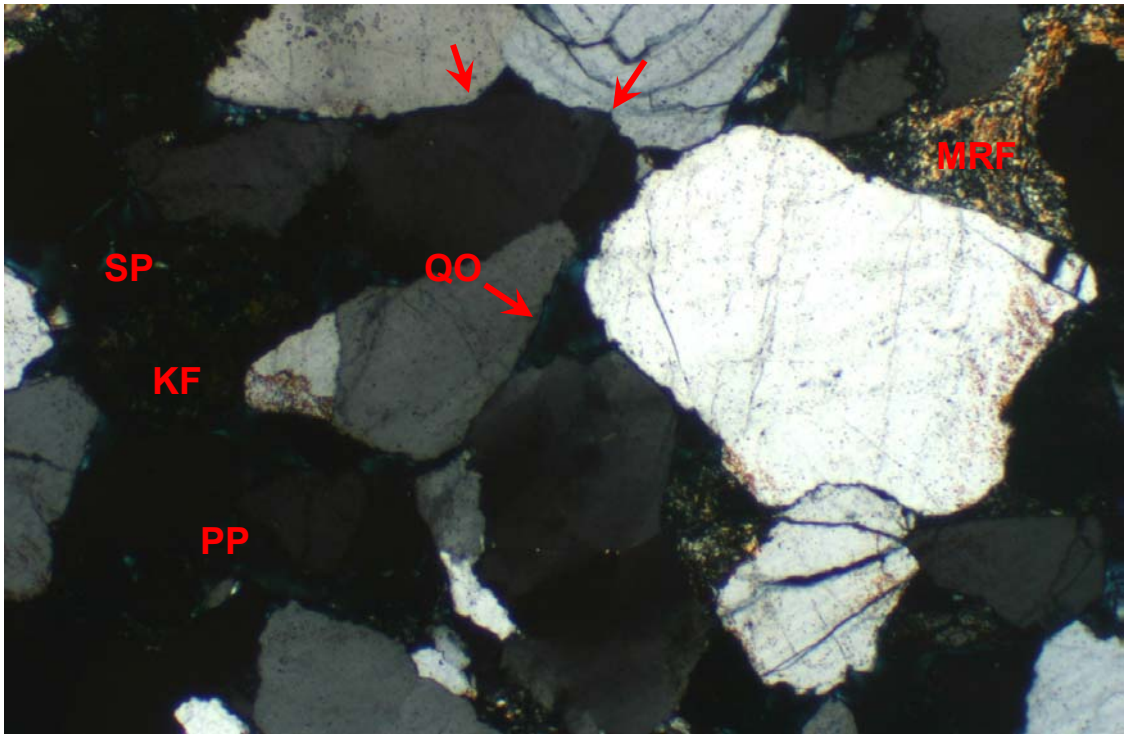

Significant porosity reduction in this coarse grained sublitharenite results from grain contact dissolution (arrows) and the compactional deformation of an illitic, low-grade metasedimentary rock fragment (MRF), but the sandstone still contains good primary intergranular porosity (PP) that is supplemented by minor secondary porosity (SP) that results from K-feldspar (KF) (stained dark brown) dissolution. Quartz grains are thinly enveloped by quartz overgrowths (QO). Detail is shown in Plate 31. K = 921mD

PLATE 31 #3 3449.0m (cont.)

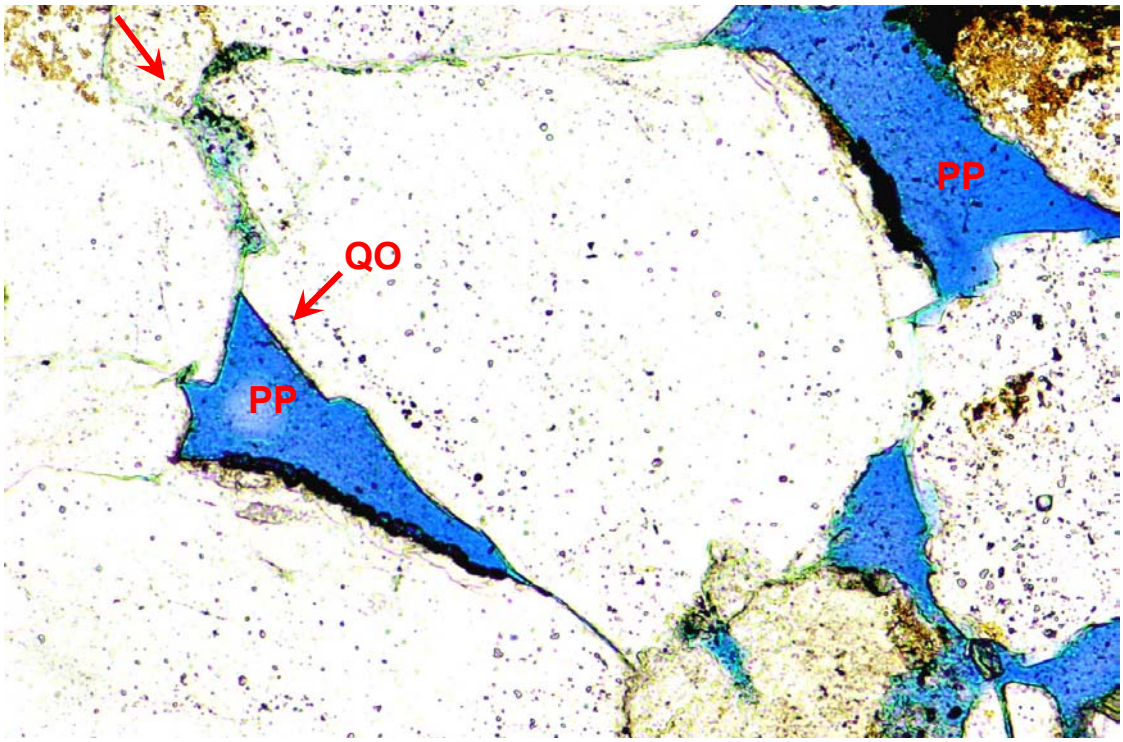

FIGURE 1 Plane polarised light

FIGURE 2 Crossed polarisers

0.2 mm

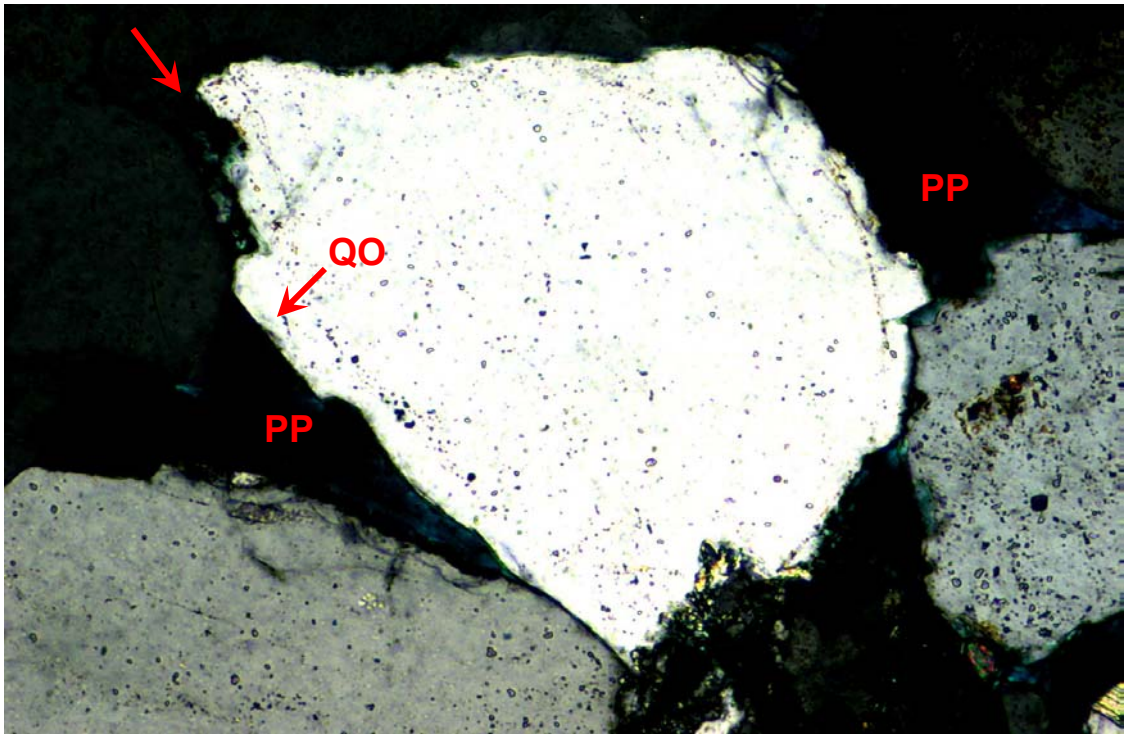

Between some quartz grains, grain contact dissolution has advanced sufficiently so as to largely or completely eliminate intergranular porosity (arrow), and there has also been porosity reduction by minor quartz overgrowth (QO) cementation. However, primary intergranular pores (PP) are still sufficiently common to be well interconnected throughout the sandstone. K = 921mD